CHALMERS
UNIVERSITY OF TECHNOLOGY

Annex 55
Reliability of Energy Efficient Building Retrofitting- Probability Assessment of Performance and Cost (RAP-RETRO)

Stochastic Data

NUNO M. M. RAMOS University of Porto, Portugal

JOHN GRUNEWALD TU Dresden, Germany

International Energy Agency

EBC
Energy in Buildings and Communities Programme

Department of Civil and Environmental Engineering
CHALMERS UNIVERSITY OF TECHNOLOGY
Gothenburg, Sweden 2015

Stochastic Data

Editors: Nuno M. M. Ramos, John Grunewald
Authors:
Canada: [BCIT] Fitsum Tariku, Wendy Simpson
Denmark: [DTU] Christopher Just Johnston, Carsten Rode
Estonia: [TUT] Targo Kalamees, Simo Ilomets, Kalle Kuusk, Endrik Arumagi
Finland: [TTU] Elina Mannelius, Anssi Laukkarinen, Juha Vinha
Germany [IBP] Florian Antretter, Marcus Fink
Germany: [TUD] John Grunewald, Jianhua Zhao
The Netherlands: [TUE] Mike van der Heijden
Portugal: [UP] Nuno M. M. Ramos, António Curado
Sweden: [CTH] Angela Sasic Kalagasidis, Vahid Nik, Simon Pallin,
Sweden: [LTH] Lars-Erik Harderup, Johan Stein
Sweden: [LTH] Petter Wallentén
Sweden: [SP] Kristina Mjörnell
United Kingdom: [UCL] Payel Das, Michael Davis
Reviewer: Peter Matiasovsky, Fitsum Tariku

Report 2015:3
ISSN 1652-9162

Department of Civil and Environmental Engineering
Division of Building Technology
Chalmers University of Technology
SE-412 96 Gothenburg
Sweden
Telephone + 46 (0)31-772 1000

Published by Chalmers University of Technology, SE-412 96 Göteborg, Sweden

ISSN 1652-9162

Participating countries in EBC:

Australia, Austria, Belgium, Canada, P.R. China, Czech Republic, Denmark, Finland, France, Germany, Greece, Ireland, Italy, Japan, Republic of Korea, the Netherlands, New Zealand, Norway, Poland, Portugal, Spain, Sweden, Switzerland, Turkey, United Kingdom and the United States of America.

Additional copies of this report may be obtained from:

EBC Bookshop

C/o AECOM Ltd

Colmore Plaza

Colmore Circus Queensway

Birmingham B4 6AT

United Kingdom

Web: www.iea-ebc.org

Email: essu@iea-ebc.org

Preface

The International Energy Agency

The International Energy Agency (IEA) was established in 1974 within the framework of the Organisation for Economic Co-operation and Development (OECD) to implement an international energy programme. A basic aim of the IEA is to foster international co-operation among the 28 IEA participating countries and to increase energy security through energy research, development and demonstration in the fields of technologies for energy efficiency and renewable energy sources.

The IEA Energy in Buildings and Communities Programme

The IEA co-ordinates research and development in a number of areas related to energy. The mission of the Energy in Buildings and Communities (EBC) Programme is to develop and facilitate the integration of technologies and processes for energy efficiency and conservation into healthy, low emission, and sustainable buildings and communities, through innovation and research. (Until March 2013, the IEA-EBC Programme was known as the Energy in Buildings and Community Systems Programme, ECBCS.)

The research and development strategies of the IEA-EBC Programme are derived from research drivers, national programmes within IEA countries, and the IEA Future Buildings Forum Think Tank Workshops. The research and development (R&D) strategies of IEA-EBC aim to exploit technological opportunities to save energy in the buildings sector, and to remove technical obstacles to market penetration of new energy efficient technologies. The R&D strategies apply to residential, commercial, office buildings and community systems, and will impact the building industry in five focus areas for R&D activities:

- Integrated planning and building design
- Building energy systems
- Building envelope
- Community scale methods
- Real building energy use

The Executive Committee

Overall control of the IEA-EBC Programme is maintained by an Executive Committee, which not only monitors existing projects, but also identifies new strategic areas in which collaborative efforts may be beneficial. As the Programme is based on a contract with the IEA, the projects are legally established as Annexes to the IEA-EBC Implementing Agreement. At the present time, the following projects have been initiated by the IEA-EBC Executive Committee, with completed projects identified by (*):

Annex 1: Load Energy Determination of Buildings (*)
Annex 2: Ekistics and Advanced Community Energy Systems (*)
Annex 3: Energy Conservation in Residential Buildings (*)
Annex 4: Glasgow Commercial Building Monitoring (*)
Annex 5: Air Infiltration and Ventilation Centre
Annex 6: Energy Systems and Design of Communities (*)
Annex 7: Local Government Energy Planning (*)
Annex 8: Inhabitants Behaviour with Regard to Ventilation (*)
Annex 9: Minimum Ventilation Rates (*)
Annex 10: Building HVAC System Simulation (*)
Annex 11: Energy Auditing (*)
Annex 12: Windows and Fenestration (*)
Annex 13: Energy Management in Hospitals (*)

Annex 14: Condensation and Energy (*)
Annex 15: Energy Efficiency in Schools (*)
Annex 16: BEMS 1- User Interfaces and System Integration (*)
Annex 17: BEMS 2- Evaluation and Emulation Techniques (*)
Annex 18: Demand Controlled Ventilation Systems (*)
Annex 19: Low Slope Roof Systems (*)
Annex 20: Air Flow Patterns within Buildings (*)
Annex 21: Thermal Modelling (*)
Annex 22: Energy Efficient Communities (*)
Annex 23: Multi Zone Air Flow Modelling (COMIS) (*)
Annex 24: Heat, Air and Moisture Transfer in Envelopes (*)
Annex 25: Real time HVAC Simulation (*)
Annex 26: Energy Efficient Ventilation of Large Enclosures (*)
Annex 27: Evaluation and Demonstration of Domestic Ventilation Systems (*)
Annex 28: Low Energy Cooling Systems (*)
Annex 29: Daylight in Buildings (*)
Annex 30: Bringing Simulation to Application (*)
Annex 31: Energy-Related Environmental Impact of Buildings (*)
Annex 32: Integral Building Envelope Performance Assessment (*)
Annex 33: Advanced Local Energy Planning (*)
Annex 34: Computer-Aided Evaluation of HVAC System Performance (*)
Annex 35: Design of Energy Efficient Hybrid Ventilation (HYBVENT) (*)
Annex 36: Retrofitting of Educational Buildings (*)
Annex 37: Low Exergy Systems for Heating and Cooling of Buildings (LowEx) (*)
Annex 38: Solar Sustainable Housing (*)
Annex 39: High Performance Insulation Systems (*)
Annex 40: Building Commissioning to Improve Energy Performance (*)
Annex 41: Whole Building Heat, Air and Moisture Response (MOIST-ENG) (*)
Annex 42: The Simulation of Building-Integrated Fuel Cell and Other Cogeneration Systems (FC+COGEN-SIM) (*)
Annex 43: Testing and Validation of Building Energy Simulation Tools (*)
Annex 44: Integrating Environmentally Responsive Elements in Buildings (*)
Annex 45: Energy Efficient Electric Lighting for Buildings (*)
Annex 46: Holistic Assessment Tool-kit on Energy Efficient Retrofit Measures for Government Buildings (EnERGo) (*)
Annex 47: Cost-Effective Commissioning for Existing and Low Energy Buildings (*)
Annex 48: Heat Pumping and Reversible Air Conditioning (*)
Annex 49: Low Exergy Systems for High Performance Buildings and Communities (*)
Annex 50: Prefabricated Systems for Low Energy Renovation of Residential Buildings (*)
Annex 51: Energy Efficient Communities (*)
Annex 52: Towards Net Zero Energy Solar Buildings (*)
Annex 53: Total Energy Use in Buildings: Analysis & Evaluation Methods (*)
Annex 54: Integration of Micro-Generation & Related Energy Technologies in Buildings
Annex 55: Reliability of Energy Efficient Building Retrofitting - Probability Assessment of Performance & Cost (RAP-RETRO)
Annex 56: Cost Effective Energy & CO2 Emissions Optimization in Building Renovation
Annex 57: Evaluation of Embodied Energy & Greenhouse Gas Emissions for Building Construction
Annex 58: Reliable Building Energy Performance Characterisation Based on Full Scale Dynamic Measurements
Annex 59: High Temperature Cooling & Low Temperature Heating in Buildings
Annex 60: New Generation Computational Tools for Building & Community Energy Systems
Annex 61: Business and Technical Concepts for Deep Energy Retrofit of Public Buildings
Annex 62: Ventilative Cooling
Annex 63: Implementation of Energy Strategies in Communities

Annex 64: LowEx Communities - Optimised Performance of Energy Supply Systems with Exergy Principles
Annex 65: Long-Term Performance of Super-Insulating Materials in Building Components and Systems
Annex 66: Definition and Simulation of Occupant Behavior in Buildings
Annex 67: Energy Flexible Buildings
Working Group - Energy Efficiency in Educational Buildings (*)
Working Group - Indicators of Energy Efficiency in Cold Climate Buildings (*)
Working Group - Annex 36 Extension: The Energy Concept Adviser (*)

Table of Contents

Abbreviations and Acronyms

BC	Housing British Columbia Housing Corporation
BCIT	British Columbia Institute of Technology
BSCE	Building Science Centre of Excellence
CDF	Cumulative distribution function
CISBO	Centre for Indoor Environment and Health in Homes
DHW	Domestic hot water
EBC	Energy in Buildings and Communities
ECBCS	Energy in Buildings and Community Systems Programme
ECDF	Empirical cumulative distribution function
E-level	Energy performance indicator (E-level corresponding regional EPBD-regulation)
EPV	Energy performance value
GLM	Generalised Linear Models
HLC	Heat loss coefficient
HVAC	Heating, ventilation, and air conditioning
IEA	International Energy Agency
IECH	Indoor Environment and Children's Health
IWT	Flemish government agency for Innovation by Science and Technology
KNMI	Royal Dutch Meteorological Institute
K-S test	Kolmogorov-Smirnov test
LCC	Life Cycle Cost
LR	Living room
MFH	Multi-family house
MSE	Mean squared error
MSI	Mould Severity Index
Net	Energy reduction for heating and cooling
NOW	Total number of hours that windows are open divided by the number of days
OECD	Organisation for Economic Co-operation and Development
PDF	Probability density functions
R&D	The research and development

RH	Row house
SDH	Semi-detached house
SFH	Single family house
SH	Space heating
SHGC	Solar Heat Gain Coefficient
SMHI	Rossby Centre
S-W test	Shapiro-Wilk test
TD	Time of the day
TUD	Experimental assessment of material properties
UHASSELT	PHL University College
UHI	Urban heat island
UHII	Urban heat island intensity at a specific time
WFS	Warm Front Study

Nomenclature

Latin characters

A	Cross-sectional area of the specimen	[m^2]
ACH	Air change rate	[h^{-1}]
A_w	Water absortion coefficient	[$kg/m^2s^{0.5}$]
A_{facade}	Facade area	[m^2]
A_f	Ground floor area	[m^2]
C	Indoor CO_2 concentration after measurements	[g/m^3]
c	Specific heat capacity	[J/kgK]
C_0	Indoor CO_2 concentration before measurements	[g/m^3]
C_v	CO_2 concentration of outdoor air	[g/m^3]
d	Thickness of the specimen	[m]
DD	Heating degree days calculated over the monitoring period	
E-value	Normalized space heating fuel consumption	[$W/K/m^2$]
g	Gravity acceleration	[m/s^2]
K_{eff}	Saturated liquid conductivity	[s]
Kl	Unsaturated liquid conductivity	[s]

Kl(θ)	Liquid water conductivity	[s]
Kv(θ)	Water vapour permeability	[s]
m	CO_2 production	[g/h]
N	Normal distribution	
n_{50}, ACH_{50}	Air change rate at 50 Pa	[h^{-1}]
$p_{v,sat}$	Saturated vapour pressure	[Pa]
q_{50}	Air permeability	[m^3/ (hm^2)]

Greek characters

α	Predefined significance level	
Δp	Pressure difference between two sides of the specimen	[Pa]
$\Delta\nu$	Moisture excess	[g/m^3]
ΔV	Volume of liquid water flowing through the material	[m^3]
θ(pC)	Moisture retention function	[m^3/m^3]
θ_{cap}	Capillary saturation	[m^3/ m^3]
θ_e	Outdoor air temperature	[°C]
θ_i	Indoor air temperature	[°C]
θ_{por}	Open Porosity	[m^3/ m^3]
λ(θ)	Thermal conductivity	[W/ (mK)]
λ_{dry}	Thermal conductivity	[W/ (mK)]
λ	Thermal conductivity coefficient	[W/ (mK)]
μ	Opening probability	
$\mu_{\Delta\nu}$	Average value of indoor moisture excess	[kg/m^3]
μ_{μ}	Average value of averages	
μ_{σ}	Average of standard deviation values	
μ_{dry}	Dry cup value	
ρ	Bulk density	[kg/m^3]
$\sigma_{\Delta\nu}$	Standard deviation of indoor moisture excess	[kg/m^3]
σ_{μ}	Standard deviation of averages	
σ_{σ}	Standard deviation of standard deviation values	
τ	Time	[h]

Φ^{-1}	Inverse normal cumulative distribution function	[kg/m^3]
φ k	Phase change for a specific harmonic	
ω0	Angular velocity	[rad/s]

1 INTRODUCTION

1.1 Motivation and Objectives

The probability assessment of performance and cost intended in Annex 55 is only possible if stochastic data are available. Subtask 1 was therefore designed to gather data that could be used in the intended assessment. That data should define a set of parameters with attached statistical distributions. Although apparently simple to implement, the definition of the best strategy was quite complex as a match between the available raw data from different sources and the desired input data for different stochastic analysis procedures had to be found.

Taking Life Cycle Cost (LCC) variability evaluation as a sound objective for this project, the desired input data can be identified in the relevant available analysis tools. Assuming that hygrothermal analysis is decisive for the success in that objective, still a wide list of parameters could be found, as available codes use different simulation strategies.

Current hygrothermal tools execute mainly deterministic simulations due to the fact that each parameter uses a desired value. The corresponding outputs will be a predictably determined value/ values. However, the simulation inputs, e.g., user behaviour, material properties, and weather condition, in the real world will not always follow the way defined in the simulation. For instance, material properties obtained from reference laboratory condition may differ from those at environmental conditions when the material was incorporated in the building envelope due to the change of the surrounding environment or ageing. Weather condition used in the simulation either is the measured data of past years or the synthetic data, e.g., test reference year. The stochastic nature of the inputs leads to the variations in the simulation outputs.

The objective of Subtask 1 was to make available stochastic data for application in hygrothermal analysis. Given the current state of the art, it was decides that the following goals should be achieved:

- Define a structure for the data so that they can be useful for researchers and practitioners;
- Identify source projects that could supply stochastic data;
- Synthetize the methodologies that allowed for the data collection and analysis;
- Assemble the data.

1.2 Structure

The structure of this document was determined by the need to clearly state the context of the presented data to allow for their correct application.

The second chapter presents the source projects where the information was gathered, identifying specific features of the sample that define the resulting data.

The third chapter presents the Input Data arranged in the following group of parameters: stochastic material data base, ventilation and airtightness, indoor loads and weather. Each subchapter is arranged so that each set of collected raw data is introduced, the analysis to derive statistical distributions that was performed on the raw data is explained and the final stochastic data sets are presented. The focus was put on ensuring that the connection to measured data wouldn't be lost.

The fourth chapter presents work on synthetic data, demonstrating how additional sets of valuable information can be prepared with more advanced analysis. Completing material data sets, window opening and heat island are hence presented as examples.

The fifth chapter addresses energy use data, presenting examples that can be used for validation of stochastic methodologies, using the input data presented in chapter three.

This document includes sets of electronic data resulting from the work presented in chapters three to five.

2 SOURCE PROJECTS

2.1 Introduction

This report was built on data previously collected in different projects. In this chapter, a synthesis of the projects carried out by each institution are presented. Details from the developed experimental campaigns, including specific features, sample sizes, methodologies and analysed parameters are described.

2.2 Belgium [KUL] – IWT TETRA BEP2020 (2011-2013)

IWT TETRA BEP2020 is a two-year research project which investigated reliable solutions for energy efficiency of new dwellings. The main research question was how to realise robust low energy dwellings. To answer this question it was investigated which design decisions and energy measures have the largest impact on the actual performance of the dwelling and are the least influenced by user behaviour. The project was performed by Department of Arts & Architecture at PHL University College (UHasselt) and Building Physics Section at KU Leuven, Belgium. Several Flemish enterprises and institutions were involved in the project and it was partly subsidised by these partners and partly by the Flemish government agency for Innovation by Science and Technology (IWT).

One major part of the research project is a measurement campaign of 70 new dwellings in Flanders. In this campaign, the energy use, indoor climate and air tightness have been measured. In the second major part, representative dwelling simulations determine the feasibility of (net) energy reduction for heating and cooling.

In this report, the air tightness measurements are collected as they are most valuable for renovation development.

2.3 Canada [BCIT] – Indoor Temperature and Humidity in a Multi-Unit Residential Building

To assess the indoor temperature and humidity distributions in a multi-unit residential building in Vancouver, the Building Science Centre of Excellence (BSCE) at the British Columbia Institute of Technology (BCIT) monitored the temperature and humidity of twenty-two rooms in four Suites for about seventeen months. The collected data is also used to obtain statistical information on the seasonal variations and ranges of indoor temperature and relative humidity conditions of Suites in the same building. The residential building is six-storey and has a total of 60 units. It is surrounded by low to mid-rise buildings and two major streets in the east and north orientations,

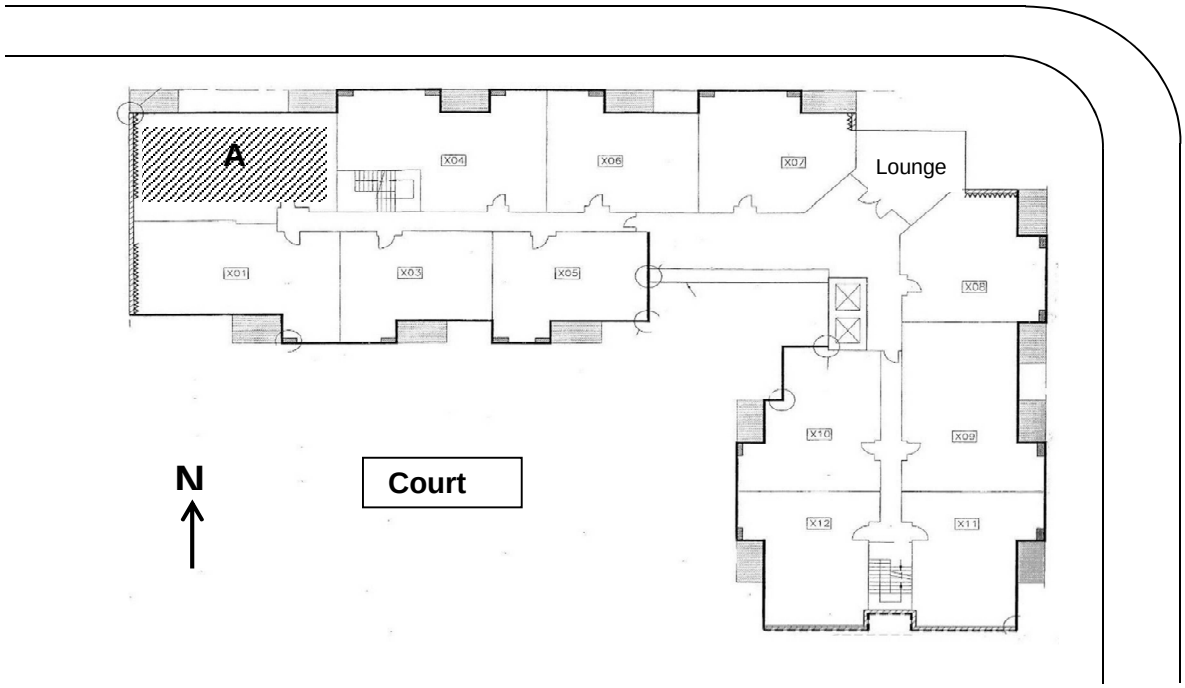

Figure *2.1*.

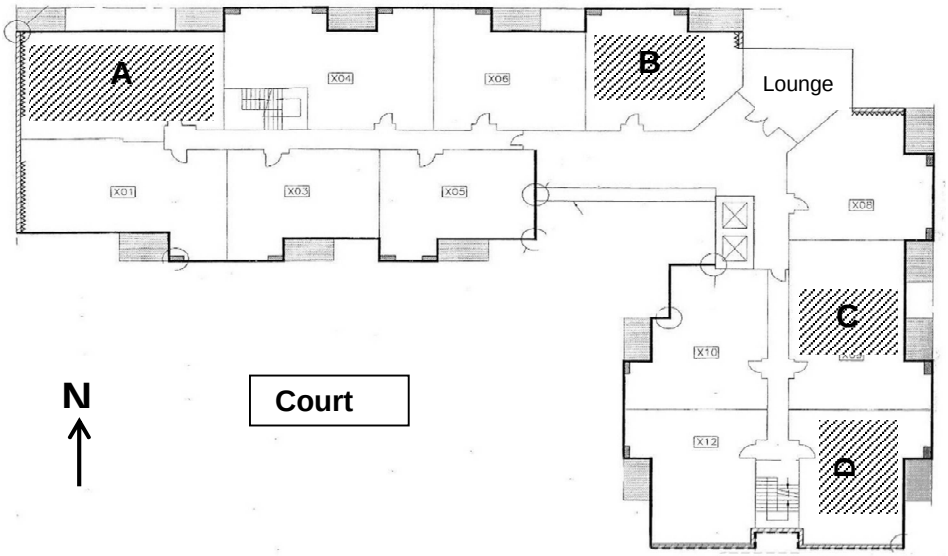

Figure 2.1 Monitored Suite locations on the fifth floor in Princess Place.

The four Suites that are considered in the study are all on the fifth floor, and they represent different occupant density, floor area and physical orientations. They are chosen to be on the same height level to allow similar outdoor and corridor environmental exposures including stack and mechanical corridor pressures. Suite 'A' and Suite 'D' are end units and Suite 'B' is adjacent to a Lounge room in the east and a neighbour Suite in the west. The corridors of the Suites, except that of Suite 'B', are pressurized and conditioned. Two of the Suites (Suite 'B' and 'D') have two bedrooms and the other two (Suite 'A' and 'C') have three bedrooms. Each Suite has also an open style Kitchen (facing to a foyer and a living room), a Bathroom and a Living room with a balcony. The two bedroom suites have a floor area of 643 and 654 sq. ft., whereas the three bedrooms have a floor area of 892 sq. ft each. The number of occupants in the suites varies from two to six. Table 2.1 shows occupant density, type and bedrooms use in the respective Suites.

Table 2.1 Tested Suites' occupant density, type and bedroom use.

Suites	Floor Area (square feet)	Number of Occupants	Number of Bedrooms (Number of Occupants)		
A	892	3 (1 adult, 2 children)	Master bedroom (1 or 2)	Bedroom #2 (1 or 2)	Bedroom #3 (Storage)
B	643	4 (2 adults and 2 children)	Master bedroom (3)	Bedroom #2 (1)	
C	892	6	Master BR (2)	Bedroom #2 (2)	Bedroom #3

		(2 adults and 4 children)			(2)
		2	Master BR	Bedroom #2	
D	654	(1 adults and 1 child)	(1)	(1)	

Mechanical ventilation is provided using the Bathroom exhaust fans (Panasonic FV-1VQ3), which have manufacturer rating of 110 CFM and actual measured ventilation rate capacity of 50 to 70 CFM and sonic level of 0.8 Sone. The operations of the fans are automatically controlled with pre-set ventilation time schedule: eight hours a day, 4 hours in the morning (7 to 11 am) and another 4 hours in the evening (6 to 10 pm). The same time-controlled ventilation strategy is implemented in all Suites to synchronize the fans operations and avoid intra Suite airflow. Suites are heated by electric baseboard heater while the corridors are heated by forced air heating system.

The project was financially supported by the British Columbia Housing Corporation (BC Housing), Affordable Housing Societies and the School of Construction and the Environment of the British Columbia Institute of Technology.

2.4 Denmark [DTU] – Indoor Environment and Children's Health (IECH)

During the late winter and spring of 2008 an investigation (Indoor Environment and Children's Health (IECH)) of the indoor environments in 500 family homes was undertaken on the island of Funen in Denmark. The primary focus of the investigation was to supply data to help test the hypothesis that there is a relation between the indoor environment in which young children grow up and the diseases they experience; the main focus was on allergies and asthma. The data was collected from children's bedrooms over the course of 2-4 days (with an average of 2.5 days).

The form of the collected data allows for uses other than epidemiological. From the data it has been possible to obtain information on means, standard deviations and confidence intervals for temperatures, relative humidities, moisture productions and air change rates in family homes, using children's bedrooms as proxies for family homes. For the Annex, the data is divided in two groups: Single and multi-family homes. Of the 500 family homes 440 are single and 60 are multi-family homes.

2.5 Estonia [TTU] – Technical condition and indoor climate of Estonian apartment buildings

The research has been conducted as a result of the project "Reducing the environmental impact of buildings through improvements of energy performance, *3.2.0801.11-0035"* (financed by *European Union through the EuropeanRegional Development Fund and* SA Archimedes) and project "Nearly-zero energy solutions and their implementation on deep renovation of buildings, IUT1−15" (financed by *Estonian Ministry of Education and Research*). The study utilizes the measuring data of the following national research projects financed by KredEx, by the Ministry of Economic Affairs and Communications, and Tallinn University of Technology:

- On brick apartment buildings built between 1955 and 1990: "Technical condition and service life of Estonian brick apartment buildings" (2008-2010);
- On wooden apartment buildings built between 1880-1940: "Technical condition and service life of Estonian wooden apartment buildings" (2009-2011).

The purposes of the study were:

- Indoor climate and technical survey of apartment buildings with different ages;
- To analyse the collected data and to assess the current condition, need for improvement and future perspectives;
- To systematize collected data for future analysis and for working out solutions for determined problems.

The study consisted following parts:

- Determination of studied apartment buildings based on building typology and age distribution of buildings;
- Investigation of building structures (durability, service life);
- Building physical studies (hygrothermal performance of structures, hygrothermal loads, thermal bridges, thermal transmittance, airtightness of building envelope);
- Indoor climate studies (thermal comfort, indoor air quality);
- Survey of building service systems (ventilation, heating, water supply, sewerage, electricity);
- Questioning of inhabitants of studied buildings.

2.5.1.1 Measurement methods

Technical survey was done for whole building. Building physical and indoor climate studies were done in 1 to 3 apartments in each building.

All together 48 apartments in 30 brick apartment buildings and in 41 apartments in 29 wooden apartment buildings were investigated.

The values of temperature (*t*) and relative humidity (*RH*) were measured with data loggers at one–hour intervals, mainly from master bedrooms. The information about air change in bedrooms was determined based on measurement of the dynamics and level of CO_2 produces from occupants.

For estimation of air change rate in bedrooms was determined based on measurement of the dynamics and level of CO_2 produces from occupants at 10 min. intervals during 2-3 week period during winter and summer period.

The air tightness of building fabric was measured with the standardized

[1] fan pressurization method, using "Minneapolis Blower Door Model 4" equipment with an automated performance testing system (flow range at 50 Pa 25 m^3/h – 7.800 m^3/h, accuracy ±3 %). To determine the air tightness of the building envelope, depressurizing and pressurizing tests were conducted. All the exterior openings: windows and doors were closed; ventilation ducts and chimneys were sealed. To compare different buildings, the air flow rate at the pressure difference 50 Pa was divided by the external envelope area (resulting air leakage rate at 50 Pa) or by the internal volume of the building (result air change rate at 50 Pa, n_{50} value).

To determine typical air leakage places and their distribution, an infrared image camera FLIR Systems E320 (accuracy ±2 % or ±2 °C , measurement range; -20 to 500 °C) and a smoke detector were used. All the thermography tests were made later during the winter period. The difference between the indoor and the outdoor air temperature was at least 20 °C . Thermography investigations were done twice. First, to determine the normal situation, the surface temperature measurements were performed without any additional pressure difference. Next, to determine the main air leakage places, the 50 Pa negative pressure under the envelope was set with fan pressurization equipment. After the infiltration airflow had cooled the inner surface (~30 to 45 min) of the envelope, the surface temperatures were measured with the infrared image camera from the inside of the building.

Based on measurements of indoor CO_2 levels in bedrooms and estimated CO_2 (as tracer gas) emissions from residences during the night (≈20:00h to 8:00h), the air change in bedrooms was estimated:

$$C = C_v + \frac{m}{\dot{V}} - (C_v + \frac{m}{\dot{V}} - C_0) \cdot (e^{-\dot{V}\tau}) \qquad (2.1)$$

Where: m is CO_2 production, g/h; $\dot{V}$ is air flow rate, l/h; C_v is CO_2 of outdoor air, g/m^3; C is CO_2 concentration indoors after measurements, g/m^3; C_0 is CO_2 concentration indoors before measurements, g/m^3; τ is time, h.

The actual use of energy was determined for the building as a whole and differences between apartments were not determined. Analysis includes measurements of electricity, gas, water, hot water, and heating (space heating and heating of ventilation air) over a 3-year period: 2006–2009 in brick apartment buildings and 2007–2010 in wooden apartment buildings. As wooden apartment buildings were primarily heated by stoves, it was difficult to determine energy for space heating. For buildings, where all energy using components were available, the primary energy use in the building is calculated.

2.5.1.2 Studied buildings

Old wooden apartment buildings were built between 1880-1940. Apartments consisted of one, two or three rooms, with a separate kitchen, entry, and sanitary rooms. Apartments were heated with wooden stove (65 %; original heating system) or with radiators (23 %: water or 8 %: electricity) where the heat source was a gas boiler or district heating. Average living density was 26 m^2/person.

Old brick apartment buildings (Figure 2.2) were built between 1955 and 1990. Apartments consisted of one, two or three rooms, with a separate kitchen, entry, and sanitary rooms. Buildings were heated with district heating and one-pipe radiator heating systems. Typically, radiators were not equipped with special thermostats, therefore individual control of the room temperature was impossible. Room temperature for the whole building was controlled in heat substations depending on outdoor temperature.

Typically, the studied dwellings had natural passive stack ventilation. In some apartments kitchens were supplied with a hood. In all of the dwellings studied, windows could be opened for airing purposes. Most of the apartments studied were in private ownership.

Figure 2.2 Example of measured brick apartment buildings (left) and wooden apartment buildings (right).

In many cases buildings were insufficiently heated and ventilated. This resulted in bad indoor climate and high indoor humidity loads, but also provided low energy bills for inhabitants. Unfortunately many inhabitants are more concerned with low energy bills rather than high quality of indoor air.

Old brick apartment buildings were typically five to nine storey with cellar. The thickness of external walls was typically 42 to 51 cm, including ~5 to 6 cm thermal insulation (mineral wool $\lambda \approx 0.05$ W/(m·K). The thickness of the wall behind the batteries is thinner, see Figure 2.3. Internal surface of the wall is plastered as a rule. External surface can be plastered or not (brick surface). Window is tightened into wall with tow (not really airtight connection) and windows were designed to be leaky to guarantee the natural ventilation (Figure 2.4 and Figure 2.5).

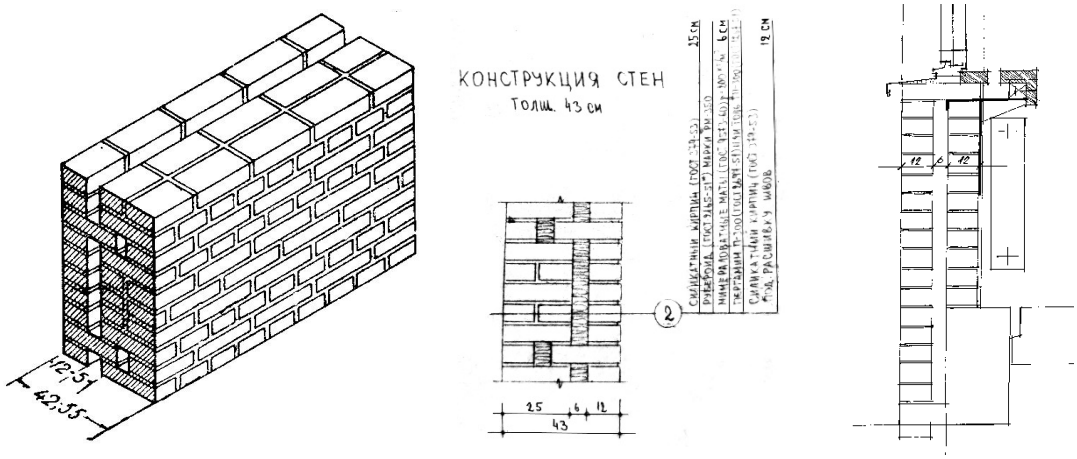

Figure 2.3 Sections of typical external walls of studied brick apartment buildings.

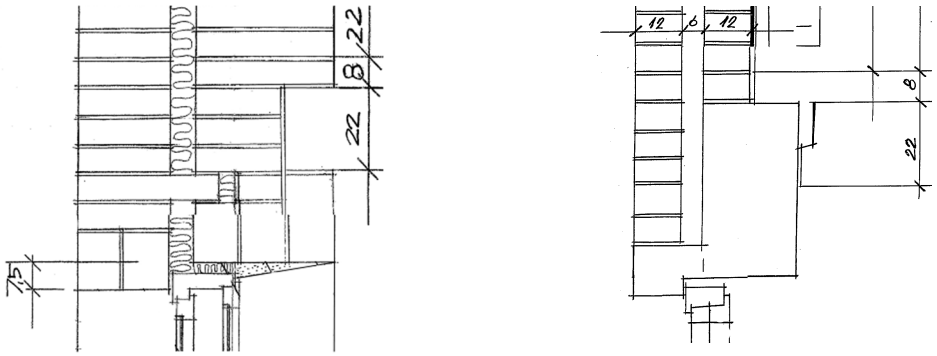

Figure 2.4 Connection of the external wall and window of studied brick apartment buildings.

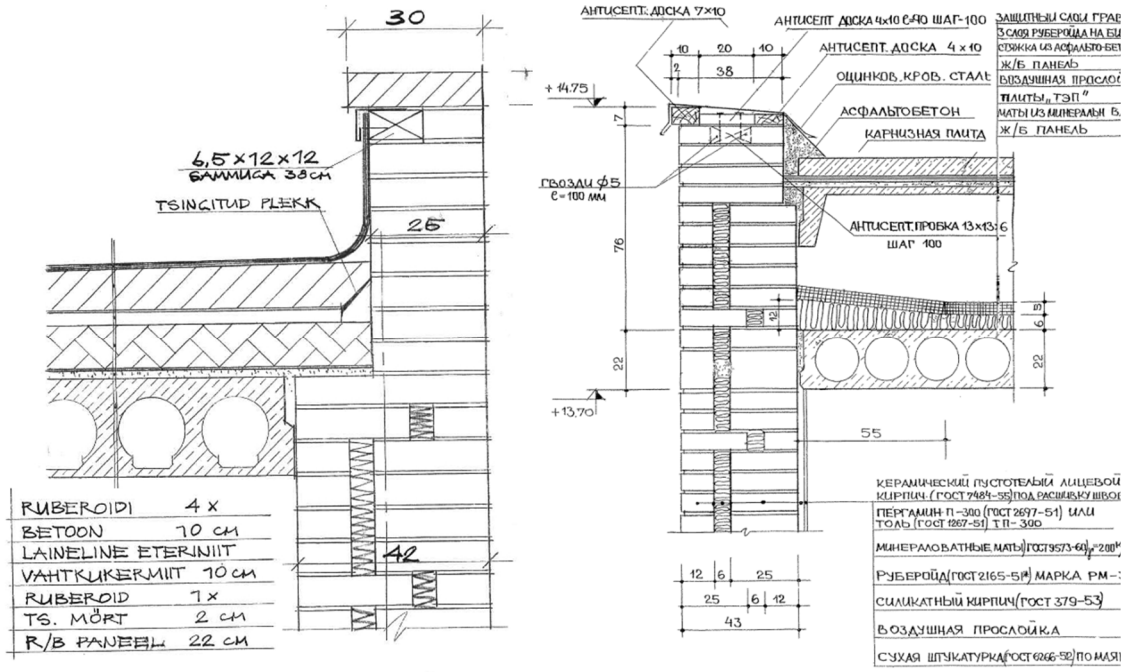

Figure 2.5 Connection of the external wall and roof of studied brick apartment buildings.

Old wooden apartment buildings were typically two and three storey buildings with cellar. External walls were built with log or as timber-frame structure, see. Internal surface of wall was plastered or covered with cardboard. External finishing of walls was wooden panelling or plaster (Figure 2.7).

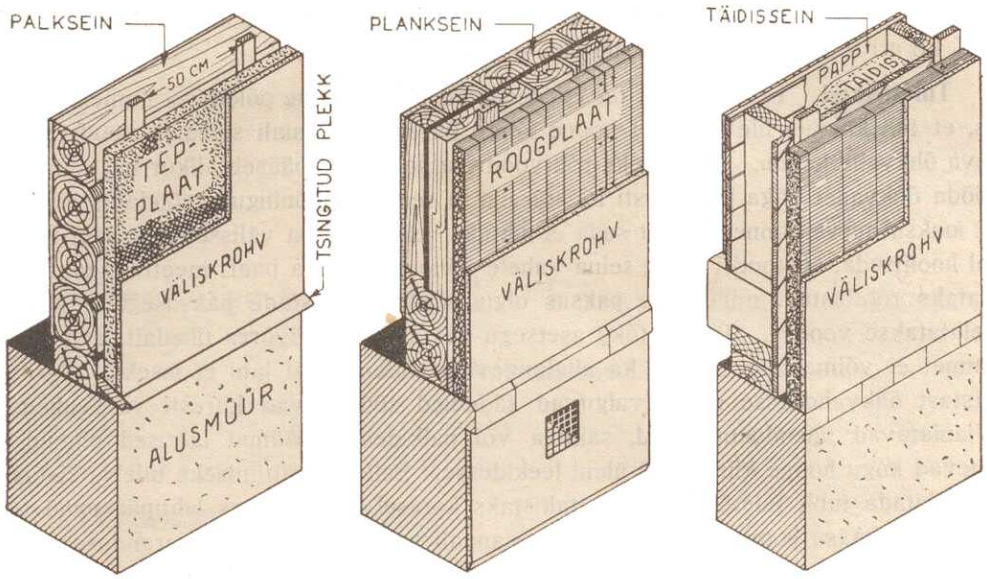

Figure 2.6 Sections of typical external walls of studied wooden apartment buildings.

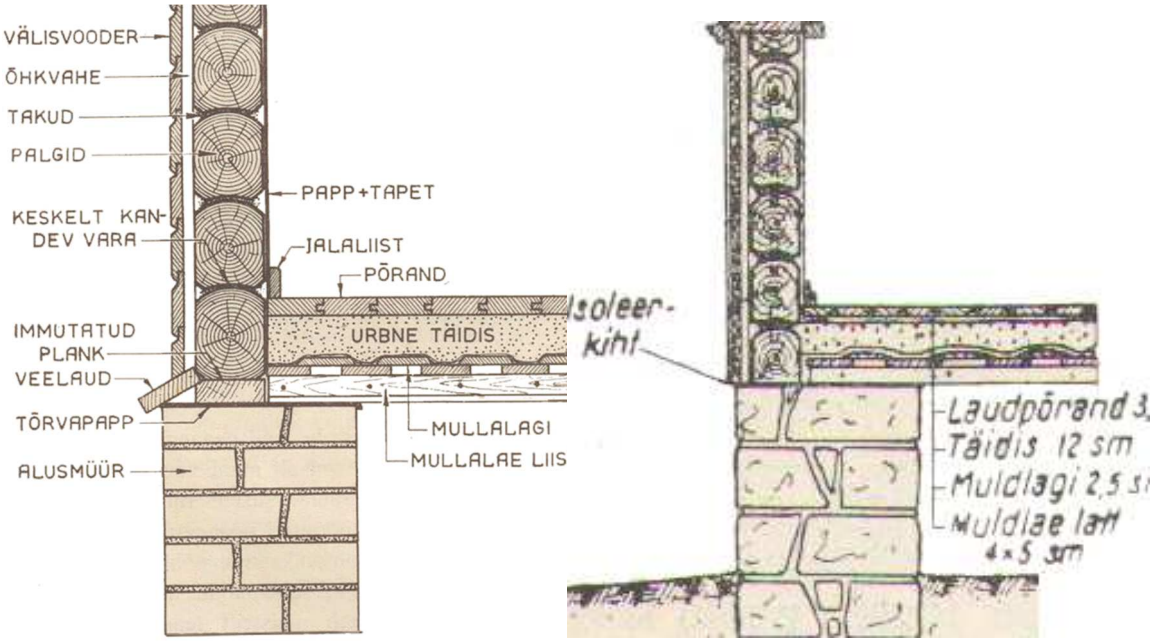

Figure 2.7 Connection of the external wall, foundation and base floor of studied wooden apartment buildings.

2.6 Finland [TUT]

2.6.1 Timber-framed detached houses

Tampere University of Technology (Laboratory of Structural Engineering) and Helsinki University of Technology (Laboratory of Heating Ventilating and Air-Conditioning) studied with field surveys the indoor climate, ventilation and air tightness of Finnish timber-framed single family houses [4]. The research included 100 timber-framed houses that were moderately new. The houses differed from each other by structure, ventilation type, age and construction method. The measurements were done during 2002-2004.

The 100 timber-framed houses under investigation represent the typical Finnish construction practice. Figure 2.8 gives an example of a typical measured house. The average volume of the houses is 405 m^3, floor area 160 m^2 and façade area 405 m^2. It should be noted that the whole group of timber-framed houses is not a random sample because the purpose was to gather proper subgroups of different types of houses.

Figure 2.8 Typical timber-framed house and an example of the outer wall structure.

2.6.2 Heavyweight detached houses

Tampere University of Technology (Department of Civil Engineering/Structural Engineering) and Helsinki University of Technology (Department of Heating Ventilating and Air-Conditioning) studied with field surveys the indoor climate, ventilation and air tightness of Finnish heavyweight detached houses [5]. The research included 50 detached heavyweight concrete and masonry houses (10 autoclaved aerated concrete, 10 lightweight aggregate concrete, 10 brick, (5 calcium silicate brick and 5 burnt clay brick), 10 shuttering concrete block and 10 concrete element houses) and 20 log houses. The measurements were done during 2005-2008.

The 70 concrete, masonry and log houses represent the typical Finnish one-family houses built with heavyweight structures. The average volume of this set of houses is 534 m^3, floor area 195 m^2 and façade area 472 m^2. Figure 2.9 gives an example of a heavyweight building and a brick wall. The purpose of the selection of houses was that the subgroups would represent different heavyweight structure types (AAC, LWAC, brick, concrete block and concrete element).

Figure 2.9 Typical heavyweight detached house and an example of the outer wall structure.

2.6.3 Individual air tightness measurements in apartment buildings

During the years 2009-2012 the air tightness of 25 apartment buildings was measured. The measurements were done for the whole building or at least for one whole stair case. All of the buildings have similar concrete element structures. The average volume of the measured buildings was 6560 m^3, floor area 2440 m^2 and façade area 2370 m^2. Examples of the apartment building and the outer wall structure are shown in Figure 2.10.

Figure 2.10 Typical apartment building and the outer wall structure.

2.7 Germany

2.7.1 Introduction measured Houses (IBP)

Within the framework of several research projects in order to analyse energy consumption of German residential buildings, the Fraunhofer-Institute for Building Physics has carried out many measurements on different locations including manual window opening. In total 114 units have been investigated in different measuring timespans lasting from one to four years.

In order to create energy balances for each hour, measurements of energy consumption for space heating, DHW and power consumption of home devices, HVAC system and photovoltaic have been taken. Together with characteristic values of the building like U-value of the envelope or air tightness (n_{50}) and the outdoor climate conditions, the heat flow was determined.

Most of the research projects have been carried out in Germany (see Figure 2.11) hence the presented data is only representative for Middle European climates. Nevertheless, some general statements can be deduced such as dependencies of window openings and outdoor temperature.

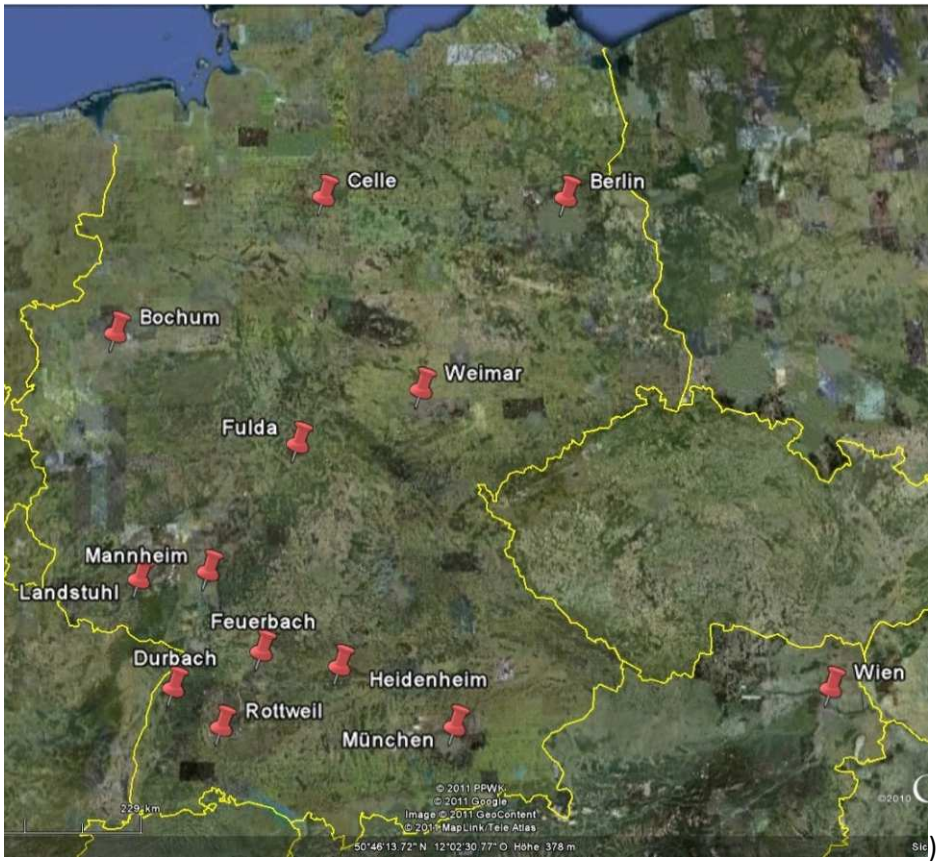

Figure 2.11 Location of the Projects- Google Earth®.

The majority of the buildings do have relatively well constructed and isolated envelopes and proper HVAC systems which comes close to the passive house standard (some are passive

houses). This has to be considered, as it is not representative of the current building stock in Germany. The year of construction for the buildings is between 1970 and 2000. Some building examples are shown in

Figure 2.12, Figure 2.13, Figure 2.14 and Figure 2.15.

Figure 2.12 Celle - 3-LitreBuilding.

Figure 2.13 Durbach - Project Weber 2001.

Figure 2.14 Stuttgart Feuerbach - Passive House Estate.

Figure 2.15 Fulda - Hybrid HVAC Building.

2.7.1.1 Description of the data

Two types of data are collected: data collected before the actual continuous data recording and the measured data in hourly values over a certain timespan.

Data recorded before the continuous measuring are considered to be constant during the measurement. Those values include an air tightness test at 50 Pa (blower door test), localization of thermal bridges via thermographic inspection and additional parameters regarding the building, HVAC system and boundary conditions.

The following list provides an overview of the constant measurements:

- Building: type, treated floor area, HVAC system, site situation, location;
- Apartment: number of occupants, room types, volume;
- Envelope: air tightness, U-values, SHGC;
- Weather station: site situation, location.

The continuous data is measured by sensors in different time intervals (60min, 10min, 1min). However, if the data is not hourly measured it is converted to hourly values by their mean. Thereby, each monitoring point (e.g. between 18:01h and 19:00h) gets aggregated to one value for each hour of the day (e.g. 19:00h). It consequently reduces the amount of data in the database, but also implicates certain loss of measured information.

The following data is measured during the monitored period, however not every parameter is available and analysed for each building:

- Temperature: indoor air, surface, DHW, exhaust air;
- Humidity: rel. humidity indoor, surface, exhaust air;
- Energy / Electricity: home devices, HVAC, photovoltaic, total;
- Window opening in seconds per hour (max. 3600 sec/hr);
- Outdoor climate: solar, temperature, rel. humidity. The outdoor climate is measured one meter above the highest point of the building for each location.

For the window openings it should be pointed out that the sensor only measured the status of the window, which could be open or closed. So it doesn't distinguish between tilting or complete opening and it does not monitor the opening angle.

Unfortunately, the recording of the occupancy has not been realised, which would have been of much interest.

2.7.1.2 Database, Data Format

Initially, the whole data has been recorded and saved in Excel format for each project, while one sheet lists the hourly values of the measured data and the other ones contain the static data. Compiling all projects would result in an enormous amount of data which is not suitable for Excel. Therefore a central MS SQL Server database has been set up, which stores all information given in the Excel files.

This opens more possibilities for analysing the data, as several projects can be cross-linked and compiled by external tools via SQL queries. The database is structured in tables which contain the static data of the projects and tables which list the monitored data. Basically each sensor has its own table in the database. The static tables are linked via Primary Key and Foreign Key, however, this is not the case for the sensor data tables.

The advantage is a significant faster SQL query and much less redundant data, but makes the query much more difficult to construct. The database structure is shown in Figure 2.16.

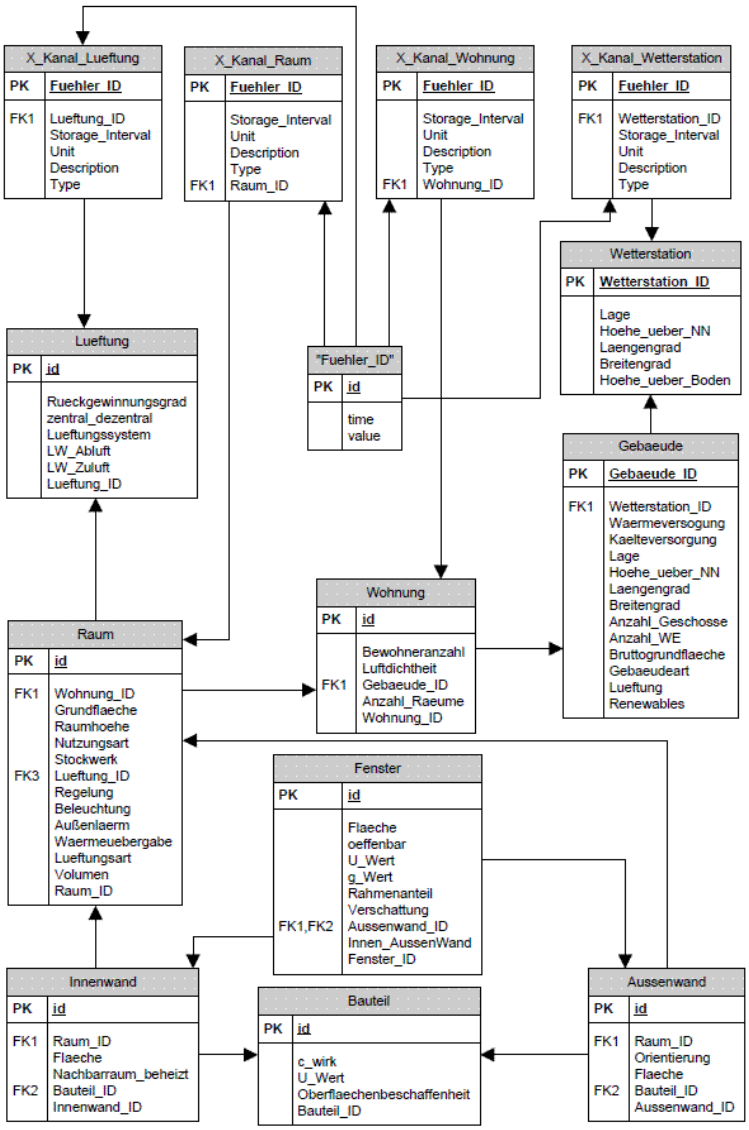

Figure 2.16 Database Layout.

The sensor tables consist of columns for the ID, measured data and a time stamp in hourly values. There has been no plausibility check when entering the data in the database (eg. Relative humidity > 100 %), hence the raw data does contain errors caused by failures of the sensors or other circumstances.

Those incorrect values are filtered during the SQL query before further analysis:

- Temperature: -30 °C to 50 °C;
- Relative Humidty: 0 % to 100 %;
- Electricity: 0 kWh to 10 kWh;
- Window opening: 0 sec/hr to 3600 sec/hr.

The analysis itself has been accomplished with R, a free software environment for statistical computing and graphics. R can be enhanced by packages, which enable SQL queries. As R being designed to handle large amount of data, it makes it the ideal tool for the analysis.

2.7.2 Experimental assessment of material properties [TUD]

The TUD dedicates to make a wide material data collection that resulted from more than 15 year's laboratory assessment of material properties. The evaluated materials have a broad variability, covering both historical and new-developed building materials on market. Standard measurement procedures include:

Table 2.2 Experimental measurements and corresponding standards.

Measurement	Standard
Bulk density, matrix density and porosity	DIN ISO 11272 (2001) [6]
Thermal conductivity	ASTM C177 (2010) [7], ASTM C518 (2010) [8] and DIN EN 12664 (2001) [9]
Specific heat capacity	ASTM E1269 (2011) [10]
Hygric sorption isotherm	ASTM C1498 (2004) [11] and DIN EN ISO 12571 (2000) [12]
Water retention	ASTM C1699 (2009) [13]
Water vapor transmission	ASTM E96 /E96M (2010) [14] and DIN EN ISO 12572 (2001) [15]
Water absorption coefficient	DIN EN ISO 15148 (2003) [16]

Moreover, a set of experiments to access the moisture transport knowledge in the porous material are executed, e.g., drying test, head permeameter and tension infliltrometer [17]; [18]. Those measurements together with the standard procedures deliver enough information for material characterization. So far, more than 200 high-quality material data from different material categories are ready for hygrothermal simulation.

2.7.2.1 Drying test

Drying process of a porous material gives insight into the moisture transport characteristics in the low moisture content range. A drying apparatus is presented inFigure 2.17. Prior to the test, the effectively saturated specimen is sealed on the lateral and bottom sides, allowing only the top side exposing to the specific environment. During the test, the specimen is periodically weighed to get the information of water mass loss and the corresponding time. The drying process is strongly influenced by the climatic conditions and boundary conditions, as well as the material properties of specimen itself. Therefore, the detailed information regarding to those conditions should be recorded.

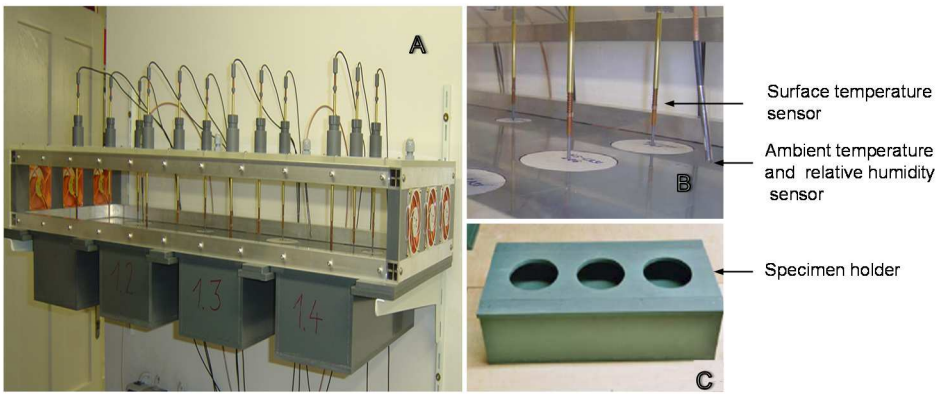

Figure 2.17 Automated drying apparatus (A); Temperature and relative humidity sensors (B); Specimen holder (C).

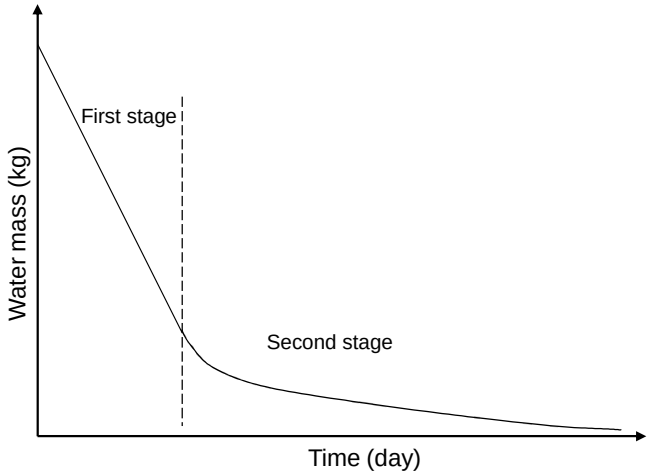

Figure 2.18 Schematic drawing of the drying process.

Drying process is comprised of two stages, as shown in Figure 2.18. The first stage, beginning at high moisture content, is characterized by a linear water mass loss over time and mainly impacted by the boundary conditions, i.e., air flow rate above the evaporation surface. In this stage, the specimen is able to deliver stored liquid water to the evaporation surface. The surface temperature will decrease due to the water evaporation. In the second stage, the drying rate becomes slow and moisture transport is dominated by the water vapor flow within the material. This process is mainly governed by material properties of the specimen itself. Therefore, the dry process presents a transition of moisture transport from liquid water to water vapor transport. This transition can be detected when surface temperature of the specimen increases or linear mass decrease over time is no longer maintained.

The measured drying curves of various building materials are shown in Figure 2.19 [18]. The values are normalized to remove the difference in the initial moisture content and the geometry of the specimen for easy comparison. The environmental conditions and boundary conditions mainly determine the length of the first drying stage, whereas the liquid water conductivity in the low moisture content range primarily affects the second drying stage. The plaster has a low liquid conductivity in this range, so it owns a longer second drying stage. Calcium silicate has a

relatively higher liquid conductivity, so it undergoes a fast second drying stage. For spruce, the liquid water transport in longitudinal direction is much faster than that in radial direction.

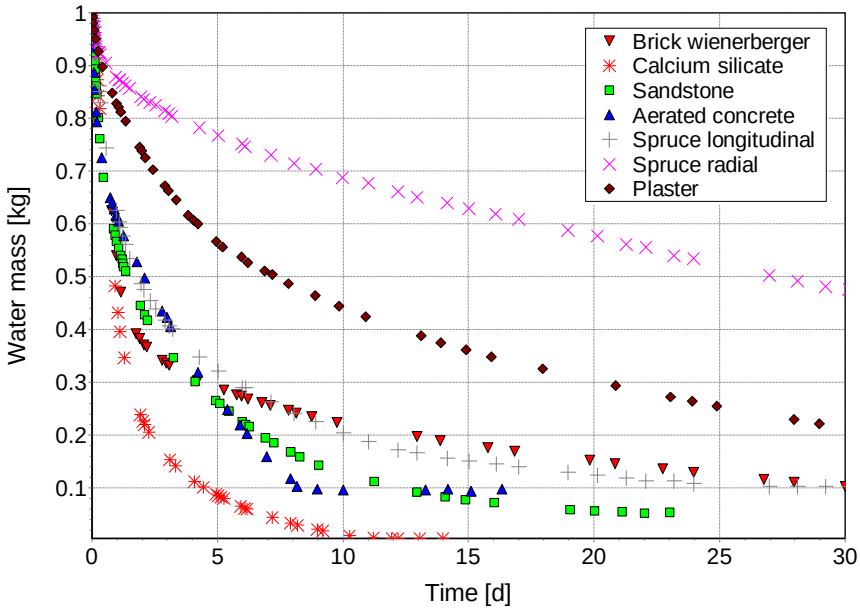

Figure 2.19 Drying behaviours of various building materials.

2.7.2.2 Unsaturated liquid conductivity, Kl

The unsaturated liquid conductivity measures the ability of liquid water transport through a porous material near the saturation moisture content region. The unsaturated liquid conductivity can be obtained by using a tension infiltrometer, which is composed of a water-filled tube and a porous ceramic plate connected by a vacuum pump as shown in Figure 2.20.

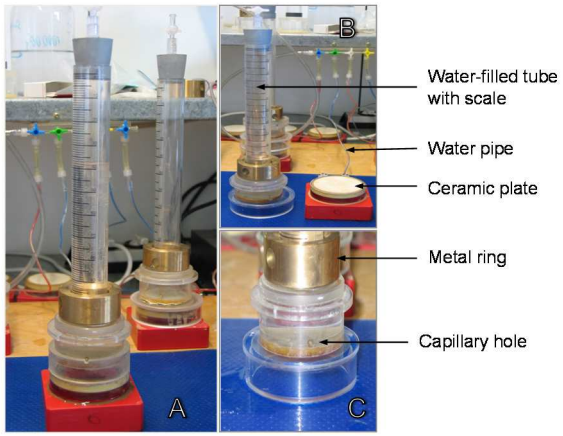

Figure 2.20 Tension infiltrometer apparatus (A); water filled tube and ceramic plate (B); Capillary hole on the lateral –bottom side of the tube (C).

The water-filled tube with a small-diameter capillary at the lateral-bottom side provides a threshold pressure on the top of the specimen. The constant suction pressure is kept up by inducing the air bubble through the capillary into the water-filled tube if the pressure falls below the desired threshold pressure. Before measurement, the moistened specimen is attached on the ceramic plate by the kaolin paste to enhance their contact. The heavy metal ring is used to

tighten the contact between the specimen and water-fill tube by its gravity. If the applied suction pressure on the bottom side of the ceramic plate exceeds the threshold pressure, then the pressure gradient will force the liquid water flowing through the specimen to form a steady state flux rate. The different degrees of moisture saturation are achieved by adjusting the suction pressures.

The liquid water conductivity at certain degree of moisture saturation is calculated by:

$$K_l = \frac{\Delta V}{t} \cdot \frac{d}{A \cdot \Delta p \cdot g}, \tag{2.2}$$

where Δ*V i*s the volume of liquid water flowing through the material (m^3), *t* is the time during the measurement (*s*), *d* is the thickness of the specimen (*m*), *A* is the cross-sectional area of the specimen (m^2), Δ*p* is the pressure difference between two sides of the specimen (*pa*), and *g* is the gravity acceleration (m/s^2).

The unsaturated liquid water conductivities of various building materials at certain degree of saturation are listed in Table 2.3 [18].

Table 2.3 Unsaturated liquid water conductivities of various building materials at certain degree of saturation.

Material	Moisture content [m^3/m^3]	Mean suction pressure [Pa]	Liquid conductivity [s]
Brick Wienerberger	0.304	8650	2.0e-09
Sandstone Hildesheim	0.21	395	1.8e-07
Calcium silicate	0.87	1441	8.5e-09
Lime plaster	0.22	710	6.8 e-09
Mortar	0.39	4466	1.1 e-09
Aerated concrete	0.18	2205	9.3 e-12
Spruce longitudinal	0.69	1473	2.7e-09
Spruce radial	0.32	1453	2.7 e-09
Gypsum board	0.42	870	2.7e-10

2.7.2.3 Saturated liquid conductivity, K_{eff}

The saturated liquid conductivity can be measured by a head permeameter apparatus as shown in Figure 2.21.

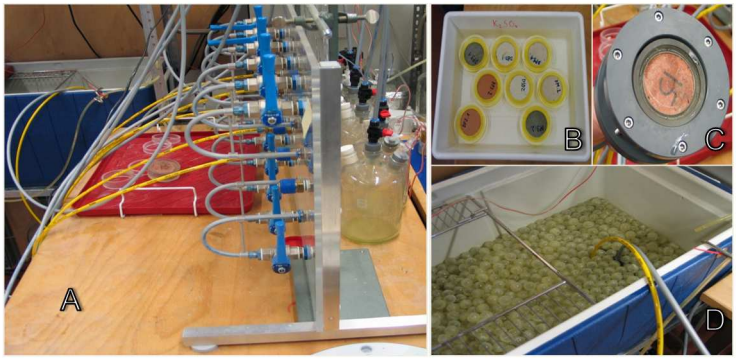

Figure 2.21 Head permeameter apparatus (A); laterally sealed specimens (B): head permeameter with specimen (C); water container (D).

It is composed of a head permeameter connected to a vacuum pump and a water container. The lateral sealed specimen is initially saturated and installed in the head permeameter, allowing one dimensional liquid water flow. The head permeameter with the specimen is then put into the water container with controlled temperature. With the application of suction pressure via the vacuum pump from one side of specimen, the liquid water will flush the specimen and flow into a glass flask through a capillary tube. The steady liquid flow rate can be calculated by measuring the increasing weight in the glass flask in the defined time intervals. By converting mass flow rate to volumetric flow rate, the saturated liquid conductivity can be determined by the equation 2.2.

2.8 The Netherlands [TUE] – Uncertainties in weather data caused by the urban heat island

Howard reported in 1818 that the temperature of the city of London was not to be considered as that of the rural climate [19], [20]. The causes of this phenomenon, later called the urban heat island (UHI), were reported by e.g. [21], [22], [23], [24] who indicated that the UHI is a result of: low-albedo, air pollution, reduction of the sky view factor, anthropogenic heat, heat storage, decrease in evaporation and a reduction of wind speed. Nowadays the existence urban heat island is a well-established and well documented phenomenon e.g. [25], [26], [27], [28], [29]. Studies on the impact of elevated temperatures reveal that increased temperatures result in increased human mortality [30], the latter being apparent in heat wave events [31], [32], [33]. Many of the additional deaths during a heat wave are likely to be caused by an enhanced UHI during the heat wave [34]. The effect of the UHI on building energy consumption has been described in several studies. Based on [35] and [36] it can be concluded that the UHI influences the energy demand significantly. [24] concluded that cooling loads could almost double, which was supported by [37] who stated that the cooling energy loads could increase by as much as 100 %. IPCC assessment report 4 reports that the UHI can affect comfort, health, labour productivity, leisure activities and climate control within buildings [38]. Recent studies have demonstrated several methods to account for the UHI in the weather data. These methods were divided in four categories by [39] and [40]. They consist of (1) Climatology models (e.g. [41], [29]) (2) Empirical models which use heat balance equations and empirically derived coefficients (e.g. [42], [43], [44], [45]) (3) Computational Fluid Dynamics models (e.g. [46]) and (4) Statistical regression methods (e.g. [47], [48], [49]), probability methods and artificial neural networks (e.g. [50], [39], [51], [52], [35]).

The latter predict the UHI intensity as a function of the main climatic parameters [25]. These models can potentially be used to account for the uncertainty in weather data caused by the UHI. Weather data might be generated by these UHI models and subsequently be used in Building Energy simulations. Section 3.5.1of this report provides an overview of the measured UHI intensity in the city of Rotterdam. In section 4.4 the measurements of Rotterdam are used to show the predictive capability of statistical methods for UHI intensity prediction.

2.9 Portugal [UP] – Social housing refurbishment in Porto

A large social housing retrofitting program was implemented in Porto, Portugal. The interventions included the upgrade of roofs, windows and ventilation systems. One of the renovated neighbourhoods was chosen as case study for this work. The neighbourhood has 4 detached buildings with similar typologies. The renovation work was performed in 2009 and 2010 by two different companies, based on the same design project for all buildings. The neighbourhood has a total of 179 dwellings, including the following typologies: 19 T1 (1 bedroom) dwellings, 31 T2, 72 T3, 56 T4 and 1 T5.

In the retrofit solution, the original natural ventilation system was improved by introducing continuous mechanical extraction in the kitchens, including a fan of variable flow. A mechanical fan was installed in the bathrooms, to be turned on when the facility is used. In the main rooms self-regulating air inlets were installed. The laundry had a fixed air inlet of 1x30cm^2. It must be stressed that the retrofitting process had several constraints, including a low budget and a very small allocation period of each dwelling tenants.

The sample included 25 measured dwellings. The dimensions of the types subject to test and the number and total area of windows is presented in Table 2.4.

Table 2.4 Dimensions of the Studied Dwellings.

Typology	Volume (m^3)	Net floor Area (m^2)	Exterior Walls Area (m^2)	Windows Area (m^2)
T1	100	40	44.3	9.4
T3	160	64	36.8	12.1
T4 – A	185	74	57.5	13.4
T4 – B	185	74	46.8	13.4

Additionally, a questionnaire was submitted to the users, collecting information for each of the days that measurements took place, including window opening action.

This work was funded by FEDER funds through the Programa Operacional Factores de Competitividade – COMPETE and by National Funds through the FCT – Fundação para a Ciência e a Tecnologia on the frame of the project FCOMP-01-0124-FEDER-041748 and EXPL/ECM-COM/1999/2013.

2.10 Sweden

2.10.1 Future climate scenarios for Sweden [CTH]

Division of Building Physics at Chalmers has collected a number of weather data parameters from different climate scenarios during a PhD project 'Sustainability of the Swedish built environment towards climate change. Hygrothermal effects and design criteria for buildings with respect to future climate scenario', performed by Vahid Nik during 2007 to 2012. The weather data have been received from a climate modelling research unit at SMHI - the Rossby Centre, and then processed to be applied in building physics applications. Examples of the data can be found in Figure 2.22 and Figure 2.23 below. More details about the data can be found in section 3.5.2.

Building Physics Chalmers offers to act as a partner and support the development of the climate data sets for research.

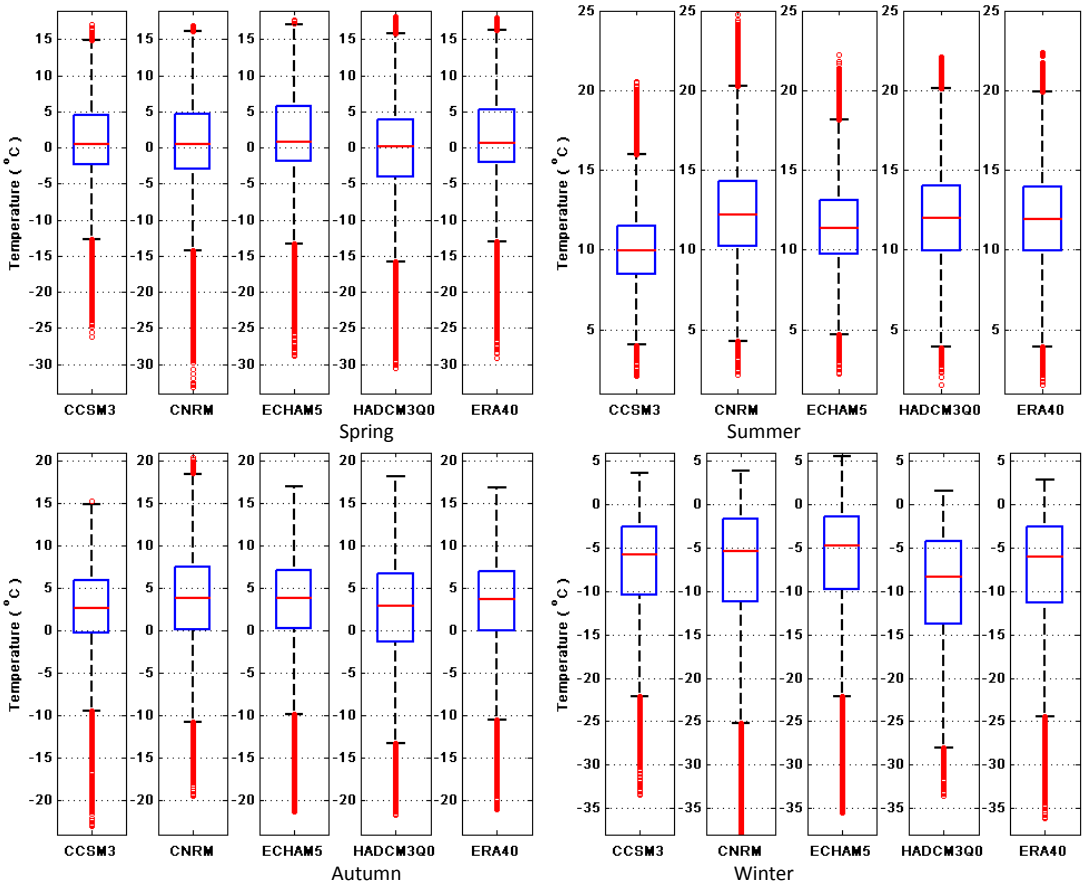

Figure 2.22 Outdoor temperature distribution in Stockholm for different global climate models (GCMs) during 1961-1990.

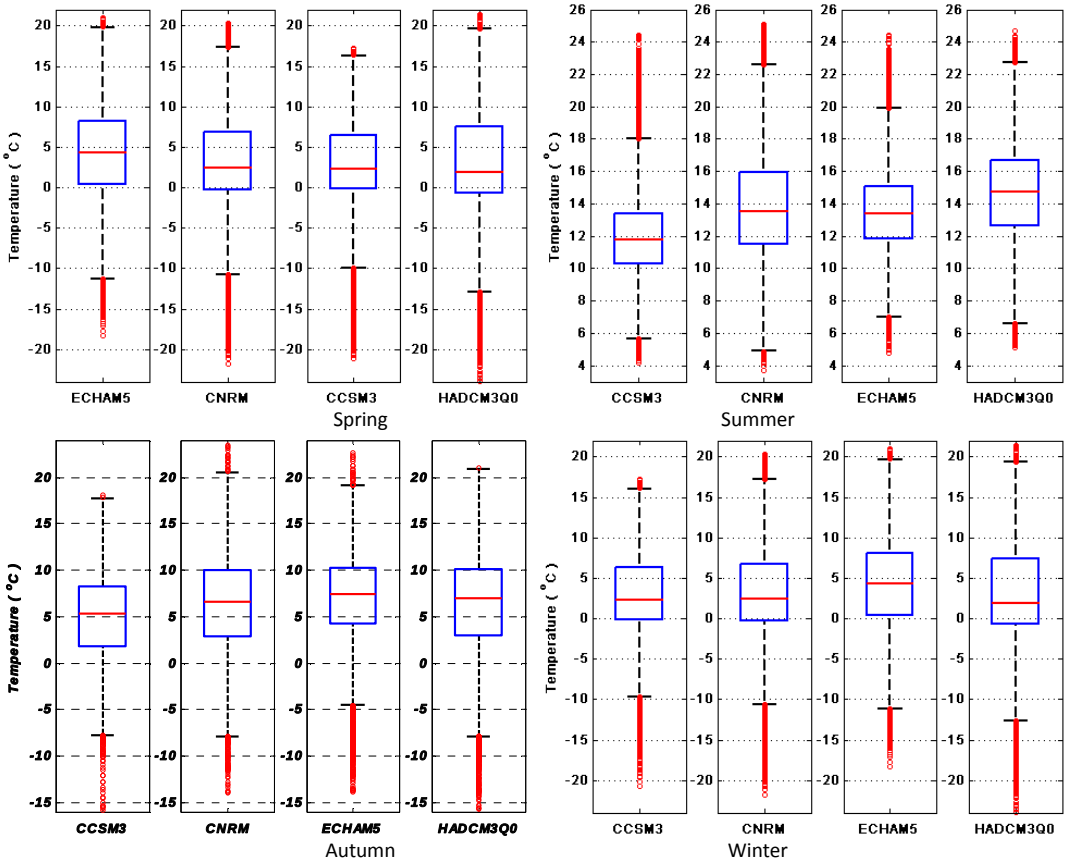

Figure 2.23 Outdoor temperature distribution in Stockholm for different GCMs during 2070-2100.

2.10.2 Source project for indoor moisture production simulation [CTH]

The variability of the indoor moisture production has been simulated in 10000 Swedish households by taking into consideration magnitudes of various moisture sources, type of families and their living styles. The result from the simulations is based on measurements, statistical data and qualified assumptions. An example of the results can be seen in Figure 2.24.

More details can be found in [53].

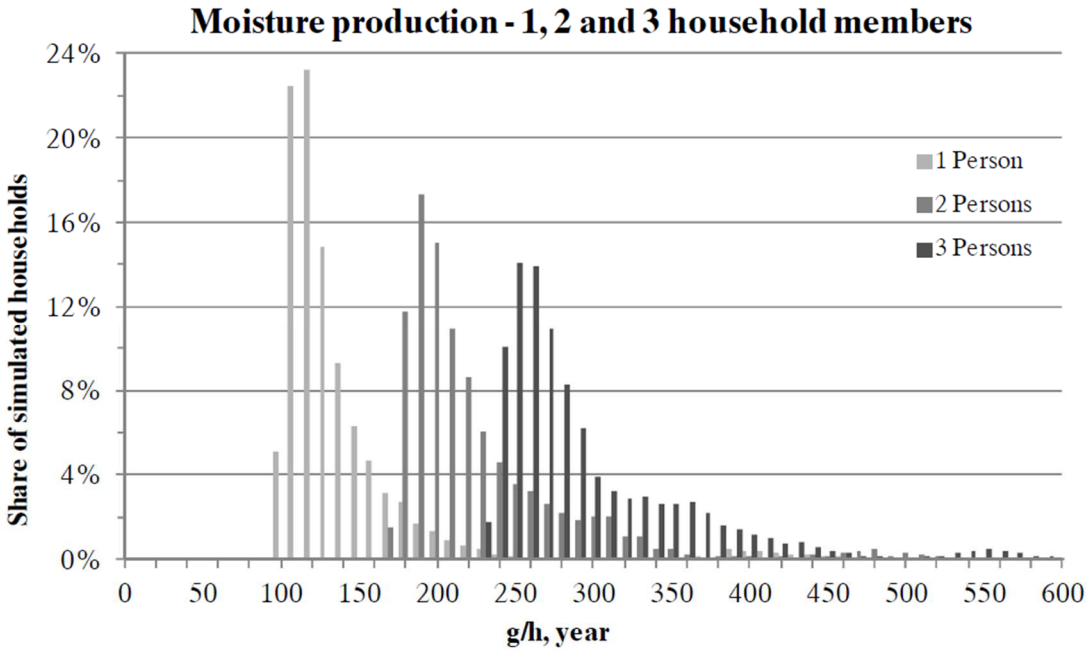

Figure 2.24 The histograms present the result from 10000 simulations of the moisture production rate in Swedish multi-family dwellings. The number of households is fixed on either one, two or three family members. The moisture production rate is presented as an annual average rate per hour.

2.10.3 Studied building – Case Sigtuna [LTH1]

Building Physics at Lund University has collected a lot of measurements from two apartments in a two-storey building close to Stockholm. More information about the buildings can be found in [54]. The studied building is part of a block of approximately 50 similar two-storey buildings built between the years 1972 and 1973, see Figure 2.25. The buildings have no basement and the upper floor apartments are accessed by external galleries. The ground slab should supposedly have been poured on loose filled expanded clay aggregate but samplings could not confirm this in all locations. There are two types of external walls in the buildings. Loadbearing walls that originally consisted of exterior masonry veneer (120 mm), airspace (30 mm), mineral wool (110 mm) and concrete (150 mm), see Figure 2.26 a). Curtain walls that were originally built up of masonry veneer (120 mm), airspace (30 mm), tempered hardboard, mineral wool and wooden studs(140 mm) and gypsum board with a plastic vapour retarding coating, Figure 2.26 b). District heating is being used for water and space heating, with hot water radiators typically placed below the windows.

Figure 2.25 Overview of the area with the studied building.

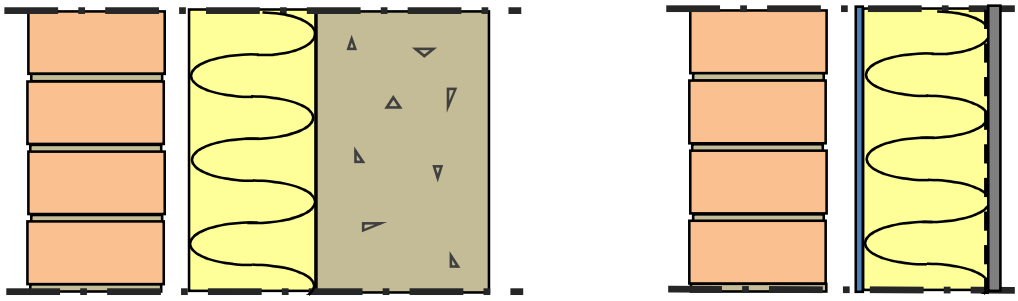

Figure 2.26 a) Original exterior load-bearing wall (North & South). b) Original curtain wall (East).

The building is situated at approximately 59° 38´ North and 17° 51´ East.

2.10.3.1 Objective of the retrofit

The goal of the municipal property owner was to reduce the total amount of bought energy (electricity and district heating) by 50 % and during the initial planning it was decided upon the listed improvements described in next subsection.With the energy use per square meter of heated floor area before improvements being approximately 177 kWh/m^2 per year, the energy use after improvements should be at the most 89 kWh/m^2 per year to be below 50 %, [55]. The Swedish governmental energy-demand at the time of the retrofit was 110 kWh/m^2 per year for new-builds in southern Sweden, excluding household electricity. To meet, for example conservational aspects retrofitted buildings can if necessary be allowed to use more energy. As a part of the planning the property owner employed consultants to evaluate the resulting effect of the retrofits on moisture levels in the construction. This evaluation, which included one-dimensional non-stationary moisture calculations and two-dimensional heat flow calculations, considered the measures later taken as sufficient.

2.10.3.2 Retrofit

The interior of the exterior walls of the house were retrofitted with 70 mm of mineral wool added between light-gauge steel studs and covered with polyethylene membrane and gypsum board. Existing gypsum board with a plastic coating on the old curtain walls was removed before adding the new layers, see Figure 2.29 and Figure 2.30. A thin and uneven layer of mineral wool in the attic is replaced with 400 mm of cellulose loose fill insulation. The ground-floor slab is

covered with a polyethylene membrane and 30 mm of polystyrene insulation below chipboard. The windows were upgraded with a new efficient inner pane and argon fill. The studied house has also been equipped with an air-to-air ventilation heat exchanger. As a part of the retrofit, kitchens and bathrooms were completely replaced and instrumentation allowing measurements of energy use (including domestic water, hot tap water and heating) were made in an effort to affect the behavior of the tenants, [55]. The choices concerning materials, design and execution of retrofit is entirely made by the property owner.

2.10.3.3 Method

Temperature and relative humidity in two apartments, outdoors and within the construction has been measured using silicon based relative humidity sensors.

Measurements were started during the construction phase in April 2009 and continued in full scale till June 2013 with the exception of a few shorter power outs. Measurements of temperature and relative humidity are taken every five minutes at 20 different places within the walls, rooms as well as on the exterior.

2.10.3.4 Measurement system

The measurement setup uses a serial interface based on the RS-485 standard. A distributed bus network (Figure 2.27) with small addressed control circuits connected by 4-core telephone cable manages one temperature and relative humidity sensor each. The network is controlled by a small PC-computer accessible by a high-speed wireless internet connection. The wired sensors, as opposed to wireless battery powered sensors, make it possible to use higher sample-rates during longer time periods and considerably reduce the size of the built-in equipment. In an effort to reduce possible interference from the size and heat produced by the control circuitry, the sensor was separated by a wire, see Figure 2.28.

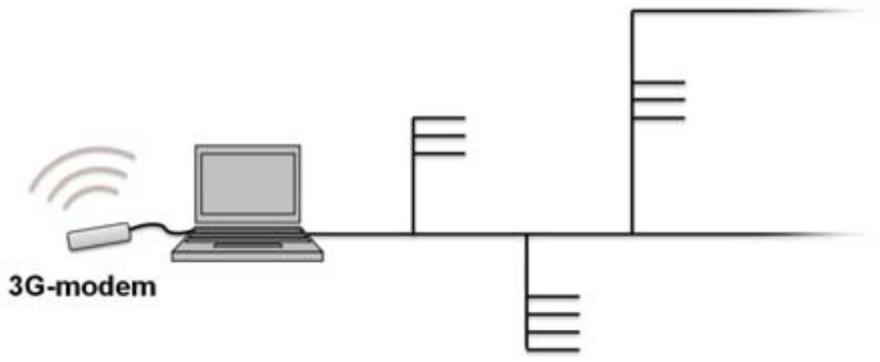

Figure 2.27 The distributed bus network simplifies installation and reduces the amount of cabling.

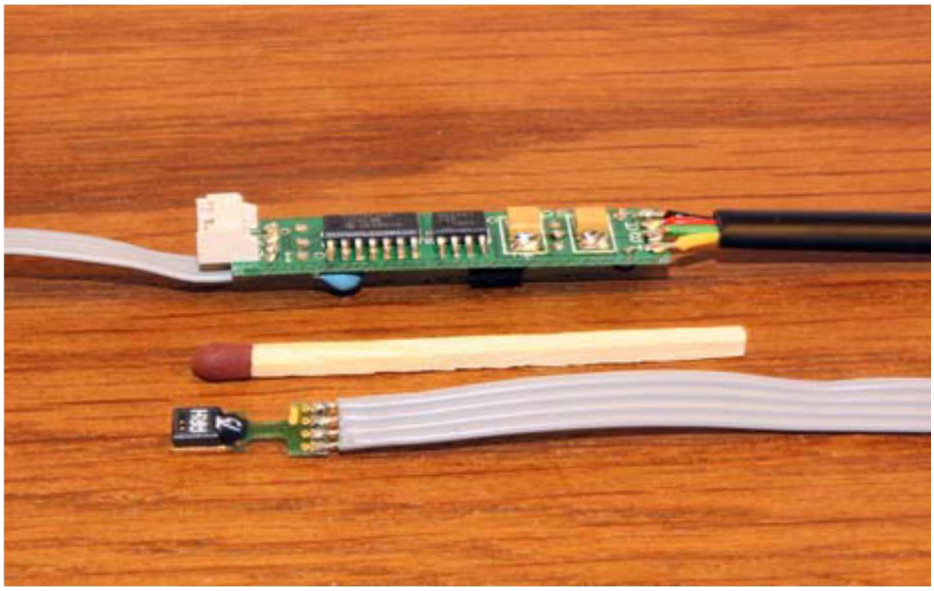

Figure 2.28 Sensor and control circuit separated by wire.

This is made possible without negative consequences due to the sensor's digital data output. With the small size and a power consumption of 5 µW during stand-by the influence of the sensor should be minimal as long as care is taken during placement and wiring.

2.10.3.5 Calibration

All of the sensors that are used in the project are calibrated in a certified precision humidity chamber at Lund University. The calibration was made at six different relative humidity levels and two different temperatures.

2.10.3.6 Placement of sensors

Sensors were placed in the ground slab, in the ground sill near external corners and at three separate locations in the different layers of the wall, see Figure 2.29, Figure 2.30 and Figure 2.31. These sensors were placed at different depth and centered between studs to make it possible to later on compare measurements with one-dimensional simulations. Additionally two sensors were placed outside facing north as well as three sensors within the two studied apartments that were placed approximately two meters above the floor on interior walls to represent the average indoor environment. Only results from the sensors placed in the two apartments and outdoors will be presented in this study.

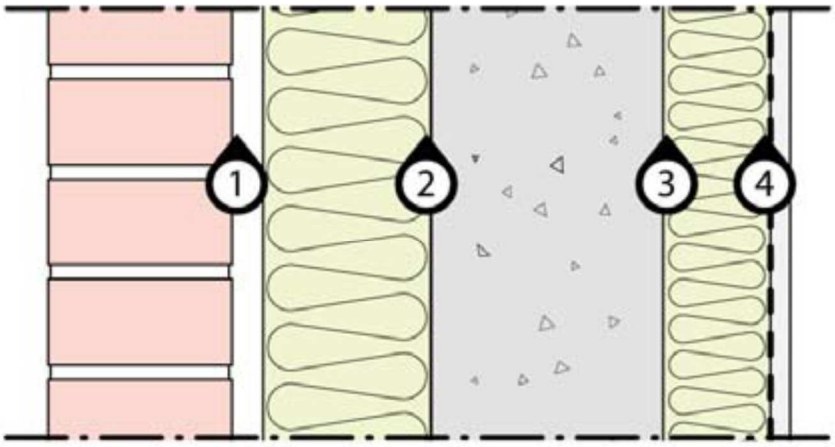

Figure 2.29 Exterior load-bearing wall (North and South) with new interior layer and sensor placements marked.

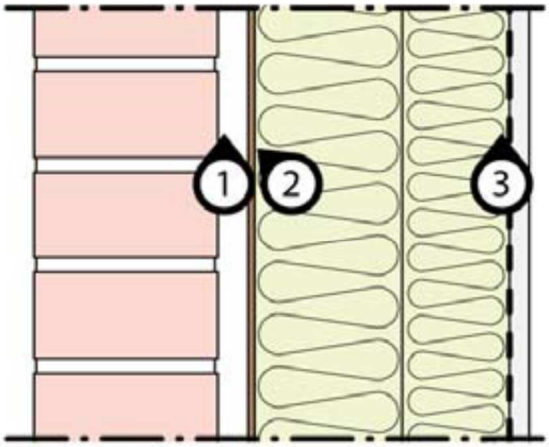

Figure 2.30 Curtain wall (East) with new interior layer and sensor placements marked.

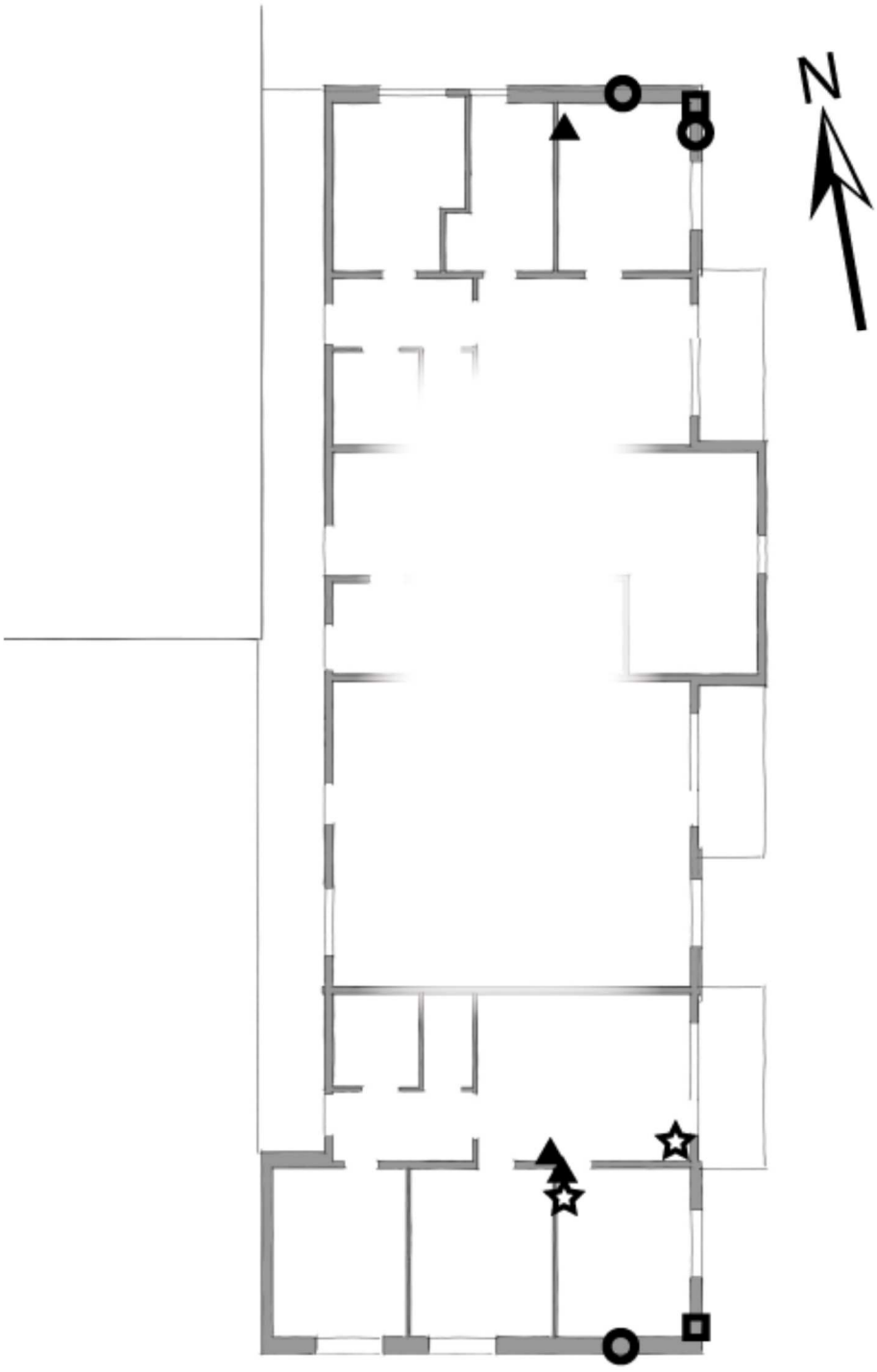

Figure 2.31 Placement of sensors in the building. A circle indicates sensors in a wall, square a sill and stars on the ground slab and triangle indoor sensors.

2.10.3.7 Findings during placement of sensors

To comply with new governmental demands concerning accessibility for wheelchairs it was necessary widening some of the doorways. The procedure used cooling water which was allowed flooding on the newly grinded concrete floor, leaving large areas damp and noticeably wet surfaces several hours after the procedure. At some point urea-formaldehyde foam has been injected into many of the wall airspaces of the building. The foam was previously unknown and probably injected during the late 1970s, only a few years after the buildings were completed.

2.10.4 Weather data for hygrothermal simulations [LTH2]

Climate data for 4 cities (Lund, Stockholm, Borlänge, Luleå) in Sweden are provided.

The data is adapted for the WUFI *.wac format and as Excel files and includes:

- Temperature (°C);
- Relative humidity (0 – 100 %);
- Global solar radiation on horizontal surface (W/m^2);
- Diffuse solar radiation on horizontal surface (W/m^2);
- Longwave (sky) radiation on horizontal surface (W/m^2);
- Precipitation (mm/h);
- Wind direction (0-360°);
- Wind speed (m/s).

The data is based on 9 consecutive years of measured data (90-98). When this raw data was analysed it was noted that:

- There were periods of completely missing data;
- The precipitation was measured on 12 or 24 hour basis;
- There were periods of missing long wave (sky) radiation data.

The relative humidity was clearly erroneous due to sensors being stuck in states where 95 % relative humidity was never reached or sudden leaps in sensor behaviour. (Perhaps due to adjustment or battery change.)

2.10.5 Airtightness measurements in renovated Swedish buildings [SP]

Airtightness measurements were performed in Swedish buildings in the following conditions:

- Measured values are for individual apartments
- In some cases measurements are reported before and after renovation but mostly before renovation
- No measures are taken to avoid air leakage to adjacent apartments during airtightness measurements
- The air leakage is given as air leakage rate (l/s liter per second), as air leakage rate per m^2 (that is envelope area facing the outside, not including envelope area facing adjacent

apartments, l/s m^2) and as air change rate at 50 Pa n_{50} (this rate is usually not reported in Sweden and in some cases the volume of the tested object have been approximated).

2.11 United Kingdom [UCL] – The Warm Front study

Warm Front was a government-funded energy efficiency initiative running between 2000-2013, targeted at providing grants for energy efficiency improvements to vulnerable households in England to tackle fuel poverty. Grants were provided for the installation of cavity wall insulation, loft insulation, draught proofing, and depending on the householder's qualification for the scheme, the option of gas wall convector heaters or a gas central heating system. The *Warm Front Study* (WFS) aimed to examine the effect of this major domestic energy efficiency refurbishment programme on winter internal temperatures [56], risk of mould growth [57], domestic space heating fuel consumption [58], thermal comfort [59], and the temperature 'take-back factor' [60]. This report summarizes the data collected and analysed in this series of papers and presents them in a format useful for stochastic analyses.

A sample of 3099 dwellings from five urban areas of England (Birmingham, Liverpool, Manchester, Newcastle, and Southampton) were surveyed, interviewed, and monitored over two successive winters (2001/2002 and 2002/2003) to reflect the effects of a wide range of environments and housing types. The dwellings (Figure 2.32) were a mixture of properties which had received Warm Front interventions mostly in the preceding six months and those due to receive interventions. 3489 sets of data were collected with 390 properties surveyed both pre-intervention in 2001/2002 and post-intervention in 2002/2003.

Figure 2.32 A selection of dwellings forming part of the Warm Front sample.

The main conclusions of this study were:

1. Air infiltration rate measurements demonstrated that Warm Front interventions designed to increase air-tightness may have little effect if a gas central heating system is additionally installed, particularly where the pipe work is laid under the suspended floor boards.
2. Warm Front interventions result in higher internal temperatures in the bedroom and living room (by about 2^{o}C). Installing a heating system and insulation simultaneously is most effective, followed by installing a heating system only, and then installing insulation only.
3. Cavity wall and loft insulation interventions were found to reduce the space heating fuel consumption by 10 % in centrally heated properties and 17 % in non-centrally heating properties. The introduction of a gas central heating system however had no significant impact in reducing fuel consumption.
4. The higher internal temperatures resulting from Warm Front interventions lead to lower relative humidities and therefore a lower incidence of mould.

3 INPUT DATA

3.1 Introduction

In this chapter input data is presented and divided into the categories described below. Different codes may require different sets of stochastic data, which means that these cannot be considered ready to use stochastic sets but rather a base for each practitioner to build his required set of input data.

Stochastic material data base: The source of uncertainty in the material data was addressed and uncertainty in different data levels was analysed.

Ventilation and airtightness: Analysis of n_{50} parameter in units with different characteristics (Blower door mechanism, CO_2 and tracer gas measurements were used).

Correlations between the air change rate and the values collected related to outdoor temperatures, moisture production, building age, window type, unit height, structural system, ventilation system, building size, number of occupants and window opening activity, were established.

Indoor loads: Indoor temperature and humidity distributions were recorded for different rooms at different times of the year. Also CO_2 concentrations were analyzed and correlated with relative humidity values presented by buildings with different construction materials.

Weather: The variability of diverse climates was recorded and correlated with pre-existing data, allowing for extrapolation.

Each subchapter is arranged so that each set of collected raw data is introduced. The analysis to derive statistical distributions that was performed on the raw data is explained and the final stochastic data sets are presented. The focus was put on ensuring that the connection to measured data wouldn't be lost.

3.2 Stochastic material data base: Germany [TUD]

3.2.1 Concept of building a stochastic material data base

Uncertainty in material properties may result from the material's natural inhomogeneity, the production and measurement, and modelling methodology concerning the functionalization of material data [18].

Material data can be presented in the following forms:

- A specific material is an individual material, usually associated with a specific producer. It has its particular name to differentiate from others. Its material properties are obtained by measuring representative samples of the production line;
- A generic material is a "derived" or "artificial" material from one material cluster. First, material cluster is identified from a collection of specific materials, according to the similarity between specific materials by comparing their differences. Then, synthetic process is applied to derive a generic material from each identified cluster. Generic material represents one type of specific materials which have similar characteristics.

The definitions of these terms can be exemplified as follows: historical "brick ZM" and "brick ZE" are specific materials. These two bricks have similar material properties and can be grouped into a brick cluster called "historical brick fabricated by the classic loam and clay", represented by one generic material named "historical building brick".

3.2.1.1 Uncertainty in specific material

Material properties include basic parameters and functionalized data. Figure 3.1 presents a template for characterization of specific material in a stochastic material data base. In the template, hygrothermal basic parameters contain general material properties, e.g., density and thermal conductivity obtained from standard measurement procedure. In additional, measured data related to moisture storage and moisture transport is used to further generate continuous functionalized data, e.g., moisture retention curve and liquid water conductivity function. The template accounts for uncertainty in material properties using the statistical data from experimental measurements: mean value, standard deviation, maximum, and minimum values calculated from several specimens. This approach is straightforward and considers the possible range of each property of a specific material. The limitation is that adequate specimens are required to get reliable statistical information, especially for the inhomogeneous materials.

Hygrothermal basic parameters

Parameter	Symbol	Unit	Mean	StdDev	Min	Max	Remarks
Bulk density	ρ	[kg/m³]	1786.2	9.3	1770.7	1805.2	
Specific heat capacity	c	[J/kgK]	889	10.8	872	901	
Thermal conductivity	λ_{dry}	[W/mK]	0.548	0.042	0.492	0.612	
Open Porosity	θ_{por}	[m³/m³]	0.354	0.003	0.347	0.359	
Capillary saturation	θ_{cap}	[m³/m³]	0.262	0.004	0.259	0.267	
Dry cup value	μ_{dry}	[---]	18.01	0.32	17.78	18.24	
Water absorption coefficient	A_w	[kg/m²s$^{0.5}$]	0.199	0.015	0.181	0.209	

Water Retention (Desorption)

Arguments		Mean	StdDev	Min	Max	Remarks
pc [hPa]	T [°C]	θ_l [m³/m³]				
0	20.0	0.319	0.005	0.308	0.323	
50	20.0	0.301	0.005	0.295	0.310	
100	22.3	0.299	0.005	0.294	0.308	
300	18.5	0.291	0.006	0.285	0.303	
600	14.0	0.275	0.007	0.269	0.287	
1000	21.8	0.265	0.007	0.258	0.278	
2000	23.5	0.209	0.013	0.187	0.228	
3000	22.0	0.172	0.013	0.148	0.196	
4000	22.7	0.143	0.011	0.123	0.160	
10000	22.9	0.103	0.009	0.086	0.113	
14000	20.5	0.075	0.009	0.060	0.088	

Sorption Isotherm (Desorption)

Arguments		Mean	StdDev	Min	Max	Remarks
φ [%]	T [°C]	θ_l [m³/m³]				
96.9	21.4	0.033	0.007	0.024	0.045	
96.0	22.4	0.026	0.006	0.018	0.035	
90.0	20.2	0.019	0.004	0.014	0.023	
84.3	22.9	0.016	0.003	0.013	0.019	
75.2	21.4	0.010	0.001	0.008	0.012	
57.6	22.4	0.006	0.000	0.005	0.007	
43.2	20.2	0.004	0.000	0.004	0.004	
32.8	22.2	0.002	0.001	0.000	0.003	

Water vapor permeability

Arguments		Mean	StdDev	Min	Max	Remarks
φ_{inside} [%]	$\varphi_{outside}$ [%]	μ [-]				
5.0	37.0	18.01	0.32	17.78	18.24	DryCup
84.0	53.0	12.04	2.18	10.50	13.58	Wetcup

Liquid water conductivity

Arguments		Mean	StdDev	Min	Max	Remarks
θ_l [m³/m³]	mean pc [Pa]	K_l [s]				
0.304	8560	2.0E-09	3.1E-10	1.5E-09	2.3E-09	

Sorption Isotherm (Adsorption)

Arguments		Mean	StdDev	Min	Max	Remarks
φ [%]	T [°C]	θ_l [m³/m³]				
32.8	20.40	0.00050	0.00019	0.00021	0.00071	
43.2	24.20	0.00123	0.00019	0.00091	0.00144	
57.6	20.60	0.00180	0.00034	0.00121	0.00213	
75.2	20.40	0.00267	0.00043	0.00195	0.00308	
84.3	24.20	0.00488	0.00055	0.00372	0.00547	
90.0	20.60	0.00630	0.00048	0.00554	0.00708	
96.0	20.60	0.00901	0.00086	0.00808	0.01029	

Figure 3.1 Data summary sheet of brick Wienerberger.

The functionalized data, also called material functions, correspond to properties that are dependent on state variables such as moisture content. It suffers from the uncertainty in the relevant basic material parameters, depending on the adopted mathematical model. For instance, open porosity and water vapour diffusion resistance factor are related to water vapour permeability function; effective saturation moisture content is the upper limit of moisture content in moisture retention function and liquid water conductivity function. When those basic parameters vary, the corresponding material functions will also shift in a certain range. For the engineering model [61], material functions and related basic material parameters are listed in Table 3.1.

Table 3.1 Material functions and their related material parameters.

Material function	Unit	Symbol	Parameters that affect material function
Moisture retention function	m^3/m^3	θ(pC)	θ_{eff}
Water vapour permeability	s	Kv(θ)	θ_{por} and μ_{dry}
Liquid water conductivity	s	Kl(θ)	θ_{eff} and K_{eff}
Thermal conductivity	W/m·K	λ(θ)	θ_{eff}

Moisture retention curve, thermal conductivity, water vapour permeability and liquid water conductivity of brick with the uncertainty are shown in Figure 3.2 [18]. In each graph, the red curve presents the design material function for the deterministic simulation. The grey shadow region is the possible variation range of material functions obtained from total 400 randomly generated samples.

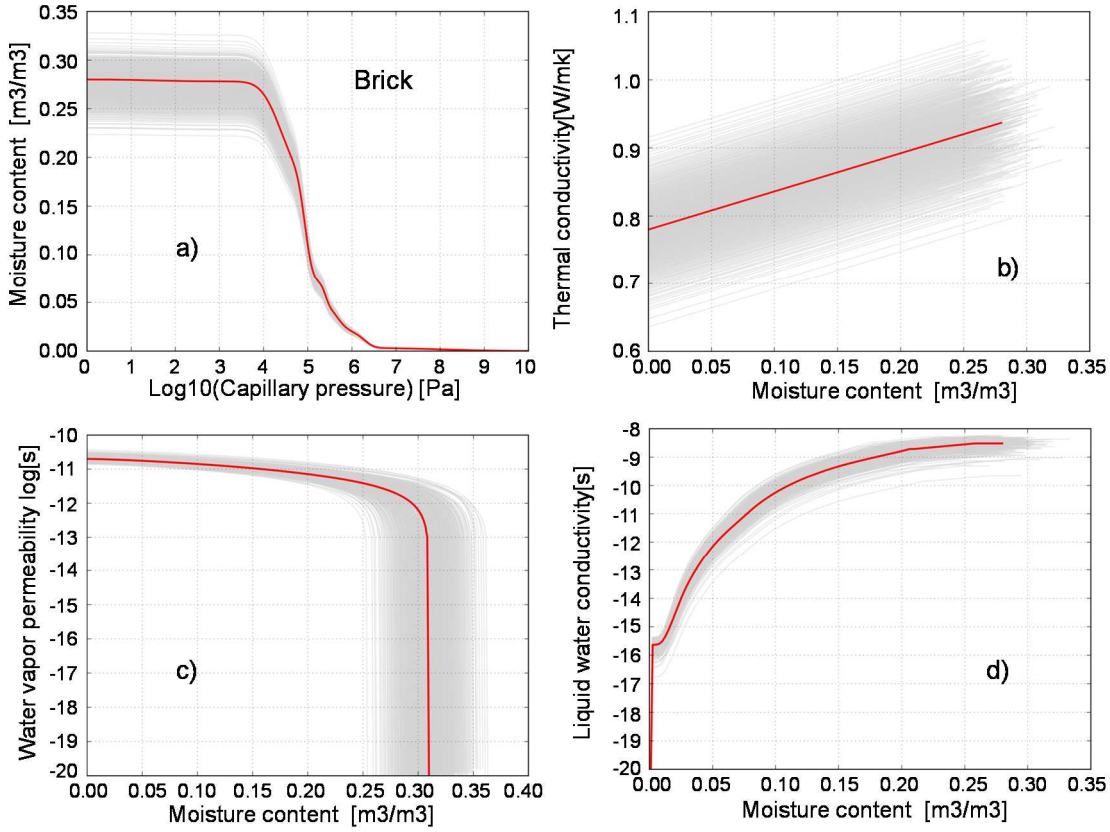

Figure 3.2 Material functions of brick a) moisture retention curve b) thermal conductivity c) water vapour permeability d) liquid water conductivity.

3.2.1.2 Uncertainty in generic material

Generic material is a derived material that represents one type of specific materials with common characteristics in material properties. Application of generic material in the hygrothermal simulation has the distinctive advantages. No detailed material information is

required any more in the building design stage, only the knowledge of the type of the material is sufficient. The generic material can be instead applied in the simulation to reduce the risk of improper selection of specific material properties and increase the reliability of the simulation results. Moreover, generic materials can be applied to qualify the incomplete material data [62].

To obtain generic material, cluster analysis is first applied to identify material clusters from a bunch of specific materials in material category. Cluster analysis is a multivariate procedure for exploring natural groups in data so that the objects or individuals in one group are similar to each other and different from the individuals in the other groups [63]. The clustering is a process that successively fuses specific materials into groups until a single group containing all the specific materials, as shown in Figure 3.3.

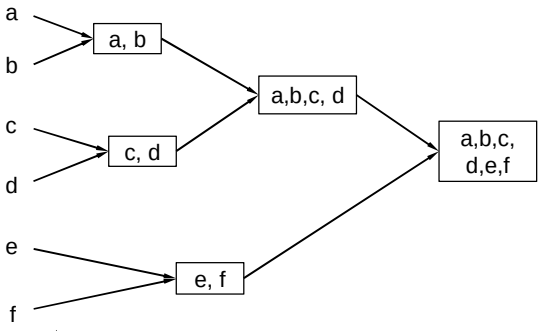

Figure 3.3 The process of clustering individuals to a single group.

Cluster analysis relies on criterion variables that determine based on which standard the distance is measured between two individuals or groups. In [18], the selected criterion variables include basic material parameters and characteristic moisture contents, in consideration of correlations between material parameters. The dissimilarity between two specific materials is determined by their distance. The Euclidean distance is most commonly used to determine the dissimilarity between two objects. The larger the distance, the more dissimilar two specific materials. The most similar specific materials are then aggregated into one cluster. The distance between clusters or groups of materials depends on the select algorithms, e.g., complete linkage and ward's method [63]. The clustering results may not be the same by applying different algorithms.

Here, one example to derive generic materials from a group of 23 specific bricks in brick category is presented. First, the Euclidean distance between each pair of specific bricks is calculated. The specific bricks with the smallest distance are joined into one cluster. Thereafter, the complete linkage and Ward's clustering methods were applied to calculate the distance between different clusters or groups of specific bricks. The "closest" clusters or groups of individuals are fused together. This clustering process continues until all the specific bricks are agglomerated to one set. The tree diagrams of the clustering results are presented in Figure 3.4.

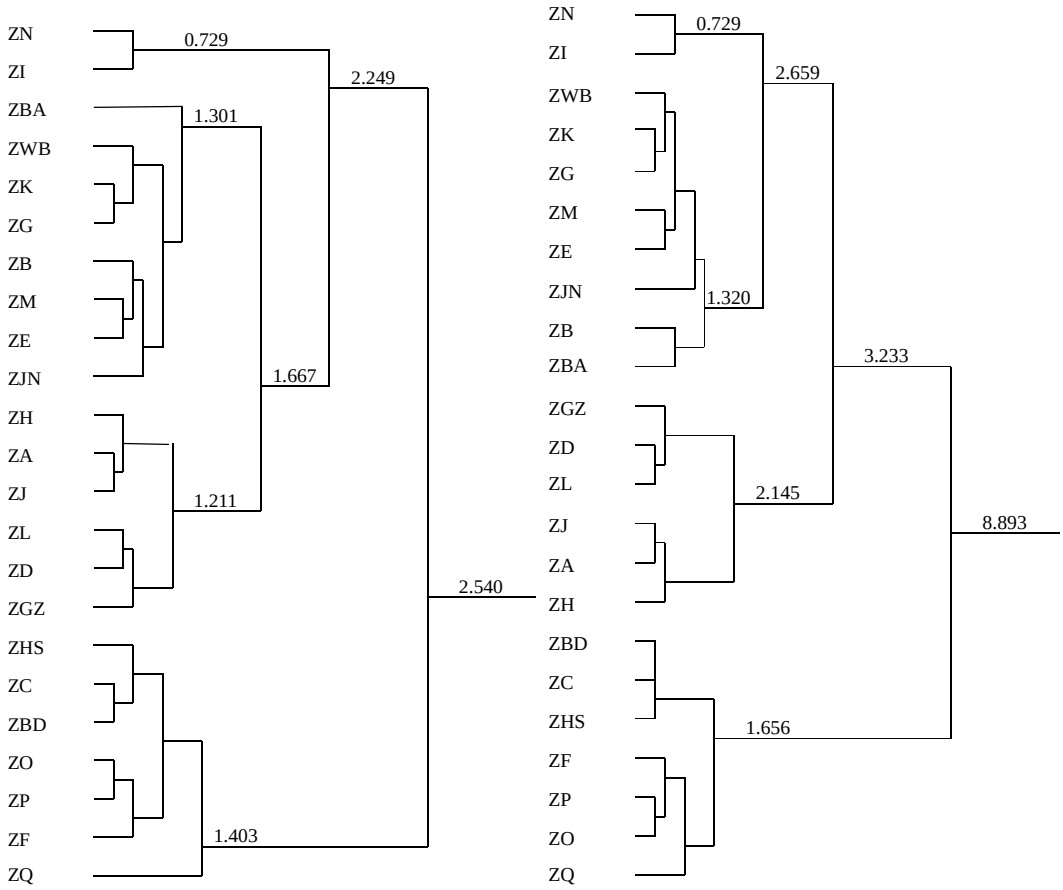

Figure 3.4 Tree diagrams of clustering of specific bricks by using complete linkage method and ward's method.

As presented in Figure 3.4, both clustering methods identify four clusters among 23 specific bricks: Cluster 1 includes bricks ZN and ZI. Cluster 2 contains bricks ZB, ZE, ZG, ZK, ZM, ZBA, ZJN, and ZWB. Cluster 3 is comprised of bricks ZA, ZD, ZJ, ZH, ZL, and ZGZ. And cluster 4 includes bricks ZC, ZF, ZO, ZP, ZQ, ZBD, and ZHS. Moisture storage data of the specific bricks in each cluster are demonstrated, respectively, in Figure 3.5 [18].

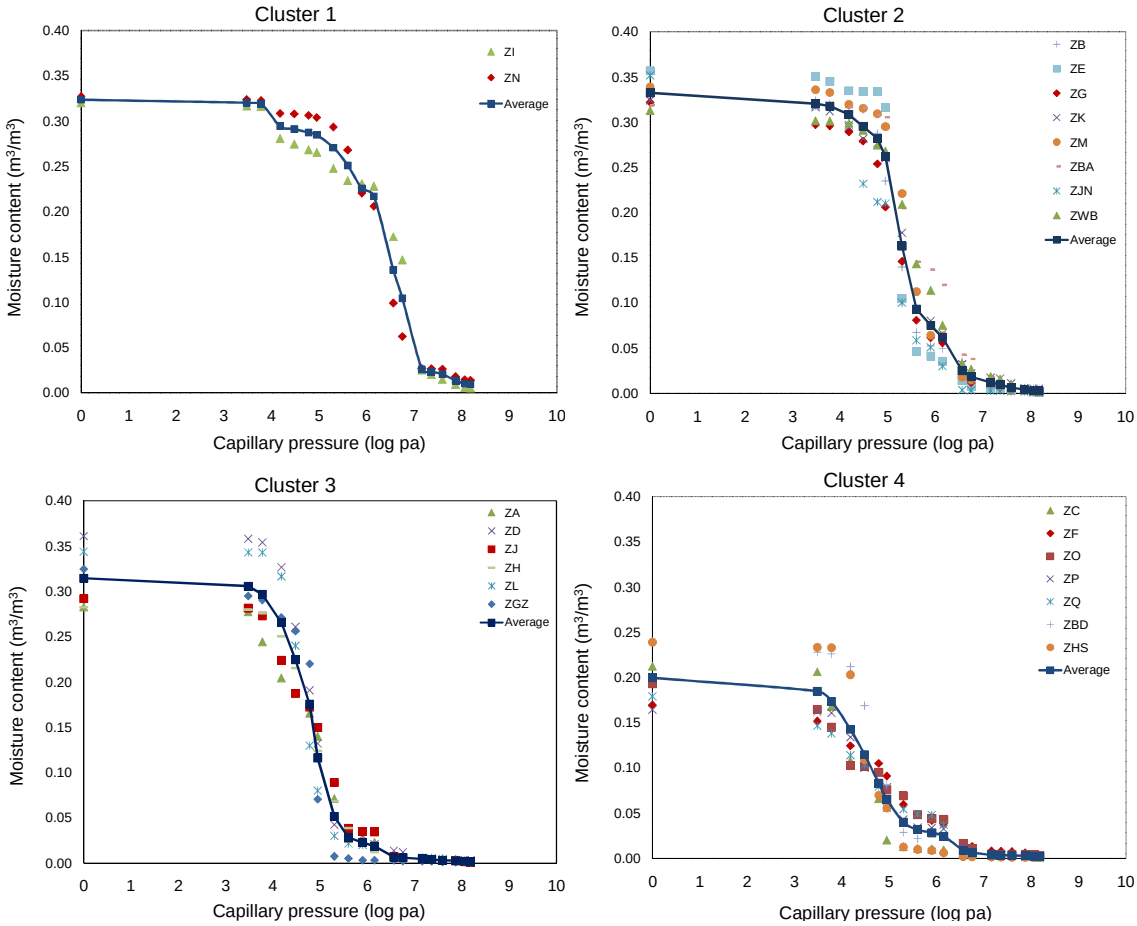

Figure 3.5 Measured moisture storage data and their means in each cluster.

Once the material clusters are identified, the generic synthesis process is conducted thereafter. The properties of generic brick can be gained by arithmetically averaging material properties of the specific bricks in one cluster. Thus, the generic brick has the common characteristics of one type of the specific bricks with a relatively small deviation in the material property.

Each material property of a generic material also includes statistical information, e.g., maximum, minimum, mean value, and standard deviation, which summarizes the material properties of specific materials in one material cluster. Comparing to the deviation in material property of a specific material which accounts for the uncertainty among the specimens, the deviation in material properties of a generic material provides the knowledge of the possible variation range of material property of this type of specific materials in the stochastic simulations. Thus, generic materials, together with specific materials, comprise of a stochastic material database.

3.2.2 Probability distribution of material properties

Uncertainty can be quantified from a probability distribution, which approximates the possible range and distribution of the variable. Probability distribution of the inputs will influence the range and distribution of the outputs, thus they should be carefully selected. Three statistical tests were carried out in the analysis of the distribution of material property: Chi-squared test, Kolmogorov-Smirnov test (K-S test), and Shapiro-Wilk test (S-W test). Chi-squared test and

Kolmogorov-Smirnov test can test if the data follows the specified distribution. Shapiro-Wilk test is used to examine if the sample is drawn from a normally distributed population. The null hypothesis is that the data comes from a particular theoretical distribution. The null hypothesis is accepted, if the calculated p-value is larger than the predefined significance level α.

As stated in [18], building materials can be classified into thirteen categories according to their physical properties and usages in the building components. Each material category has its characteristics, so probability distribution of material property was investigated in the scope of material category. Material data collected from IBK laboratory measurement (TUD), [64], [65], and [66] were analysed.

Probability density functions of material properties in building brick category, plaster and mortar category, natural stone category, and insulation category were evaluated. Histogram plots of density, specific heat capacity, thermal conductivity, capillary saturation moisture content, effective saturation moisture content, water absorption coefficient, liquid water conductivity at saturation moisture content, and water vapour diffusion resistance factor were presented in the Appendix 3.1.4. The number of materials analysed for each property was also indicated. Chi-squared test, Kolmogorov-Smirnov test, and Shapiro-Wilk test were conducted for each material category. The significance level α is set to 0.05.

3.2.3 Material data template

The first part of the data sheet includes general information related to material identification, e.g., its category and the producing method. Those descriptions give an insight into the material's natural characteristics. Good data organization is convenient to quickly search and investigate materials. For easy organization, each material is classified into certain material categories. Table 3.2 lists total thirteen material categories. Each material will be assigned to at least one but no more than three categories [18].

Table 3.2 Material category for data organization.

Category	Material description
01	Coating
02	Plaster/ mortar
03	Building brick
04	Natural stone
05	Cement containing building material
06	Insulation material
07	Building board
08	Wood
09	Natural material
10	Soil
11	Cladding panel and ceramic tile
12	Foil and waterproofing product
13	Miscellaneous

Some measurements aim to obtain basic parameters, e.g., thermal conductivity and specific heat capacity, while others are designed for further material modelling, e.g., water vapour permeability and water retention measurements. For the functional data, the measurement conditions are listed, e.g., pressure, relative humidity and temperature at which the measurements are executed. The statistical data from those measurements, including mean, maximum, minimum and standard deviation, is summarized in the data sheet, respectively. In addition, the special comment regarding to the measurement can be added into each "Remarks" column.

3.2.4 Appendix

Histogram plots and statistical analyses of material properties of bricks are presented in Figure 3.6, Figure 3.7, Figure 3.8, and Figure 3.9.

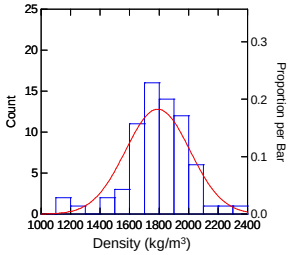

Distribution: Normal Number of materials: 70
Mean = 1791.02 SD = 216.75
Chi-square test statistic = 2.58, df = 3, p-value = 0.46
K-S test statistic = 0.092, Lilliefors probability (2-tail) = 0.15
S-W test statistic = 0.954, p-value = 0.012

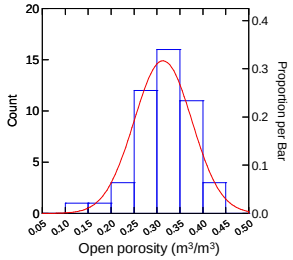

Distribution: Normal Number of materials: 47
Mean = 0.313, SD = 0.063
Chi-square test statistic = 1.13, df = 3, p-value = 0.77
K-S test statistic = 0.071, Lilliefors probability (2-tail) = 0.82
S-W test statistic= 0.977, p-value = 0.465

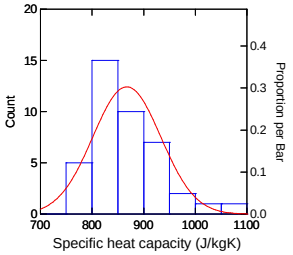

Distribution: Normal Number of materials: 41
Mean = 867.32, SD = 65.07
Chi-square test statistic = 3.71, df = 3, p-value = 0.30
K-S test statistic = 0.113, Lilliefors probability (2-tail) = 0.21
S-W test statistic = 0.923, p-value = 0.011

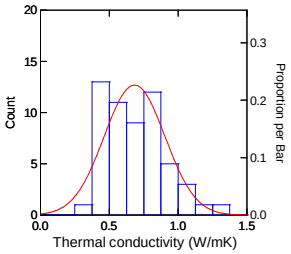

Distribution: Normal Number of materials: 56
Mean = 0.684, SD = 0.218
Chi-square test statistic = 3.61, df = 4, p-value = 0.46
K-S test statistic = 0.108, Lilliefors Probability (2-tail) = 0.11
S-W test statistic for normality = 0.95, p-value = 0.022

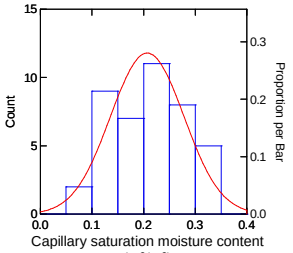

Distribution: Normal Number of materials: 42
Mean = 0.207, SD = 0.07
Chi-square test statistic = 4.22, df = 3, p-value = 0.24
K-S test statistic = 0.097, Lilliefors probability (2-tail) = 0.397
S-W test statistic for normality = 0.973, p-value = 0.413

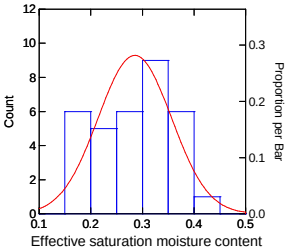

Distribution: Normal Number of materials: 33
Mean = 0.285, SD = 0.07
Chi-square test results may not be good for this sample size.
K-S test statistic = 0.155, Lilliefors probability (2-tail) = 0.044
S-W test statistic for normality = 0.95, p-value = 0.135

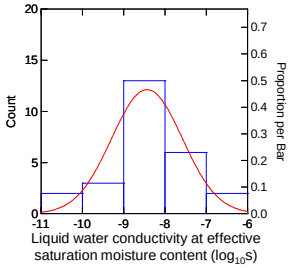

Distribution: Normal Number of materials: 26
Mean = -8.44, SD = 0.84
Chi-square test results may not be good for this sample size.
K-S test statistic = 0.146, Lilliefors Probability (2-tail) = 0.164
S-W test statistic for normality = 0.96, p-value = 0.34

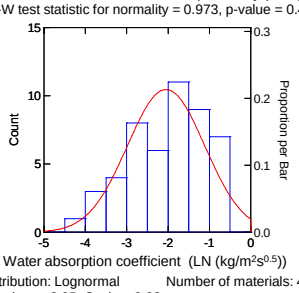

Distribution: Lognormal Number of materials: 49
Location = -2.05, Scale = 0.93
Chi-square test statistic = 2.23, df = 3, p-value = 0.53
K-S test statistic = 0.128, Lilliefors probability (2-tail) = 0.044
S-W test statistic for normality = 0.95, p-value = 0.03

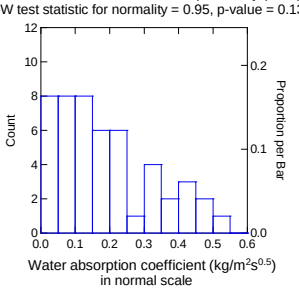

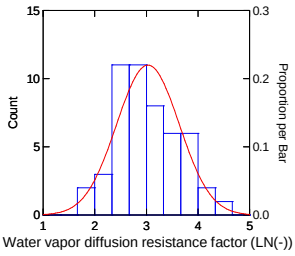

Distribution: Lognormal Number of materials: 50
Location = 3.031, Scale = 0.599
Chi-square test statistic = 4.99, df = 4, p-value = 0.29
K-S test statistic = 0.085, Lilliefors probability (2-tail) = 0.47
S-Wtest statistic for normality = 0.9802, p-value = 0.56
Note: the values larger than 100 are excluded in the analysis

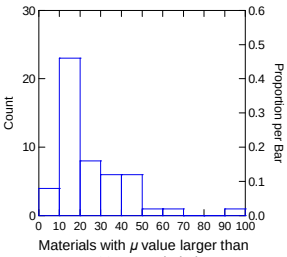

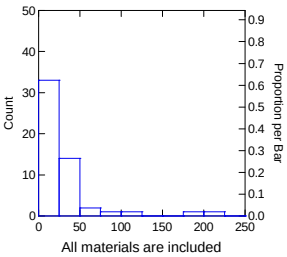

Figure 3.6 Histogram plots and statistical analyses of material properties of bricks.

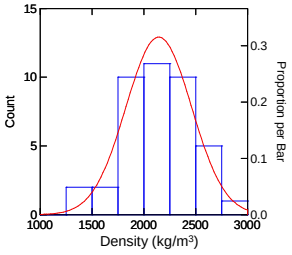

Distribution: Normal Number of materials: 41
Mean = 2143.28, SD = 312.58
Chi-square test statistic = 4.14, df = 2, p-value = 0.126
K-S test statistic = 0.114, Lilliefors Probability (2-tail) = 0.189
S-W test statistic for normality = 0.976, p-value = 0.519

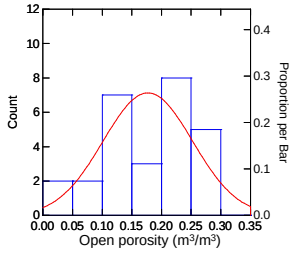

Distribution: Normal Number of materials: 26
Mean = 0.177, SD = 0.074
Chi-square test results may not be good for this sample size.
K-S test statistic = 0.129, Lilliefors Probability (2-tail) = 0.289
S-W test statistic for normality = 0.939, p-value = 0.114
Note: Tuffs with the values larger than 0.45 are not included

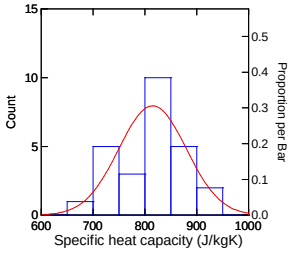

Distribution: Normal Number of materials: 26
Mean (mu) = 814.83, SD = 63.95
Chi-square test results may not be good for this sample size.
K-S test statistic = 0.144, Lilliefors Probability (2-tail) = 0.175
S-W test statistic for normality = 0.941, p-value = 0.142

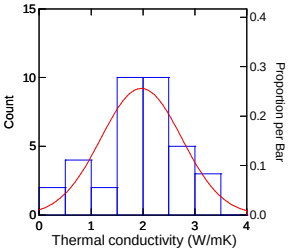

Distribution: Normal Number of materials: 36
Mean = 1.97, SD = 0.769
Chi-square test results may not be good for this sample size.
K-S test statistic = 0.113, Lilliefors Probability (2-tail) = 0.284
S-W test statistic for normality = 0.971, p-value = 0.439
Note: materials with the values larger than 5 are excluded

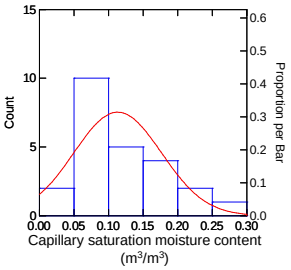

Distribution: Normal Number of materials: 24
Mean = 0.113, SD = 0.062
Chi-square test results may not be good for this sample size.
K-S test statistic = 0.138, Lilliefors Probability (2-tail) = 0.273
S-W test statistic for normality = 0.958, p-value = 0.40

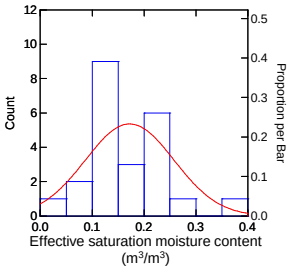

Distribution: Normal Number of materials: 23
Mean = 0.172, SD = 0.084
Chi-square test results may not be good for this sample size.
K-S test statistic = 0.143, Lilliefors Probability (2-tail) = 0.255
S-W test statistic for normality = 0.968, p-value = 0.645

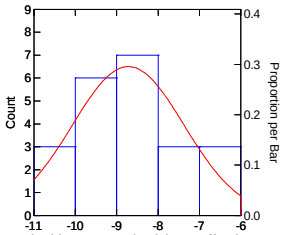

Distribution: Normal Number of materials: 22
Mean = -8.72, SD = 1.32
Chi-square test results may not be good for this sample size.
K-S test statistic = 0.136, Lilliefors Probability (2-tail) = 0.364
S-W test statistic for normality = 0.962, p-value = 0.540

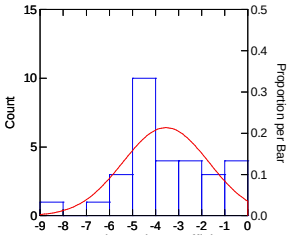

Distribution: Lognormal Number of materials: 30
Location = -3.549, SD = 1.837
Chi-square test results may not be good for this sample size.
K-S test statistic = 0.141, Lilliefors Probability (2-tail) = 0.130
S-W test statistic for normality = 0.958, p-value = 0.282

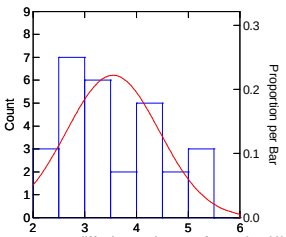

Distribution: Lognormal Number of materials: 28
Location = 3.546, SD = 0.883
Chi-square test results may not be good for this sample size.
K-S test statistic = 0.163, Lilliefors Probability (2-tail) = 0.054
S-W test statistic for normality = 0.922, p-value = 0.039
Note: materials with μ values larger than 200 are excluded.

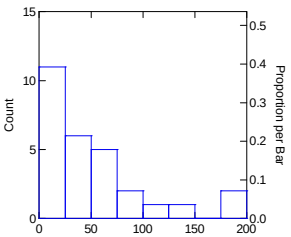

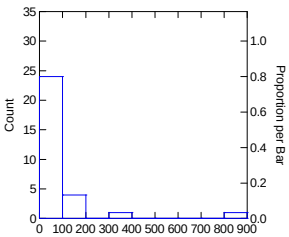

Figure 3.7 Histogram plots and statistical analyses of material properties of natural stones.

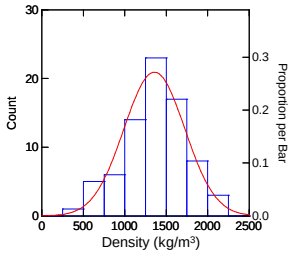

Distribution: Normal Number of materials: 77
Mean = 1356.91, SD = 364.58
Chi-square test statistic = 3.83, df = 5, p-value = 0.574
K-S test statistic = 0.084, Lilliefors Probability (2-tail) = 0.184
S-W test statistic = 0.984, p-value = 0.432

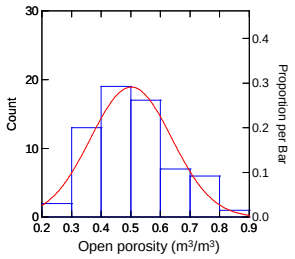

Distribution: Normal Number of materials: 65
Mean = 0.501, SD = 0.136
Chi-square test statistic = 1.939, df = 5, p-value = 0.858
K-S test statistic = 0.096, Lilliefors Probability (2-tail) = 0.134
S-W test statistic = 0.977, p-value = 0.26

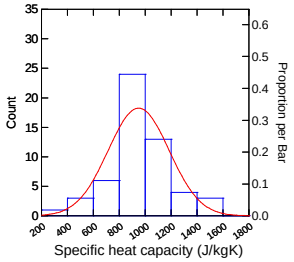

Distribution: Normal Number of materials: 54
Mean = 949.37, SD = 234.03
Chi-square test statistic = 9.09, df = 4, p-value = 0.059
K-S test statistic = 0.104, Lilliefors Probability (2-tail) = 0.147
S-W test statistic = 0.972, p-value = 0.23

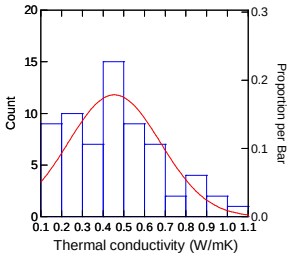

Distribution: Normal Number of materials: 66
Mean = 0.454, SD = 0.221
Chi-square test statistic = 3.137, df = 5, p-value = 0.679
K-S test statistic = 0.074, Lilliefors Probability (2-tail) = 0.454
S-W test statistic = 0.963, p-value = 0.0484
Note: materials with the values larger than 1.5 are excluded

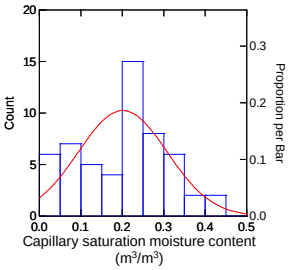

Distribution: Normal Number of materials: 55
Mean = 0.201, SD = 0.106
Chi-square test statistic = 8.233, df = 4, p-value = 0.083
K-S test statistic = 0.107, Lilliefors Probability (2-tail) = 0.115
S-W test statistic = 0.961, p-value = 0.074

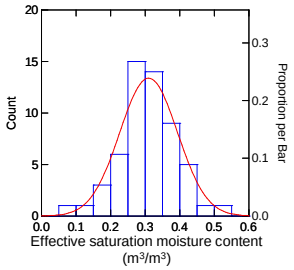

Distribution: Normal Number of materials: 56
Mean = 0.310, SD = 0.083
Chi-square test statistic = 1.344, df = 3, p-value = 0.719
K-S test statistic = 0.079, Lilliefors Probability (2-tail) = 0.493
S-W test statistic = 0.984, p-value = 0.658

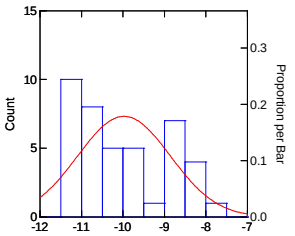

Distribution: Normal Number of materials: 41
Mean = -9.98, SD = 1.10
Chi-square test statistic = 8.508, df = 3, p-value = 0.037
K-S test statistic = 0.150, Lilliefors Probability (2-tail) = 0.021
S-W test statistic = 0.906, p-value = 0.003

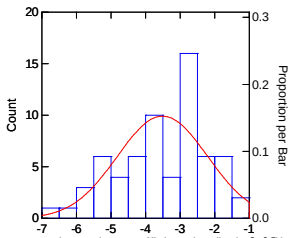

Distribution: Lognormal Number of materials: 65
Location = -3.51, Scale = 1.297
Chi-square test statistic = 3.148, df = 4, p-value = 0.533
K-S test statistic = 0.116, Lilliefors Probability (2-tail) = 0.030
S-W test statistic = 0.979, p-value = 0.325

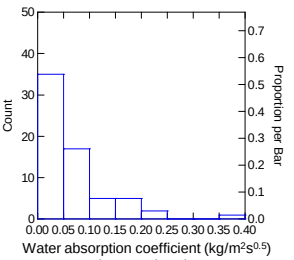

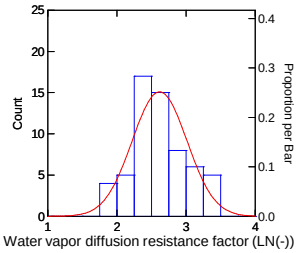

Distribution: Lognormal Number of materials: 49
Location = 2.617, Scale = 0.393
Chi-square test statistic = 8.73, df = 5, p-value = 0.120
K-Stest statistic = 0.116, Lilliefors Probability (2-tail) = 0.042
S-W test statistic = 0.968, p-value = 0.11
Note: Materials with μ values larger than 40 are excluded.

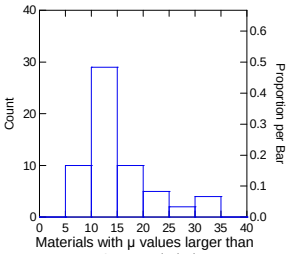

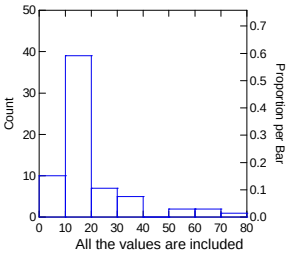

Figure 3.8 Histogram plots and statistical analyses of material properties of plasters and mortars.

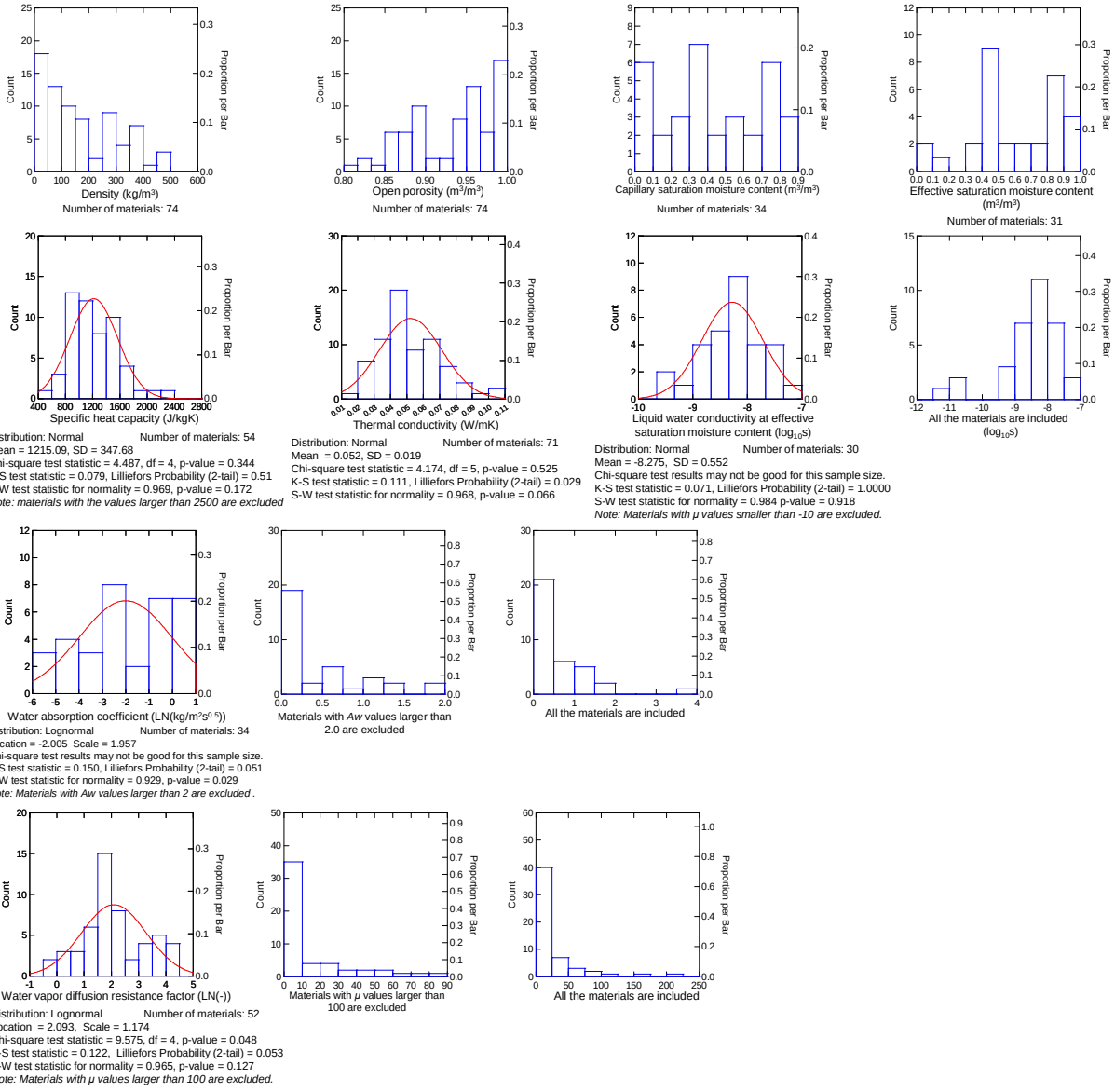

Figure 3.9 Histogram plots and statistical analyses of material properties of insulations.

3.3 Ventilation and airtightness

3.3.1 Belgium input - Air tightness of 54 new Flemish dwellings (IWT TETRA BEP2020) – [KUL]

The air change rates at 50Pa pressure difference (n_{50}) of 54 new dwellings were collected in Flanders, Belgium, between 2010 and 2013. In addition to this data, insulation level (the so-called K-level, which corresponds to a kind of overall heat loss coefficient (HLC)), energy performance indicator (E-level corresponding regional EPBD-regulation), typology, compactness and internal volume are collected as well.

The air tightness measurements in this project were performed by several researchers and equipment, but are all based on standard

[1], which makes them comparable. However, it is possible that the execution of the measurements influenced the results. Measurement errors can be expected for both flow measurement and dimensions.

The cumulative distribution function of the n_{50} values is shown in Figure 3.10.The average value of the sample is 2.22 h^{-1} with standard deviation 2.38 h^{-1}. Correlations between the input parameters were investigated. A strong correlation was found between the n_{50} values and both overall HLC and E-level, which are correlated as well. This indicated that dwellings are more airtight when attention is paid for the energy performance and thus also insulation level of the dwellings (see Figure 3.11). Note that in Belgium for passive house certificates a n_{50} value lower than 0.6h^{-1} is required. In other cases, there are no requirements regarding air tightness.

To investigate other parameters influencing the air tightness, more measurements and more details on the dwellings are needed. Nevertheless, the measured n_{50} values reflect the spread on air tightness for newly built dwellings in Flanders, Belgium.

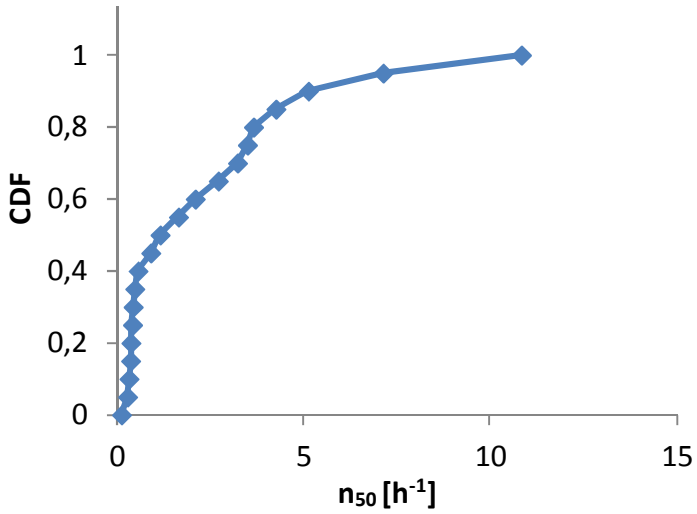

Figure 3.10 Cumulative distribution function of measured n_{50} values.

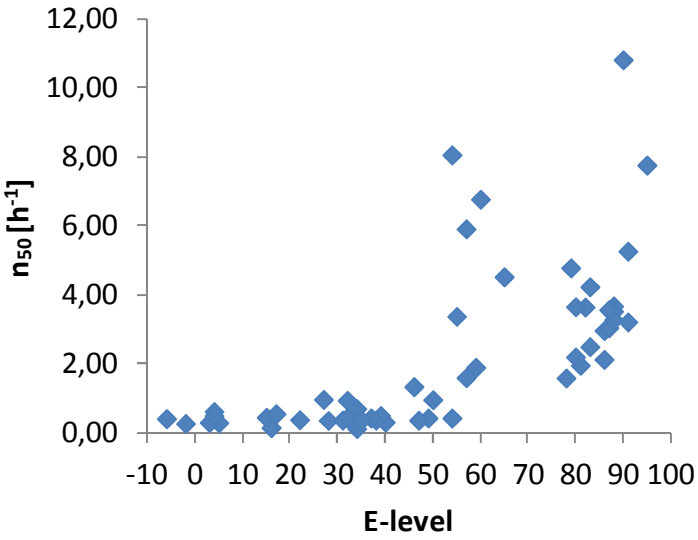

Figure 3.11 Scatter plot of n_{50} value and E-level (based on EPBD-regulation) of dwellings.

3.3.2 Denmark input

The collected data that is presented in the following text was obtained as part of the Indoor Environment and Children's Health (IECH) study undertaken by DTU. A short introduction to the research project can be found in section 2.4 that containing the contribution from Denmark (DTU).

The following text contains a description of the method used to calculate the air changes in 500 Danish family homes. The report also includes simple graphs depicting correlations between proxies for occupant behaviour (air changes and moisture excess) and ambient environment. For the Annex, the data is divided in two groups: Single and multi-family homes. Of the 500 family homes 440 are single and 60 are multi-family homes. All data is from measurements done in Odense, Denmark, between 10 March and 18 May 2008.

3.3.2.1 Method

The method section is an excerpt from [67]. The excerpt has been edited lightly to conform to the purposes of Annex 55.

The homes of the children were located within a radius of 20 km from the city centre. In order to estimate the CO_2 emission rate in the room during the period of the measurements, the parents were asked to record the number of occupants in the room for each day and each night [68], [69]. They were also asked to record if anyone left the room for a longer period during the night. They provided the weight and height of each person sleeping in the room and they indicated in a diary whether the windows and doors were closed, ajar or fully open during the monitored days and nights. The families were asked to maintain their regular routine regarding opening the doors and windows. The volumes of all the rooms were measured by the research teams. The measurements were performed between 10 March and 18 May 2008.

Carbon dioxide data obtained in the time period between 21:00h and 7:00h each measured night, were extracted for data analyses and calculation of the ventilation rate [68], [69]. This

time period was selected to represent the conditions when the child spent most of the time in his/her room. The activity and occupancy were assumed to be constant during the night, unless otherwise indicated by the parents. When these factors were known to change during the night, the night period was divided into shorter periods and the ventilation rate was determined separately for the period with known occupancy. Data from periods when the child was not in the room were omitted.

Three different patterns in the obtained CO_2 concentrations were used to estimate the ventilation rate in the room for the respective night:

- Concentration build-up: Primarily, periods of clear concentration build-ups were used to calculate the ventilation rate. When the data were noisy and the behaviour in the room was not well documented, the initial concentration build-up was the only one used. A spread sheet (Excel) was developed to estimate the air change rate in the room by fitting a non-linear curve to the measured pattern of the CO_2 concentration at a given CO_2 emission rate (calculated from the data obtained from the parents), room volume and outdoor CO_2 concentration. The spread sheet employed the carbon dioxide mass balance equation.
- Concentration decay: Decays of the CO_2 concentration were only used when the occupancy and behaviour in the room were precisely documented for the entire night. The spread sheet described above was used for the calculation.
- Steady-state concentration: Occasionally, no well-defined build-up or decay was available within the selected data. In such a case the ventilation rate was predicted using a mass balance model applied on the estimated steady-stateCO_2 concentration.

Only the most trustworthy fractions of the 10-hour period extracted for each night were used for further data treatment. The final estimated ventilation rate in a bedroom is the time-weighted average of the ventilation rates obtained for each relevant time period. The ventilation rates were estimated using the average outdoor CO_2 concentration over the 10-week experimental period.

The average and the highest 20-minute running average of the CO_2 concentration were determined for each bedroom. The same time periods as for calculating the ventilation rate, were used to determine the average and highest CO_2 concentration.

3.3.2.2 Collected raw data

To see the indoor CO_2 concentration levels measured in the children's bedrooms, then see section 3.4.2. This chapter and section focuses solely on the air changes. The air changes are calculated on the data on CO_2 concentration levels presented in section 3.4.2.

The measurements were performed between 10 March and 18 May 2008. The distribution of indoor air change rates can be described by the log-normal distribution.

Table 3.3 Air changes calculated for family homes in Denmark in spring 2008.

Air changes [h^{-1}]	All homes (500)	Single-family (440)	Multi-family (60)
Average	0.61	0.63	0.48
Median	0.46	0.47	0.37
Standard Deviation	0.53	0.55	0.38
Confidence Interval95	0.56	0.58	0.39
	0.66	0.68	0.58
Maximum	4.72	4.72	2.52
Minimum	0.05	0.05	0.10

Standard deviations are calculated using theory applicable for samples and log-normal distributions. The confidence intervals are calculated using modified version of the Cox method [70] using the Student's t variate, instead of the standard normal z variate, for a α-value of 0.05; this gives 95 % confidence intervals.

For reference the outdoor temperature distribution in the measured period has been listed below. The table contains the same data as Table 3.12 presented in section 3.4.2.

Table 3.4 Outdoor temperature distribution in % in measured period.

Temperatures [°C]	Distribution [%]
>30	0.4
30>X≥ 25	4.6
25>X≥20	10.0
20>X≥15	13.7
15>X≥10	25.6
10>X≥5	26.0
5>X≥0	15.2
0>X≥-5	4.4
-5>	0.2

The following graphs (Figure 3.12,Figure 3.13 and Figure 3.14) display the data collected on indoor air change rates in Danish homes along with probability functions and probability density functions (PDF). The probability functions are calculated as the frequency of a measurement occurring in a bin (air change rate interval) divided by the total amount of bins. The displayed probability density functions have been drawn from their respective means and standard deviations and the calculated probability of occurrences in the individual bins.

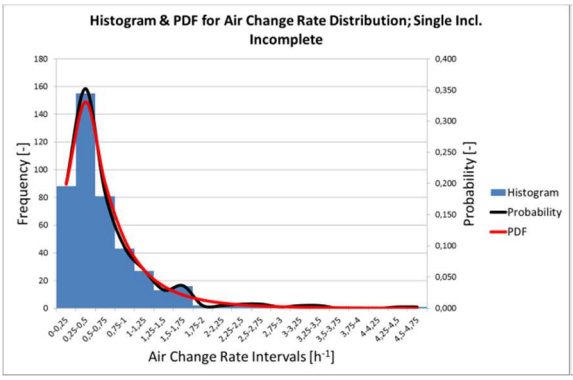

Figure 3.12 Distribution and PDF of indoor air change rates in Danish single-family homes.

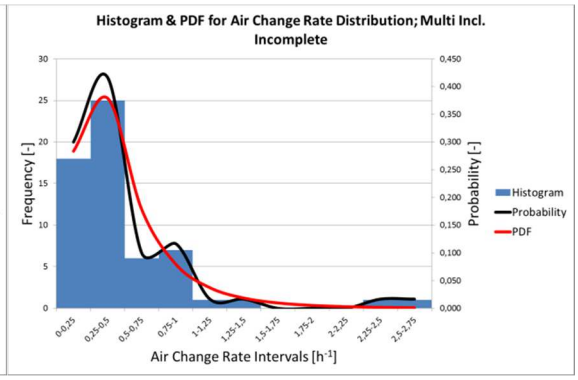

Figure 3.13 Distribution and PDF of indoor air change rates in Danish multi-family homes.

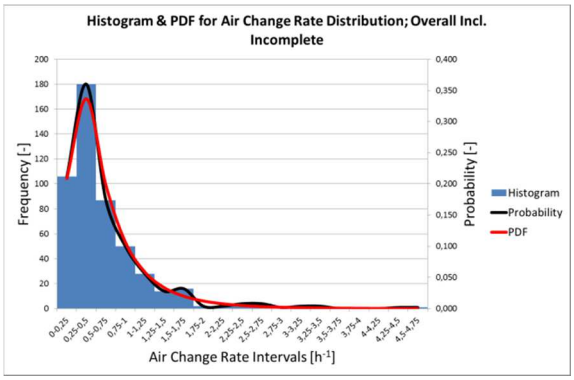

Figure 3.14 Distribution and PDF of indoor air change rates in general Danish family homes.

3.3.2.3 Analysis

3.3.2.3.1 Air change rates

Figure 3.15 and Figure 3.16 show how outdoor temperatures influence air changes (n) in Danish homes. Due to a lack of weather data for the first few days of the study it is only data from 480 of the 500 homes that is included in the figures (18 single-family and 2 multi-family homes are missing). The air change levels are stable over the temperature variations in the measured period. In Denmark it is uncommon to have mechanical ventilation systems in homes; therefore venting (airing out by opening windows) is the most common form of cooling found in Denmark. Venting a home without changing other occupant behaviour significantly will result in air change levels to rise. So it would be expected that families will open windows more during periods with higher temperatures. The presented data does not support this chain of reasoning.

However, the data used to calculate the air changes is from 22:00h to 7:00h, which is the night time. The period during which measurements were done was during the Danish spring. Nights would have been relatively cool. It is considered unlikely that people who did not keep windows open in colder periods would have opened them during this spring.

So the presented data represents the air changes present in homes with closed windows and doors. This presented data can be said to be the base air change for the homes.

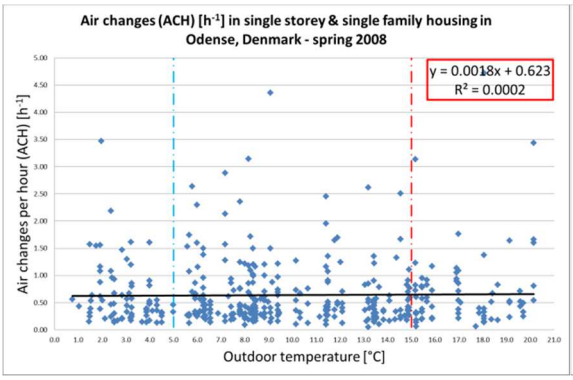

Figure 3.15 Correlation between air change rates (n) and outdoor temperatures in single-family homes.

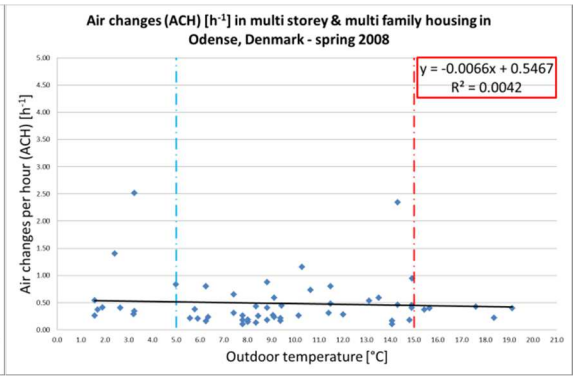

Figure 3.16 Correlation between air change rates (n) and outdoor temperatures in multi-family homes.

The air changes were calculated using occupant generated CO_2 as a tracer gas. Using this method introduces possible errors. Discussing these errors is outside the scope of this report. For a discussion regarding the possible errors introduced with this procedure, see [67] and Appendix A [71]. The APPENDIX is a (unpublished) conference paper written for the Indoor Air 2011 conference held in Austin, Texas. The paper discusses the findings of a research project where three methods used to determine the air change of a home are compared. The three methods are the occupant-generated CO_2 method, the tracer gas method (TG) and the passive tracer gas method (PFT).

A single zone mass balance of occupant generated CO_2 was used to calculate the ventilation rate during 4 to 5 nights in each bedroom of the five Danish homes. Only data from night periods was used. At the same time the air change rates in the homes were measured using Freon® as a tracer gas. Constant concentrations of the tracer gas was maintained throughout the dwellings, with a tracer gas dosing and sampling point in up to six rooms in each home, including the bedrooms. These measurements were conducted in all four seasons of the year.

Passive tracer gas (PFT) measurements of the average monthly air changes for the entire dwellings were also done in the five homes. The measurements were done during the winter season in time periods comparable with the periods the active tracer gas measurements were done.

Some of the findings of the research project are shown in Figure 3.17. The figure compares the air changes as they were determined by the occupant generated CO_2 method with air changes determined by the tracer gas method. The figure show how the total ventilation rates (influenced by airflows both from outdoors and adjacent spaces) determined by the CO_2 method were several times larger than the outdoor ventilation rates obtained by the guarded tracer gas measurement.

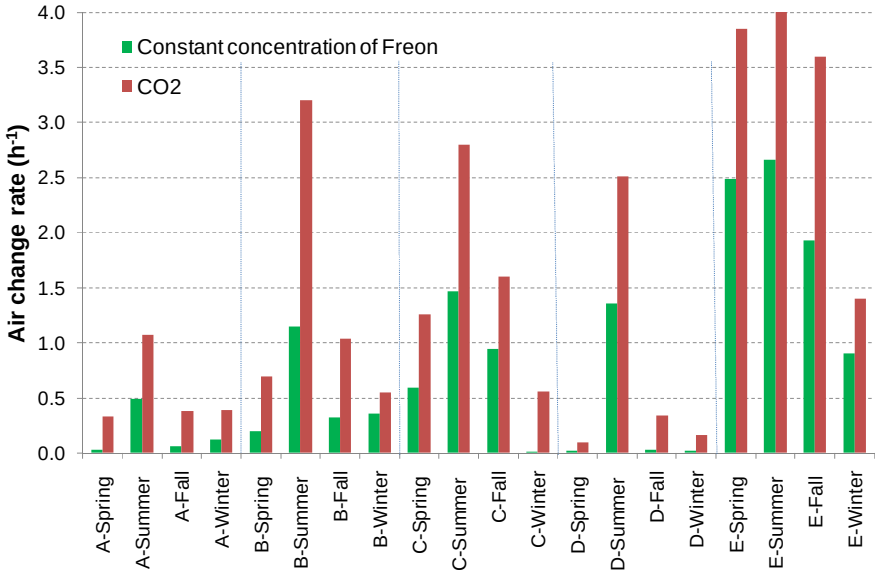

Figure 3.17 Comparison of air changes rates as determined by the occupant generated CO_2 method and the tracer gas method using Freon® as tracer gas.

The active tracer gas method is widely believed to be the most accurate ventilation method available in buildings where multi-zone effects are important. The results from the research projects suggest that the total ventilation rates calculated from the IECH data are higher than the outdoor ventilation rates. This in turn suggests that using the occupant generated CO_2 method to determine air changes leads to overestimating overall air changes for multi-zone homes.

Danish homes are supposed to have a minimum air change of 0.5 h^{-1}. The calculated average air change for single-family homes is 0.64 h^{-1} and 0.49 h^{-1} for multi-family homes. With respective medians values of 0.44 and 0.38 h^{-1} it can be seen that more than half of the participating homes have air changes below the minimum requirement. Considering the above brief discussion of the quality of the method used and the possible effects on the resulting calculated air changes, it is quite possible that the air changes in Danish homes are even lower than those presented in the tables above.

In conclusion it can be said that outdoor ventilation rates in ordinary Danish homes a low and that the presented air changes are subjected to sources of error. The reported air changes are quite possibly higher than the actual air changes present in Danish homes. However, the spread (calculated variances) in the results is believed to be accurate to the extent of the purposes of Annex 55.

3.3.2.3.2 Air change rates and moisture excesses

Figure 3.18 and Figure 3.19 show how air changes influence moisture excess in Danish homes. Moisture excess levels can be seen to be falling with rising air changes. This is as could be expected. With higher ventilation rates the indoor absolute humidity levels will come to be closer to outdoor levels, which, more often than not, are lower.

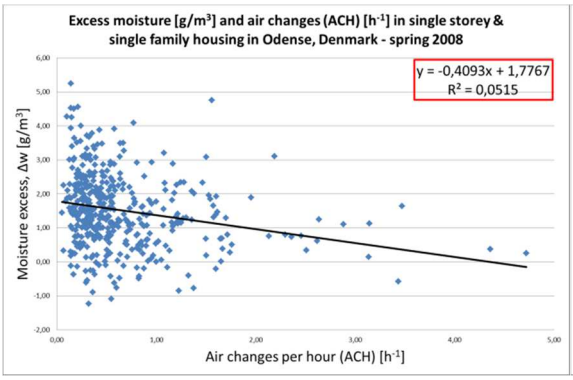

Figure 3.18 Correlation between moisture excesses (moisture production) and air change rates (n) in single-family homes.

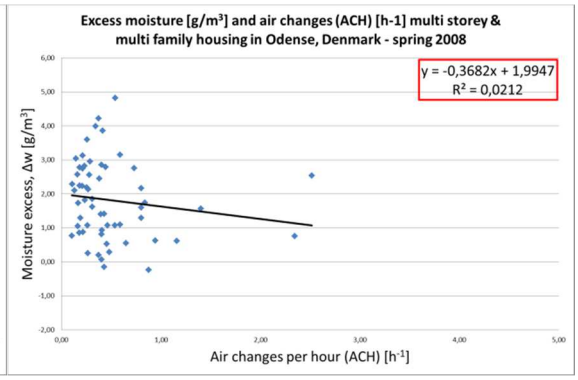

Figure 3.19 Correlation between moisture excesses (moisture production) and air change rates (n) in multi-family homes.

The homes included in the above graphical representations of the dependence of indoor moisture excess levels on air changes per hour are 20 less (18 single-family and 2 multi-family homes) than the overall total of homes included in the study. This is due to a lack of weather data for the first few days of the study.

3.3.3 Estonia [TTU] – Ventilation and airtightness in Estonian buildings

3.3.3.1 Performance of ventilation

According to standard [72] ventilation airflow in bedrooms should be at least 1 l/(s·m^2) for indoor climate category II and at least 0.6 l/(s·m^2) for indoor climate category III.

The average ventilation airflow in bedrooms of brick apartment buildings was 0.46 l/(s·m^2) (st.deviation 0.29 l/(s·m^2)), see Figure 3.20. Air flow per person was between 0.5…9.3 l/(s·person) with average value of 3.8 l/(s·person). Average air change in bedrooms was 0.65 h^{-1} (st.deviation 0.41 h^{-1}); variation from different apartments was 0.10…1.5 h^{-1}.

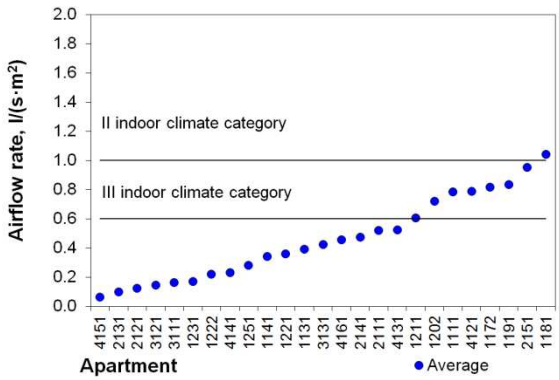

Figure 3.20 Ventilation airflow rates in bedrooms of brick apartment buildings.

During winter the average ventilation airflow in bedrooms of wooden apartment buildings was 0.43 l/(s·m^2) (st.deviation 0.32 l/(s·m^2)), see Figure 3.21 left. Air flow per person was between 1.0…10.3 l/(s·person) with average value was 3.7 l/(s·person). Average air change in bedrooms was 0.56 h^{-1} (st.deviation 0.32 h^{-1}); variation from different apartments was 0.12…2.0 h^{-1}.

During summer the average ventilation airflow in bedrooms of wooden apartment buildings was 0.58 l/(s·m^2) (st.deviation 0.44 l/(s·m^2)), see Figure 3.21 right. Air flow per person was between 1.5…8.4 l/(s·person) with average value was 3.9 l/(s·person). Average air change in bedrooms was 0.79 h^{-1} (st.deviation 0.60 h^{-1}); variation from different apartments was 0.09…2.2 h^{-1}.

Ventilation airflow was compared in wooden apartment buildings between apartments with old-original windows and changed-modern windows. In apartments with old-original windows the airflow was 0.12…1.1 h^{-1}and average was 0.45 h^{-1}. In apartments with modern-changed windows the airflow was 0.12…1.2 h^{-1}and average was 0.57 h^{-1}. The difference in airflows between changed and original windows was not significant.

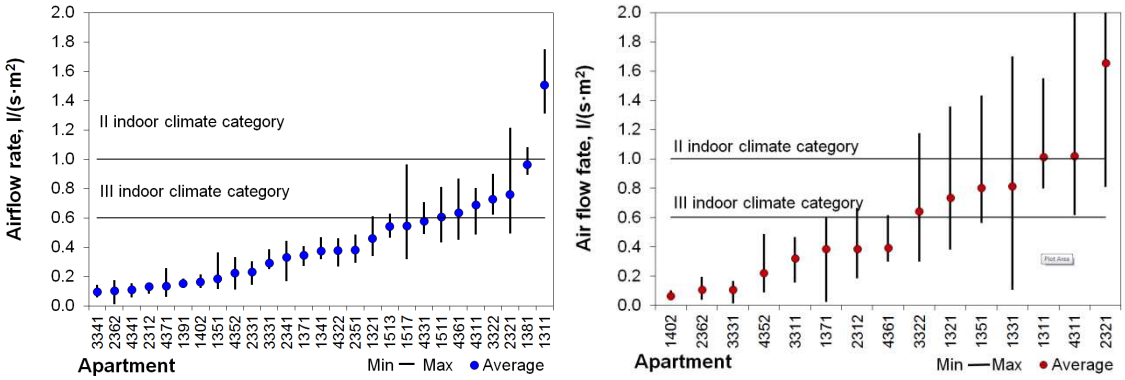

Figure 3.21 Ventilation air flow in bedrooms of wooden apartment buildings during winter (left) and summer (right).

3.3.3.2 Airtightness of building envelope

Average air leakage rate of building envelope of brick apartment building was q_{50} = 4.0 m^3/(h·m^2) (st.dev = 1.4 m^3/(h·m^2)) and air leakage rate @ 50Pa wasn_{50} = 5.7 h^{-1} (st.dev = 2.0 m^3/(h·m^2)), see Figure 3.22. Older buildings were slightly leakier (see Figure 3.23 left), but due to the large variation in results the difference was not significant. In comparison of airtightness with changed windows and old windows difference was not significant (p=0.37), see Figure 3.23 (right).

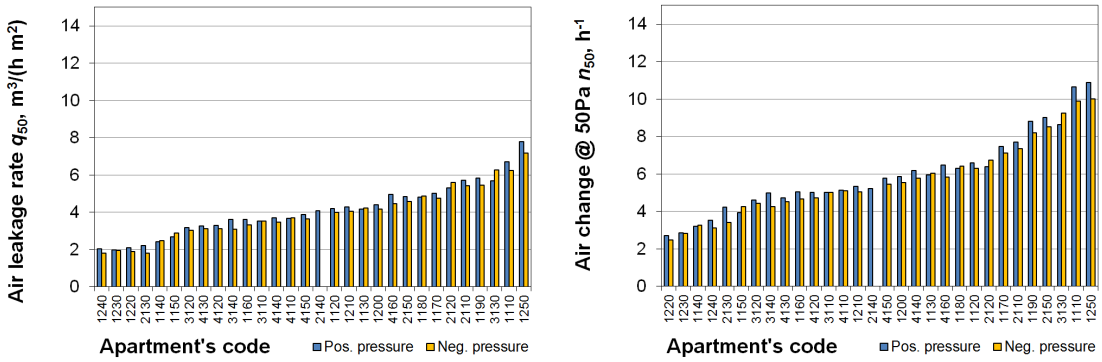

Figure 3.22 Air leakage rate q_{50} *(left) and air change rate @ 50Pa* n_{50} *(right) of brick apartment buildings.*

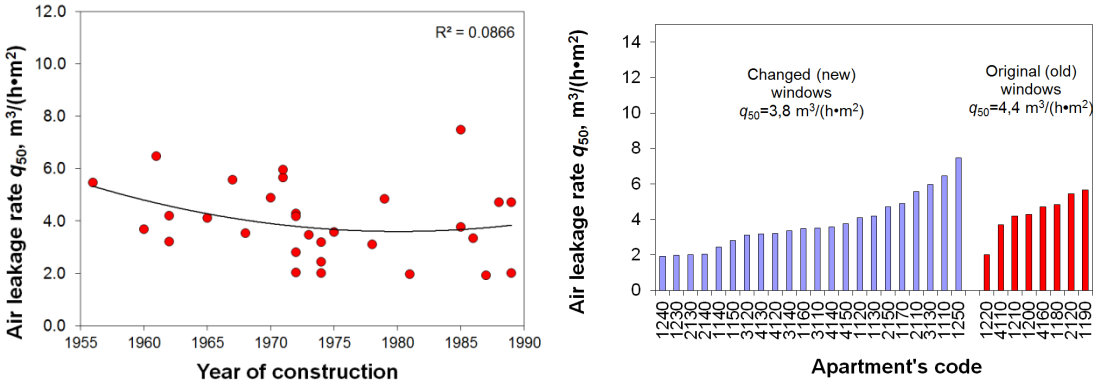

Figure 3.23 The influence of age of building (left) and the type of windows (right) on air tightness of brick apartment buildings.

Average air leakage rate of wooden apartment building was q_{50} = 9.7 m³/(h·m²) (st.dev = 4.0 m³/(h·m²)) and air leakage rate @ 50Pa wasn_{50} = 13 h^{-1} (st.dev = 4.9 m³/(h·m²)), see Figure 3.24. Older buildings were slightly leakier (see Figure 3.25 left), but due to the large variation in results the difference was not significant. In comparison of apartments in upper and bottom floor, apartments in upper floor were significantly leakier due to leaky attic floor, see Figure 3.25 right). The change or restoration of windows did not influence significantly the airtightness of windows.

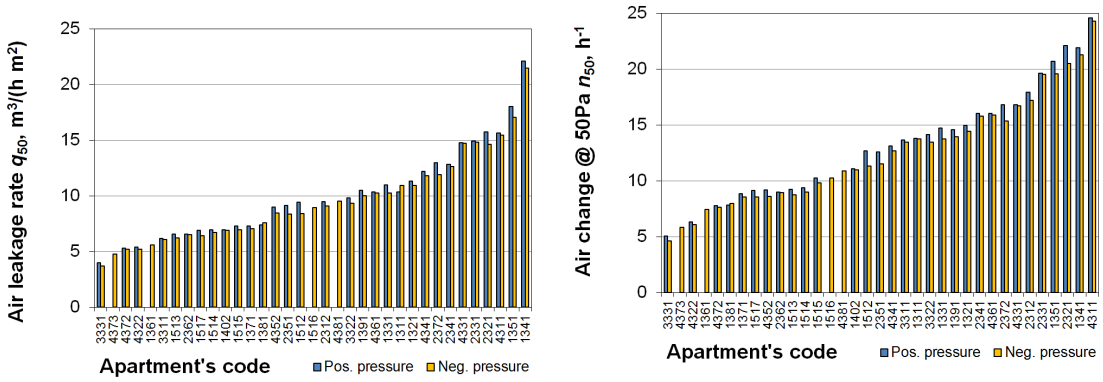

Figure 3.24 Air leakage rate q_{50} *(left) and air change rate @ 50Pa* n_{50} *(right) of wooden apartment buildings.*

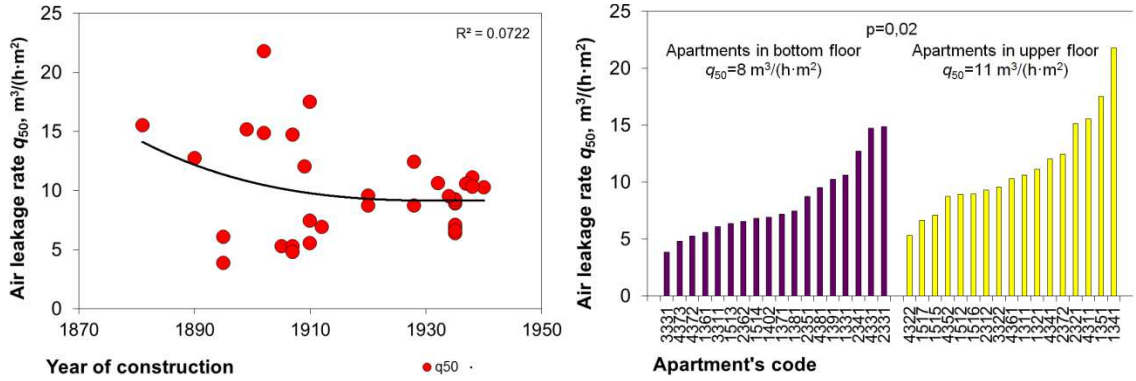

Figure 3.25 The influence of age of building (left) and the floor of the apartment (right) on air tightness of wooden apartment buildings.

Occupants' opinions concerning indoor climate and thermal comfort collected from the questionnaires and the results of air tightness measurements were compared. According to the questionnaire, the main problems in apartments with large air leakage rate were too dry air (significant difference during winter and summer), uniformity and unstability of temperatures in apartments, Figure 3.26.

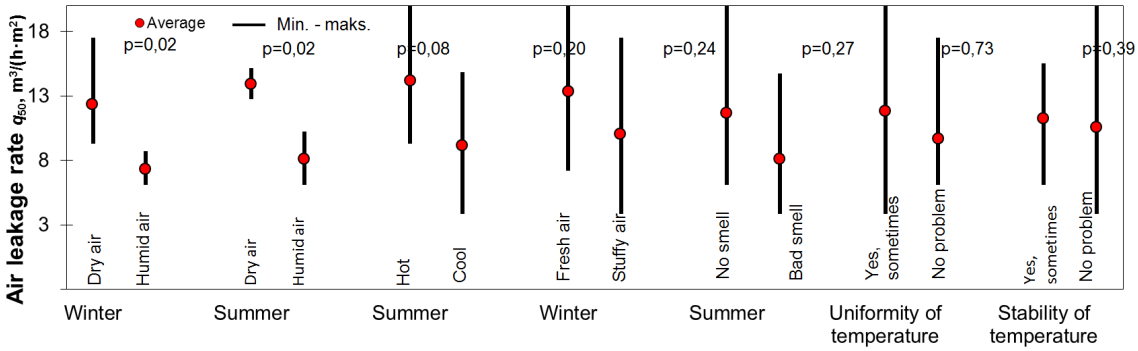

Figure 3.26 The difference in airtightness in apartment divided according to opinion of inhabitants.

3.3.4 Finland [TUT] – AISE and KVTP –projects

Airtightness values n_{50} and q_{50} are greater than or equal to zero. If normal distribution is used to describe these or other values with similar physical restrictions, then additional conditions (e.g. $q_{50} \geq 0$ m³/(m²h)) must be used when creating random numbers from that distribution. Another possibility would be to use some non-negative distribution with suitable parameters or the original probabilities of the measurement sample.

3.3.4.1 Ventilation in timber-framed and heavy weight detached houses

Air change rates in 100 timber-framed and 70 heavyweight detached houses were analyzed. The measurements have been done with Airflow LCA 6000 VA -vane anemometer by measuring the exhaust air flow rates at every exhaust ventilator at the operation level of the ventilation machine. The distribution of air change rates for timber-framed houses is shown in Figure 3.27 and for heavyweight houses in Figure 3.28. Also normality of the data has been investigated by

plotting the normal probability plots. It seems that the air change rate is almost normally distributed.

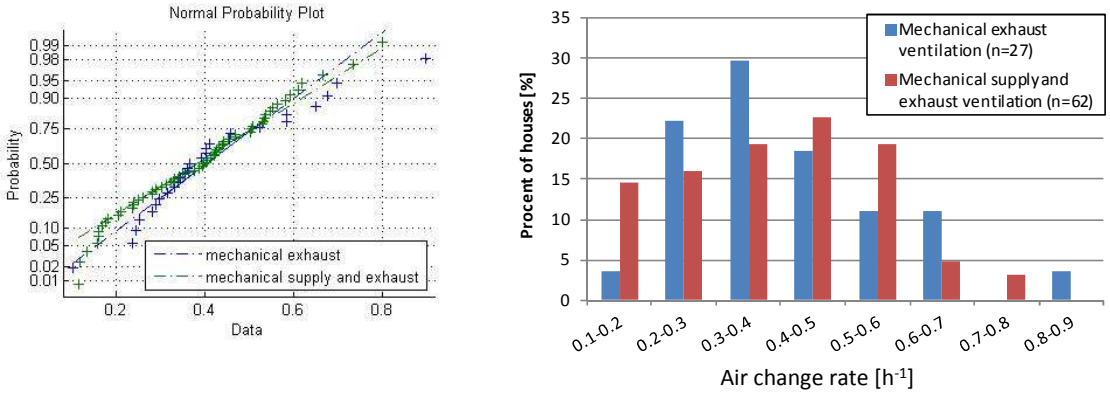

Figure 3.27 Distribution and normal probability plots for air change rate [h^{-1}] in timber-framed houses according to ventilation type.

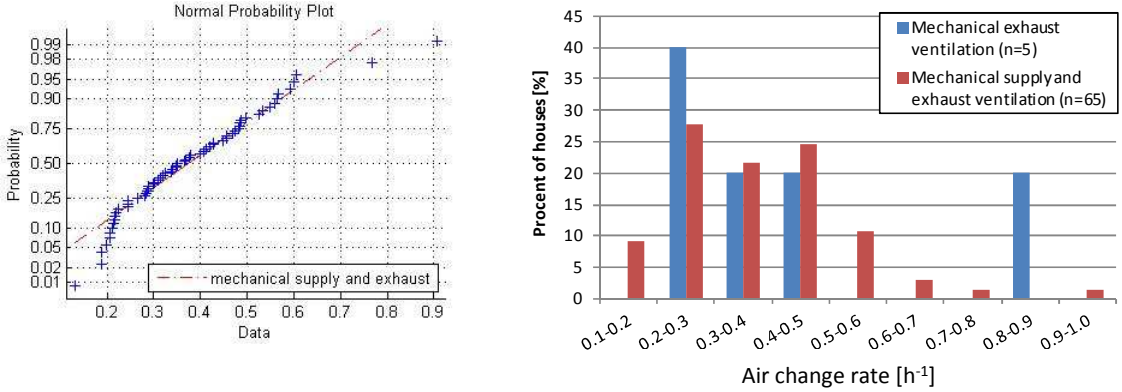

Figure 3.28 Distribution and normal probability plots for air change rate [h^{-1}] in heavy-weight houses according to ventilation type.

The average and standard deviation of air change rates according to ventilation type (mechanical exhaust or mechanical supply and exhaust) are shown in Figure 3.29. Average air change rate for all detached houses was 0.39 h^{-1} (st.dev. 0.16).

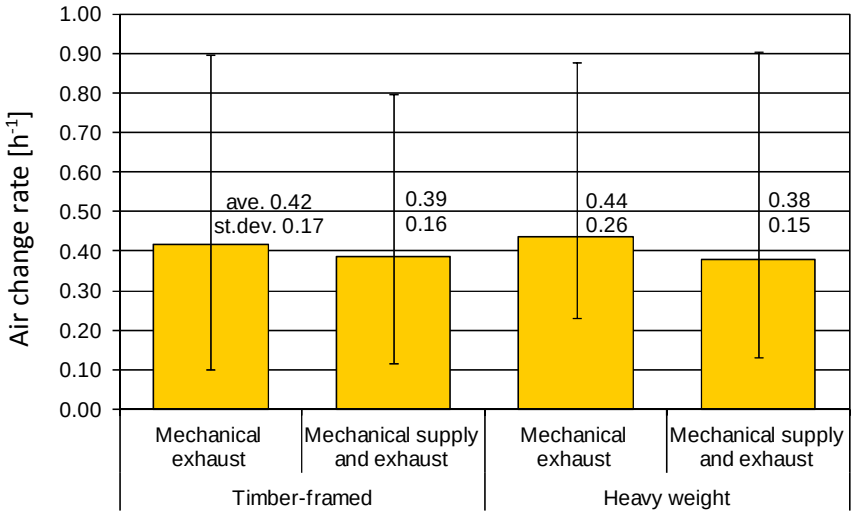

Figure 3.29 Average and standard deviation of air change rates in timber-framed and heavy weight detached houses.

3.3.4.2 Air tightness of timber-framed and heavy weight detached houses

Air tightness data from 100 timber-framed, 50 stone and 20 log houses was analyzed. The air tightness measurements have been performed with fan pressurization method according to the standard

[1].

First the normality of the data was analysed. The distributions of air change rate [h^{-1}] and air permeability [$m^3/(hm^2)$] for timber-framed, stone and log houses can be seen from Figure 3.30. Also the normal probability plots of the data sets have been plotted. Visually it seems that the data is close to normally distributed.

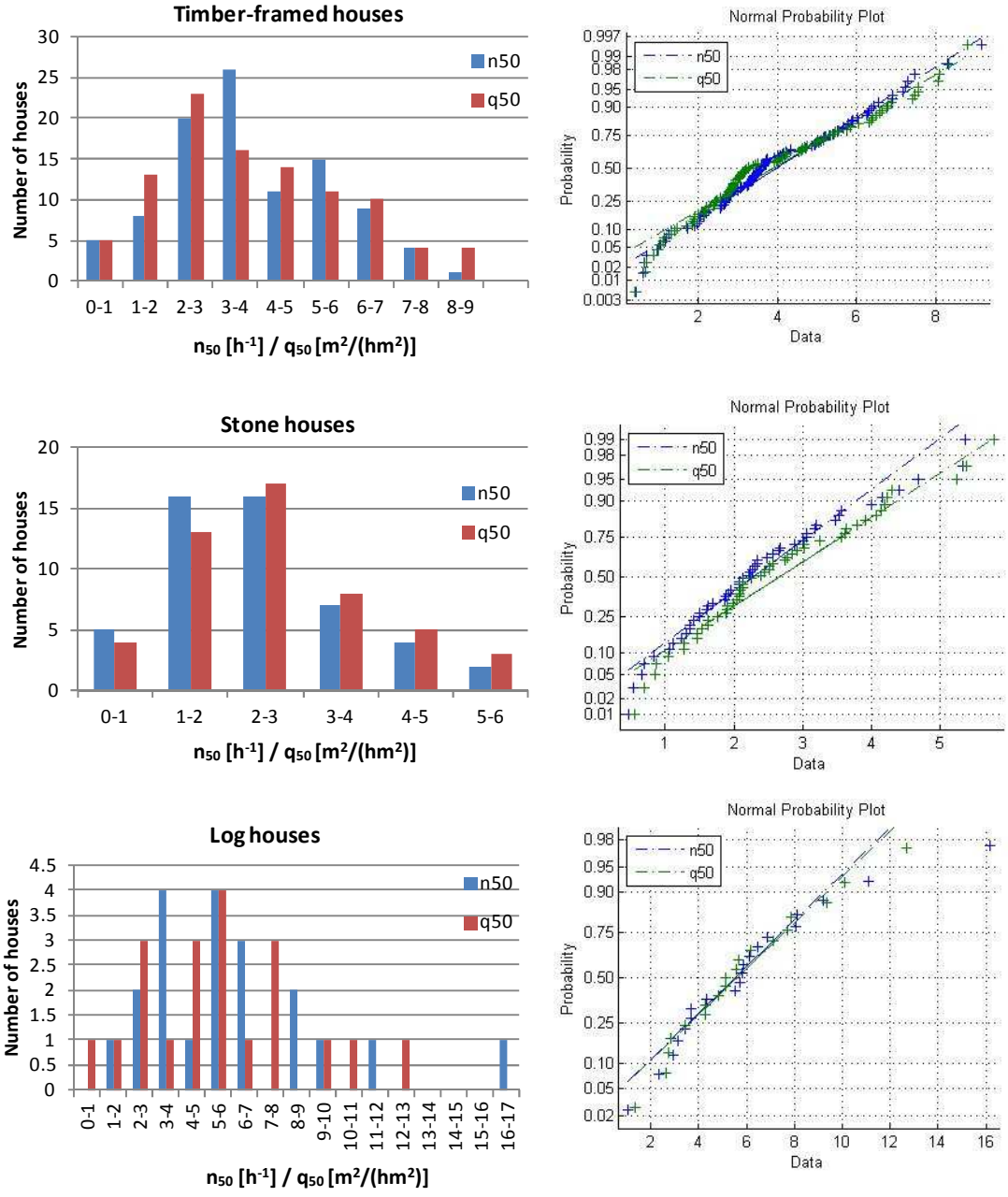

Figure 3.30 Distributions and normal probability plots of air change rate and air permeability. Air tightness tests for timber-framed, stone and log houses are presented.

Average air tightness and standard deviations of different house types are shown in Figure 3.31. It can be seen that there is difference between houses that have been built with different types of structures. Timber-framed houses and log houses have the highest average air permeability values. On the other hand, in every type of house there are also good air tightness values, which mean that good air tightness can be reached regardless of the choice of structure.

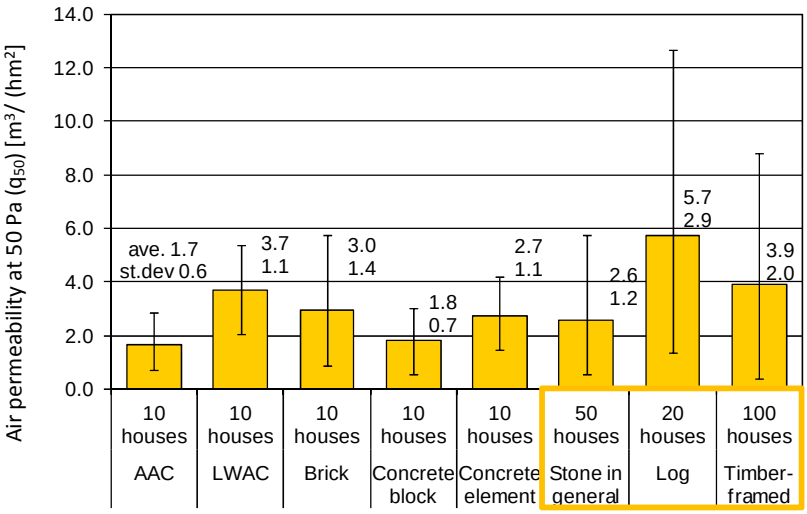

Figure 3.31 Air permeability q50 [m³/ (hm²)] of detached houses divided by different types of structures (stone-based, log and timber-framed houses). The mean values with standard deviations and the range of the results are shown.

The influence of the age of the house on the air tightness is shown in Figure 3.32. There are no statistically significant signs which would suggest that the age of the house influences the air tightness of the house. It should be noted that the measurement sample contains results only from a certain time period. For example the emphasis on building air tightness has changed clearly both in building practice and in regulations in Finland in the past ten years.

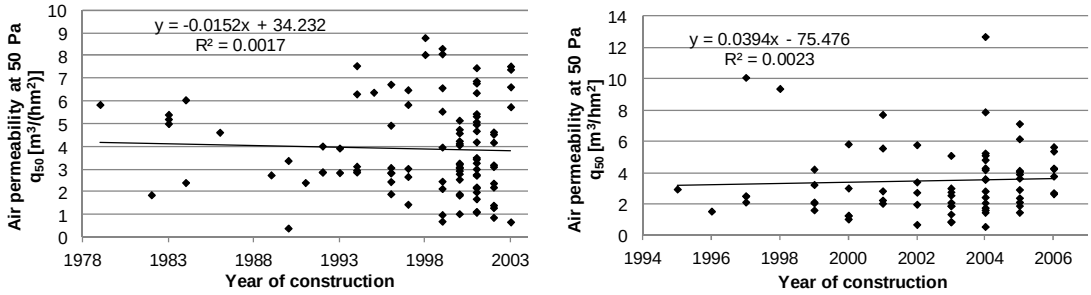

Figure 3.32 Influence of year of construction on air tightness of timber-framed houses (left) and heavy weight houses (right).

The subgroups of timber-framed houses were studied more thoroughly. The average air tightness of timber-framed houses grouped by ventilation type and combination of insulation and air barrier can be seen in Figure 3.33. It seems that houses with mechanical ventilation have been built more air tight than houses with natural ventilation. Also houses with polyurethane insulation seem to have been built more air tight than houses with mineral wool & plastic film or cellulose insulation & paper sheet.

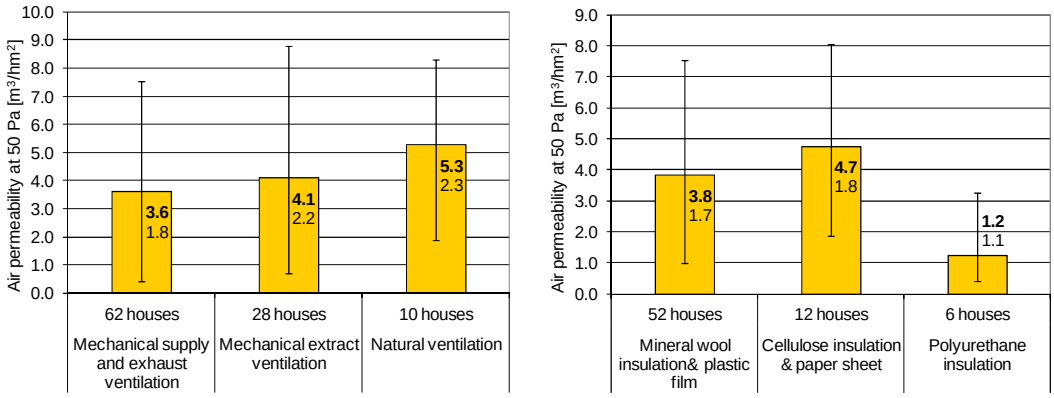

Figure 3.33 Air permeability of timber-framed houses at 50 Pa [$m^3/(hm^2)$] grouped by ventilation system (left) and by combinations of insulation and air barrier materials (right). The mean values with standard deviations and the range of the results are shown.

Also the influence of the way of construction was investigated in Figure 3.34. It seems that houses constructed on site are less air tight than prefabricated houses or houses built with pre-cut elements. The reason for houses constructed on site being less air tight, might be the need for manual labor and therefore the quality of workmanship.

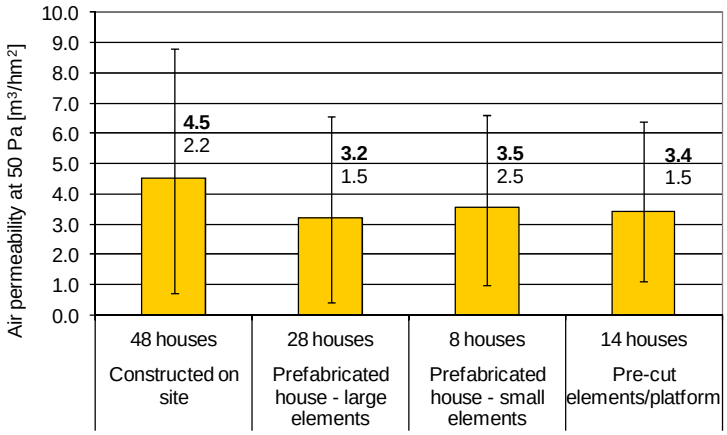

Figure 3.34 Air permeability of timber-framed houses at 50 Pa [$m^3/(hm^2)$] grouped by way of construction. The mean values with standard deviations and the range of the results are shown.

Also the heavyweight detached houses were studied more thoroughly. The influence of the ceiling type was investigated because according to thermal imaging the joint between the ceiling and the outer wall is the most common place for air leakages. The results are shown in Table 3.5. Although the sample size was small, the results suggest that when using a timber-framed ceiling the air change rate and air permeability of the house increases.

Table 3.5 Air change rates [h^{-1}] and air permeability [m^3/hm^2] of heavyweight houses divided by ceiling type.

Type of house	Houses with concrete or AAC ceiling			Houses with timber-framed ceiling		
	Amount of houses	Average n_{50}-value [h^{-1}]	Average q_{50}-value [m^3/hm^2]	Amount of houses	Average n_{50}-value [h^{-1}]	Average q_{50}-value [m^3/hm^2]
Autoclaved aerated concrete	9	1.5	1.6	1	2.3	2.0
Shuttering concrete block	3	1.2	1.6	7	1.8	2.0
Concrete element	2	1.2	1.6	8	3.0	3.0
Lightweight aggregate concrete	1	1.9	2.4	9	3.3	3.8
Total	**15**	**1.5**	**1.8**	**25**	**2.6**	**2.7**

3.3.4.3 Air tightness of apartment buildings

Air tightness measurements from 25 apartment buildings were investigated. The air tightness measurements have been performed for the whole buildings or at least for the whole stair case. When considering big buildings (multistory apartment building etc.) the air change rates and air permeability values differ from each other. The volume of the house increases faster compared to the area of the façade. For the 25 investigated apartment buildings the average n_{50}-value was 0.4 h^{-1} (st.dev. 0.2) and the average q_{50}-value 1.1 $m^3/(hm^2)$ (st.dev. 0.5). In Figure 3.35 is shown the distribution of air tightness measurements.

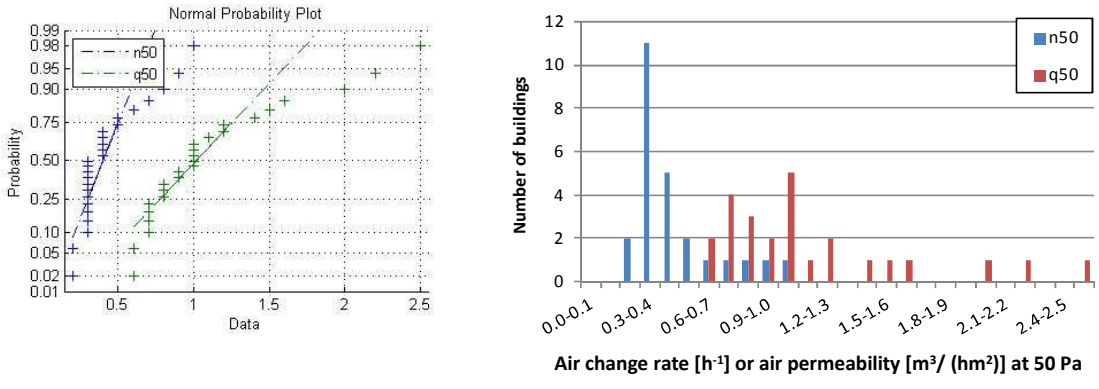

Figure 3.35 Distribution and normal probability plot of air change rate [h^{-1}] and air permeability at 50 Pa pressure difference in apartment buildings.

The influence of the shape of the house was investigated by comparing the n_{50}- and q_{50}-values with the shape factor of the house (Figure 3.36).

The shape factor is calculated by:

$$\frac{A_{facade}}{V} \tag{3.1}$$

where A_{facade} [m^2] is the area of the facade and V [m^3] the volume of the house.

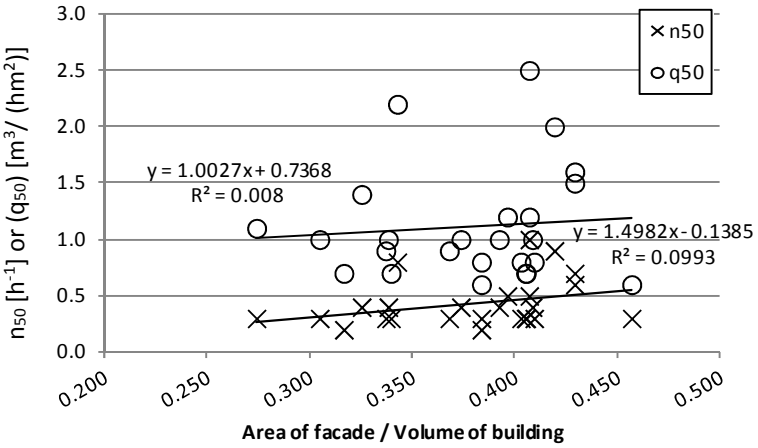

Figure 3.36 Effect of the shape factor (A_{facade}/V) on the air tightness of buildings (n_{50} [h^{-1}] or q_{50} [$m^3/(hm^2)$]).

3.3.5 Germany input (IBP)

3.3.5.1 Air tightness distribution

Air tightness of 81 residential buildings has been investigated. The measurements have been done via a blower door test by measuring the exhaust air flow rates at 50 Pa pressure difference caused by an exhaust ventilator located at the front door. The test has been performed according to [73] respectively

[1].

The principle is shown in Figure 3.37, Figure 3.38 shows an installed ventilator for a blower door test.

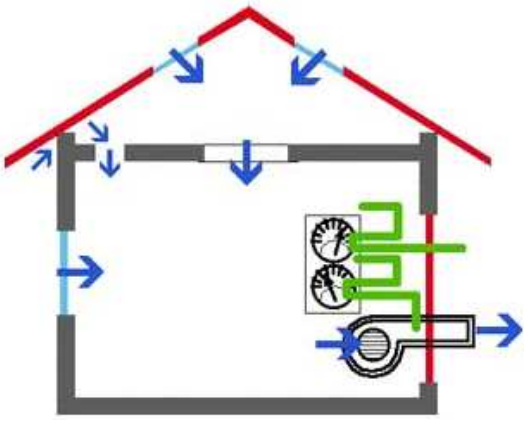

Figure 3.37 Principle of a blower door test.

Figure 3.38 Installed ventilator of blower door test (source: Wikipedia).

The distribution of air change rates (n_{50}) is shown in Figure 3.39 and cumulative distribution function in Figure 3.40. Most of the values are measured around 1.3 h^{-1}while the mean of the data is 1.77 h^{-1} with a standard deviation of 1.22. More information can be found in Table 3.6.

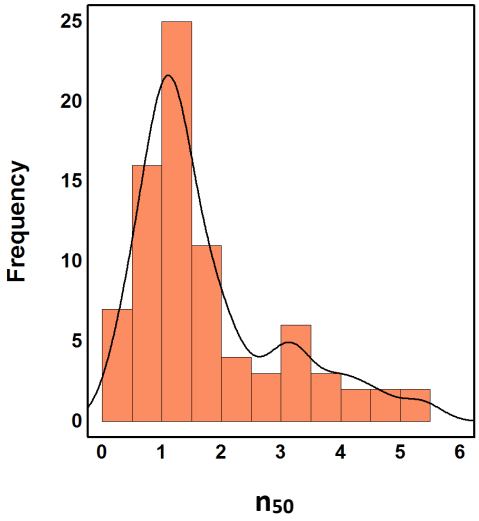

Figure 3.39 Distribution of air permeability at 50 Pa

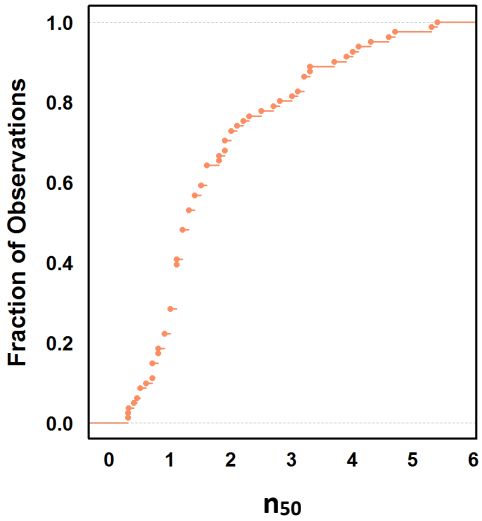

Figure 3.40 Empirical Cumulative Distribution Function of air permeability at 50 Pa

Table 3.6 Summary n_{50} data.

Min.	1st Qu.	Median	Mean	3rd Qu.	Max.	SD
0.03	1.00	1.30	1.77	2.20	5.4	1.22

It has also been investigated, if the n_{50} data follows the normal distribution. The results are shown in the normal probability plot of Figure 3.41.To verify this assumption a Shapiro Wilk test with has been performed. The results show a very high possibility that the data follows the normal distribution (probability of 3e-07 to reject the hypothesis of normal distribution).

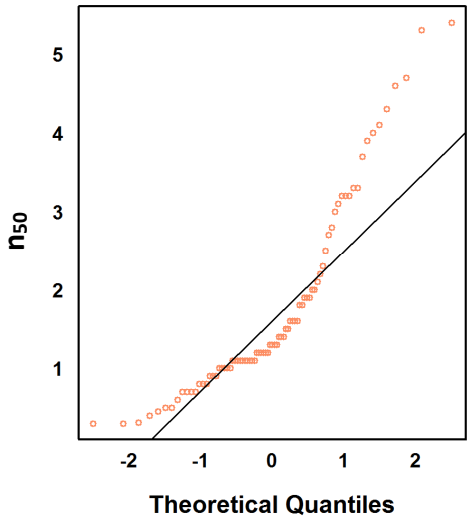

Figure 3.41 Normal probability plot for n_{50} values.

3.3.5.2 Air tightness per building type

Average air tightness and standard deviations of different house types are shown in Figure 3.42.

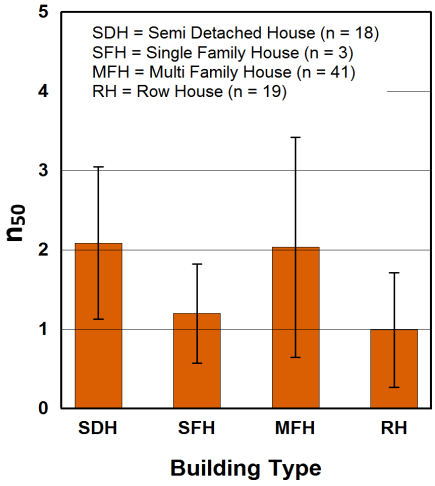

Figure 3.42 Mean n_{50} values grouped by building type and their error bars (standard deviation).

Differences in n_{50} values between the buildings types can be identified; however, the statistical significance of deviations has not been tested via anova. The lowest n_{50} measurements have been taken at single family and row houses, however, with a relative small sample size only 3 single family houses being measured.

3.3.5.3 Air tightness correlations

The following section analyses if there is a correlation between n_{50} values and other parameters of the building.

At first the influence of the building volume and size of the enclosing external area have been investigated (Figure 3.43, Figure 3.44). The plots indicate that there seems to be no correlation between air tightness and the building volume or surrounding area. The values are rather wide spread and the linear correlation does not show any tendencies. This assumption is supported by Spearman's correlation tests which suggest only a correlation of 0.05 for both the building volume and external area.

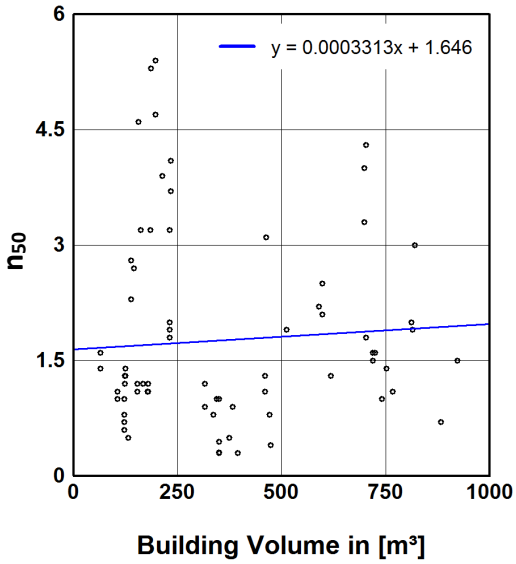

Figure 3.43 Correlation between n_{50} and building volume.

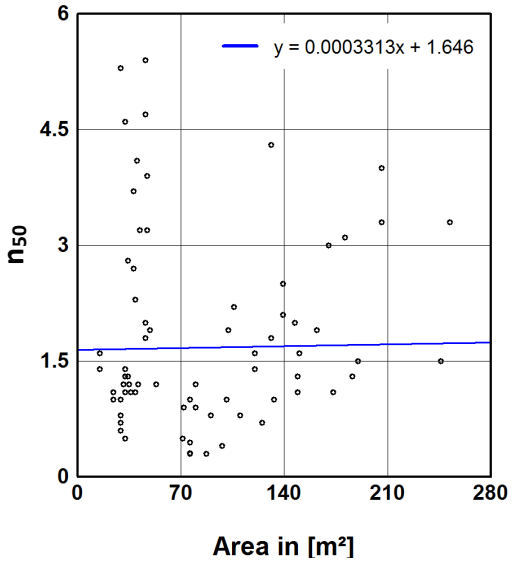

Figure 3.44 Correlation between n_{50} and building envelope area.

In contrast, the number of occupants is likely to be linked to the air tightness, while the occupancy per m² treated floor area remains uncertain. At least a mathematical correlation can be found by using the Spearman correlation test which result in-0.53 for testing number of occupants and 0.14 for occupancy per floor area. The scatterplots including the regression lines are shown in Figure 3.45 and Figure 3.46.

.

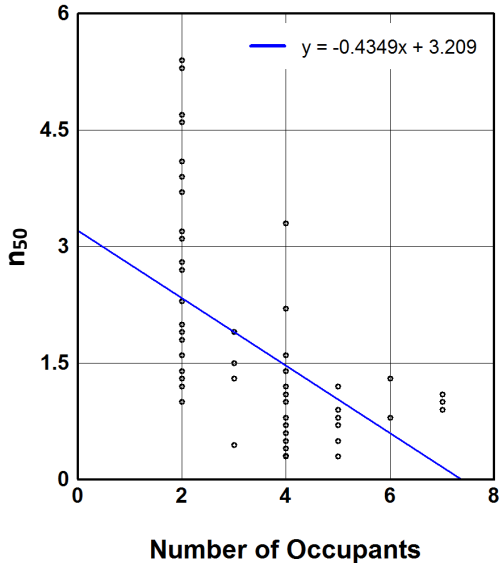

Figure 3.45 Correlation between n_{50} and number of occupants.

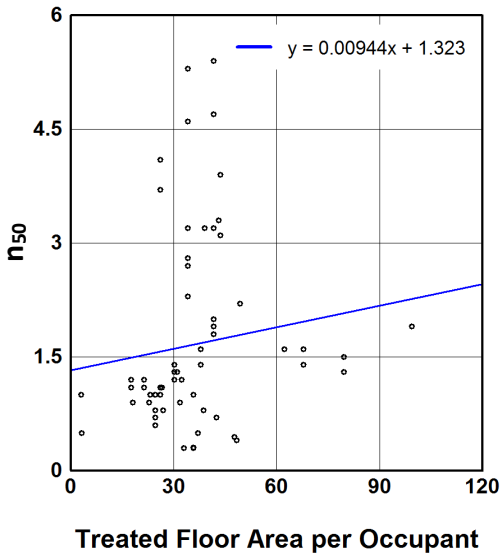

Figure 3.46 Correlation between n_{50} and treated floor area per occupant.

Not unexpected comes the negative correlation between construction year and n_{50} measurements (Figure 3.47). As building regulations are continuously getting stricter and improvements in building construction have been made over the years, the air leakage is steadily decreasing.

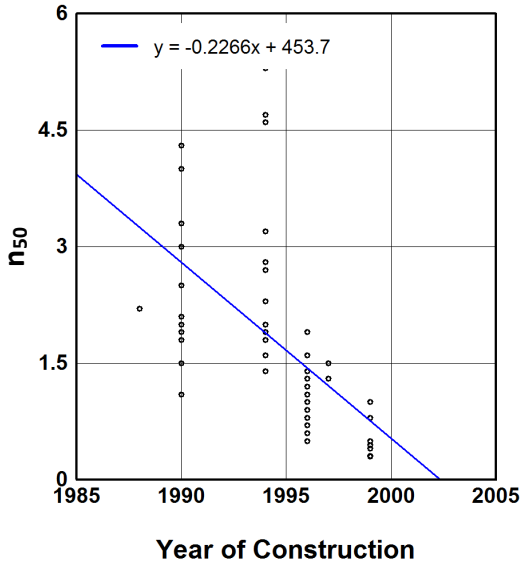

Figure 3.47 Correlation between n_{50} and year of construction.

3.3.6 Portugal [UP] – Airtightness in refurbished social housing of Porto

3.3.6.1 Collected raw data

The air permeability measurements were carried out using the Retrotec1000 blower door model. The standard

[1] was applied in the tests, following method A described in the standard. In each dwelling, both pressurization and depressurization tests were performed. The in situ measurements were done in four days of two consecutive weeks during spring, with average temperature ranging from 13.5 °C to 21.0 °C . The wind velocity during tests varied between 1.2 m/s and 2.4 m/s. The values obtained in the tests of pressurization and depressurization were averaged and are presented in Figure 3.48. The dwellings without modifications are shaded in the graph.

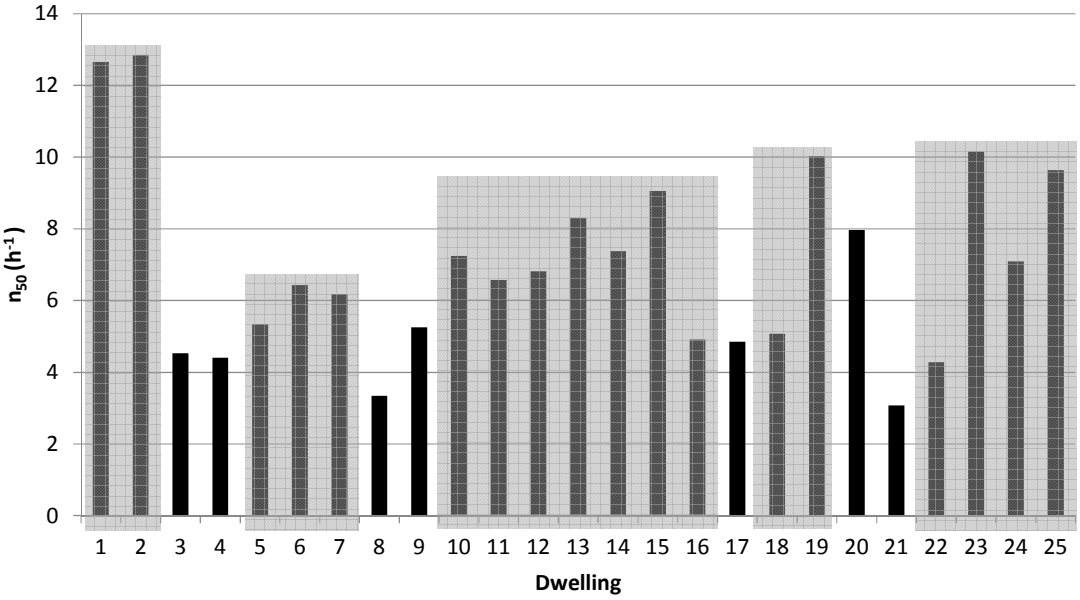

Figure 3.48 Measured n_{50} values (shaded results correspond to non-modified dwellings).

3.3.6.2 ANALYSIS AND STOCHASTIC DATA

The cumulative distribution of the measured data is presented in Figure 3.49.

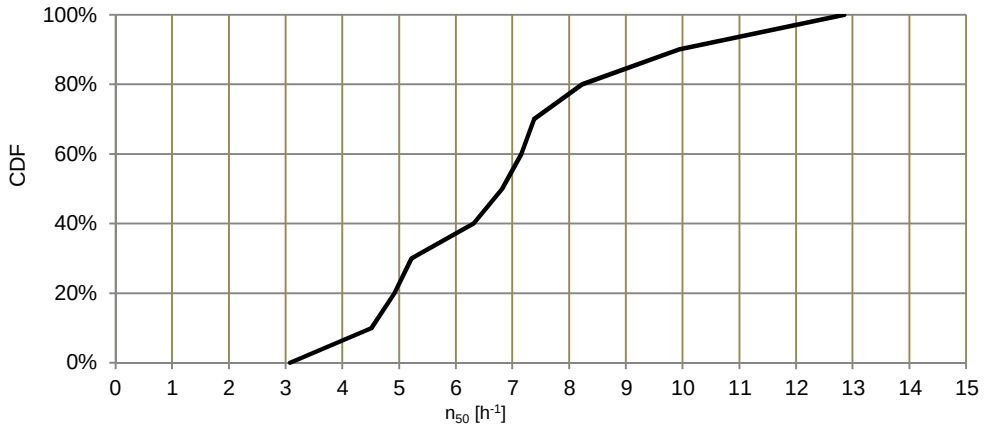

Figure 3.49 CDF of Measured n_{50} values.

The evaluation of window opening action relied on questionnaires that were supposed to be filled every day of the surveying period. The outdoor temperature effect was therefore considered to be the same for all the dwellings. With that information, the total number of hours

users said the windows were opened was divided by the number of days the survey took place in each dwelling resulting in the NWO parameter, expressed in hours/day. The correlation between that parameter and airtightness is presented in Figure 3.50. It shows a tendency of decreasing hours of opened windows with the increase of n_{50} especially if the number of users per dwelling is included in the analysis. This observation confirms that, turning the dwellings more airtight without a working ventilation system compels the users to increase ventilation by opening windows. Of course that this is more a trend than an actual correlation as user behaviour is complex and cannot be assessed in a too simplified way.

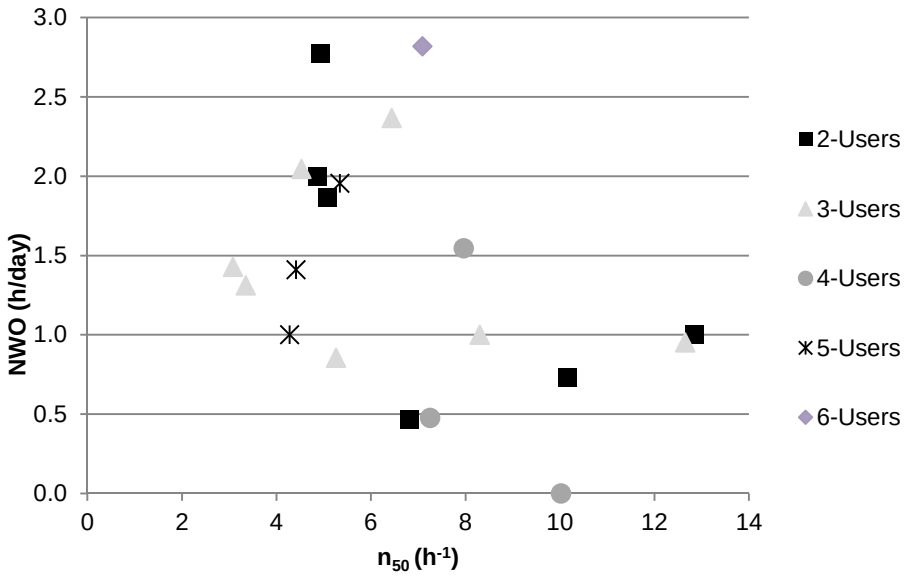

Figure 3.50 n_{50} vs. NWO.

3.3.7 Sweden [SP] – Airtightness in refurbished Swedish buildings

The detailed data for 15 measured apartments is presented in the Digital Appendix. Figure 3.51 presents the overall results.

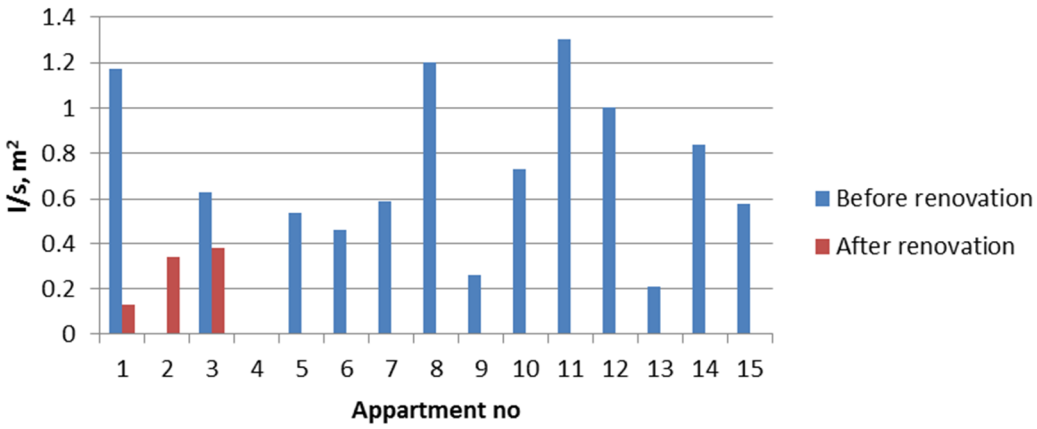

Figure 3.51 Measured air-tightness of 15 apartments.

3.3.8 United Kingdom [UCL] – Airtightness in the Warm Front study

3.3.8.1 Collected raw data

A total of 221 (40 pre- intervention, 113 post-intervention, and 30 both pre- and post-intervention) sets of data were collected from a subsample of dwellings with physical dwelling characteristics given in

Table 3.7. The sample dwellings were principally terraced and constructed between 1900-1950. The walls are most likely to be cavity masonry with most of the remaining dwellings having solid brick walls.

Table 3.7 Dwelling characteristics of sample in which air infiltration rate measurements were taken.

Age		Wall type		Building type	
Pre 1900	15 %	Cavity masonry	66 %	Terraced	57 %
1900-1950	50 %	Solid brick	33 %	Semi-detached	33 %
1951-1976	32 %	Timber framed	0.5 %	Flats	9 %
Post 1976	3 %	Other	0.5 %	Detached	1 %

A fan pressurization test was used to measure the whole dwelling air flow rate due to infiltration at a pressure differential of 50Pa. All open flues and vents were kept open during the test in order to measure infiltration under normal operating conditions.

3.3.8.2 Analysis

3.3.8.2.1 Post-processing of raw data

To compare different buildings, the air flow rate at the pressure differential of 50Pa was divided by the building envelope area to obtain the permeability ($m^3/hr/m^2$). Measurements for dwellings tested twice with no intervention in between replaced with the mean permeability of both tests.

3.3.8.2.2 Statistical summary

Table 3.8 Summary statistics for distribution of permeabilities in pre- and post-intervention samples.

	Pre-Warm Front	Post-Warm Front
Number of dwellings	60	127
Mean permeability ($m^3/hr/m^2$)	17.7	16.7
Median permeability ($m^3/hr/m^2$)	16.6	15.8
Standard deviation permeability ($m^3/hr/m^2$)	7.0	7.2

Carrying out a two-sample Kolmogorov-Smirnov test on the pre- and post- intervention permeabilities (Table 3.8) finds the null hypothesis that the two distributions are drawn from the original parent distribution cannot be rejected at the 5 % significance level.

3.3.8.3 Stochastic data sets

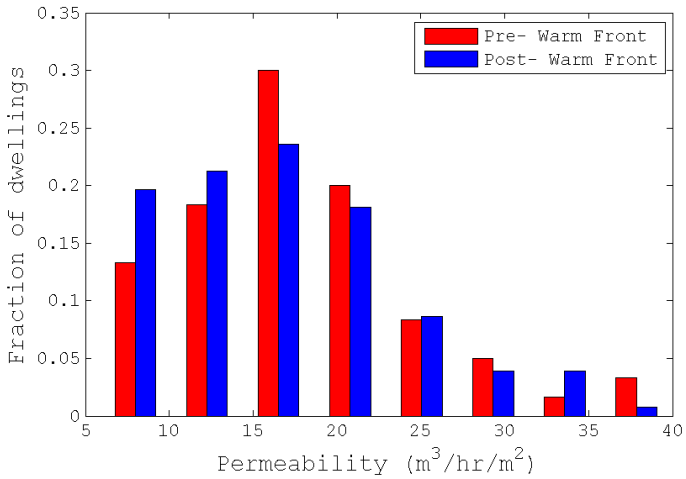

Figure 3.52 Distribution of permeabilities for dwellings pre- Warm Front intervention and post-Warm Front intervention.

Figure 3.52 shows the distribution of permeabilities for the pre- and post- intervention samples that can be used in stochastic analyses.

3.4 Indoor loads

3.4.1 Canada input: Indoor Temperature and Humidity Distributions in 22 Rooms of a Multi-Unit Residential Building [BCIT]

Brief description of the project is presented in section 2.3, where the indoor temperature and excess humidity distributions of the 22 rooms during the winter and summer periods are presented. Excess humidity is defined as the difference between the indoor and outdoor absolute humidities, quantities that are derived from the simultaneously measured temperature and relative humidity of the indoor and outdoor locations. In this study, the winter and summer periods are defined from December to February and from June to August, respectively.

3.4.1.1 Measurement methods

To assess the level of variations in temperature and humidity among the rooms in the same Suite, temperature and relative humidity data loggers (HOBO Onset U12-011 and Onset U12-013) are placed in each bedroom, kitchen, bathroom and living room of each suite. In addition, two data loggers are installed in the north and east corridors, one each, to simultaneously capture the corridor air temperature and relative humidity conditions. The HOBOs' log data every two minutes, and the data is downloaded on a computer once a month. To correlate the indoor and outdoor climatic conditions, the local outdoor air temperature and relative humidity are measured every minute and downloaded to a computer once a month. The weather sensors are bought for the project and assumed to be within the manufacturer's calibration range. The indoor temperature and humidity data loggers (HOBOs) are calibrated in-house using a climatic chamber. Figure 3.53 shows the temperature and relative humidity readings of the data loggers at the three reference environments: 35 %, 52 % and 70 % relative humidity and 21^{o}C. As shown in the figure, the HOBOs readings at all three settings are consistent. The relative humidity difference between the maximum and the minimum readings at given set points are under 2.5 %. Thus in general, the accuracies of the data loggers are within the range of the manufacturer specifications (2.5 %).

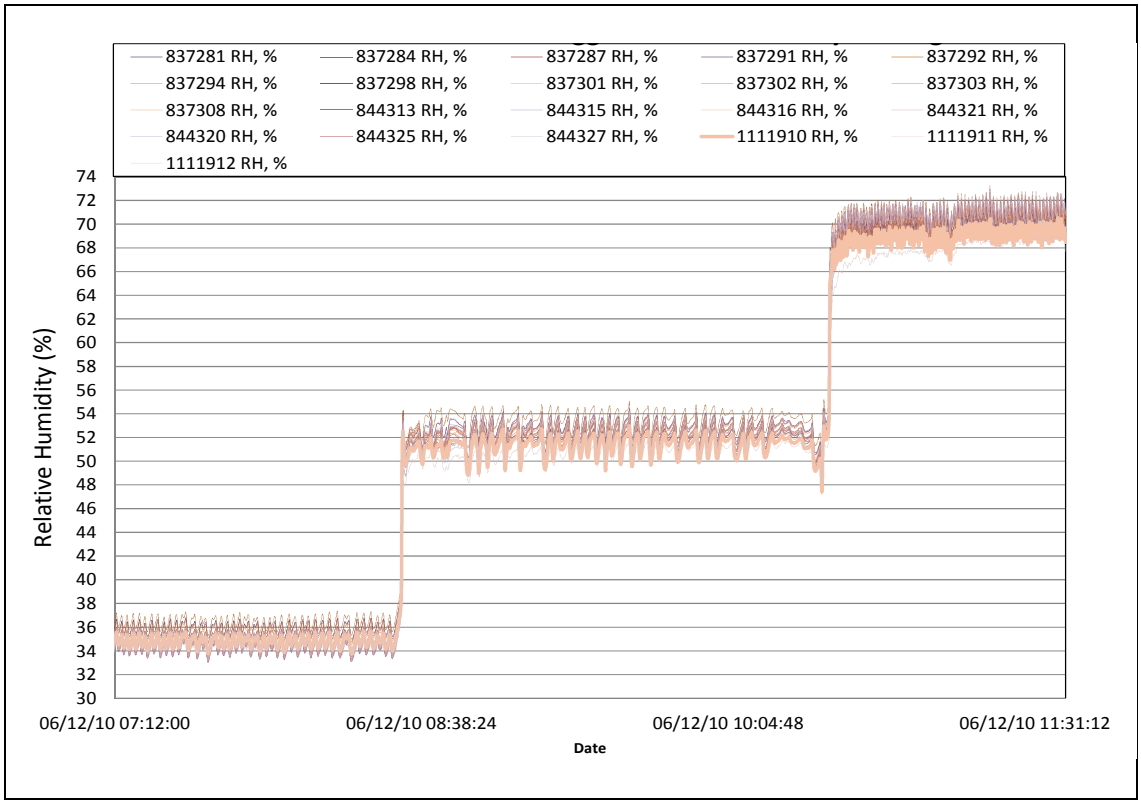

Figure 3.53 Relative humidity readings of HOBO data loggers during the calibration process.

3.4.1.2 Indoor temperature distributions within Suites

3.4.1.2.1 Winter period

The average winter temperatures of the 22 rooms are shown in Figure 3.54 (a). During the winter period, the seasonal average temperature of the rooms in Suite 'A' can vary from 17.9 °C (in the Living Room) to 20.7 °C (in the Master Bedroom), which results in a maximum seasonal average temperature difference of 2.8 °C. The average temperature in the Kitchen, Bathroom and Bedroom-2 are about the same (19.5 °C). Temperature variation within the rooms is relatively higher in the Living Room followed by the occupied bedrooms as shown in the standard deviation plots in Figure 3.55. The Living Room temperature has a standard deviation of 1.7 °C, and is between 14.5 °C and 21.3 °C for 95 % of the winter period. In comparison, the Bathroom and the Kitchen have a relatively narrower temperature variation (standard deviation of 0.8 °C). The seasonal average temperatures of the rooms in Suite 'B' vary from 16.8°C (in the Bedroom-2) to 17.8 °C (in the Bathroom). Not only the seasonal average temperatures of the rooms are about the same (difference between rooms less than 1 °C), but also the magnitude of temperature variations within the rooms are similar. The standard deviations of the temperature variation in the Suite vary from 0.8 °C (in the Master Bedroom) to 1.2 °C (in the Living room and Bathroom), Figure 3.55. In Suite 'C', the Bathroom has the highest seasonal average temperature (23.6 °C), followed by the Living Room (21.5 °C). The Bedrooms have similar seasonal average temperatures (20.0 °C), which is about 3.6 °C less than the Bathroom temperature. The temperature variations within the rooms seem to be low as the standard

deviation values (0.7 °C to 1.0 °C) are indicated in Figure 3.55. Similar to Suite 'C', the Bathroom and the Living Room in Suite 'D' have high seasonal average temperatures, 22.5 °C and 21 °C, respectively. In comparison to the other rooms, the Kitchen has the lowest seasonal average temperature (18.9 °C) and relatively high temperature variation (standard deviation of 1.2 °C). In general, the Bathrooms in Suite 'C' and 'D' have relatively high temperatures, and the temperature difference between the rooms excluding the bathrooms are within 1.0 °C to 2.0 °C.

3.4.1.2.2 Summer period

Figure 3.54 (b) and Figure 3.55 show the average summer temperature in different rooms of the four Suites as well as the corresponding standard deviations, respectively. The seasonal average temperature in Suite 'A' varies from 25.0°C in the Bathroom to 23.4°C in the Bedroom-3, and around 24°C in the other four rooms. Thus, the maximum seasonal variation between the rooms in Suite 'A' is in the range of 1.0 to 1.5°C. The temperature fluctuations within the rooms are relatively high in the summer when compared to that of the winter period as shown in the standard deviation plots in Figure 3.55. In general, the rooms have about the same temperature fluctuation (standard deviation of 1.8°C) in the summer period, while slightly different temperature fluctuations in different rooms are observed during the winter period (standard deviation of 0.8 to 1.6°C). The rooms in Suite 'B' have about the same seasonal average temperatures (24°C) except the Bathroom room, which has 1°C more than the other rooms. In this Suite, the temperature fluctuations within the rooms are nearly the same and have standard deviation about 1°C, Figure 3.55. The rooms in Suite 'C' have relatively higher seasonal average temperature compared to the other Suites, Figure 3.54. The temperature differences between the rooms except the Bathroom are less than 0.7°C. The seasonal average temperature in the Bathroom is 29.8°C, which is about 3.5°C more than the other rooms. The temperature fluctuations within the rooms are about the same (standard deviation of 2°C). As in Suite 'A', the temperature fluctuations within the rooms are relatively high during the summer period when compared to that of the temperature fluctuation during the winter period (in the cases of Suite 'C' about two times). The seasonal average temperatures of the rooms in Suite 'D' are nearly the same (24.9°C to 25.5°C), which a variation of below 0.6°C. Inconsistent with the observation made in Suite 'A' and Suite 'C' the temperature variation within the rooms in Suite D during the summer period are relatively high (standard deviation between 2.2 to 2.5°C standard deviation).

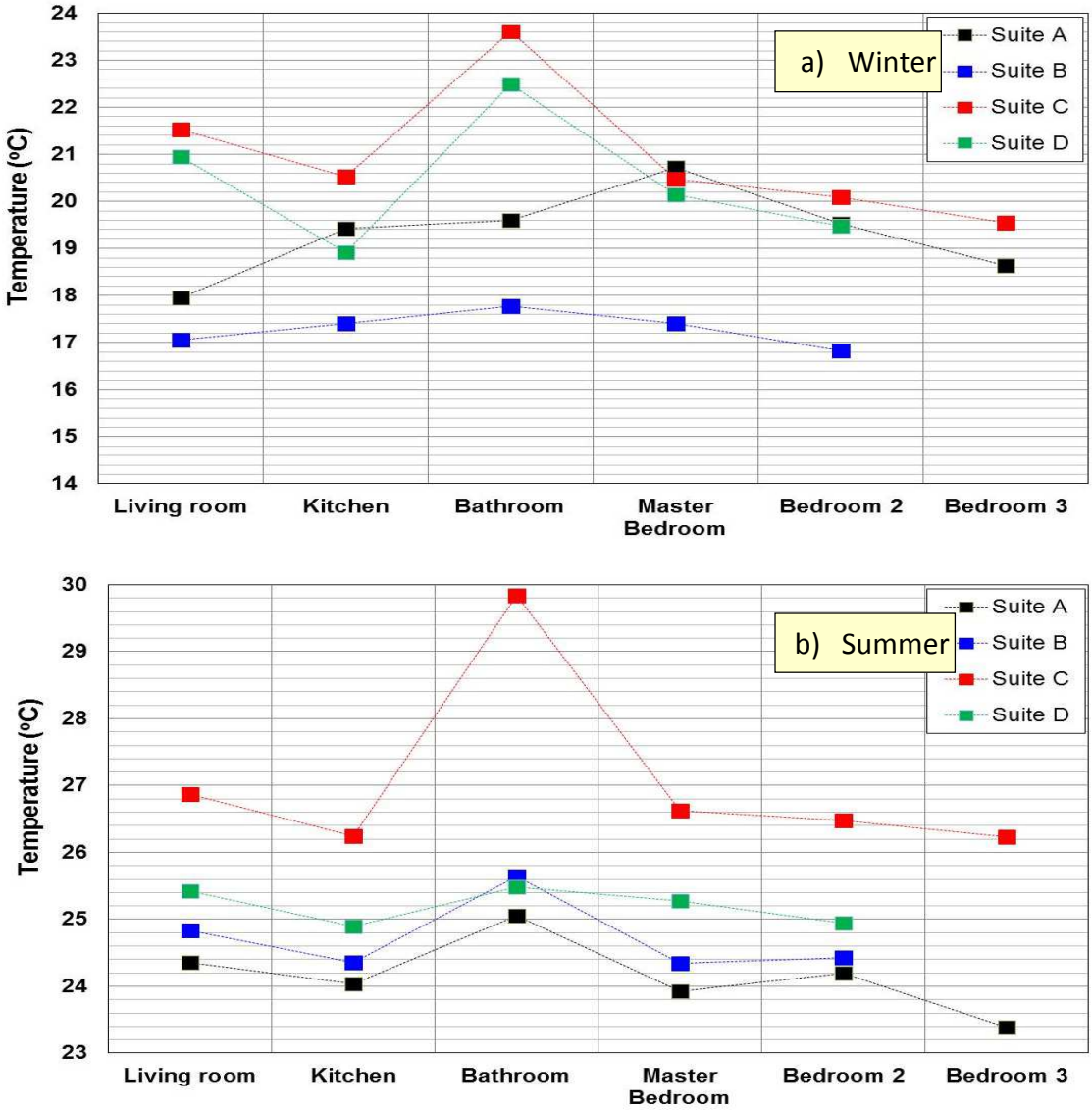

Figure 3.54 Average temperatures of the rooms during the Winter (a) and Summer (b) periods.

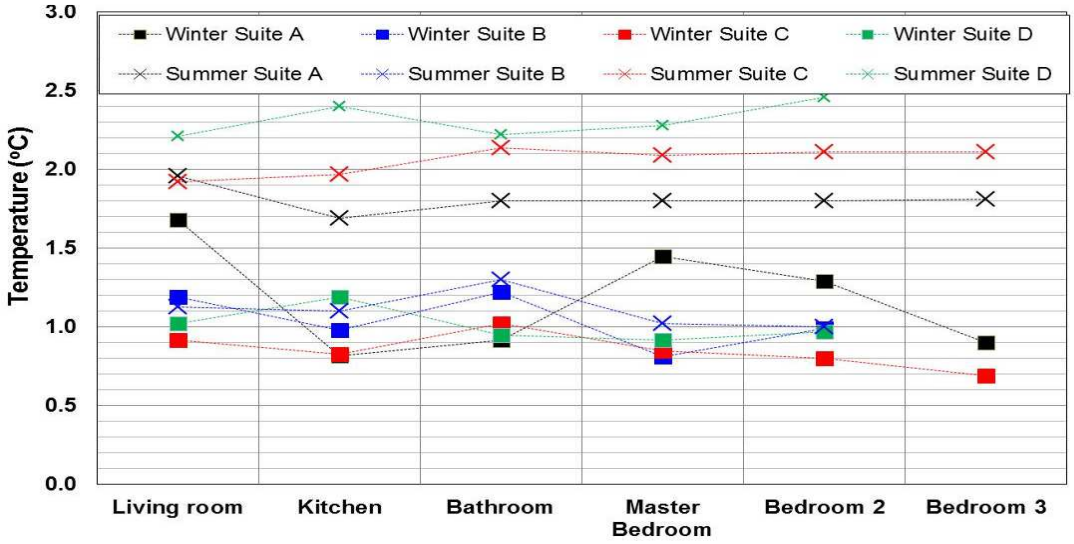

Figure 3.55 Standard deviation of temperature variations in the rooms during the Winter and Summer periods.

3.4.1.3 Excess humidity distribution within Suites

3.4.1.3.1 Winter period

The seasonal average excess humidity in the Living rooms, Kitchens, Bathrooms and Bedrooms of the four Suites are presented Figure 3.56. As can be seen in the figure, the excess humidity in Suite 'A' varies from 2.5 g/m^3 in the Bedroom-3, which is used as storage, to 4.5 g/m^3 in the Master Bedroom. The Living room and Bathroom have excess humidity of 2.7 g/m^3 and 2.9 g/m^3, respectively. The excess humidity fluctuation in the Master Bedroom is significantly high (standard deviation of 1.5 g/m^3) compared to the other rooms, which varies between 0.8 to 1.0 g/m^3, Figure 3.58. The relatively high excess moisture variations between rooms in Suite A is due to the change in occupant habits (occupants occasionally use a portable humidifier during the winter period). In Suite 'B' the seasonal average excess humidities in the rooms are nearly the same (4.5 g/m^3), Figure 3.56. Similarly, as shown in Figure 3.58, the excess humidity fluctuations within the rooms are about the same (1.2 g/m^3). A similar situation is observed in Suite 'C', where the excess humidity in the rooms have about the same seasonal average values (4.3 to 4.8 g/m^3) and fluctuations (standard deviations 1.0 to 1.2 g/m^3). Based on the average and standard deviation values presented here, the excess humidity in Suite 'B' and 'C' can be assumed to be distributed uniformly within the respective Suites. As can be seen in Figure 3.56, the excess humidity in Suite 'D' is significantly high in the Kitchen (3.1 g/m^3) when compared to the other rooms, which have seasonal average of 2.3 to 2.5 g/m^3. The excess humidity fluctuations in all the rooms except the Kitchen are about the same (standard deviation of 0.8 g/m^3), while the Kitchen has a standard deviation of 1.6g/m^3. Thus, the excess humidity distributions in all the rooms of Suite D except the kitchen can be represented with the same excess humidity distribution parameters.

3.4.1.3.2 Summer period

The seasonal average excess humidities of the 22 rooms and the standard deviations that indicate the excess humidity fluctuations within the rooms are presented in Figure 3.57 and Figure 3.58, respectively. As shown in the Figure 3.44, the Master Bedroom and the Kitchen have slightly higher excess moisture (2.3 and 2.5 g/m^3, respectively) compared to the other rooms, which have about 1.6 g/m^3. The excess humidity fluctuations within the rooms, however, are comparable and are within 0.75 to 1.0 g/m^3 standard deviation. The excess humidity in Suite 'B' seems to be uniform across the various rooms (seasonal average value of 3.5 g/m^3). The difference between the rooms' average excess humidity values are less than 0.5 g/m^3. Moreover, the excess humidity fluctuations within the rooms are similar and all have about 1.0 g/m^3 standard deviation. In Suite 'C', the bedrooms have slightly higher excess humidity (3.0 to 3.5 g/m^3) when compared to the Living room (2.6 g/m^3). The standard deviation of the excess humidity fluctuation within the Kitchen is 1.2 g/m^3 while the other rooms have about the same standard deviations (1.0g/m^3). The excess humidity in Suite 'D' is low compared to the other Suites. The average excess humidities in all the rooms except in the Kitchen are between 1.3 to 1.6 g/m^3, while the Kitchen has 3.0 g/m^3. Although some difference between the rooms are expected, the excess humidity deviation between the Kitchen and the other rooms are quite significant, which suggests that the HOBO in the 'Kitchen' must have been defective. Similarly, the excess humidity fluctuations within the rooms are quite the same, except in the Kitchen. They have a standard deviation of 0.8 g/m^3 while the Kitchen's is 2.8 g/m^3.

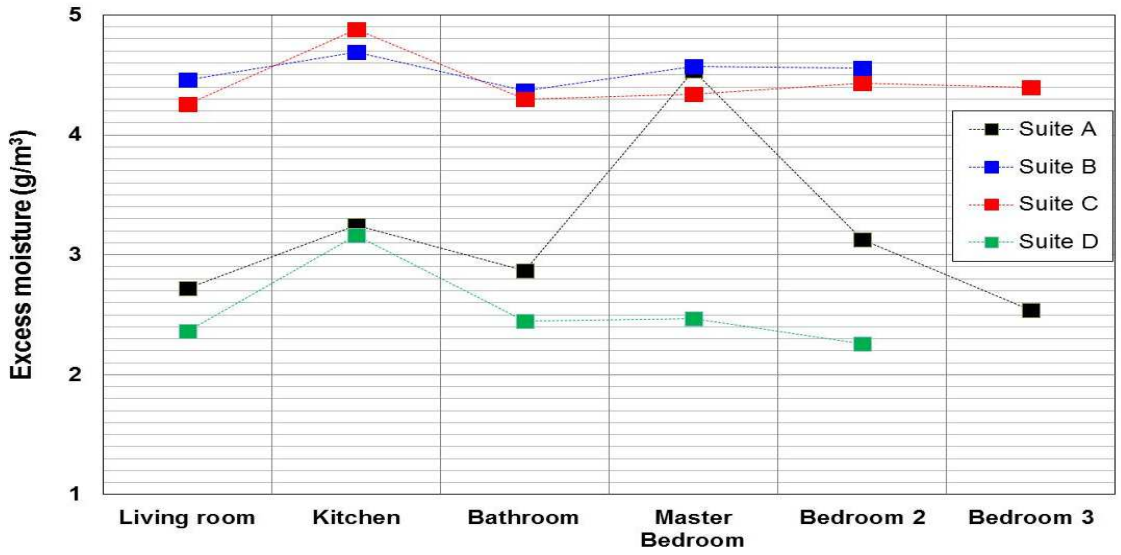

Figure 3.56 Average excess humidity of the rooms during the Winter period.

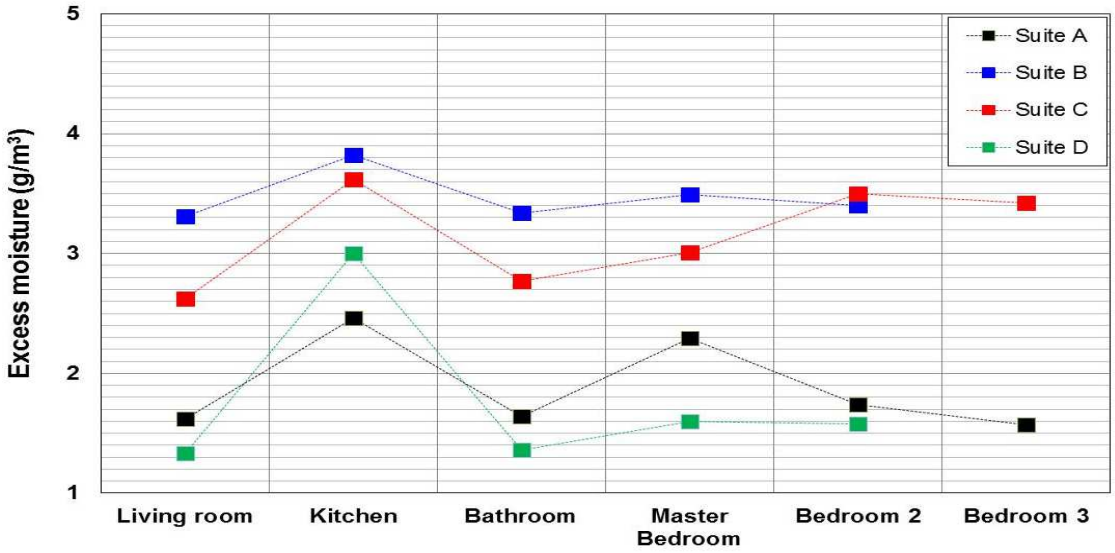

Figure 3.57 Average excess humidity of the rooms during the Summer period.

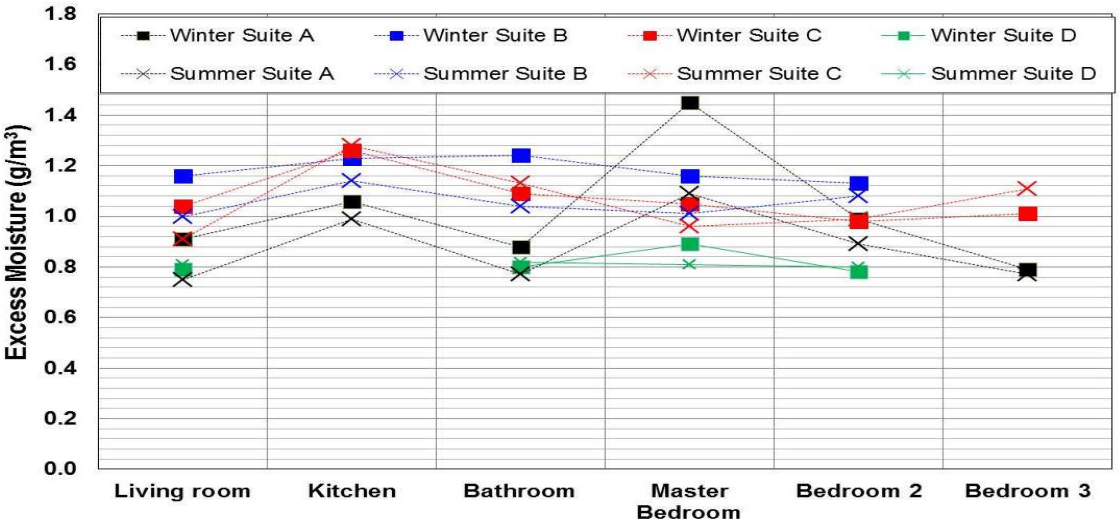

Figure 3.58 Standard deviation of excess humidity variations in the rooms during the Winter and Summer periods.

3.4.1.4 Suites' average temperature and excess humidity

The temperature and excess moisture distributions in various rooms of the four Suites are presented in the previous sections. Here, the average temperature and excess moisture distributions of the suites are presented. The measurements in the bathrooms and kitchens are excluded from the set of data used for averaging since the temperature readings in the bathrooms and the calculated excess moisture values in the kitchens tend to deviate significantly from the other rooms' data. The Suites' average temperature distributions during the winter and summer periods are presented in Figure 3.59.

During the winter period, the average indoor temperature of the Suites varies from 17°C in Suite 'B' to 20.4°C in Suite 'C', while Suites 'A' and 'D' have an average temperature of 19°C and 20.2°C, respectively. In general, Suite 'B' is relatively cold and has high temperature fluctuation (standard deviation of 1.8°C). Suites 'C' and 'D' are relatively warm and the former has slightly lower temperature fluctuation (standard deviation of 0.9°C).

The Suites average temperatures during the summer varies from 24°C in Suite 'A' to 26.6°C in Suite 'C'. Suite 'B' and Suite 'D' have an average temperature of 24.5°C and 25.2°C, respectively. As can be seen in

Figure 3.46 (b), the temperature distribution curve in Suite 'B' is narrow (lowest standard deviation value 1.0°C) while the other Suites have wider distributions (standard deviation between 1.8°C in Suite 'A' to 2.3°C in Suite 'D'). Thus, Suite 'C' can be characterized as a Suite with high summer indoor temperature and fluctuations.

Figure 3.60 shows the average excess moisture distributions in the four suites. In general, the excess moisture distributions in the suites can be classified as low, medium and high during the winter period, Suite 'D', Suite 'A' and Suites 'B' and 'C', respectively. The corresponding seasonal average values are 2.3 g/m^3, 3.2 g/m^3, and 4.3 g/m^3 and 4.5 g/m^3, respectively. Of the four Suites, Suite 'A' has a high fluctuation of excess humidity (standard deviation value of 3.8 g/m^3) when compared to the other Suites', which are in the range of 0.8 to 1.2 g/m^3. The significantly high fluctuation in Suite 'A' is caused by the occupants' use of portable humidifier during the winter period.

As can be seen in Figure 3.60, the excess humidity in the Suites during the summer period can be classified as low (Suite 'A' and 'D') and high (Suite 'B' and 'C'). The average excess humidity in Suite 'A', 'B', 'C' and 'D' are 1.8 g/m^3, 3.4 g/m^3, 3.2 g/m^3 and 1.5 g/m^3, respectively. Regardless of the high and low excess humidity grouping, the excess humidity fluctuations in all of the Suites are similar (standard deviations between 0.8 to 1.0°C). Based on the temperature and excess moisture distribution curves, Suite 'C's indoor conditions may represent the worst case scenario where the indoor temperature is low and the excess moisture is high—a combination that may result in durability issues and an increased mold growth risk.

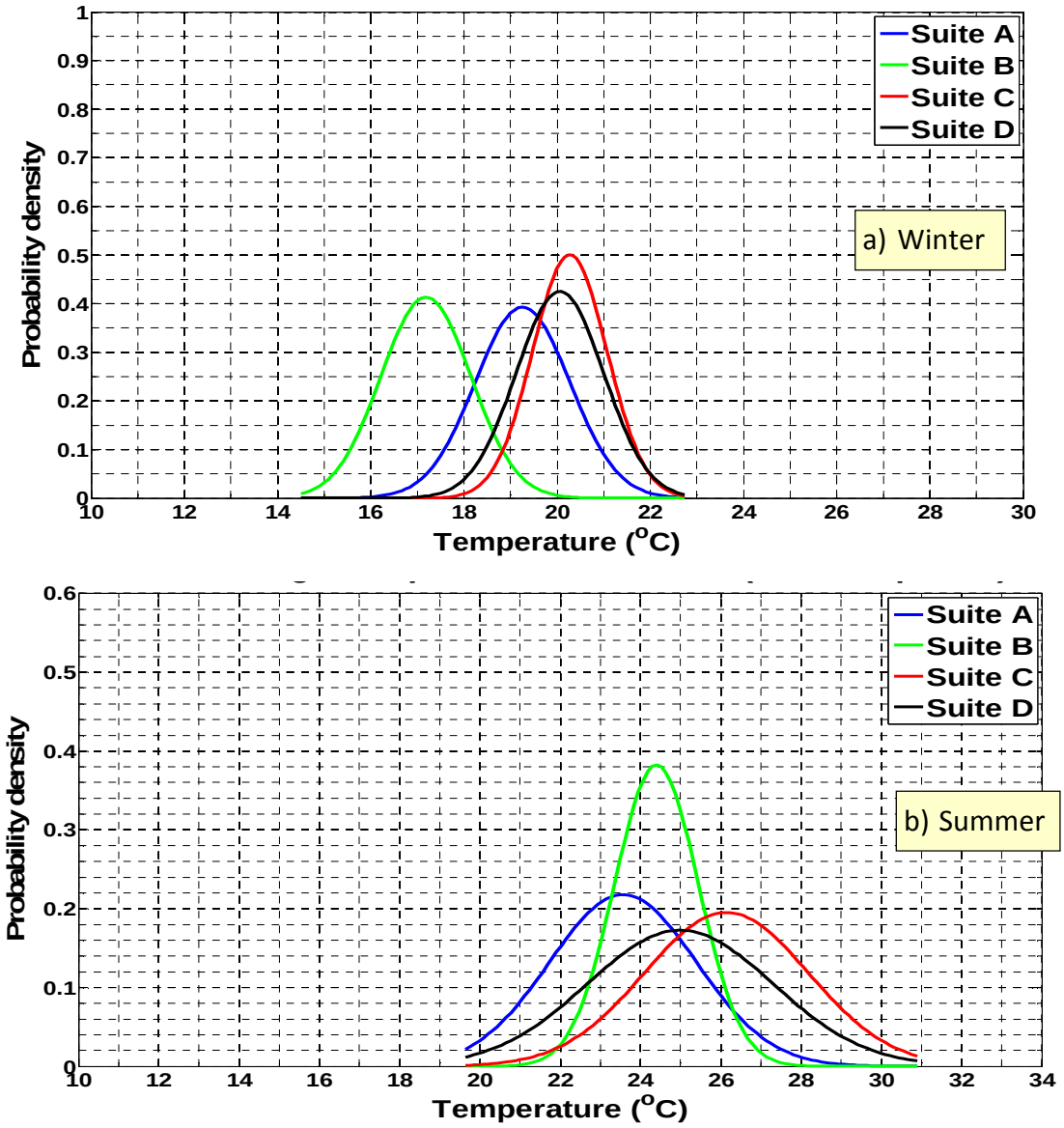

Figure 3.59 Suites average indoor temperature distributions during Winter (a) and Summer (b) period.

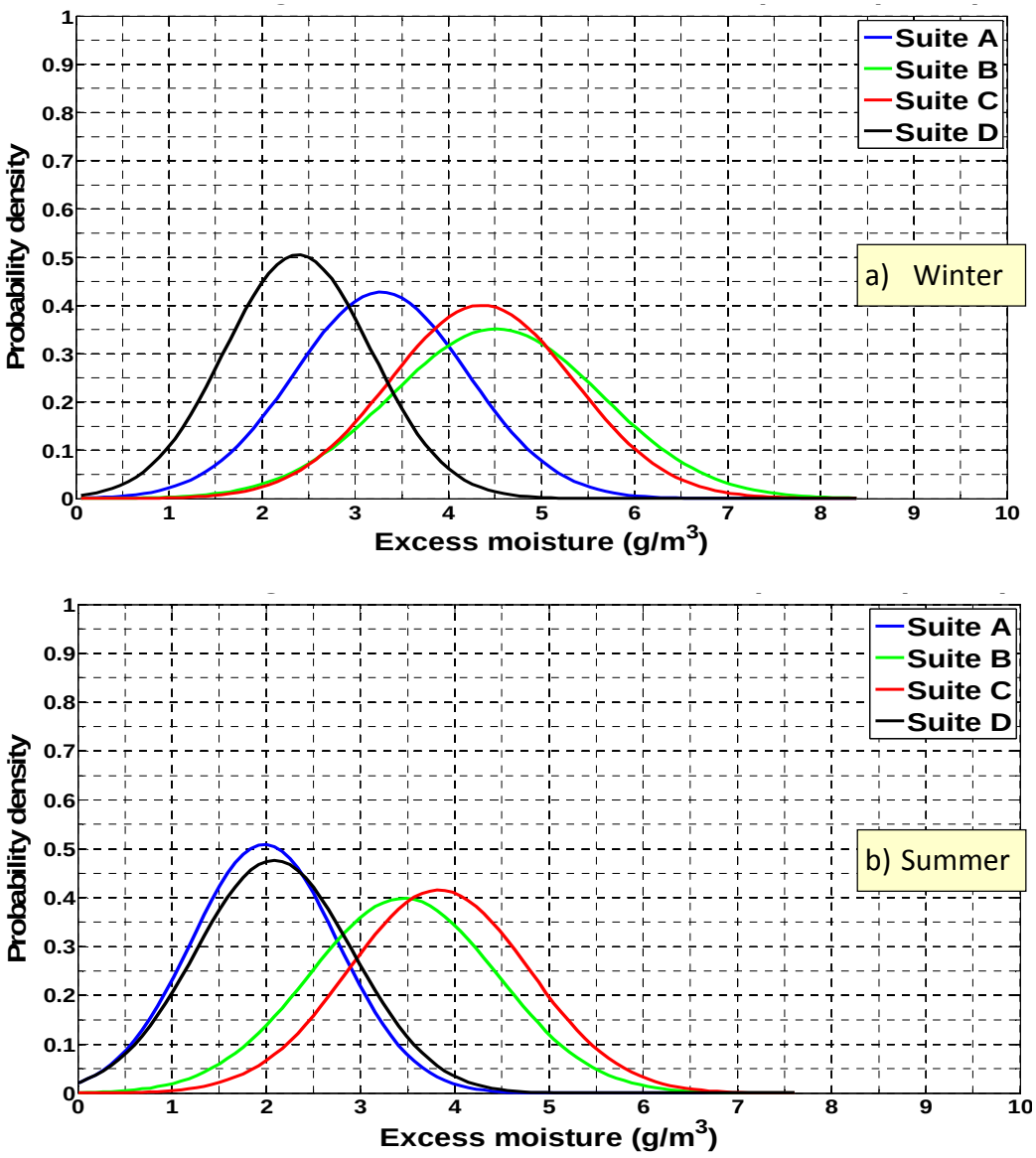

Figure 3.60 Suites' average indoor excess humidity distributions during Winter (a) and Summer (b) periods.

3.4.1.5 Summary

In general during the winter period, the indoor temperature distribution curves are narrower (lower standard deviation) and have slightly different mean values, which imply that temperature variations within the rooms are relatively low, but the temperature differences between rooms are relatively higher. During the summer period, the temperature distribution curves are wider (higher standard deviation values) and have similar mean values, which means during the summer period the temperature variation within a room can be high but the temperature difference between rooms are low. These seasonal temperature distributions are related to the levels of air movement in the two seasons. Higher natural ventilation in the summer period results higher air circulation and more uniform temperature distribution across the Suites, and the low natural ventilation and thermostat control during the winter results less

indoor air mixing and room temperature variations. During both winter and summer periods, the excess humidity differences between the rooms, excluding the Kitchens, are in the range of 0.2 g/m^3 to 1.0 g/m^3. Whereas the excess humidity fluctuations within the rooms are fairly the same and have standard deviation values between 0.8 g/m^3 and 1.0 g/m^3.

Based on the Suites considered in this study, the winter indoor temperature of a typical Suite can be characterized by a normal distribution using a mean temperature value between 17^{o}C to 21^{o}C and a standard deviation of 1^{o}C. Similarly, the summer indoor temperature of the suite can be characterized using a mean value between 24^{o}C to 27^{o}C and standard deviation of 2^{o}C. In a similar fashion, the excess humidity profile of a typical Suite can be defined using a mean excess humidity value selected between 2.5 to 4.5 g/m^3 for the winter period and 2.0 to 4.0 g/m^3 for the summer period and a standard deviation value of 0.1 g/m^3 for both winter and summer periods. Such approximation may not be valid for Suites with portable heater or humidifier. These mean and standard deviation values may be used to define different operating scenarios of different Suites representing low to high occupancy and cold to warm indoor temperature ranges in stochastic hygrothermal performance analysis.

3.4.2 Denmark input

The reporting of the data includes a description of the method used for collecting the data along with a description of the subsequent data handling. The report also includes simple graphs depicting correlations between proxies for occupant behaviour (temperature, relative humidity, CO_2 concentration) and ambient environment. Of main interest to the Annex will be the data on indoor environments and their statistical deviations.

3.4.2.1 Method

The method section is an excerpt from [67]. The excerpt has been edited lightly to conform to the purposes of Annex 55.

The concentration of carbon dioxide was continuously measured over a minimum of 2 days and 2 nights (averaging about 60 hours) in the bedrooms of the children. Eighty measuring units, each comprising a carbon dioxide monitor and a data logger, were used in the study. CARBOCAP® CO_2 monitors (GMW22, Vaisala, Finland) were used to measure the CO_2 concentration. The silicon-based Single-Beam, Dual-Wavelength NDIR sensors had a measurement range of 0-5000 ppm, an accuracy of (± 2 % of range + 2.0 % of reading) and a response time of 1 min. A HOBO U12-012 data logger (Onset Computer Corp., USA) was connected to each CO_2 monitor to record the measured value. The logger also recorded the air temperature and relative humidity in the room with an accuracy of (± 0.35 °C from 0 to 50°C and ±2.5 % from 10 % to 90 % RH). The measuring interval was 5 min. Prior to the experiment, readings of CO_2 concentrations were compared with the CO_2 concentrations measured with a factory calibrated Innova 1312 photo-acoustic multi-gas monitor (Luma-Sense Technologies A/S, Ballerup, Denmark) at various CO_2 concentrations and a correction curve was generated for each unit. The CO_2 concentrations recorded by a given unit were then corrected using the respective correction curve before further data processing.

One unit was used in each bedroom. The unit was placed at a location that would ensure minimum direct influence of sleeping occupants and windows on the measured data. Potential "dead" zones such as the space between furniture and room corners were avoided. One measuring unit was continuously operating outdoors in the yard of the research team's base, located 3 km from the city centre of Odense, Denmark.

3.4.2.2 Collected raw data

The IECH study has supplied Annex 55 with measurements of indoor and outdoor temperatures, relative humidities and CO_2 concentrations.

3.4.2.2.1 Temperatures

The measurements were performed between 10 March and 18 May 2008. The distribution of indoor temperatures can be described by the normal distribution.

Table 3.9 Temperatures measured in 500 family homes in Denmark in spring 2008.

Temperatures [°C]	Outdoor	Indoor Average	Indoor Minimum	Indoor Maximum
Average	11.4	21.0	13.2	25.2
Median	10.8	21.0	13.6	24.0
Standard Deviation		2.0	5.4	4.8
Confidence Interval95		±0.2	±0.5	±0.4
Maximum		26.4	24.8	52.6
Minimum		12.2	-3.4	18.2

Table 3.10 Temperatures measured in 440 single-family homes in Denmark in spring 2008.

Temperatures [°C]	Outdoor	Indoor Average	Indoor Minimum	Indoor Maximum
Average	11.4	20.9	12.7	25.4
Median	10.8	20.9	13.1	24.0
Standard Deviation		2.0	5.4	5.1
Confidence Interval95		±0.2	±0.5	±0.5
Maximum		26.4	24.8	52.6
Minimum		12.2	-3.4	18.2

Table 3.11 Temperatures measured in 60 multi-family homes in Denmark in spring 2008.

Temperatures [°C]	Outdoor	Indoor Average	Indoor Minimum	Indoor Maximum
Average	11.4	21.3	17.1	24.2
Median	10.8	21.4	18.4	23.7
Standard Deviation		1.9	4.3	2.7
Confidence Interval95		±0.5	±1.1	±0.7
Maximum		26.4	23.1	35.1
Minimum		16.3	2.0	18.8

The outdoor temperatures are for the entire period between 10 March and 18 May 2008. The indoor averages are the average temperatures measured in the children's bedrooms during the few days the measurement equipment was positioned in their bedrooms. The minimum values are the single lowest value measured in the child's bedroom. The maximum values are the single highest value measured in a child's bedroom.

Standard deviations are calculated using theory applicable for samples. The confidence intervals are calculated using the theory valid for the Normal Distribution for a α-value of 0.05; this gives 95 % confidence intervals.

Table 3.12 Outdoor temperature distribution in % in measured period.

Temperatures [°C]	Distribution [%]
>30	0.4
30>X≥ 25	4.6
25>X≥20	10.0
20>X≥15	13.7
15>X≥10	25.6
10>X≥5	26.0
5>X≥0	15.2
0>X≥-5	4.4
-5>	0.2

The following graphs (Figure 3.61,Figure 3.62 andFigure 3.63) display the data collected on indoor temperatures in Danish homes along with probability functions and probability density functions (PDF). The probability functions are calculated as the frequency of a measurement occurring in a bin (temperature interval) divided by the total amount of bins. The displayed probability density functions have been drawn from their respective means and standard deviations and the calculated probability of occurrences in the individual bins.

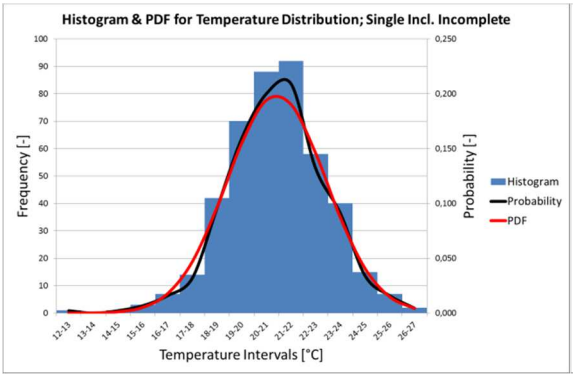

Figure 3.61 Distribution and PDF of indoor temperatures in Danish single-family homes.

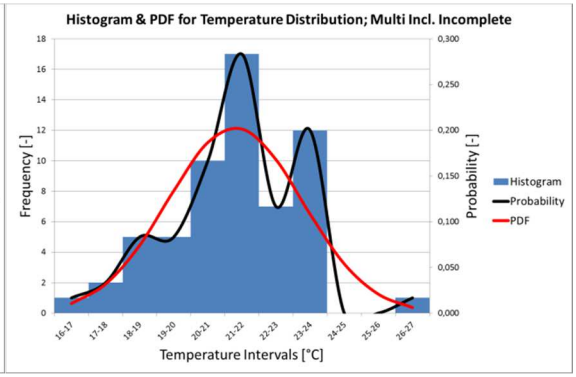

Figure 3.62 Distribution and PDF of indoor temperatures in Danish multi-family homes.

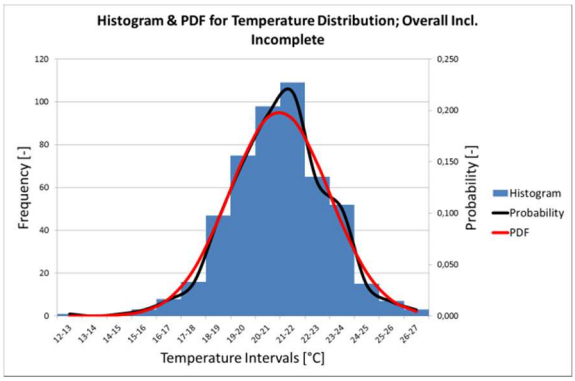

Figure 3.63 Distribution and PDF of indoor temperatures in general Danish family homes.

3.4.2.2.2 Relative humidities

The measurements were performed between 10 March and 18 May 2008. The distribution of indoor relative humidities can be described by the normal distribution.

Table 3.13 Relative humidities measured in 500 family homes in Denmark in spring 2008.

Relative humidities [%]	Outdoor	Indoor Average	Indoor Minimum	Indoor Maximum
Average	62.0	41.4	31.0	50.8
Median	65.0	41.2	30.9	50.1
Standard Deviation		5.5	5.3	7.4
Confidence Interval95		±0.5	±0.5	±0.6
Maximum		58.1	44.3	93.2
Minimum		27.4	10.8	32.2

Table 3.14 Relative humidities measured in 440 single-family homes in Denmark in spring 2008.

Relative humidities [%]	Outdoor	Indoor Average	Indoor Minimum	Indoor Maximum
Average	62.0	41.4	31.1	50.9
Median	65.0	41.3	31.0	50.1
Standard Deviation		5.4	5.3	7.4
Confidence Interval95		±0.5	±0.5	±0.7
Maximum		58.1	44.3	93.2
Minimum		27.4	10.8	32.2

Table 3.15 Relative humidities measured in 60 multi-family homes in Denmark in spring 2008.

Relative humidities [%]	Outdoor	Indoor Average	Indoor Minimum	Indoor Maximum
Average	62.0	41.1	30.3	50.0
Median	65.0	40.4	29.1	50.0
Standard Deviation		6.0	4.9	7.0
Confidence Interval95		±1.6	±1.3	±1.8
Maximum		55.0	42.3	69.9
Minimum		30.8	18.9	36.2

The outdoor relative humidities are for the entire period between 10 March and 18 May 2008. The indoor averages are the average relative humidities measured in the children's bedrooms during the few days the measurement equipment was positioned in their bedrooms. The minimum values are the single lowest value measured in the child's bedroom. The maximum values are the single highest value measured in a child's bedroom.

Standard deviations are calculated using theory applicable for samples. The confidence intervals are calculated using the theory valid for the Normal Distribution for an α-value of 0.05; this gives 95 % confidence intervals.

Table 3.16 Outdoor relative humidity distribution in % in measured period.

Relative humidities [%]	Distribution [%]
> 95	2.6
95 > X ≥ 85	11.0
85 > X ≥ 75	20.3
75 > X ≥ 65	18.8
65 > X ≥ 55	12.6
55 > X ≥ 45	12.4
45 > X ≥ 35	16.4
35 > X ≥ 25	7.4
< 25	1.2

The following graphs (Figure 3.64,Figure 3.65 andFigure 3.66) display the data collected on indoor relative humidities in Danish homes along with probability functions and probability density functions (PDF). The probability functions are calculated as the frequency of a measurement occurring in a bin (relative humidity interval) divided by the total amount of bins. The displayed probability density functions have been drawn from their respective means and standard deviations and the calculated probability of occurrences in the individual bins.

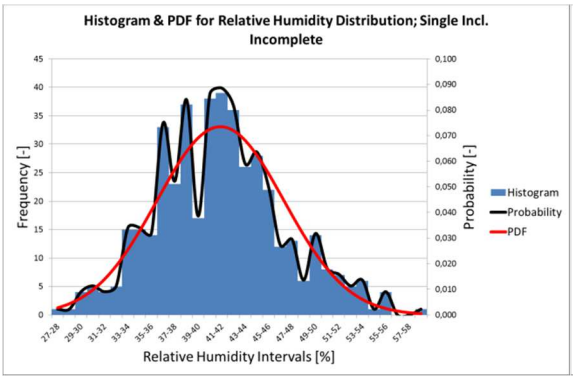

Figure 3.64 Distribution and PDF of indoor relative humidities in Danish single-family homes.

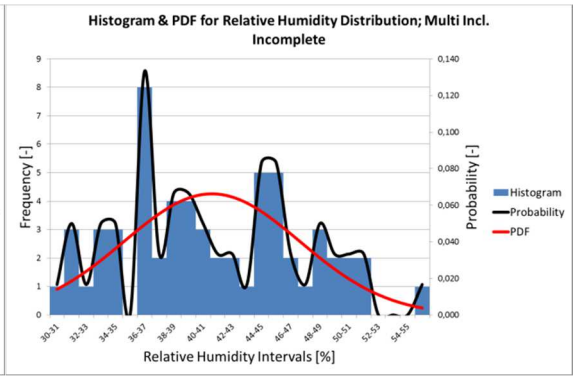

Figure 3.65 Distribution and PDF of indoor relative humidities in Danish multi-family homes.

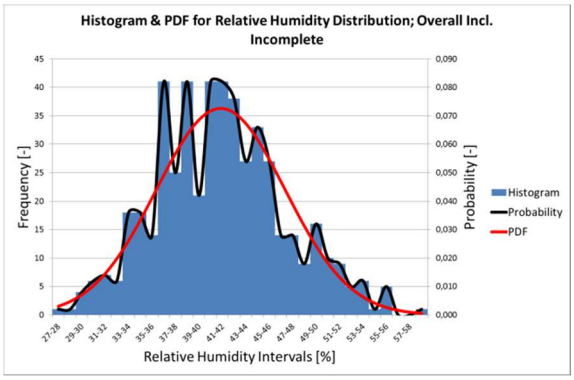

Figure 3.66 Distribution and PDF of indoor relative humidites in general Danish family homes.

3.4.2.2.3 Moisture excesses

The moisture excess (occupant generated moisture production) is calculated from the measurements of indoor and outdoor relative humidity levels and temperatures:

$$\Delta v = \left(\frac{RH_i \cdot p_{v,sat}(\theta_i) \cdot 1000 \frac{g}{kg}}{R_v \cdot (\theta_i + 273.15°C) \cdot \frac{°C}{K}} - \frac{RH_e \cdot p_{v,sat}(\theta_e) \cdot 1000 \frac{g}{kg}}{R_v \cdot (\theta_i + 273.15°C) \cdot \frac{°C}{K}} \right) \quad (3.2)$$

where

Δ symbolizes a change	–
v is the moisture excess	g/m^3
RH is the relative humidity	%
$p_{v,sat}$ is the saturated vapour pressure	Pa
θ is the temperature in Celsius	$°C$
K is the unit for temperature in Kelvin	K
R_v is the specific gas constant for water vapour	$461.5 \frac{J}{kg \cdot K}$
Subscript i is for the interior environment (indoor)	–
Subscript e is for the exterior environment (outdoor)	–

The measurements were performed between 10 March and 18 May 2008. The distribution of moisture excesses can be described by the normal distribution.

Table 3.17 Moisture excesses calculated for family homes in Denmark in spring 2008.

Moisture excess [g/m^3]	All homes (480)	Single-family (422)	Multi-family (58)
Average	1.6	1.5	1.8
Median	1.5	1.5	1.7
Standard Deviation	1.1	1.1	1.2
Confidence Interval^{95}	±0.1	±0.1	±0.3
Maximum	5.2	5.2	4.8
Minimum	-1.2	-1.2	-0.2

Standard deviations are calculated using theory applicable for samples. The confidence intervals are calculated using the theory valid for the Normal Distribution for a α-value of 0.05; this gives 95 % confidence intervals.

The homes included in the calculations of the moisture excesses are 20 less (18 single-family and 2 multi-family homes) than the overall total of homes included in the study. This is due to a lack of weather data for the first few days of the study.

The following graphs (Figure 3.67, Figure 3.68 andFigure 3.69) display the data collected on moisture excesses in Danish homes along with probability functions and probability density functions (PDF). The probability functions are calculated as the frequency of a measurement occurring in a bin (moisture excess interval) divided by the total amount of bins. The displayed probability density functions have been drawn from their respective means and standard deviations and the calculated probability of occurrences in the individual bins. In the instances where the amounts of bins are low, there can be some inconsistency between the drawn PDF and the actual PDF; this is due to rounding errors in the process of drawing the graphs and not related to the collected data. An example of this can be seen on Figure 3.68.

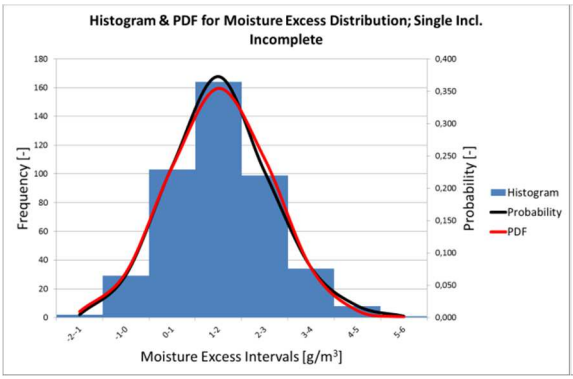

Figure 3.67 Distribution and PDF of indoor moisture excesses in Danish single-family homes.

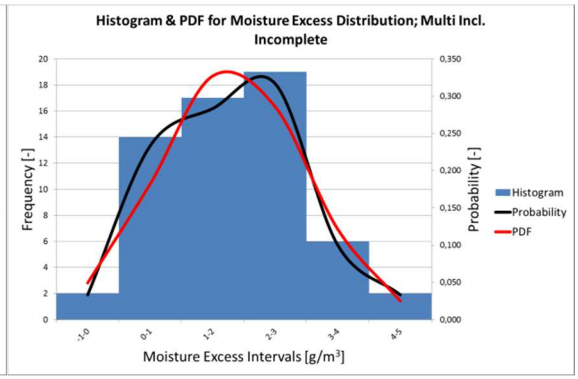

Figure 3.68 Distribution and PDF of indoor moisture excesses in Danish multi-family homes.

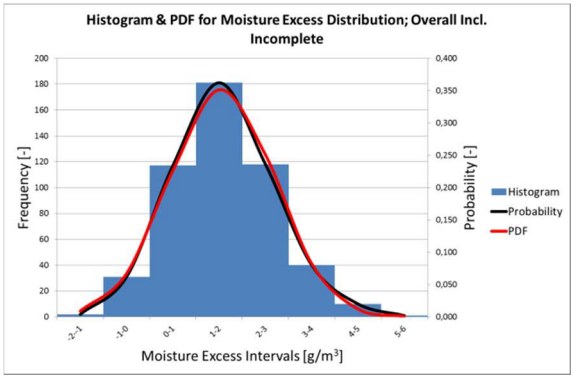

Figure 3.69 Distribution and PDF of indoor moisture excesses in general Danish family homes.

3.4.2.2.4 CO_2 concentrations

The measurements were performed between 10 March and 18 May 2008. The distribution of indoor CO_2 concentrations can be described by the log-normal distribution.

Table 3.18 CO_2 concentration levels measured in 500 family homes in Denmark in spring 2008.

CO_2 concentration [ppm]	Outdoor	Indoor Average	Indoor Minimum	Indoor Maximum
Average	403	978	472	1865
Median	392	943	469	1757
Standard Deviation		270	55	664
Confidence Interval[95]		955	467	1807
		1002	477	1924
Maximum		2225	831	4675
Minimum		481	370	687

Table 3.19 CO_2 concentration levels measured in 440 single-family homes in Denmark in spring 2008.

CO_2 concentration [ppm]	Outdoor	Indoor Average	Indoor Minimum	Indoor Maximum
Average	403	962	474	1815
Median	392	928	471	1717
Standard Deviation		262	57	622
Confidence Interval95		938	469	1758
		987	479	1874
Maximum		2225	831	4474
Minimum		481	383	687

Table 3.20 CO_2 concentration levels measured in 60 multi-family homes in Denmark in spring 2008.

CO_2 concentration [ppm]	Outdoor	Indoor Average	Indoor Minimum	Indoor Maximum
Average	403	1098	456	2237
Median	392	1058	454	2073
Standard Deviation		304	42	907
Confidence Interval95		1022	445	2015
		1179	467	2484
Maximum		2020	589	4675
Minimum		594	370	991

The outdoor CO_2 concentration levels are for the entire period between 10 March and 18 May 2008. The indoor averages are the average CO_2 concentration levels measured in the children's

bedrooms during the few days the measurement equipment was positioned in their bedrooms. The minimum values are the single lowest value measured in the child's bedroom. The maximum values are the single highest value measured in a child's bedroom.

Standard deviations are calculated using theory applicable for samples and log-normal distributions. The confidence intervals are calculated using modified version of the Cox method [70] using the Student's t variate, instead of the standard normal z variate, for a α-value of 0.05; this gives 95 % confidence intervals.

Table 3.21 Outdoor CO_2 concentration levels distribution in % in measured period.

CO_2 concentration [ppm]	Distribution [%]
> 550	0.7
550 > X ≥ 525	0.8
525 > X ≥ 500	2.1
500 > X ≥ 475	3.5
475 > X ≥ 450	6.8
450 > X ≥ 425	0.0
425 > X ≥ 400	18.0
400 > X ≥ 375	47.4
375 > X ≥ 350	18.4
350 > X ≥ 325	2.5
< 325	0.0

The following graphs (Figure 3.70,Figure 3.71 andFigure 3.72) display the data collected on indoor CO_2 concentration levels in Danish homes along with probability functions and probability density functions (PDF). The probability functions are calculated as the frequency of a measurement occurring in a bin (CO_2 concentration interval) divided by the total amount of bins. The displayed probability density functions have been drawn from their respective means and standard deviations and the calculated probability of occurrences in the individual bins.

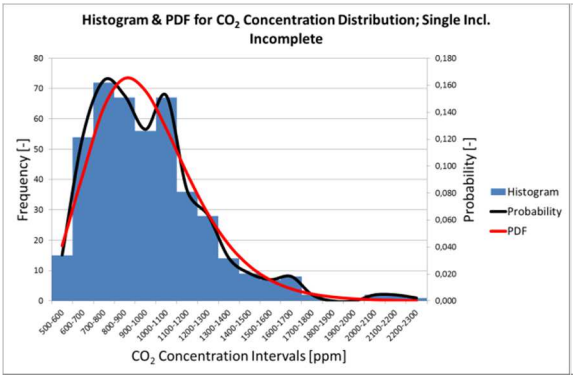

Figure 3.70 Distribution and PDF of indoor CO2 concentration levels in Danish single-family homes.

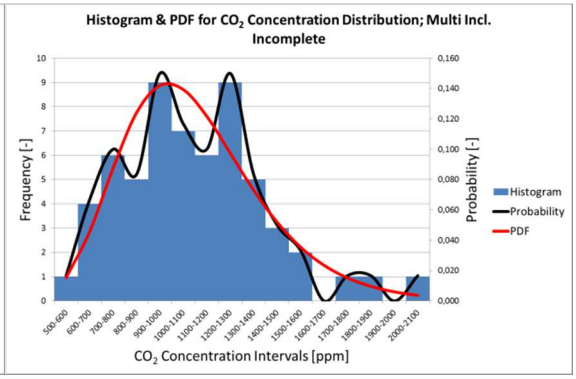

Figure 3.71 Distribution and PDF of indoor CO2 concentration levels in Danish multi-family homes.

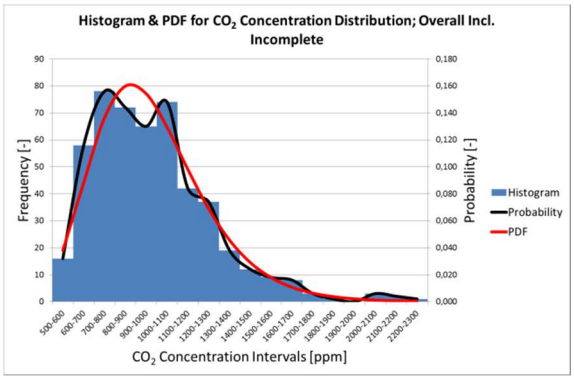

Figure 3.72 Distribution and PDF of indoor CO2 concentration levels in general Danish family homes

3.4.2.3 Analysis

3.4.2.3.1 Temperatures

Figure 3.73 and Figure 3.74 show how outdoor temperatures influence indoor temperatures in Danish homes. The indoor temperatures can be seen to be rising with the outdoor temperatures. Common Danish homes are equipped with heating systems which can maintain comfortable temperatures during the heating season. It is uncommon for homes to have mechanical cooling systems and most cooling will be done by opening windows. The Temperate Danish climate allows for this kind of cooling and venting. Danish family homes will usually try to maintain indoor temperatures around 21-23 °C.

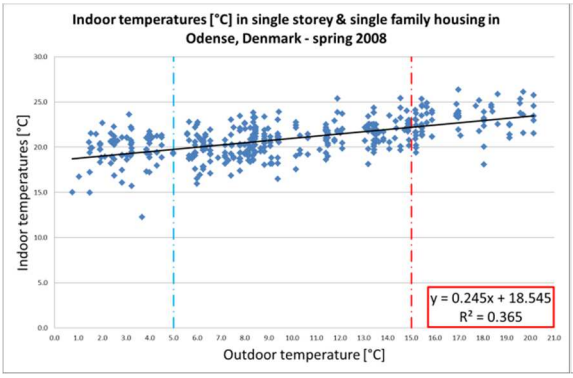

Figure 3.73 Correlation between indoor and outdoor temperatures in single-family homes.

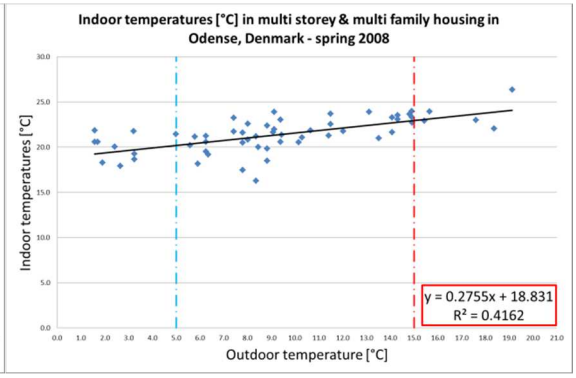

Figure 3.74 Correlation between indoor and outdoor temperatures in multi-family homes.

The homes included in the above graphical representations of the dependence of indoor temperature on outdoor temperature are 20 less (18 single-family and 2 multi-family homes) than the overall total of homes included in the study. This is due to a lack of weather data for the first few days of the study.

3.4.2.3.2 Relative humidities

Figure 3.75 and Figure 3.76 show how outdoor temperatures influence relative humidity in Danish homes. For the measured period, the average indoor relative humidity is 40 %. The

relative humidity level is stable over the temperature variations in the measured period. Higher temperatures and stable relative humidity levels mean that the homes have higher levels of absolute humidity. It is unlikely that the families that participated in the research project changed their daily routines significantly over the measured period. For this reason, it can be assumed that the moisture added to the indoor environment comes from the outside. This also fits with the assumption that with higher temperatures more venting (opening of windows) will be done. The section on moisture excess supports this analysis.

The measured period is relatively cool compared to the Danish summer. In summer the indoor relative humidities can be in the 60's. In cold winters relative humidities can drop down into the 20's. The Danish climate is quite humid and the yearly average is around 80 %.

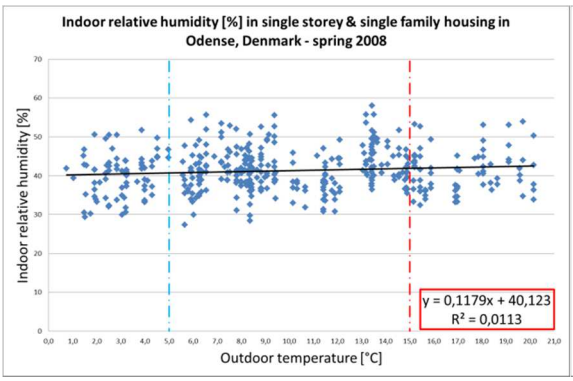

Figure 3.75 Correlation between indoor relative humidity and outdoor temperatures in single-family homes.

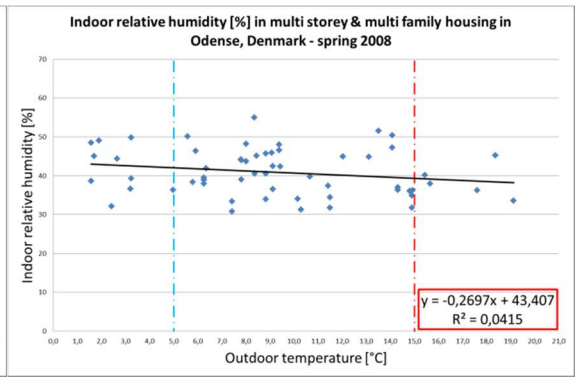

Figure 3.76 Correlation between indoor relative humidity and outdoor temperatures in multi-family homes.

The homes included in the above graphical representations of the dependence of indoor relative humidity on outdoor temperature are 20 less (18 single-family and 2 multi-family homes) than the overall total of homes included in the study. This is due to a lack of weather data for the first few days of the study.

Figure 3.77 and Figure 3.78 show how outdoor temperatures influence indoor moisture excess (moisture production) in Danish homes. Moisture excess levels can be seen to be falling with rising outdoor temperatures. In Denmark it is uncommon to have mechanical ventilation systems in homes. For this reason it is expected that families will open windows more during periods with higher temperatures. Venting a home without changing other occupant behaviour significantly will result in indoor absolute humidity levels closer to outdoor levels. The same reasoning also explains the falling moisture excess levels.

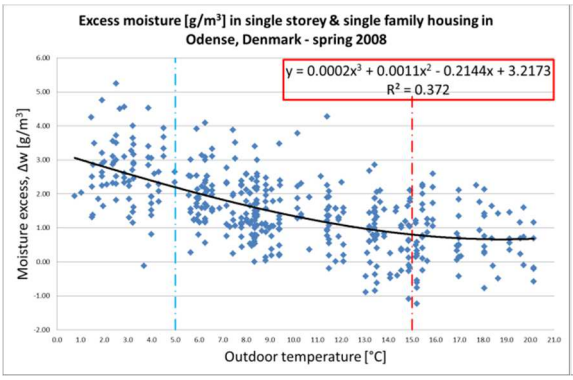

Figure 3.77 Correlation between moisture excess (moisture production) and outdoor temperatures in single-family homes.

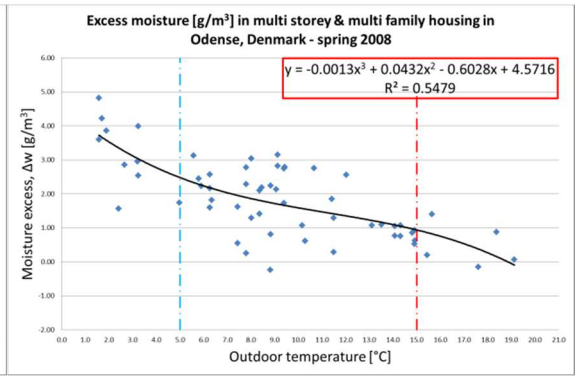

Figure 3.78 Correlation between moisture excess (moisture production) and outdoor temperatures in multi-family homes.

The homes included in the above graphical representations of the dependence of indoor moisture excess levels on outdoor temperature are 20 less (18 single-family and 2 multi-family homes) than the overall total of homes included in the study. This is due to a lack of weather data for the first few days of the study.

3.4.2.3.3 CO_2 concentrations

Figure 3.79 and Figure 3. 80 show how outdoor temperatures influence CO_2 concentration levels in Danish homes. For the measured period, the average indoor CO_2 concentration level is about 1000 ppm. The concentration levels can be seen to be falling with rising outdoor temperatures. In Denmark it is uncommon to have mechanical ventilation systems in homes. For this reason it is expected that families will open windows more during periods with higher temperatures. Venting a home without changing other occupant behaviour significantly will result in indoor CO_2 concentration levels closer to outdoor levels.

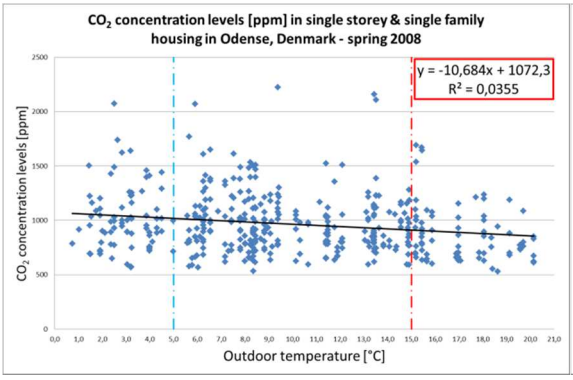

Figure 3.79 Correlation between CO_2 concentration levels and outdoor temperatures in single-family homes.

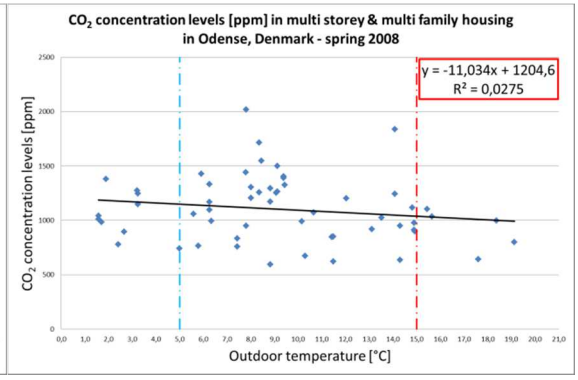

Figure 3. 80 Correlation between CO_2 concentration levels and outdoor temperatures in multi-family homes.

The homes included in the above graphical representations of the dependence of indoor CO_2 concentration levels on outdoor temperature are 20 less (18 single-family and 2 multi-family homes) than the overall total of homes included in the study. This is due to a lack of weather data for the first few days of the study.

3.4.2.4 Acknowledgements

We thank the International Centre for Indoor Environment and Energy at The Technical University of Denmark for generously supplying us with data from their research project Indoor Environment and Children's Health. Special thanks are due to Gabriel Bekö for his help with the handling of the data and for supplying the method section of this chapter.

3.4.3 Estonia [TTU] – Indoor thermal comfort and moisture loads in Estonian buildings

3.4.3.1 Assessment of indoor thermal comfort and humidity loads

Analysing the indoor climate's dependency on outdoor climate eliminates or decreases the influence of the outdoor climate.

The indoor climate was analysed separately over the measurement period as dependency on outdoor climate and during the summer seasons and winter seasons.

Moisture production indoors and ventilation/infiltration airflows make the difference between indoors and outdoors air water vapour content, i.e. moisture excess $\Delta\nu$, g/m^3:

$$\Delta\nu = \nu_i - \nu_e \tag{3.3}$$

As indoor RH depends on indoor temperature, outdoor humidity, moisture production and ventilation airflow, there are many variables. To decrease variables in presenting humidity loads by moisture or vapour excess is one possibility and is the main solution used in Estonian study.

3.4.3.2 Outdoor climate

The lowest and highest hourly outdoor temperature during measurement period were -30 °C and +34 °C . The monthly average temperature during winter in different places varied between -5.4…-8.5 °C and during summer between +16.9…+19.5 °C.

3.4.3.3 Dependence of indoor temperature and humidity on the outdoor temperature

To give the overall view of the thermal condition, the dependence of the indoor temperature on the outdoor temperature was analysed. Thin solid lightly shaded curves in Figure 3.81 shows average daily indoor temperature dependency on daily average outdoor temperature. The dotted curve in the Figure 3.81 represents the average thermal conditions from all the apartments.

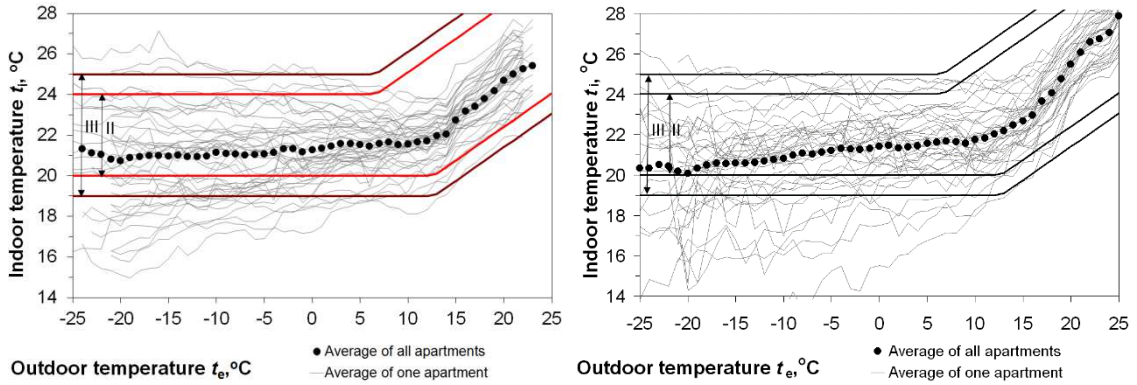

Figure 3.81 Dependence of the daily average indoor temperature on the outdoor temperature in brick (left) and wooden (right) apartment buildings.

Measurements in this study showed the dependence between the indoor temperature and the outdoor temperature. There is a turning point at ~+15 °C average daily outdoor temperature. Over ~+15 °C of average daily outdoor temperature, the slope of the indoor temperature is larger. Over ~+15 °C of average daily outdoor temperature, the indoor temperature reaching over +21…22 °C and heating is not necessary any more. The average indoor temperature curve in studied buildings rises from +20 °C (at t_e -25 °C) to +22 °C (at t_e +15 °C) in the heating season, reaching +28 °C (at t_e +25 °C) during summer, see Figure 3.16 right. Standard deviation of daily average indoor temperatures during heating season was on average 1.5 °C.

Similarly to the room temperature, the dependence of indoor RH on the outdoor temperature was also analysed. Each individual thin solid lightly shaded curve in Figure 3.82 represents the average value of the average daily indoor RH at the corresponding average daily outdoor temperature in one apartment. The dotted curve represents the average curve of all the apartments. Even though the average RH in the studied apartments stays within target values of RH in most of the apartments, we can see large variations of indoor RH.

Results of indoor RH showed a dependence on the outdoor temperature, but clear turning point is difficult to determine. It can be at t_e+15 °C. Standard deviation of average daily indoor RH during heating season was on average ~10 %.

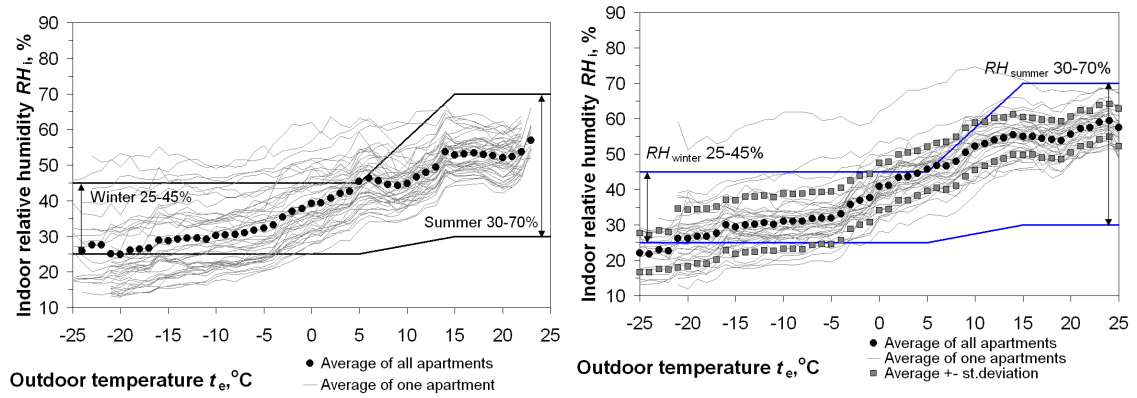

Figure 3.82 Dependence of the daily average indoor RH on the outdoor temperature in brick (left) and wooden (right) apartment buildings.

3.4.3.4 Indoor temperature and humidity conditions during winter

All the temperature measurement results in the measured dwellings during winter months are shown in Figure 3.83. Each curve represents one measured apartment. Dotted curves show the average of all the rooms. The average indoor temperature during the winter season from all the brick apartment buildings was +21.1 °C (min. average being +17.2 °C and max. average +25.3 °C) and in wooden apartment buildings it was +21.0 °C (min. average being +13.3 °C and max. average +24.8 °C; standard deviation was 2.3 °C). Even though typically the average temperature was between +19 and +22°C in most of apartments, large variations of temperatures show problems related to the control of the heating system.

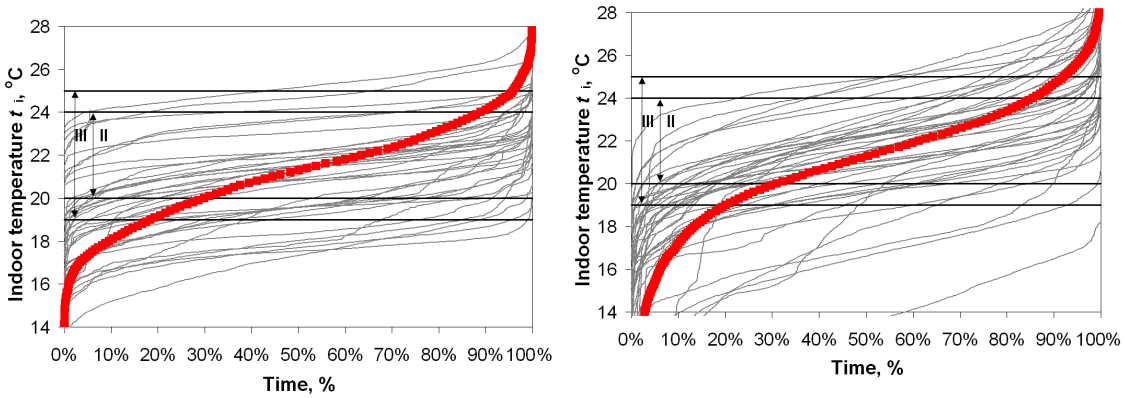

Figure 3.83 The distribution of indoor temperature during winter in brick (left) and wooden (right) apartment buildings.

The average indoor RH during the winter season from all the brick apartment buildings was 33 % (min. average being 19 % and max. average 54 %) and in wooden apartment buildings it was 31 % (min. average being 10 % and max. average 73 % and standard deviation was 11 %), see Figure 3.84. The large deviation of RH (Figure 3.84), in addition to temperature variations, indicates that problems exist in the ventilation system's performance.

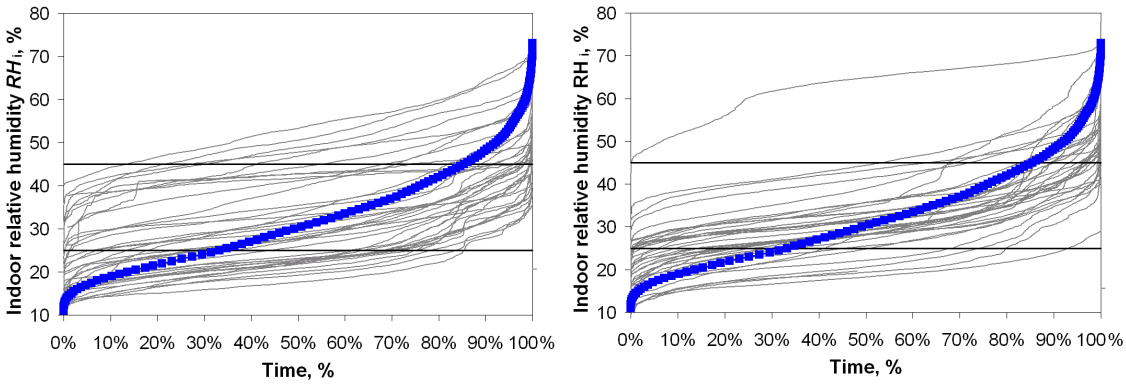

Figure 3.84 The distribution of indoor RH during winter in brick (left) and wooden (right) apartment buildings.

3.4.3.5 Indoor temperature and humidity conditions during summer

The average indoor temperature during the summer season from all the brick apartment buildings was +23.2 °C (min. average being +20.2 °C and max. average +25.8 °C) and in wooden apartment buildings it was +24.6 °C (min. average being+22.7 °C and max. average +26.8 °C, standard deviation was 1.1 °C), see Figure 3.85.

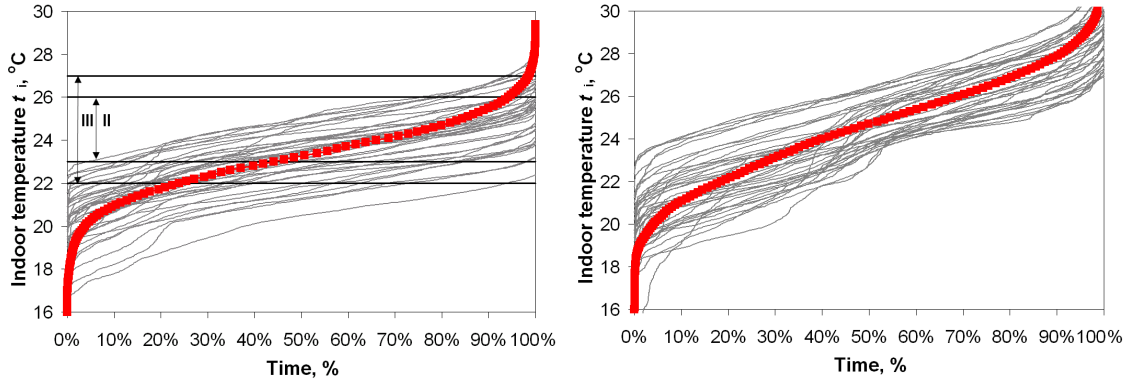

Figure 3.85 The distribution of indoor temperature during summer in brick (left) and wooden (right) apartment buildings.

The average indoor RH during the winter season from all the brick apartment buildings was +52 % (min. average being 42 % and max. average 62 %) and in wooden apartment buildings it was 56 % (min. average being 48 % and max. average 69 %, standard deviation was 6 %), see Figure 3.86.

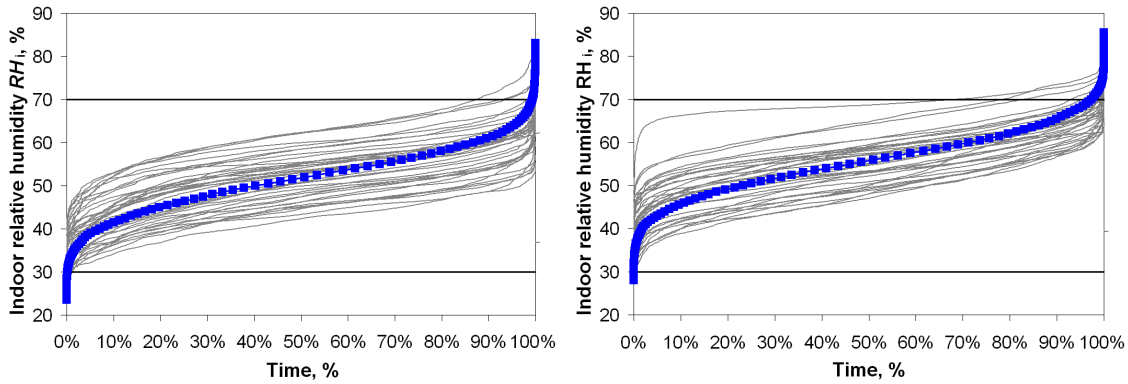

Figure 3.86 The distribution of indoor temperature during summer in brick (left) and wooden (right) apartment buildings.

3.4.3.6 Internal moisture excess

Moisture excess (i.e., the difference between indoors absolute humidity v_i, g/m^3 and outdoors absolute humidity v_e, g/m^3) Δv, g/m^3, was calculated on the basis of the measured results of the indoor and outdoor temperatures and RH.

For each apartment, moisture excess values were averaged over the cold period ($t_e \leq +5$ °C) and over the warm period ($t_e \geq +15$ °C). The comparison of average moisture excess values is shown in Figure 3.87.

In brick apartment buildings the average moisture excess during the cold period ($t_e \leq +5$ °C) was +2.9 g/m^3 (st.dev. 1.3 g/m^3) and during warm period ($t_e \geq +5$ °C) it was +0.7 g/m^3 (st.dev. 0.5 g/m^3). In wooden apartment buildings the average moisture excess during the cold period ($t_e \leq +5$ °C) was +3.0 g/m^3 (st.dev. 1.1 g/m^3) and during warm period ($t_e \geq +15$ °C) it was +0.7 g/m^3 (st.dev. 0.7 g/m^3). The maximum value from weekly average moisture excess during the cold period was +6.3 g/m^3 and during the remaining time was +2.5 g/m^3.

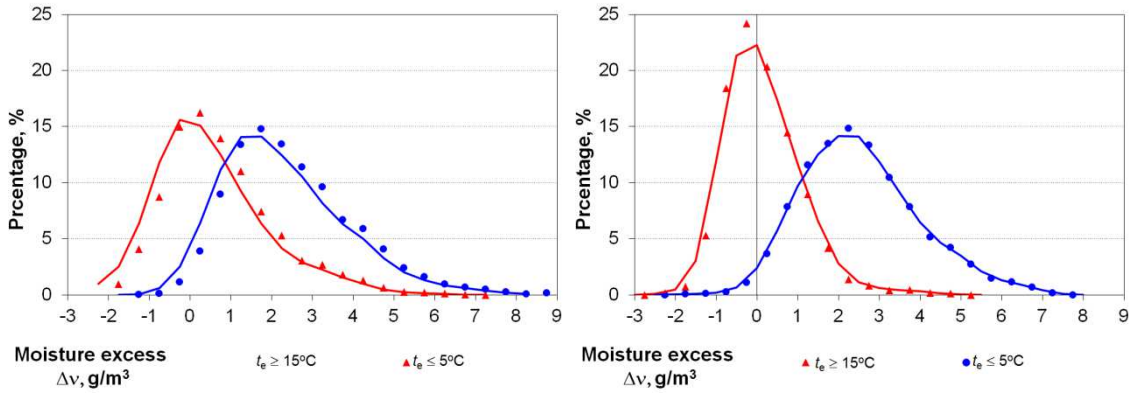

Figure 3.87 Distribution of moisture excess in brick (left) and wooden (right) apartment buildings.

In common hygrothermal design moister loads on higher critical levels is commonly used. For stochastic analysis average and minimum loads are needed. Different moisture excess levels showing moisture performance of apartments through the full range of moisture production. Figure 3.88 left shows indoor humidity loads in wooden apartment buildings on 90 %, average, and 10 % level. For hygrothermal design, more simplified and stylized curves are needed. These curves can be calculated from the moisture excess data, sorting the curves so that during the cold period ($t_e \leq +5$ °C) the average values of moisture excess are as follows: +1 g/m^3, +2 g/m^3, +3 g/m^3, +4 g/m^3, +5 g/m^3, and +6 g/m^3, see Figure 3.88 right. On the basis of these curves, moisture supply changes 1 g/m^3 during the cold period ($t_e \leq +5$ °C) and 0.5 g/m^3 during the warm period ($t_e \geq +15$…20 °C), see Figure 3.16 right.

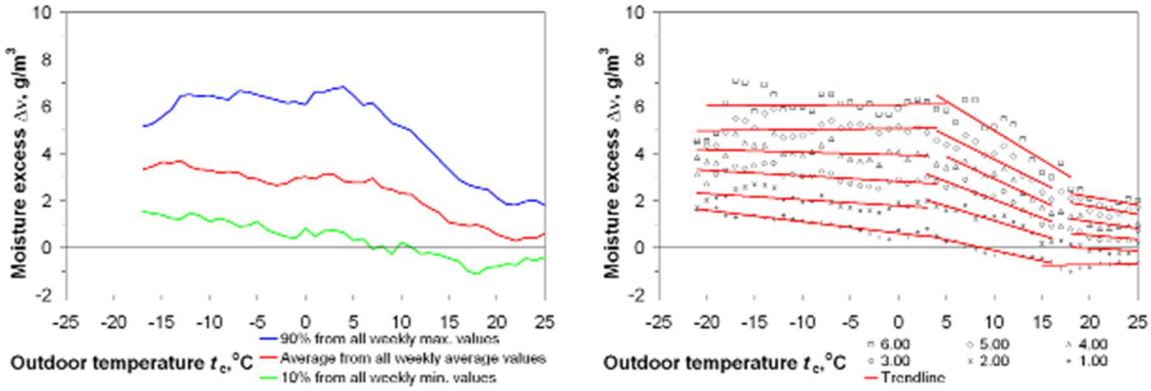

Figure 3.88 Indoor humidity loads on 90 %, average, and 10 % level in wooden apartment (left).

Figure 3.89 shows simplified and stylized indoor hygrothermal load curves. Humidity load curves can be calculated from the moisture excess data, sorting the curves so that during the cold period ($t_e \leq +5$ °C) the average values of moisture excess changes at +1 g/m^3 step. On the basis

of these curves, moisture excess changes 1 g/m^3 during the cold period ($t_e \leq +5$ °C) and 0.5 g/m^3 during the warm period ($t_e \geq +15…20$ °C),

This indoor hygrothermal load model and its change can be used in the indoor temperature calculations, where the indoor temperature should be given for program as input parameter (Delphin, WUFI 1D, Wufi 2D, hygIRC 1-D, 1D-HAM, MATCH, etc.) and is not generated by the room model of the whole buildings simulation program (IDA-ICE, WUFI+, etc.). Moving this curve up and down allows to great different indoor temperature conditions for stochastic calculations.

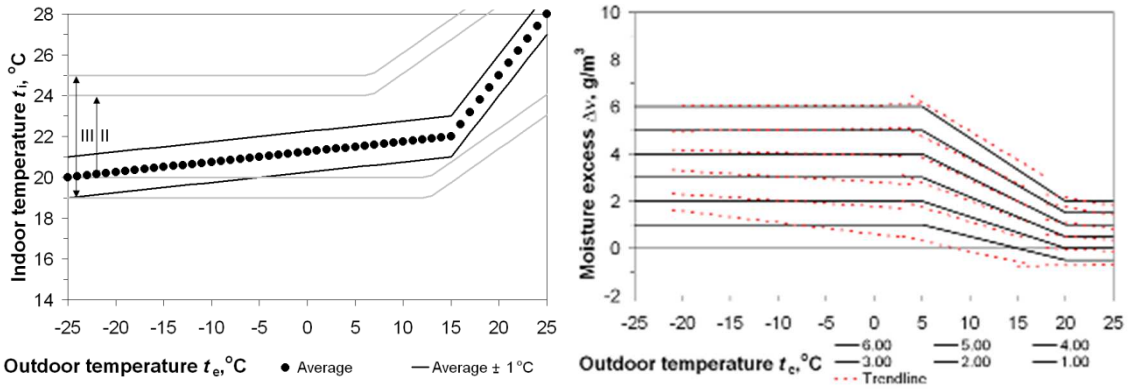

Figure 3.89 The simplified curves for indoor temperature (left) moisture excess (right) on different hygrothermal load levels.

Average indoor temperature model together with average (Δv=3 g/m^3 @ $t_e \leq +5$ °C) or design curve (Δv=6 g/m^3 @ $t_e \leq +5$ °C) of moisture excess give realistic indoor relative humidity models in cold climate conditions over whole year period, see Figure 3.90.

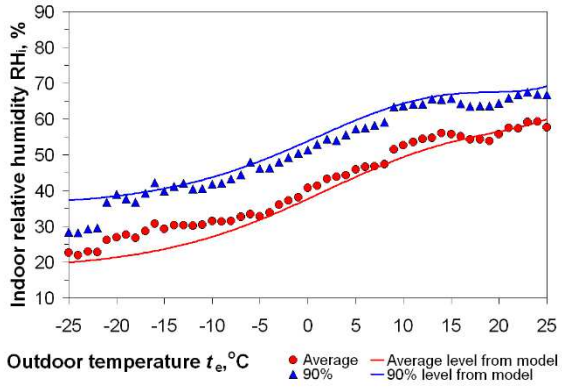

Figure 3.90 The comparison of measured and calculated indoor RH curves on different humidity load levels.

3.4.3.7 Moisture production

Moisture production values during winter are presented as hourly results (Figure 3.91, left) and as specific values per square meter (Figure 3.91, right). As these values are measured during night they show mainly moisture production from inhabitant. In addition these values may add moisture production due to common household (kitchen, shower, cleaning, ect.).

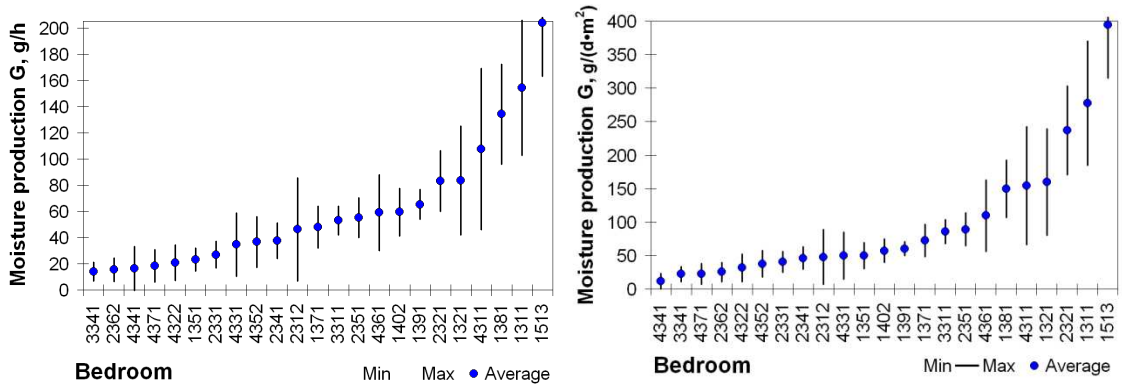

Figure 3.91 The distribution of moisture production during winter.

3.4.4 Finland [TUT] – Indoor loads in Finnish buildings

3.4.4.1 Introduction

This chapter presents results from statistical analysis on indoor moisture excess. Indoor air conditions were monitored from timber frame detached houses in 2002-2004 and from heavyweight detached houses and apartments in 2005-2008. Indoor temperature and relative humidity data was collected with Comark Diligence EV N2003 and N2013 data loggers. Outdoor data was measured at the nearest weather station by the Finnish Meteorological Institute.

The measurement sample consists of different types of buildings with different HVAC-systems. In the statistical analysis, there is data from 44 timber frame detached houses and from 112 heavyweight detached houses and apartments.

Many activities in buildings produce moisture to the indoor air, e.g. breathing, perspiration, cooking, cleaning and washing. As the outdoor air creates a base level for moisture content also in indoor air, these indoor moisture sources create a moisture excess compared to the outdoors. As the differences in indoor and outdoor air try to even out, this extra moisture e.g. increases the moisture load on building structures. The indoor moisture excess depends heavily on the moisture production rate and ventilation, which both depend on user behavior. However, it is also linked to outdoor air temperature, which we use in the following calculations.

3.4.4.2 Methods

Computer programs with statistical capabilities can produce stochastic data sets with desired probability density functions. For example, if the average and standard deviation are known, we can get values from the normal distribution [74]:

$$\Delta\nu = N\left(\mu_{\Delta\nu}, \sigma_{\Delta\nu}\right) \tag{3.4}$$

where Δν is the indoor moisture excess value [kg/m^3], N is for normal distribution, $\mu_{\Delta\nu}$ is the average value of indoor moisture excess [kg/m^3] and $\sigma_{\Delta\nu}$ is the standard deviation of indoor moisture excess [kg/m^3].

Typical values in residential buildings range between -0.001 kg/m^3 to 0.006 kg/m^3. From literature ([75]; [4]; [5]) we know that indoor moisture excess is connected to outdoor air temperature, so that the moisture excess value decreases when outdoor air temperature rises.

The higher the indoor moisture excess is, the bigger the moisture load is for structures. In IEA Annex 24 Task 2 [76] it has been recommended that the dimensioning conditions would correspond to 10 % criticality level. That way 90 % of the time conditions would be less critical than with the chosen value. In this chapter we try to find the distributions of $\mu_{\Delta\nu}$ and $\sigma_{\Delta\nu}$ that were presented in Equation (3.4). The indoor moisture excess would be written as:

$$\Delta\nu(T_e, P_{ave}, P_{std}) = N\left(\Phi^{-1}_{\Delta\nu,ave}(T_e, P_{ave}), \Phi^{-1}_{\Delta\nu,std}(T_e, P_{std})\right) \quad (3.5)$$

where T_e is the outdoor air temperature [°C], P_{ave} is the percentile of average moisture excess values in measured houses, 0…1 [-], P_{std} is the percentile of standard deviation of indoor moisture excess, 0…1 [-] and Φ^{-1} is the inverse normal cumulative distribution function [kg/m^3].

Measurement data from [4]; [5] were used to define distributions of $\mu_{\Delta\nu}$ and $\sigma_{\Delta\nu}$. First the indoor moisture excess was calculated for each time step (hour) as the difference between indoor and outdoor air moisture content. Second, the moisture excess values were divided into subgroups for each measured building/apartment and temperature degree. Third, average and standard deviation were calculated for these subgroups and presented as a function of outdoor temperature (Figure 3.92). Fourth, analytical functions were fitted to data (Figure 3.93 and Table 3.22).

Because these values don't however represent the true 10% criticality value, the 90% percentiles were calculated from the original subgroups and plotted for each building/apartment along with their average and standard deviation values (Figure 3.94). Curve fitting was used to find continuous functions that would match those values (Table 3.23).

It was noticed that the normal distribution parameters of indoor moisture excess average resemble the logistic curve in some way (Figure 3.93 and Figure 3.94). The standard deviation on the other hand can be better described with a linear and an exponential function (Figure 3.93). Simplified distribution parameter functions based on visual inspection were selected and are presented in Table 3.24.

Statistical analysis was done with Matlab R2011b. The hourly measurement data was imported from Excel-files and organized into structures. Data manipulation was done with m-files and Matlab cftool (Curve Fitting Tool). Different mathematical functions were tested to find the highest R^2-value and reasonable usability. If measurement data had long empty sections or had clearly abnormal values, the whole data set for that case was removed from the analysis.

3.4.4.3 Results

Figure 3.92 show the average and standard deviation of the indoor moisture excess corresponding to each outdoor temperature degree. One curve means one house/apartment.

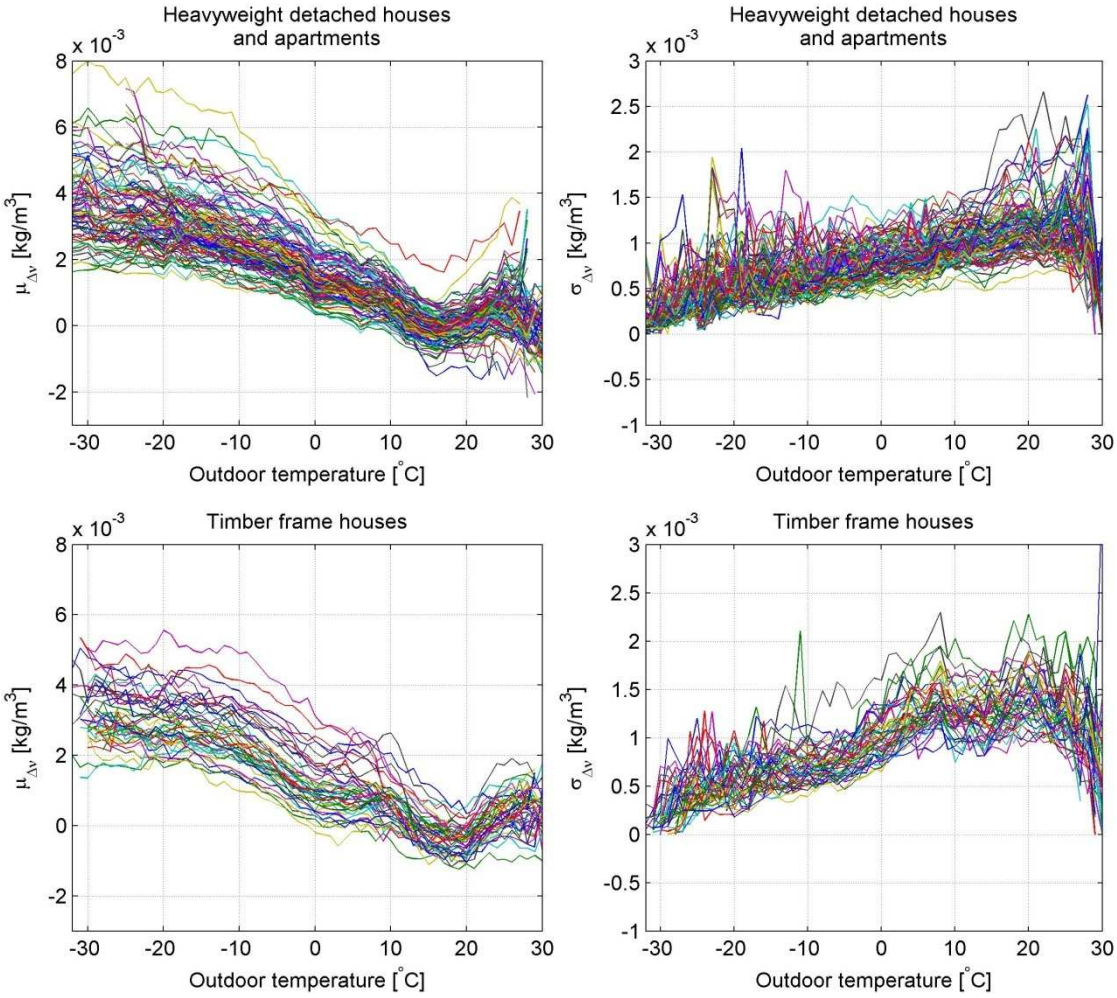

Figure 3.92 Top: Heavyweight detached houses and apartments. Bottom: Timber framed detached houses. Left: Average indoor moisture excess values for each building and temperature degree. Right: The standard deviation of indoor moisture excess in each building and temperature degree.

Figure 3.93 show the average and standard deviation of building-wise averages and standard deviations.

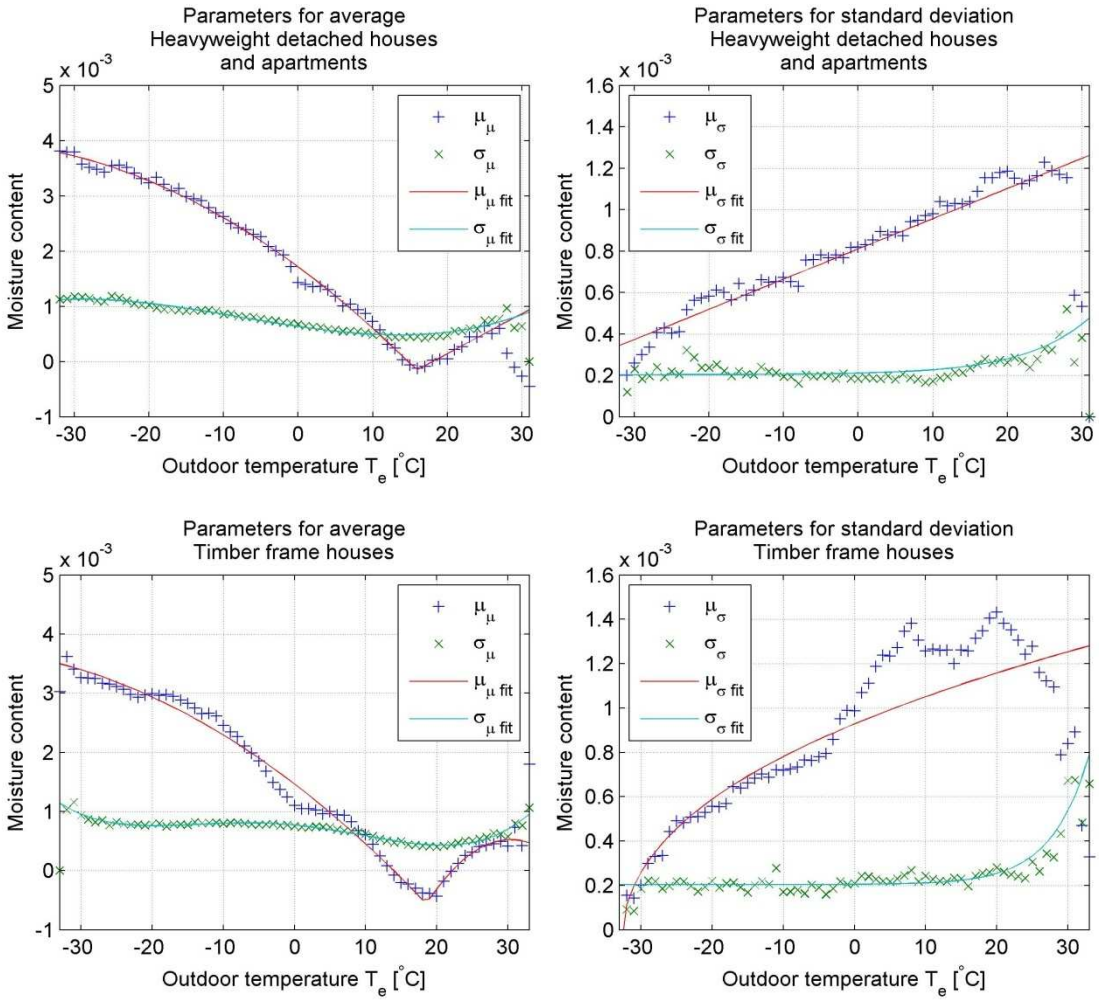

Figure 3.93 Average (left) and standard deviation (right) of indoor moisture excess. Top row: Heavyweight detached houses and apartments. Bottom row: Timber framed detached houses.

The next table shows the resulting equations from the fitting procedure.

Table 3.22 Curve fitting results. Moisture content values are in kg/m³ and temperatures in °C. Variable Te is the outdoor air temperature.

Inverse cumulative distribution function parameters for indoor moisture excess average		Inverse cumulative distribution function parameters for indoor moisture excess standard deviation
Heavyweight detached houses and apartments:		***Heavyweight detached houses and apartments:***
if Te ≤ 15	μ_μ =-1.107e-6*Te^2 -0.0001001*Te +0.001711	μ_σ=1.457e-5*Te+0.0008104
else	μ_μ =7.251e-5*Te -0.001308	
	σ_μ = 1.67e-8*Te^3 + 3.898e-7*Te^2 -1.974e-5*Te+ 0.0006364	σ_σ = exp(-11.79+0.1157*Te) +0.000203
Timber-framed one family houses:		***Timber-framed one family houses:***
if Te ≤ 18	μ_μ = -9.23e-7*Te^2-9.216e-5*Te + 0.001463	μ_σ= +0.0002557*(Te+33)^0.4098 - 0.0001431
else	μ_μ = -7.78e-6*Te^2 + 0.0004724*Te-0.006646	
	σ_μ = 1.001e-9*Te^4 + 7.842e-9*Te^3 -8.359e-7*Te^2 - 1.137e-5*Te + 0.0007692	σ_σ = 0.0002039 + exp(-13.67+0.1888*Te)

μ_μ is the average value of averages and σ_μ is the standard deviation of averages. μ_σ is the average of standard deviation values and σ_σ is the standard deviation of standard deviation values.

It is not recommended to extrapolate function values outside the range that they were made for. Suitable temperature range is approximately -30…25 °C.

From the previous equations we know the distribution of house averages. However, to get a true 10 % criticality level, we also want know the situation when 90 % of houses have lower indoor moisture content 90 % of the time. This is calculated here by choosing the 90 % cumulative distribution function value from each building and temperature degree to further analysis, while the standard deviation is kept the same as with the average values. It is not known how standard deviation changes with different indoor moisture excess levels, but this is done as the first method to get onwards. The next figures in Figure 3.94, show the 90 % indoor moisture excess values from each house and the average and standard deviation of those values.

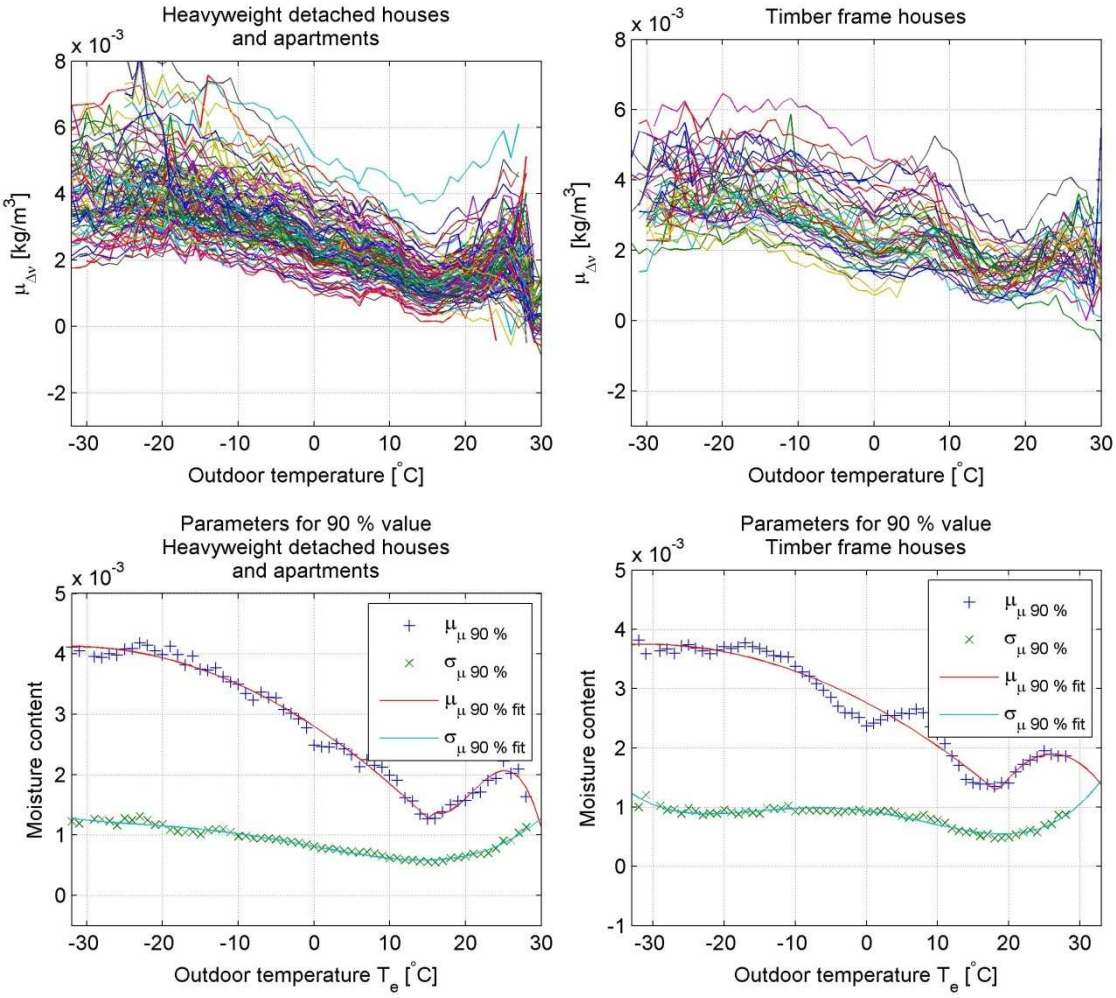

Figure 3.94 Top row: 90 % CDF values of indoor moisture excess of the temperature degree-wise subgroups. Bottom row: Average and standard deviation of the 90 % CDF values. Distribution parameters for the indoor moisture excess standard deviation are kept the same than before.

Table 3.23 Normal distribution parameters for the indoor moisture excess 90 % percentile values.

Inverse cumulative distribution function parameters for indoor moisture excess 90 % value	
Heavyweight detached houses and apartments:	
if Te ≤ 15	μ_μ =-1.282e-6*Te^2 -8.24e-5*Te +0.0028
else	μ_μ =-2.286e-6*Te3 +0.0001433*Te^2 -0.002869*Te +0.01995
	σ_μ = 5.531e-10*Te^4 +2.605e-8*Te^3 +2.849e-9*Te^2-2.292e-5*Te +0.0008123
Timber-framed one family houses:	
if Te ≤ 18	μ_μ = -1.014e-6*Te^2 -6.328e-5*Te +0.002761
else	μ_μ = -1.089e-5*Te^2 +0.000569*Te -0.005536
	σ_μ = 1.316e-9*Te^4 +1.743e-8*Te^3 -1.059e-6*Te^2 -1.559e-5*Te +0.0009331

The normal distribution parameters for the standard deviation are kept the same than before.

These type of equations are however hard to remember and somewhat difficult to use. Also in actual buildings there are many types of case-specific solutions that affect the amount of indoor moisture excess.

The average and standard deviation of average indoor moisture excess is somewhat similar to logistic function. The average of indoor moisture excess standard deviation has a linear or power function –type behavior while the standard deviation of the standard deviation has an exponential growth. Based on Figure 3.93 and Figure 3.94, if we use the logistic function and simplify the numerical values, we come up with the following functions for the inverse cumulative function parameters.

Table 3.24 Chosen values for moisture analysis.

Inverse cumulative distribution function parameters for indoor moisture excess average	Inverse cumulative distribution function parameters for indoor moisture excess standard deviation
$\mu_\mu = \frac{\mu_{\mu,\max} - \mu_{\mu,\min}}{1 + e^{\frac{T}{T_{25\%}}}} + \mu_{\mu,\min}$ $\mu_{\mu,max}$=0.004 kg/m^3 $\mu_{\mu,min}$= 0.0015 kg/m^3 $T_{25\%}$=10°C	μ_σ=1e-5 * Te + 0.001
$\sigma_\mu = \frac{\sigma_{\mu,\max} - \sigma_{\mu,\min}}{1 + e^{\frac{T}{T_{25\%}}}} + \sigma_{\mu,\min}$ $\sigma_{\mu,max}$=0.001 kg/m^3 $\sigma_{\mu,min}$=0.0005 kg/m^3	σ_σ = exp(-12+0.12*Te) +0.0002

When temperature is T = 0 °C, the indoor moisture excess has its average value. Temperature $T_{25\,\%}$ is used as a scaling parameter, where the indoor moisture excess has increased roughly 25 % from the minimum value (1/(1+e) ≈ 0.25).

Figure 3.95 shows an example with these simplified indoor moisture excess values. The average and standard deviation values correspond to 90 % percentile values both in time and among measured buildings/apartments.

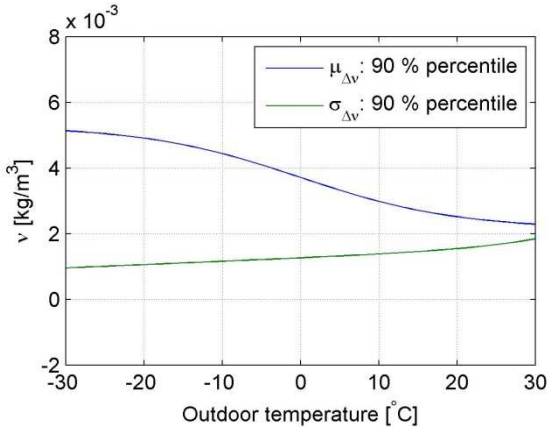

Figure 3.95 90 % percentile values of indoor moisture excess average and standard deviation. Functions are calculated from normal distributions with functions given at the previous table.

The following equation is an approximation to the outdoor air temperature dependent indoor air moisture excess, corresponding to the 10 % criticality level:

$$\Delta\nu(T) = N\left(0.002 + \frac{0.003}{1+e^{\frac{T}{10}}}, 0.001 + 2\cdot10^{-5}\cdot T\right) \quad (3.6)$$

Values depend only on the outdoor air temperature ([T] = °C).

3.4.4.4 Discussion

Indoor moisture excess average and standard deviation functions were determined and can be used in stochastic calculations. Both variables depend on the outdoor air temperature and different criticality levels can be chosen if desired.

Normal probability density function parameters for average moisture excess were calculated from both indoor moisture excess averages and from 90 % values. In winter the average values of both are quite close to 4 g/m^3, but the difference becomes bigger when the outdoor air temperature rises. The average values of each house in the summer (T_e = +15 °C) is roughly in the range -1…1 g/m^3. When 90 % values are used the moisture excess is about 0…2 g/m^3. In both cases however, the standard deviation is close to 1 g/m^3 whole year around.

The average or 90 % values correspond basically to the indoor moisture excess values given in literature e.g. in [75]. In addition to that, also standard deviation was calculated which gives information for stochastic calculations. The average standard deviation in indoor moisture excess for each house/apartment increases with outdoor temperature. With heavyweight detached houses and apartments standard deviation increases almost linearly. For timber framed houses the increase was more square root –type. The standard deviation of standard deviation was quite constant throughout the year, about 0.2 g/m^3. The variability between houses starts to increase exponentially when outdoor air temperature increases to 20 °C.

As a result of the calculations, we have equations for distributions for both indoor moisture excess average and standard deviation (Eq. 1). Sanders [76] has recommended to use 10 % critical values for loads in building physical calculations. This is clear with average moisture excess, because more moisture in the system typically has small effect on temperatures but increased moisture load increases moisture-related risks. The same criterion has been chosen also for the standard deviation, because the impact of varying conditions is unlinear [77]. It is not studied here, but the high moisture load times are assumed to have bigger negative impact on moisture conditions than the same amount of drier times has positive impact.

Histograms and normal probability plots of indoor moisture excess for each house and temperature degree were monitored during the calculations. In many cases the moisture excess had a long tail and so some other distribution might describe the process better than normal distribution, e.g. gamma distribution. However because of familiarity and reasonable accuracy the normal distribution was eventually chosen.

Also differences came up with the Matlab's graphical cftool. The resulting coefficients for the same equation might vary when changing through different options. This can be at least partly due to the initial guesses and tolerances. It is good to arrange e.g. visual check on curve fitting results.

3.4.5 Germany input (IBP)

3.4.5.1 Introduction

The following subsections address the excess moisture of the residential houses presented in section 2.7. To estimate the excess moisture, data for outdoor temperature and relative humidity as well as indoor temperature and relative humidity is necessary. In this case, only for 42 houses a complete dataset has been available.

The moisture excess is linked to indoor moisture sources such as cooking, washing, perspiration, user behavior etc. The outdoor air has a certain amount of water content depending on the weather conditions, while the indoor air water content depends on the moisture production rate and the base level of the outdoor air water content and air exchange. Physical principles imply that the differences try to even out. The data is relevant in such aspects as extra moisture increases the moisture load on building structures and therefore e.g. increases the danger of mold growth.

At first the general distribution of the excess moisture is analyzed as well as trend over the year and the differences between room types. Secondly its correlation between other parameters is investigated.The excess moisture is defined as absolute humidity indoor – absolute humidity outdoor for each hour.

3.4.5.2 Excess Moisture distribution

Figure 3.96 shows the excess moisture distribution of each single house (orange) and all data combined for each hour.

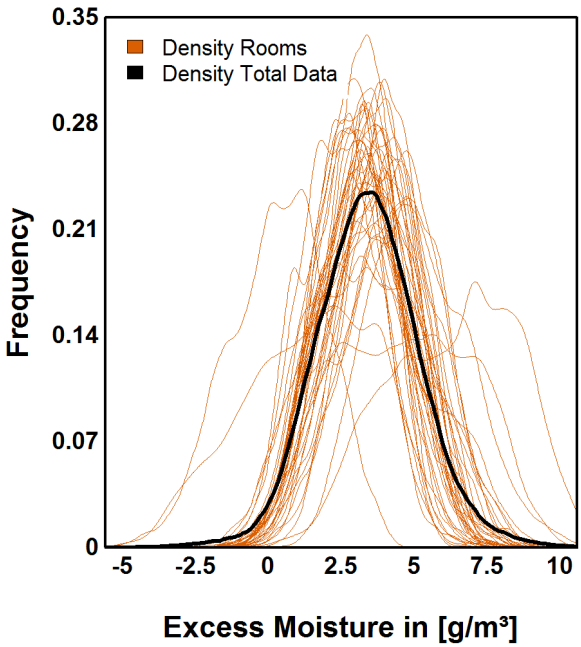

Figure 3.96 Excess moisture distribution.

The curve highly suggests a normal distribution; therefore a Shapiro Wilk test with 3000 samples has been performed to verify this assumption. The results show a very high possibility that the

data follows the normal distribution (probability of 6e-09 to reject the hypothesis of normal distribution).

For further analysis, the influence of the room types is investigated. Figure 3.97 shows the distribution function of different room types. The plot indicates that there is hardly any variance between different room types. Apart from the bathroom, which has the highest values, all rooms have more or less the same amount of moisture excess. Detailed data can be obtained in Table 3.25.

By analysing this data it can be concluded that the air moisture content spreads relatively consistent in between the building envelope; hence the room type does not play a significant role.

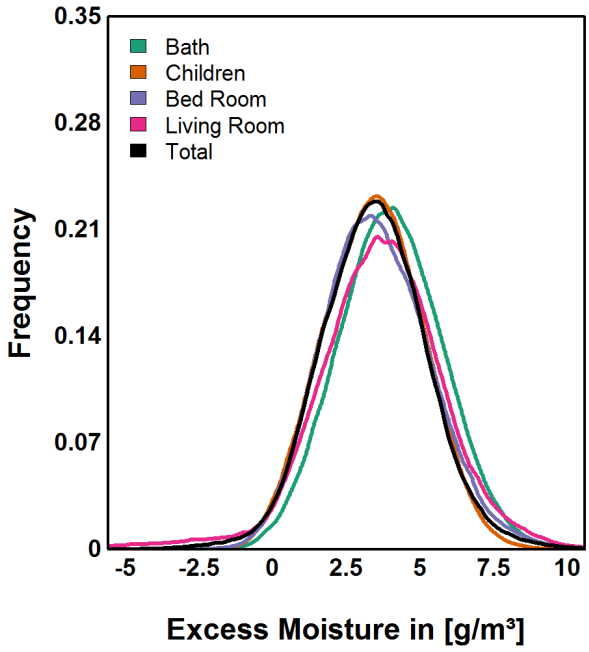

Figure 3.97 Excess Moisture distribution for different room types.

Table 3.25 Summary excess moisture data.

	Min.	1st Qu.	Median	**Mean**	3rd Qu.	Max.	SD
Bath	-3.0	2.8	4.0	**4.0**	5.2	12.8	1.8
Child	-2.3	2.2	3.4	**3.4**	4.6	10.7	1.7
Bed Room	-7.1	2.3	3.4	**3.5**	4.7	11.9	1.8
Living Room	-10.5	2.3	3.7	**3.6**	5.0	15	2.2
Total	**-10.5**	**2.2**	**3.9**	**3.4**	**4.5**	**15**	**1.8**

3.4.5.3 Excess Moisture profiles

Plotting the average excess moisture excess over the daytime does not display a significant divergence throughout the day (Figure 3.98). During night times, the excess moisture seems to be slightly lower most likely due to less activity in moisture production. However, the values only vary around 0.4 g/m³ at maximum.

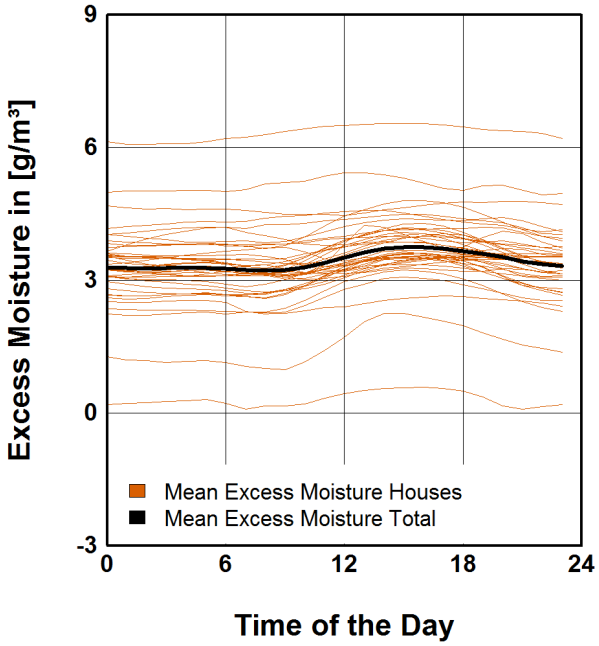

Figure 3.98 Excess Moisture day profile.

In contrast, the changes with the time of the year as Figure 3.99 confirms. Based on the assumption, that in cold months of the year the excess moisture is significant higher, the influence of the outdoor climate conditions are investigated in the following section.

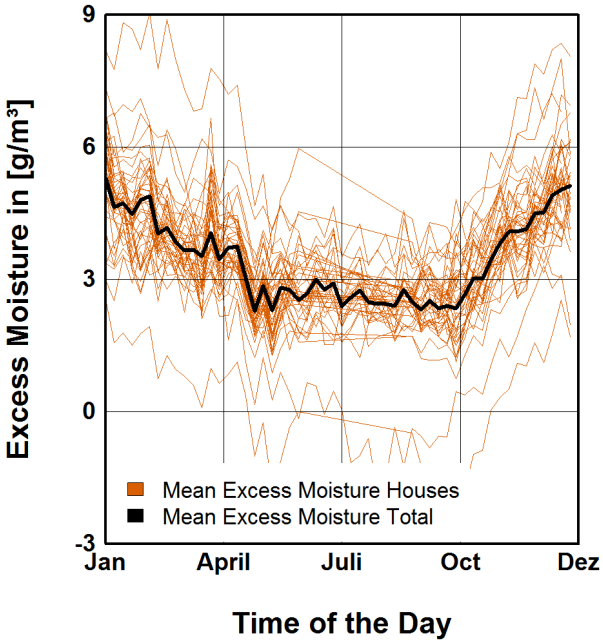

Figure 3.99 Excess Moisture year profile.

3.4.5.4 Excess Moisture in correlation with other parameters

The following plots show the average excess moisture for a certain temperature or relative humidity interval. The intervals are defined as 1 °C or 1 % (e.g. all values measured from 9.5 °C to 10.4 °C are summarised into the interval of 10 °C).

In contrast, the outdoor climate conditions clearly influence the excess moisture as Figure 3.100 and Figure 3.101 show.

The outdoor temperature is negatively correlated between -20 °C and 10 °C but increases excess moisture when increasing temperature from 10 °C to 30 °C. It should be pointed out that the data greater than 35°C is not very reliable due to the small dataset.

Pearson's product-moment correlation estimates a very strong correlation of -0.89 / -0.91 between excess moisture and outdoor temperature respectively relative humidity.

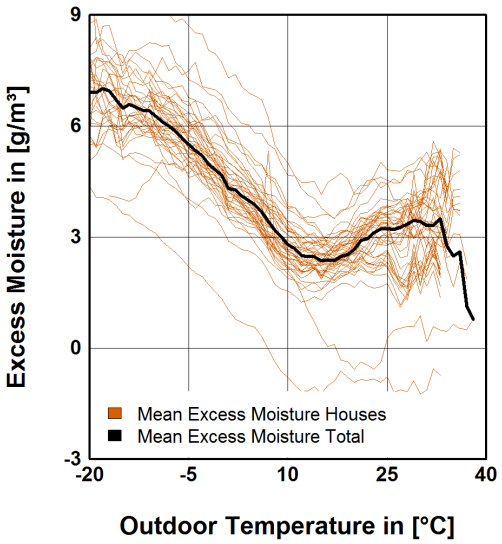

Figure 3.100 Excess Moisture in correlation with outdoor temperature.

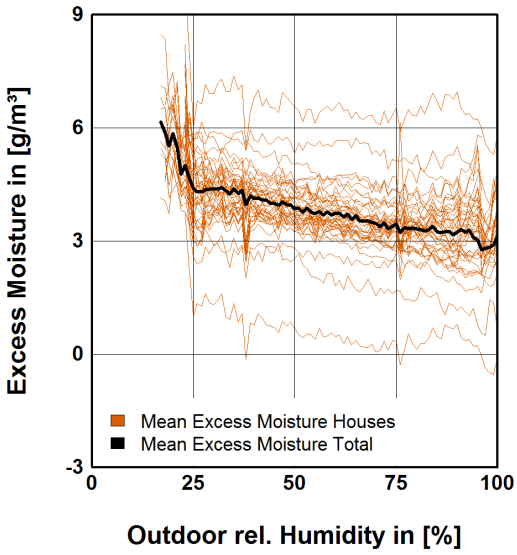

Figure 3.101 Excess Moisture in correlation with outdoor relative humidity.

3.4.6 Sweden [CTH] – Base data for moisture production estimation

The results of simulations of indoor moisture production mentioned in 2.10.2 are provided in a Excel file, in the Digital Appendix. The results are presented as annual averages for 10000 simulated households, both single and multi-family dwellings. The production rates are also presented for each activity, as annual averages. Further, the hourly variation of the indoor moisture production is presented for 1000 simulated Swedish multi-family dwellings.

Annual Averages of Indoor Moisture Production.xlsx

Simulated Indoor Moisture Production in 1000 Multi-Family Dwellings.xlsx

3.4.7 Sweden [LTH1] – Indoor loads in case Situgna

Building Physics at Lund University has measured in two apartments in a two-storey building close to Stockholm every five minute during a number of years. The measurements presented here represent two years of data from July 2009 to June 2011 with samples taken every five minutes with a few shorter breaks due to power outs during the construction phase. The data is presented unaltered with temperature (°C), relative humidity (%) and moisture supply (g/m^3) diagrams. Preliminary results from the Sigtuna study can be found in [54]. More information about indoor loads in Swedish buildings is published in [78] and [79].

3.4.7.1 Temperature and relative humidity

Measurements of temperature (°C) and relative humidity, in two dwellings and outdoors, from July 2009 to June 2011 is shown in Figure 3.102 and Figure 3.103. In March 2011 the tenant has been vacated, because of complaints from the inhabitants about the indoor environment, and a reduction in the variation and average values of both temperature and RH is notable. As

expected both the indoor temperature and RH is lower in winter than in summer. Indoor sensors In2 and In3 in Figure 3.102 and Figure 3.103 are close to each other and in the same apartment, see Figure 2.31. The differences between different indoor sensors at a given time seem generally not very big.

However, when comparing the cumulative curves in Figure 3.104 andFigure 3.105 there are obvious differences between the three sensors in the two apartments. The most apparent difference when looking at temperature is that it is always warmer in position In1.

In summer 2010 the outdoor temperature is above +30 °C, which is uncommon for Sweden. From Figure 3.88 and Figure 3.89 it is shown that also the indoor temperature is above +30 °C. The median temperature for In2-3 is around +21,5 °C and approximately +23 °C for In1. According to [78] the average temperature for multi-family dwellings in Sweden is 22,3 ± 0,2 °C during the heating season. It seems as if the measured temperature in In2-3 is somewhat lower than for the average Swedish multi-family dwelling.

In rare occasions the indoor RH can be as high as 70-75%. Since the surface temperature on exterior walls is often lower than the indoor temperature there might be a risk for mould growth.

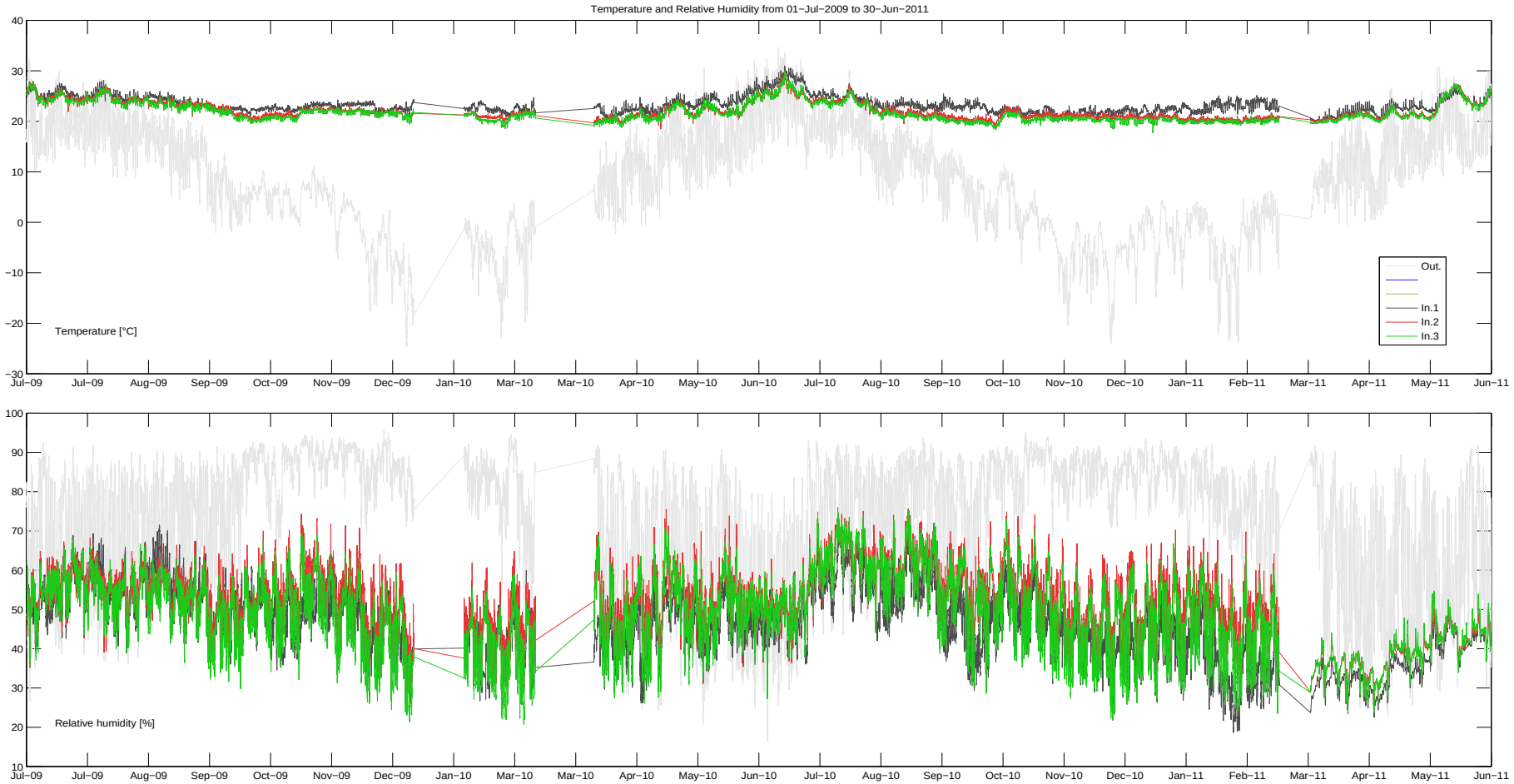

Figure 3.102 Temperature (°C) in two dwellings and outdoors in Sigtuna from July 2009 to end of June 2011.

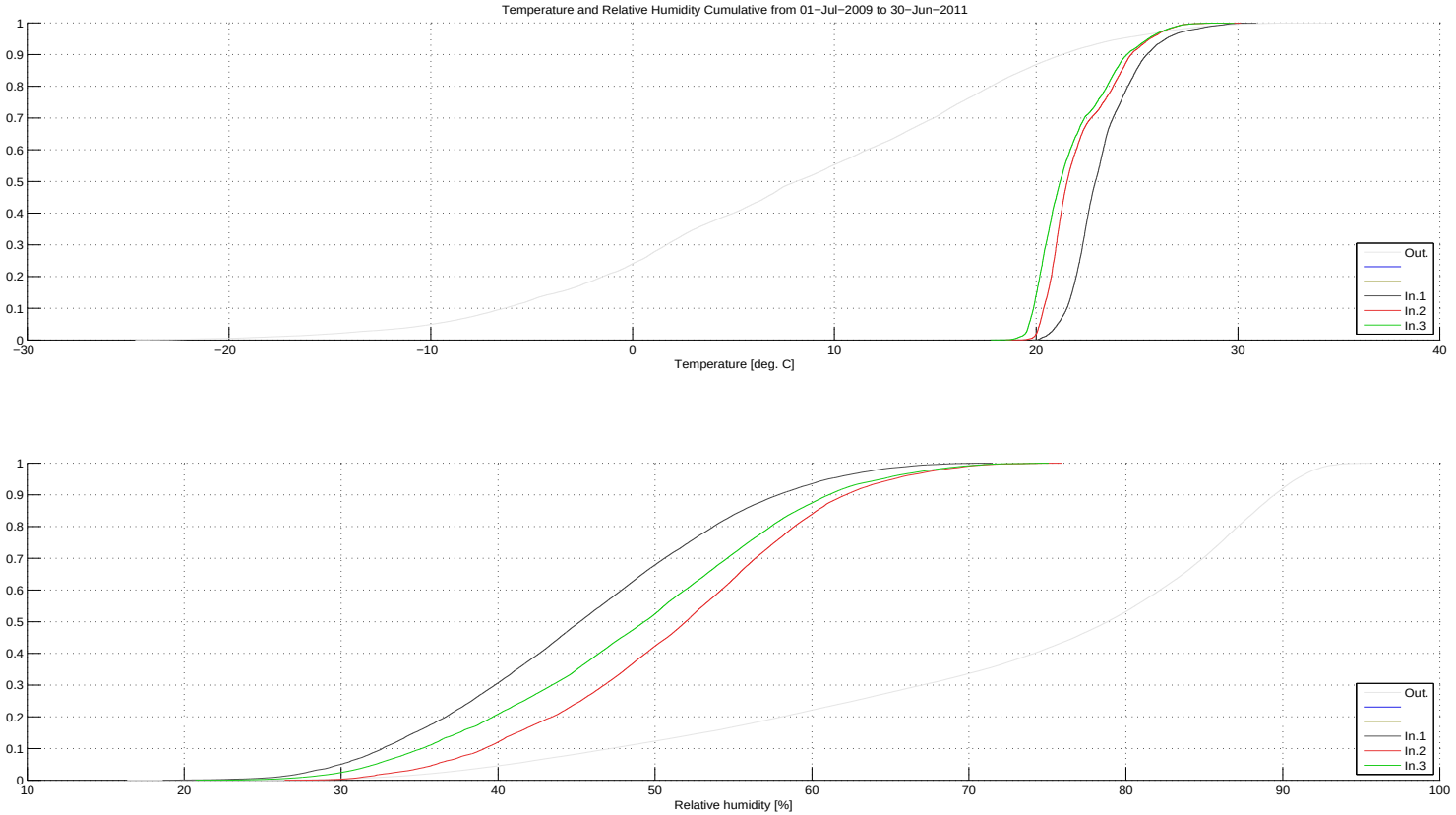

Figure 3.105 Relative humidity (%) cumulative in two dwellings and outdoors in Sigtuna from July 2009 to end of June 2011.

3.4.7.2 Moisture supply

Moisture supply (g/m^3) has been calculated from temperature and relative humidity outdoor and indoor. As always is moisture supply the difference between the vapour concentration (g/m^3) indoors and outdoors. From Figure 3.106 it is obvious that moisture supply is lower after March 2011, i.e. without people and activities from living in an apartment the moisture supply is substantially reduced. Figure 3.106 also show that the moisture supply is higher in winter than in summer. This also expected since some moisture activities as drying of clothes indoors are rare in summer. It is also probable to have higher ventilation in apartments from window opening when the outdoor temperature is high.

Figure 3.107 show the cumulative moisture supply (g/m^3) in two dwellings. The median moisture supply is higher than reported by [78]. According to [78] the average moisture supply for Swedish multi-family dwellings is approximately 1,2 g/m^3 during the heating season. A high moisture supply generally indicates that there is something wrong with the ventilation or that the inhabitants are acting in an “unexpected” way. However, it is normal to have short peaks with high moisture supply and also negative moisture supply as seen in Figure 3.106, especially in position In2, and in Figure 3.107. Negative moisture supply can occur if the outdoor climate changes rapidly. It can also happen frequently as we normally cannot take into account for the time delay between vapour concentration outdoors and indoors. A third possible reason for negative moisture supply is the “volume factor”, i.e. when cold air enters into a warm building the air will expand and thus the vapour concentration will decrease. However, in this study we have taken into account the "volume factor".

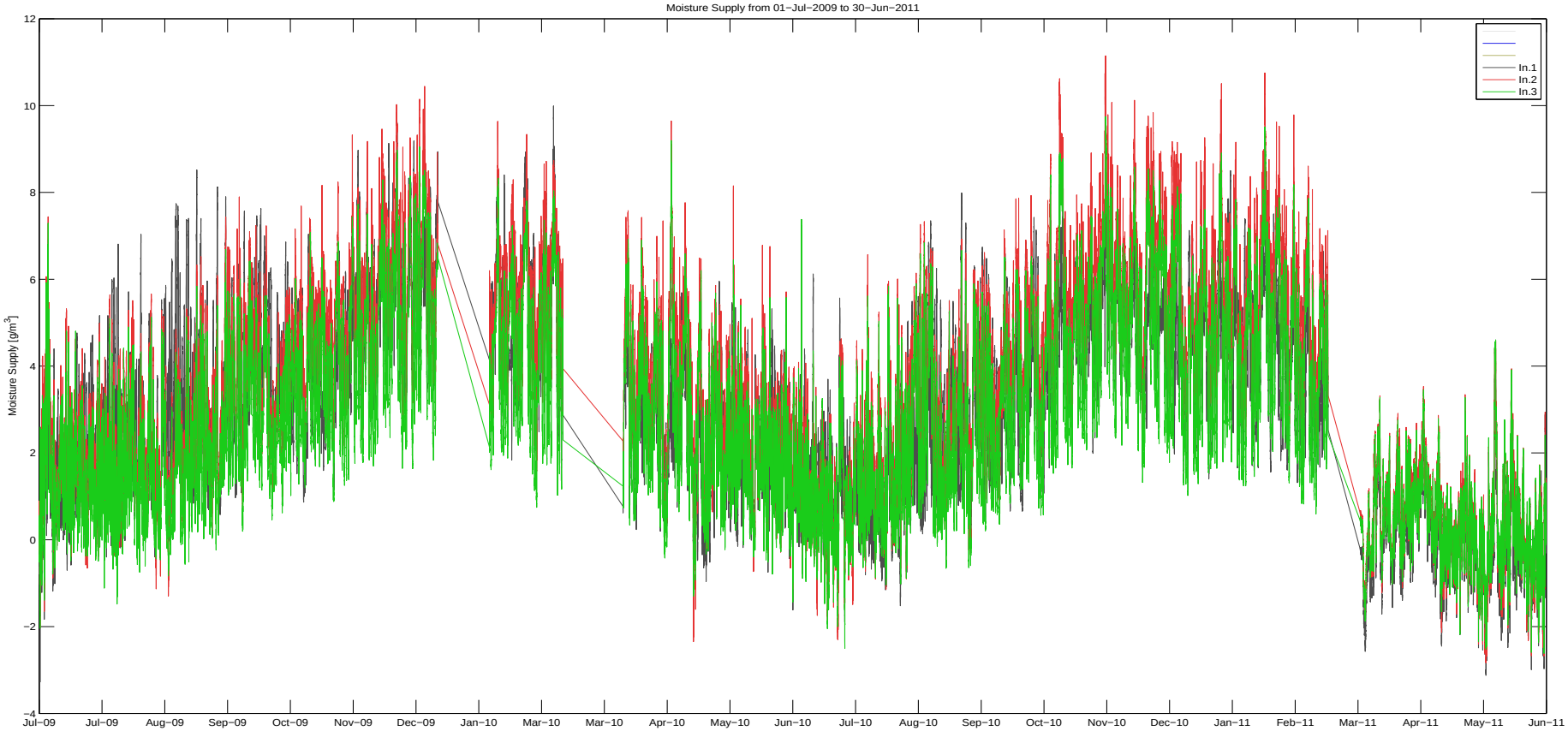

Figure 3.106 Moisture supply (g/m^3) in two dwellings in Sigtuna from July 2009 to end of June 2011.

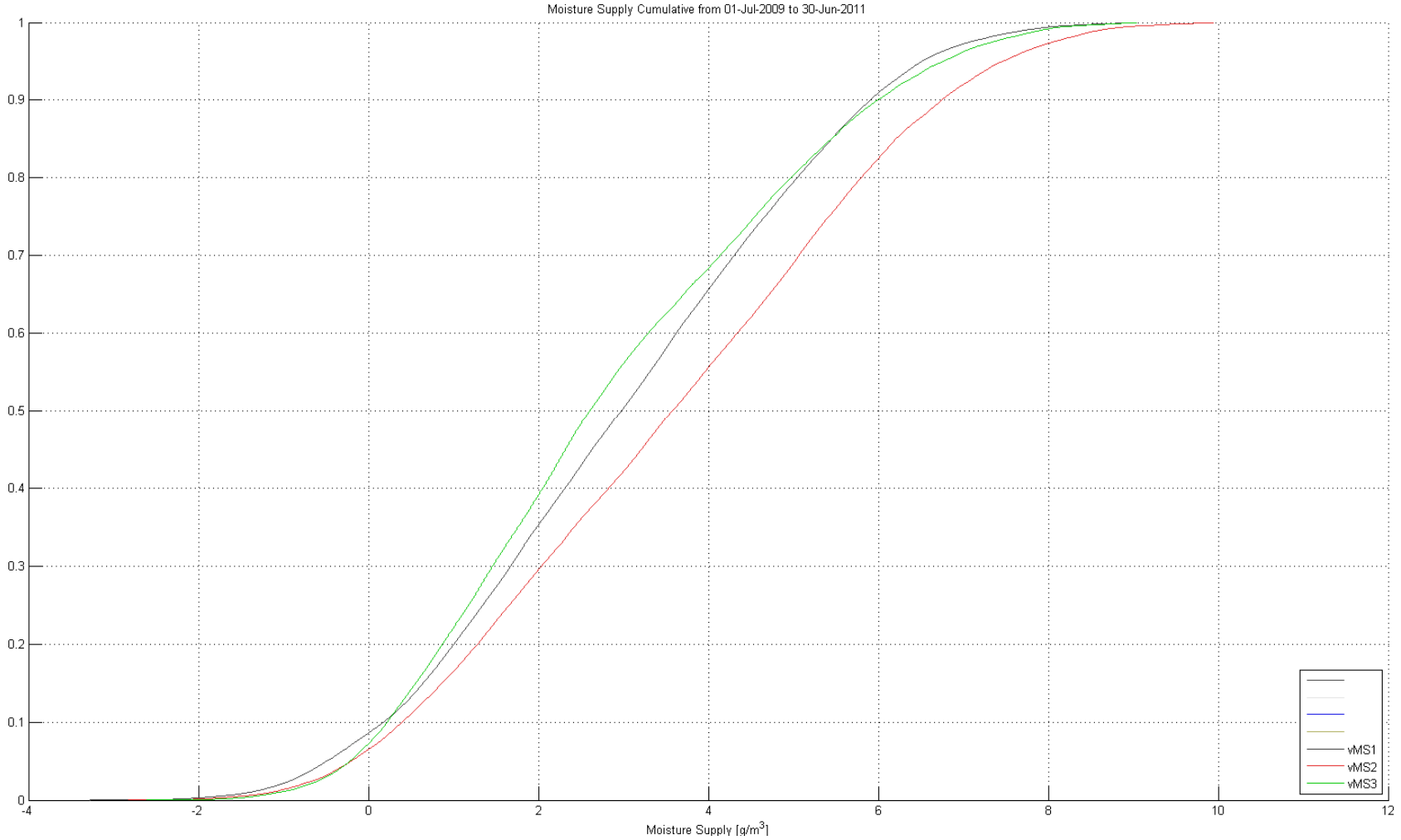

Figure 3.107 Moisture supply (g/m^3) cumulative in two dwellings in Sigtuna from July 2009 to end of June 2011.

3.4.8 United Kingdom [UCL] – Indoor loads in the Warm Front study

3.4.8.1 Collected raw data

A total of 1871 sets of living room and bedroom temperature, relative humidity, and mould data were collected from a subset of 1481 dwellings with characteristics given in Table 3.26, thus including repeat as well as both post- and pre-intervention measurements. As with the previous sample (i.e. for air infiltration rate measurements presented in section 3.3.8), this sample is dominated by dwellings built between 1900-1950 and cavity masonry walls. Most of the dwellings are however semi-detached in this sample. The data are cleaned of repeat measurements and if both pre- and post-intervention measurements exist for the same dwelling, only the pre-intervention measurements are kept so that the data represents a single stock.

Table 3.26 Dwelling characteristics of sample in which air temperature, relative humidity, and Mould Severity Index measurements were taken.

Age		Wall type		Building type	
Pre 1900	11 %	Cavity masonry	68 %	Terraced	7 %
1900-1950	52 %	Solid brick	29 %	Semi-detached	51 %
1951-1976	32 %	Timber framed	1 %	Flats	38 %
Post 1976	5 %	Other	2 %	Detached	5 %

3.4.8.1.1 Winter internal temperatures and relative humidity

The temperature and relative humidity (RH) were measured in the main living room and main bedroom using Gemini TinyTag data loggers at half-hourly intervals for periods of 2 to 4 weeks between December and early May. The sensors were positioned away from direct sources of heat and light on a sideboard or shelf at approximately 1m above the ground.

3.4.8.1.2 Winter external temperatures and relative humidity

Measurements of external temperature and RH were also recorded in central locations in each of the survey areas.

3.4.8.1.3 Mould Severity Index

Table 3.27 Interpretation of MSI.

MSI range	Significance
1-2	Slight
3-4	Moderate
>5	Severe

Each property underwent a detailed visual inspection regarding the occurrence and extent of mould on windows, walls and ceilings, though no attempt was made to identify the species. The state of mould growth was quantified using the Mould Severity Index (MSI):

MSI = the number of rooms with mould growth

+1 if there is mould in either living room

+1 if there is a match with the medium mould photograph

+2 if there is a match with the worst mould photograph (1)

Thus it is defined such that a dwelling will have an MSI of at least one if there is any mould growth in any one single room. The significance of the index is given in Table 3.27. The calculation of MSI requires the quantification of the number of rooms with mould with an extra penalty if it is found in any living rooms as these are generally heated to a higher level than other rooms in the dwelling. Then a comparison of the mould growth is made against standard photographs showing three classes of mould severity ranging from slight, medium to the worst.

3.4.8.2 Analysis

3.4.8.2.1 Post-processing of raw data

Standardized internal temperature

The living room and bedroom temperatures were standardized to an external temperature of 5°C to account for the variability in weather. This was carried out by excluding data from any day where the maximum temperature was above 15 °C (above this temperature, the heating system would normally be switched off) and from any monitoring period during which the coldest day had a maximum temperature above 7 °C. For living room temperatures, data was analysed for between 8:00h to 20:00h and for bedroom temperatures between 20:00h to 8:00h.

For each dwelling, the selected internal temperatures were regressed with the corresponding external temperatures, including quadratic terms to allow for a non-linear relationship. The internal temperature and its standard error were then estimated from this regression equation at an external temperature of 5 °C.

Standardized vapour pressure excess

The living room and bedroom relative humidities were also standardized to account for the variability in weather. Firstly, the hourly vapour pressure excess was calculated for the living room and bedroom of each dwelling based on the monitored relative humidity. For each dwelling, the internal vapour pressure excess was regressed with the external temperature using quadratic terms to allow for any non-linearities in the relationship. The internal vapour pressure excess and its standard error were then estimated for an external temperature of 5 °C.

3.4.8.2.2 Statistical summary

Table 3.28 Summary statistics for distributions of standardized internal temperature in living room and bedrooms, standardized internal vapour pressure excess in the living room and bedroom, and the mould severity index, after zero temperature and humidity entries are removed (this is why the number of dwellings vary).

	Number of dwellings	Mean	Median	Standard deviation
Standardized internal temperature in living room (°C)	1007	18.8	19.1	2.9
Standardized internal temperature in bedroom (°C)	968	17.1	17.0	3.0
Standardized internal vapour pressure excess in living room (Pa)	894	317.8	308.2	165.1
Standardized internal vapour pressure excess in bedroom (Pa)	814	327.5	315.8	167.9
Mould Severity Index	1481	0.44	0	1.19

3.4.8.3 Stochastic data sets

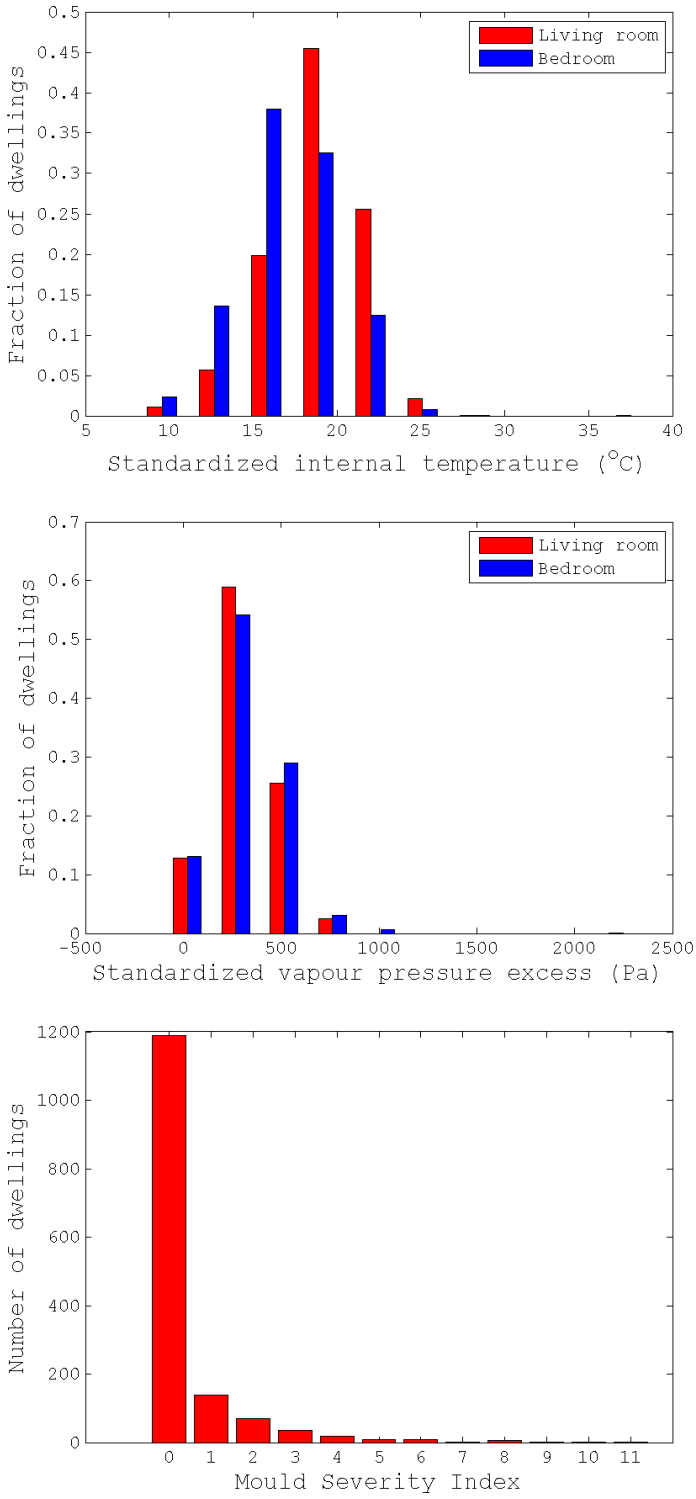

Figure 3.108 Distribution of standardized internal temperatures (top), standardized vapour pressure excesses (middle), and mould severity indices (bottom).

Figure 3.108 shows the distribution of standardized internal temperatures and standardized vapour pressure excesses for the living room and bedroom, and MSI for the whole dwelling.

3.5 Weather

3.5.1 The Netherlands [TUE] – Case study on the urban heat island

The urban heat island intensity was measured at five locations in Rotterdam, subsequently the frequency distribution of the UHI intensity was determined as well as the diurnal variation of the UHI intensity. This section will first describe the experimental set-up, followed by a description of the method used to determine the diurnal variation of the UHI. At the end of this section a description the measurement results given.

3.5.1.1 Experimental set-up

At five locations in Rotterdam the weather was measured (as shown in Figure 3.109) from 01-04-2011 to 31-10-2012 (579 days) by Standard Campbell weather stations with an added 4-component radiation sensor (Hukseflux NR01) and Black Globe temperature sensor (Sensor Data). The measured components that are used in this study are the dry bulb temperatures in the urban areas, which are compared to the dry bulb temperature in the rural area (at Rotterdam Airport). The five locations where the measurements took place in the city of Rotterdam were; (1) City center; (2) Ommoord; (3) Rijnhaven; (4) Spaanse polder; (5) Vlaardingen. For the rural area, the measurements of the Royal Dutch Meteorological Institute (KNMI) of Rotterdam were used. This station is located at Rotterdam airport roughly 5 km from the centre of Rotterdam and mainly consists of grass land. The time interval at which the data is considered is by one hour time steps, resulting in a total of 13,896 readings for each station.

Figure 3.109 Measurement locations in Rotterdam (NL).

3.5.1.2 Method for determination of diurnal variation

The diurnal variation of the UHI intensity in Rotterdam was analysed as a function of time, which enables to the time of maximum and minimum UHI intensity as well as the typical variation over a day. This diurnal variation of the UHI was determined by a Fast Fourier transformation applied to the average UHI intensity of Rotterdam. As a result the sinusoidal functions with the best fit for the diurnal variation are identified. The transformation was performed for periods of one month, this monthly period is equal to the period used to indicate the diurnal variation in e.g. [80]. The Fourier transform was performed by using the Fast Fourier transform algorithm [81] in MATLAB R2012a (version 7.14.0.739). In the evaluation of the transformation three harmonics as well as a constant were taken into account, namely with a frequency of one day, half a day and one third of a day. This leads to the following expression for the transformations for each month.

$$\mathrm{UHII(t)} = \mathrm{a_0} + \sum_{\mathrm{k=1}}^{3} \mathrm{A_k} \cdot cos(k\omega_0 t + \varphi_k) \qquad (3.7)$$

where UHII is the urban heat island intensity at a specific time, a_0 is the constant value for each month, A_k the amplitude of a specific harmonic of a specific month, ω_0 the angular velocity and φ_k the phase change for a specific harmonic.

3.5.1.3 Results of UHI measurements

The analysis of the hourly data from 01-04-2011 to 31-10-2012 showed an average urban heat island intensity over this period between 0.53 and 1.16 °C for the five locations. The maximum UHI intensity varied between 5.3 and 8.8 °C for the five locations, the maximum was found in the Center. The frequency distribution of the UHI for the five locations over the complete period are shown in Figure 3.110, the indicated distribution is the generalized extreme value distribution. A negative UHI intensity is not uncommon and is reported in several studies e.g. [21], [22], [82], [83], [84], [85], [48], [86], [87], [88], [89], [29]. [22] reported that the occurrence of a negative urban heat island intensity might be restricted to city centres with deep and narrow urban canyons (higher aspect ratios). This is supported by the measurements, the strongest negative intensity was namely found in Rijnhaven, which had the highest aspect ratio of the five locations (aspect ratio Rijnhaven: 1.11).

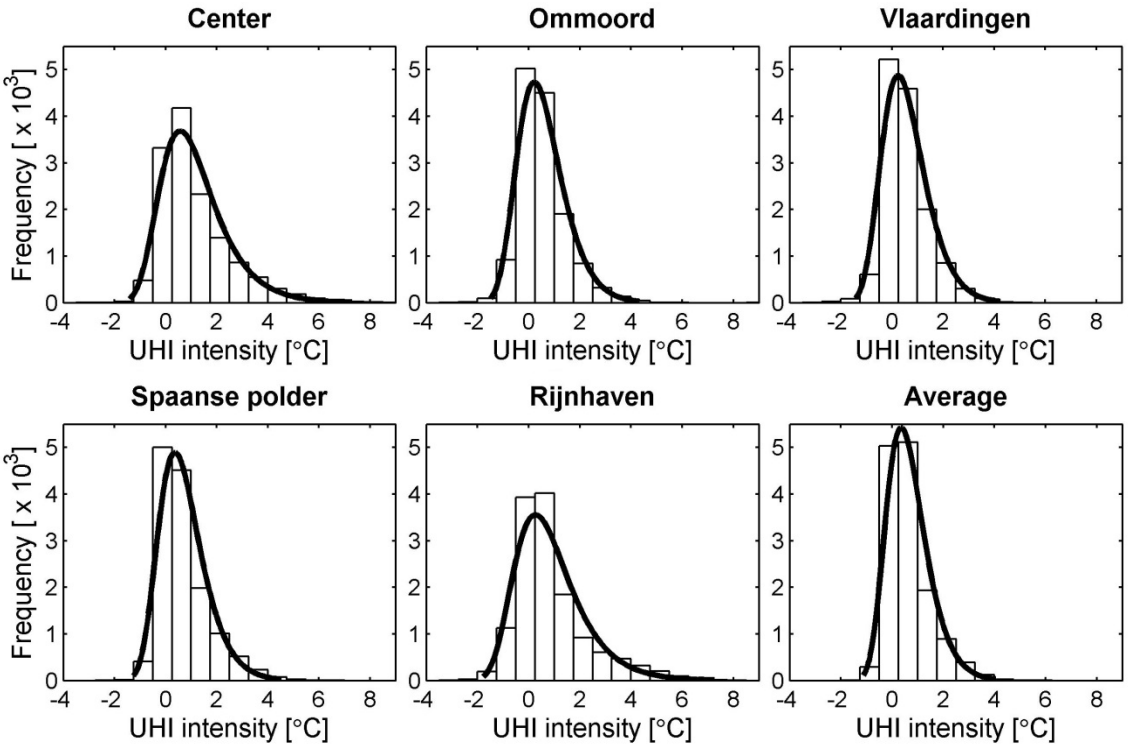

Figure 3.110 Measured UHI intensities from 01-04-2011 to 31-10-2012 for five locations as well as the average UHI intensity. The shown distribution is a fitted generalised extreme value distribution.

3.5.1.4 Diurnal variation of the urban heat island

The diurnal variation of the UHI intensity in Rotterdam was determined by a Fourier transformation of the average UHI intensity at the five locations in Rotterdam. Figure 3.111 shows the average diurnal variations for each month in one year from November 2011 to October 2012. It is shown that the variation during a day changes over the year. The maximum urban heat island intensity was found during the night and the minimum roughly at 10:00h. Moreover, it is visible from the average UHI intensity that the effect decreases rapidly during the morning and increases gradually during the day reaching its maximum during the night. The UHI intensity is relatively constant during the night (20:00h to 5:00h), which was also reported by e.g. [90].

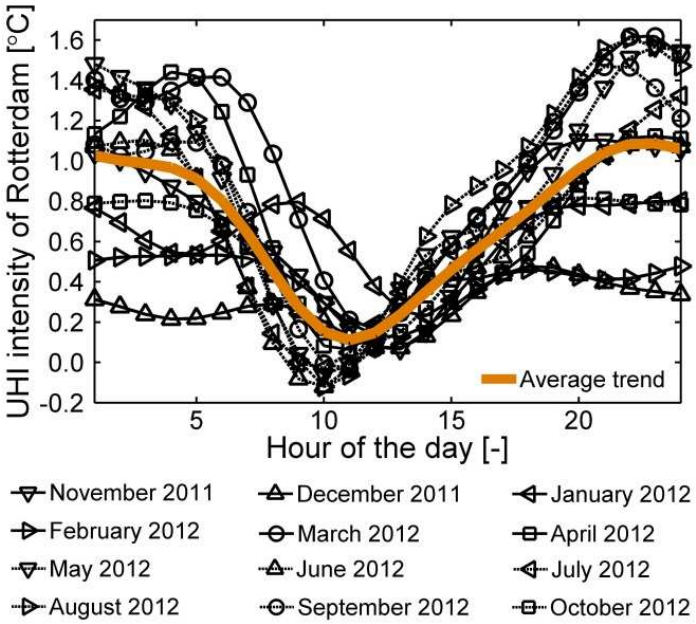

Figure 3.111 Diurnal variation of the UHI intensity in Rotterdam. The time is displayed in UTC+1 throughout the complete year.

3.5.2 Sweden [CTH] – Future climate scenarios

3.5.2.1 Available climate data (raw)

These are the raw weather parameters received from the Rossby Centre, SMHI.

Table 3.29 Raw weather parameters from Rossby Centre.

Weather parameter	Unit	Time resolution
downward longwave radiation at the surface	[W/m^2]	30 minutes
corresponding shortwave radiation	[W/m^2]	30 minutes
air temperature at the 2-metre level	[K]	3 hours
specific humidity at the 2m level	[kg water/kg air]	3 hours
WE wind speed components at the 10-metre level	[m/s]	3 hours
SN wind speed components at the 10-metre level	[m/s]	3 hours
total precipitation	[mm]	30 minutes
snow precipitation	[mm]	30 minutes
total cloud coverage	[0-1]	3 hours
total air pressure	[N/m^2]	30 minutes
cloudiness of low-level clouds	[0-1]	
cloudiness of mid-level clouds	[0-1]	
cloudiness of high-level clouds	[0-1]	
rain precipitation	[mm]	6 hours

3.5.2.2 Available climate data (processed)

The raw data have been processed and the following data sets are available for building simulations for all the climate scenarios and with the time resolution of one hour.

Table 3.30 Processed raw data available for building simulations.

Weather parameter	Unit
Air temperature	[°C]
Relative humidity	[%]
Global radiation	[W/m^2]
Diffusive horizontal radiation	[W/m^2]
Direct normal radiation or Beam	[W/m^2]
Long wave sky radiation	[W/m^2]
Wind direction	[degree]
Wind speed	[m/s]

More details about how the raw data are processed can be found in [1], chapter 2.

3.5.2.3 Available climate scenarios

Climate scenarios are result of different global climate models, regional climate models, emission scenarios, initial conditions and/or spatial resolution. Available climate data sources are shown below, and more information about them can be found in [91] and [92].

For the exact combinations of climate data sources into climate scenarios, contact Building Physics research group on info@byggnadsteknologi.se. All data sets cover the period of 1961-2100 (140 years).

Table 3.31 Climate scenarios.

Cities	Global climate models	Regional climate models	Emission scenarios	Initial conditions	Spatial resolution
Gothenburg	CCSM	RCA3	A2	1	25 x 25 km
Lund	CNRM	KNMI-RACMO2	B1	2	50 x 50 km
Stockholm	ECHAM5	DMI-HIRHAM5	B2	3	
Östersund	HADCM3		A1B		
	IPSL				

Besides, we have RCA3-ERA40 reanalysis that constitutes a realistic description of the state of the atmosphere including its evolution in time for the period 1961-2002.

3.5.3 Sweden [LTH2] – 9 years climate measurements

In order to create data suitable for heat and moisture calculations several corrections had to be made. The aim was not to create data which matched the original situation as much as possible. It was to create realistic but relatively tough data, i.e. be sure to create data with a high rather than low moisture load.

The steps taken to create the data were:

1. Sanitize the data to remove obvious strange values.
2. Complement missing days of data by using full periods before and after.
3. Complement missing hours by interpolating between hours before and after.
4. Calculate missing long wave radiation data by formulas according to [93].
5. Distribute precipitation to hourly values according to [93].
6. Adjust the relative humidity by scaling so that there was 100 % at least once every 3 month (12 weeks). This was done using a 12 week moving average as base for the scaling.

Figure 3.112 shows some of the parameters for all the locations and all the 9 years. Figure 3.113 and Figure 3.114 show the data for Lund.

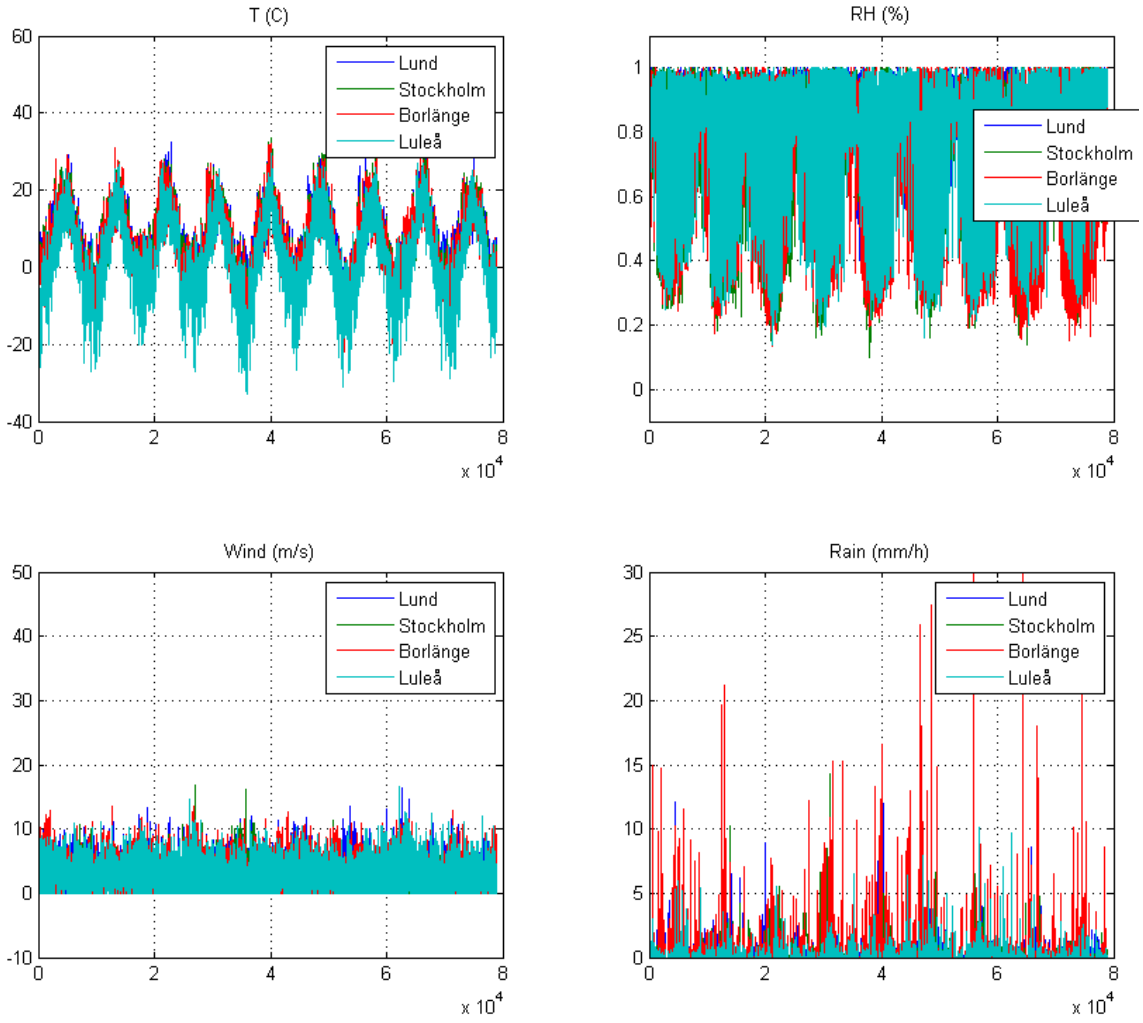

Figure 3.112 The climate for all years and all positions.

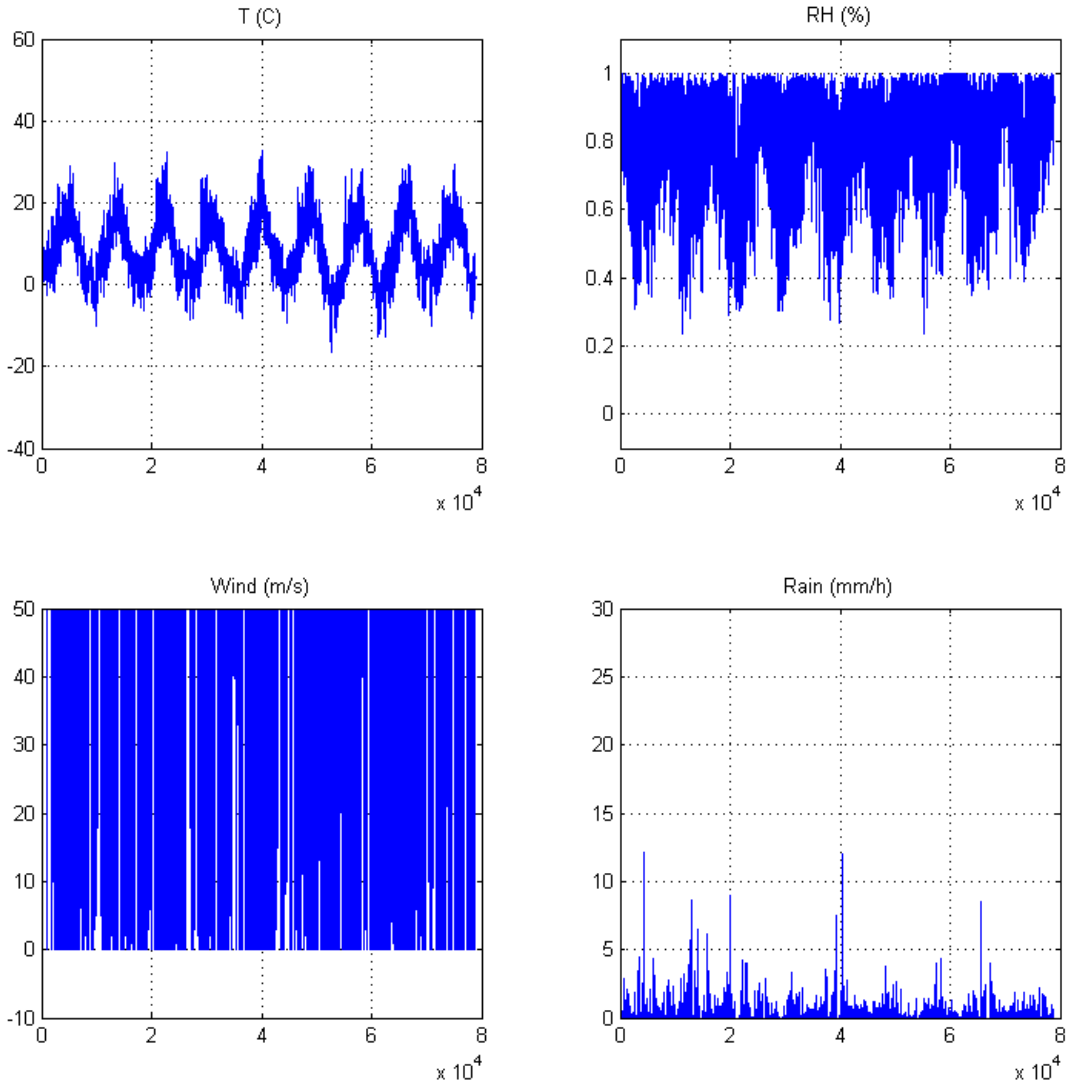

Figure 3.113 Temperature, relative humidity, wind speed and precipitation in Lund.

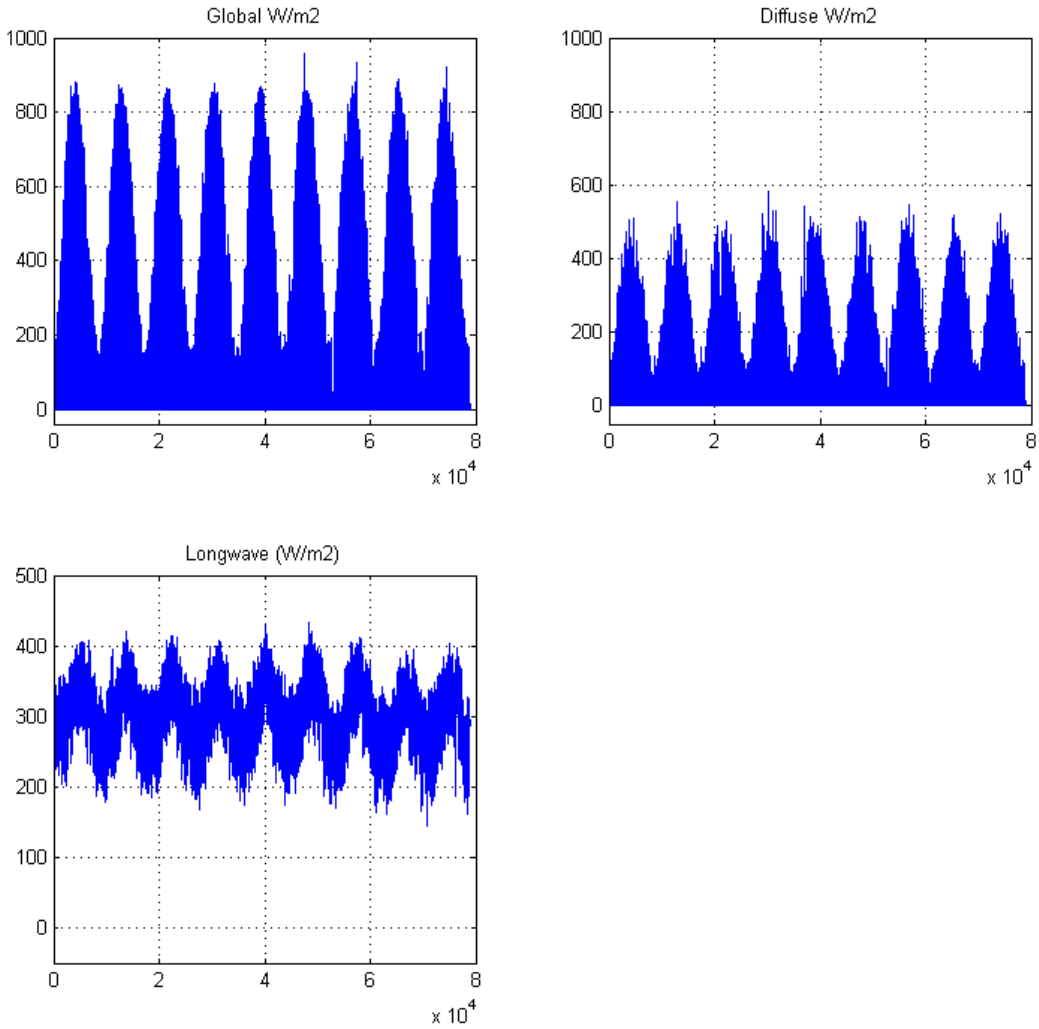

Figure 3.114 Global, diffuse and long-wave radiation for Lund.

4 SYNTHETIC DATA

4.1 Introduction

The fourth chapter presents work on synthetic data, demonstrating how additional sets of valuable information can be prepared with more advanced analysis. The following examples are provided:

- Extrapolation of material properties from comparison of incomplete material data with generic materials and via regression analysis.
- Determination of window opening behaviour according to recorded temperatures and building type, area and airtightness.
- UHI intensity determination using data on wind speed, relative humidity, global horizontal irradiance and cloud cover.

4.2 Germany [TUD]: Extrapolation of incomplete material data

Material data in the literature is not always complete, i.e., the density and thermal conductivity are known, but other properties are missing. This kind of data is not qualified for simulation use, but still a valuable source for the simulation tools and should be utilized to expand a material database. In this section, the methods to extrapolate missing properties of incomplete material data set are illustrated.

As shown in Figure 4.1, missing properties of incomplete material data can be completed by two ways:

1. By comparing the available properties of the incomplete material data with those of generic materials (Section 3.1) in the same physical material group, a most similar generic material is selected. The missing properties of the incomplete material data can be supplemented by the material properties of the most similar generic material. This approach actually uses the average material property from one material cluster to substitute the missing property of the incomplete data.
2. The relationships among material properties, deduced from the measured high-quality data by regression analysis, can be applied to complete the missing properties. Regression analysis can be based on the physical material group level, which means more materials are included for the analysis but may lead to a wide range of uncertainty, or based on the material cluster level, which results in a narrow range of uncertainty since fewer materials are involved but may have the problem with statistics basis. The decision on which level to choose is dependent on the number of materials in the physical material group and in the material cluster, and the quality of the regression model, e.g., the coefficient of determination R^2.

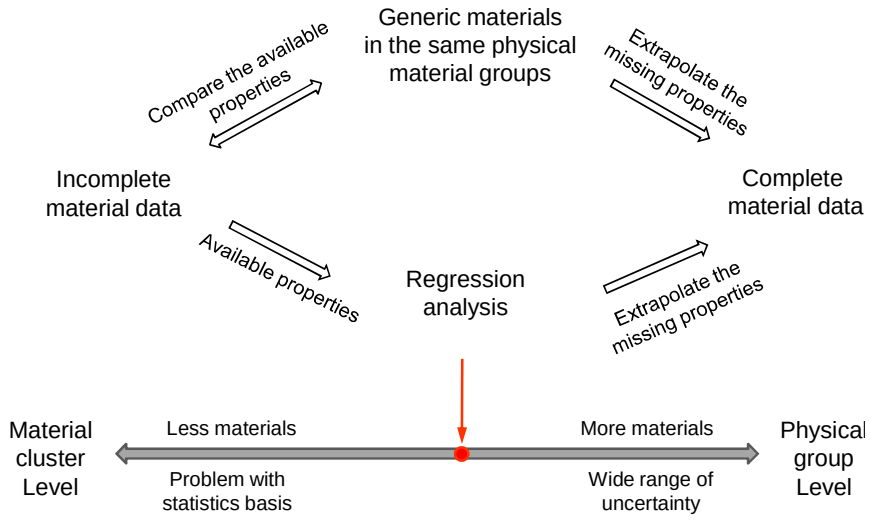

Figure 4.1 Extrapolation of the missing properties of incomplete material data by the application of generic materials and regression analysis.

Relations between basic parameters in building brick category were investigated as one example for the application of regression method. Material data was collected from IBK laboratory measurement (TUD), [64], [65], and [66]. For bricks, most parameters have a linear relationship with density (Figure 4.2). While water absorption coefficient and water vapour diffusion resistance factor cannot be directly deferred from density, the relation between them can be clearly expressed by a nonlinear regression equation. Thus, if one of the parameters is not available, the other one can be estimated by the regression equation.

Open porosity, θ_{por}:

$$0.994-0.000372\cdot\rho \qquad (R^2=0.966,\ 45\ \text{materials}) \qquad (4.1)$$

Capillary moisture content, θ_{cap}:

$$0.880-0.000379\cdot\rho \qquad (R^2=0.631,\ 40\ \text{materials}) \qquad (4.2)$$

Effective saturation moisture content, θ_{eff}:

$$1.028-0.000411\cdot\rho \qquad (R^2=0.726,\ 33\ \text{materials}) \qquad (4.3)$$

Specific heat capacity, c_0:

$$1415.357-0.305\cdot\rho \qquad (R^2=0.550,\ 39\ \text{materials}) \qquad (4.4)$$

Thermal conductivity, λ:

$$-0.712+0.001\cdot\rho \qquad (R^2=0.553,\ 56\ \text{materials}) \qquad (4.5)$$

Water vapor diffusion resistance factor, μ_{dry}:

$$0.087\cdot\exp(0.003\cdot\rho) \qquad (R^2=0.289,\ 52\ \text{materials}) \qquad (4.6)$$

Water absorption coefficient, A_w:

$$1.135-0.001\cdot\rho \qquad (R^2=0.293,\ 49\ \text{materials}) \qquad (4.7)$$

Water vapor diffusion resistance factor, μ_{dry}:

$$9.397+1.715/A_w-0.002/A_w^2 \quad (R^2=0.578,\ 45\ \text{materials}) \qquad (4.8)$$

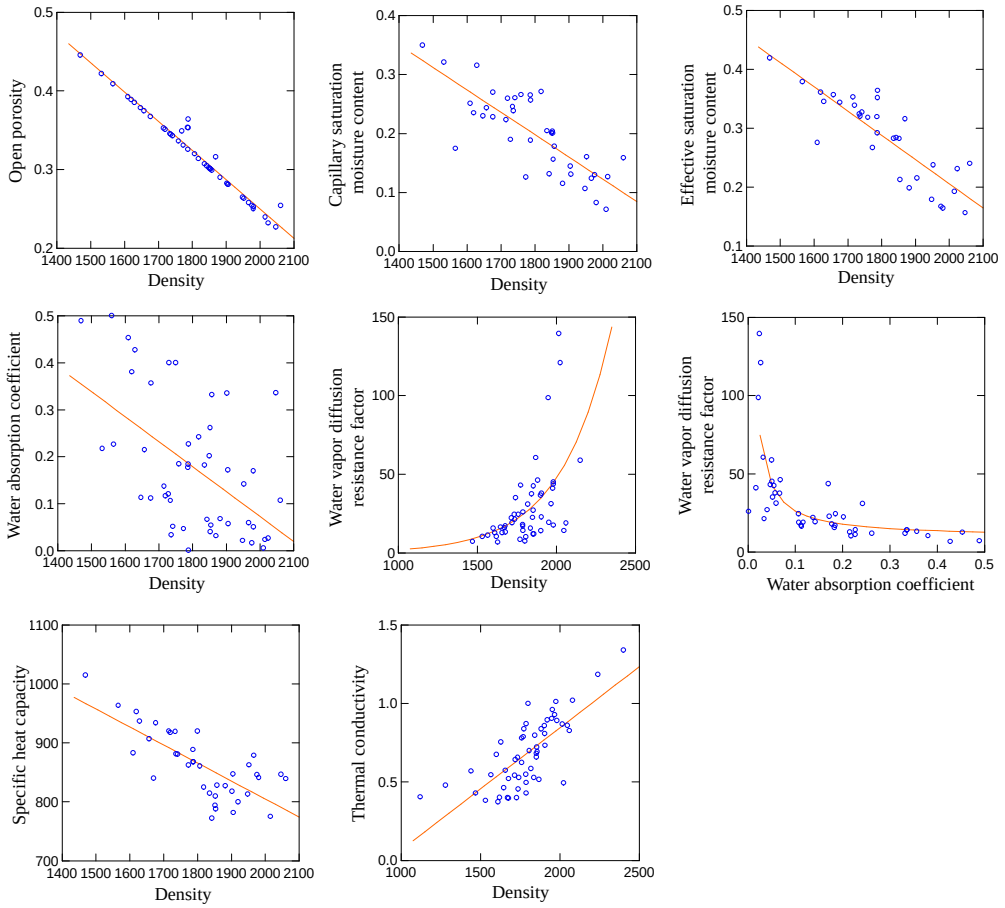

Figure 4.2 Scatter plots of material properties of specific bricks.

Moisture storage capacity is one of the most important material characteristics. It describes the amount of moisture accumulated in the material pores at the consecutive environmental conditions. In general, it can be achieved by two tests: sorption isotherm measurement in the hygroscopic range and pressure plate measurement in the over hygroscopic range. These two measurements usually take several weeks or months to reach the equilibrium condition. Therefore, measurement steps are not always sufficiently complete to derive a continuous moisture retention curve in the literature. In cases where only some data are available, regression analysis can be applied to estimate unmeasured moisture contents based on the available data.

For instance, moisture contents in the over hygroscopic range can be predicted by moisture contents *w0*, *w4.78*, and *w5.60* [18]. The coefficients of regression models are summarized in Table 4.1. For convenience, logarithmic capillary pressures is represented by *pC* (*pC=log*$_{10}$*(-P*$_c$*)*). The symbol *w4.78* denotes moisture content at *pC4.78*. *w6.56 (97.4 %)* denotes moisture content at 97.4 % relative humidity, corresponding to *pC6.56*. In the table, Ro denotes that regression coefficients and R^2 are derived from robust regression analysis, which is developed as an alternative to the least-squares estimation. It keeps the outlier in the dataset but tries to dampen its influence on the estimation of the regression coefficients. So robust regression

model will not be sensitive to these unusual outliers. Other coefficients are based on least-squares regression.

Table 4.1 Coefficients of regression models based on w0, w4.78, and w5.60 in the building brick category.

	constant	*w0*	R^2
w3.48	-0.025	1.053	0.985
w3.78	-0.046	1.100	0.966
w4.18	-0.093	1.178	0.926
	constant	*w4.78*	R^2
w4.48	0.041	0.888	0.961(Ro)
w4.95	-0.028	1.033	0.964
	constant	*Log(w5.60)*	R^2
Log(w5.30)	0.161	0.987	0.908
Log(w5.90)	-0.103	0.970	0.979 (Ro)
Log(w6.15)	-0.162	0.986	0.940

For example, the regression equation can be expressed by

$$w3.48 = -0.025 + 1.053 \cdot w0 \tag{4.9}$$

$$Log(w5.30) = 0.161 + 0.987 \cdot Log(w5.60) \tag{4.10}$$

After transformation, equation 4.10 becomes:

$$w5.30 = 10^{0.161} \cdot w5.60^{0.987} \tag{4.11}$$

75.4 % relative humidity is easily achieved by *NaCl* solution, so moisture content at 75.4 % RH can be used to predict unmeasured moisture contents in the hygroscopic range. The coefficients of regression models based on *w7.59 (75.4 %)* are summarized in Table 4.2.

Table 4.2 Coefficients of regression models based on w*7.59 (75.4%) in the building brick category*

	constant	*Log(w7.59(75.4 %))*	R^2
Log(w6.56(97.4 %))	1.102	1.288	0.846(Ro)
Log(w6.75(96.0 %))	0.747	1.199	0.861(Ro)
Log(w7.16(90.0 %))	0.196	1.029	0.956
Log(w7.36(84.7 %))	0.249	1.075	0.974(Ro)
Log(w7.87(58.2 %))	-0.464	0.848	0.953(Ro)
Log(w8.06(43.2 %))	-0.824	0.748	0.831
Log(w8.18(32.9 %))	-0.915	0.749	0.693

With the values of capillary saturation moisture content, water absorption coefficient, and open porosity, moisture contents of building bricks in the over hygroscopic range can be derived by these three parameters. The regression coefficients are listed in Table 4.3 [18]. The relationships between them provide a possibility to quickly estimate moisture storage data without any moisture measurement.

For instance, moisture contents *w*3.48, *w*4.48, and *w*5.60 can be estimated by the following equations.

$$w3.48 = 0.0365 + 1.163 \cdot \theta_{cap} \quad (4.12)$$

$$w4.48 = -0.056 + 1.472 \cdot \theta_{cap} - 0.267 \cdot A_w \quad (4.13)$$

$$Logw5.60 = -5.930 + 9.945 \cdot \theta_{por}^{0.5} - 2.752 \cdot A_w^{0.5} \quad (4.14)$$

After transformation, equation 4.14 becomes:

$$w5.60 = 10^{-5.930 + 9.945 \cdot \theta_{por}^{0.5} - 2.752 \cdot A_w^{0.5}} \quad (4.15)$$

Table 4.3 Coefficients of regression models based on basic material parameters in the building brick category.

	constant	ϑ_{cap}	A_w	R^2
w0	0.056	1.108	-	0.936
w3.48	0.0365	1.163	-	0.919
w3.78	0.017	1.210	-	0.894
w4.18	-0.029	1.312	-	0.880
w4.48	-0.056	1.472	-0.267	0.883(Ro)
w4.78	-0.100	1.655	-0.369	0.864(Ro)
w4.95	-0.134	1.805	-0.516	0.864(Ro)
w5.30	-0.090	1.439	-0.640	0.877
	constant	$\vartheta_{por}^{0.5}$	$A_w^{0.5}$	R^2
Log(w5.60)	-5.930	9.945	-2.752	0.803(Ro)
Log(w5.90)	-5.782	9.580	-2.760	0.858(Ro)
Log(w6.15)	-5.788	9.542	-2.845	0.870

4.3 Germany [IBP]: Window opening

4.3.1 Literature Background

There has been an extensive literature research regarding manual window opening carried out by C. Mayer which can be summarised as follows:

- The main influencing factor on user behaviour is the temperature. However, there are different opinions on whether the indoor or outdoor temperature is more significant.
- Most research relating to user behaviour has been done for office buildings. Manual window openings in residential buildings have not been investigated thoroughly yet.
- The occupancy does play an important role
- Disparities in user behaviour between different climate regions have not been analysed
- For the modelling of the user behaviour various mathematical methods have been used. Those are logistic regression, Markov-Chains and survival analysis.
- The angle of the window opening has not been considered yet

4.3.2 Influencing Parameter

4.3.2.1 Building, room type and size

Current research suggests that the type of the building has a significant influence on the window opening behaviour. For instance, the occupancy of residential buildings and offices are completely dissimilar, while activities like cooking or showering require other air flow rates than common office work. In general, the user behaviour in residential buildings tends to be more complex, as a substantial room dependency can be found (Figure 4.3).

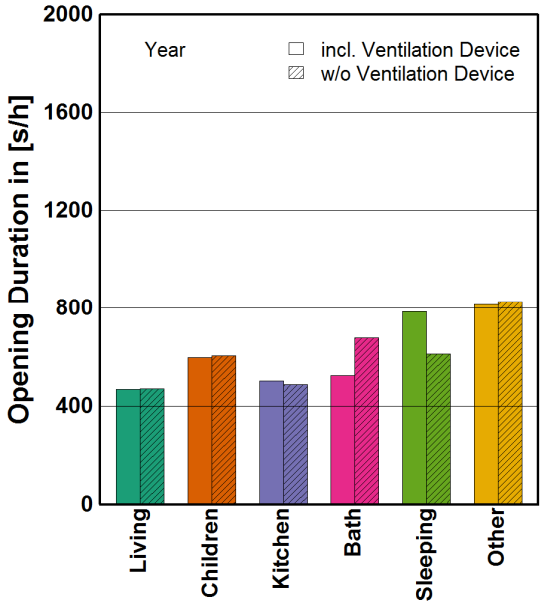

Figure 4.3 Mean Window opening duration over room type.

Rooms like kitchen, bathroom and bedrooms are differently ventilated and the occupancy and user behaviour are more difficult to predict.

Moreover, the average occupancy (treated floor area per inhabitant) seems to have a correlation to the window opening duration (Figure 4.4).

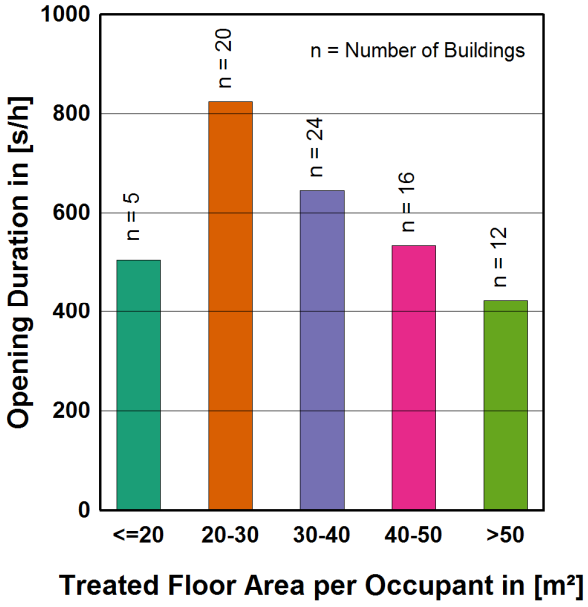

Figure 4.4 C Mean Window opening duration over average occupancy.

4.3.2.2 Building envelope, air tightness

Thermal insulation and air tightness don't have a direct influence on manual window opening behaviour (Figure 4.5). Nevertheless, the better the building envelope standard and air tightness, the greater the influence of the windows opening to the overall energy losses.

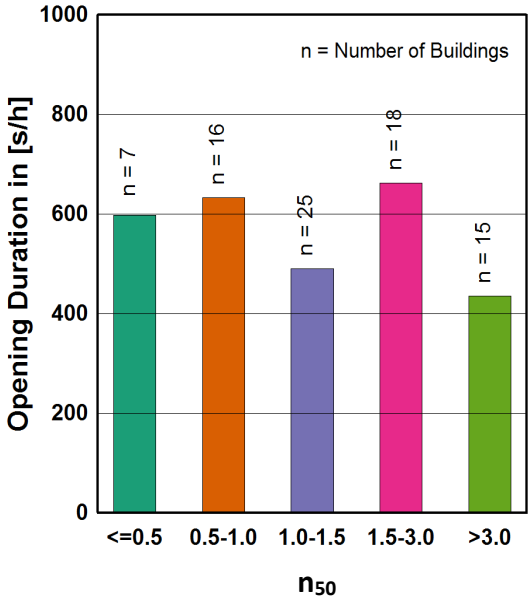

Figure 4.5 Mean window opening duration over air tightness (blower door test at 50 Pa).

4.3.2.3 Outdoor / indoor temperature

The outdoor temperature is one of the main influencing parameter to the user behaviour. Generally, the greater the difference between indoor and outdoor temperature at cold periods, the shorter the opening duration is. The opposite is true for the summer period (>28 °C), when warm outdoor temperature heats up the indoor climate (Figure 4.6)

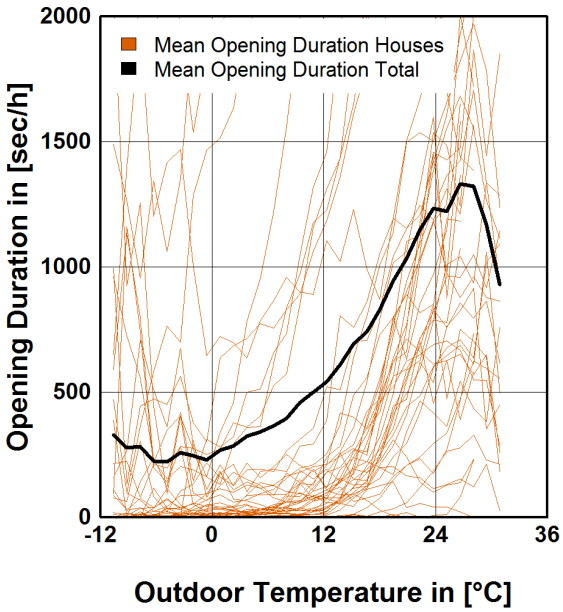

Figure 4.6 Correlation between window opening and outdoor temperature.

Accordingly, the indoor temperature correlates with the window opening duration as well. Up to 23 °C there is no relation while exceeding 23 °C results in longer opening durations until 28 °C when the outdoor climate conditions heat up the indoor climate too much (Figure 4.7).

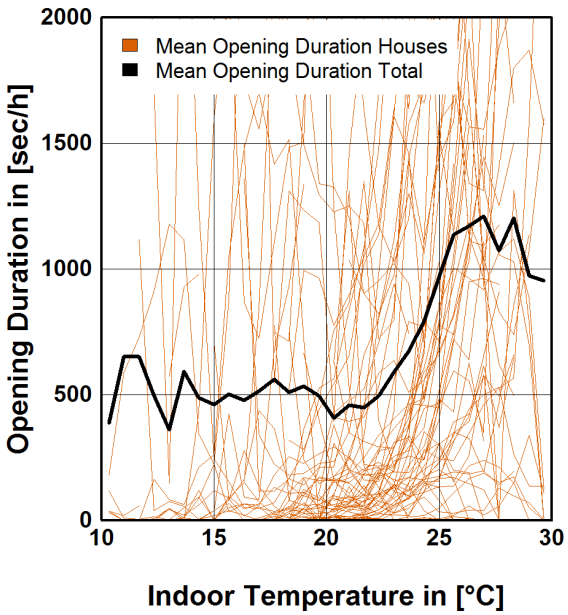

Figure 4.7 Correlation between window opening and indoor temperature.

4.3.2.4 Other outdoor climate parameters

Former researches suggest that there is no correlation between window opening and wind speed up to 6 m/sec. In Germany, 80 % of the year there is less wind speed than 6 m/sec, hence wind speed is not regarded as an important factor. In addition, local site conditions can have great impact to the wind speed and angle which should be considered in the climate file for the simulation, nevertheless those are hard to determine. Analysis of the investigated building doesn't show any correlation at all (Figure 4.8). The same applies for rain direction (graph not shown here).

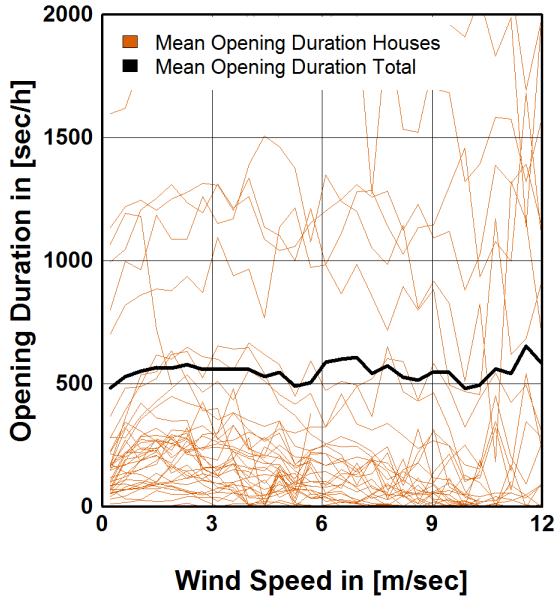

Figure 4.8 Correlation between window opening and wind speed.

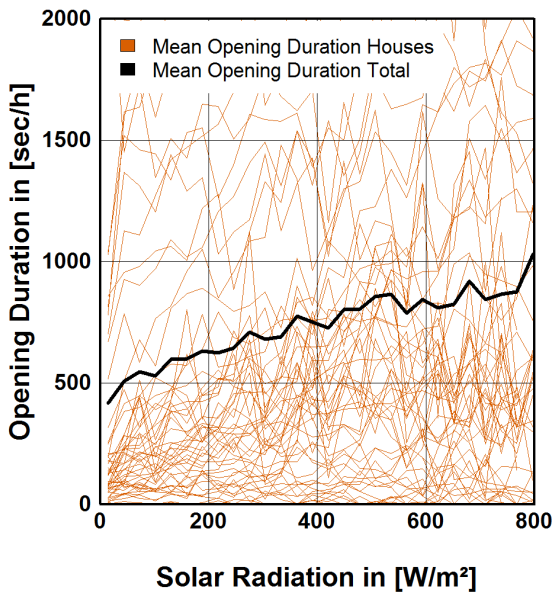

Figure 4.9 Correlation between window opening and solar radiation.

In contrast to wind speed, the solar radiation shows a significant correlation to manual window opening (Figure 4.9). Increased solar radiation results in increased window opening duration. As a matter of course this correlation is only viable during daytime when daylight is available.

4.3.2.5 Mechanical Ventilation

In literature there is a disagreement if mechanical ventilation has impact on the manual window opening behaviour. The analysis of the current dataset does not support such thesis, although there haven't been enough buildings without mechanical ventilation available to make a reliable conclusion (Figure 4.10).

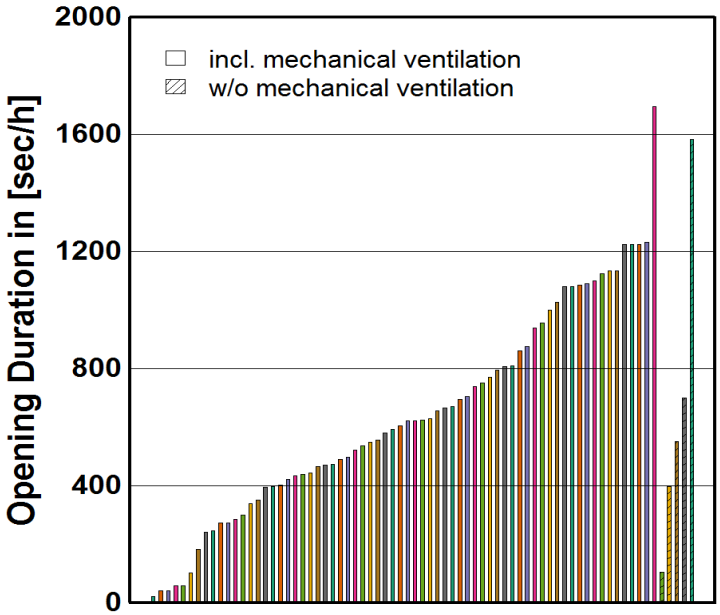

Figure 4.10 Buildings with mechanical ventilation and without.

4.3.2.6 Time of the day and user preferences

The user behaviour also depends on the daytime (Figure 4.11) and personal preferences (Figure 4.12 and Figure 4.13). For instance, some people like to keep the window open during night and some people are more sensitive to the indoor climate comfort.

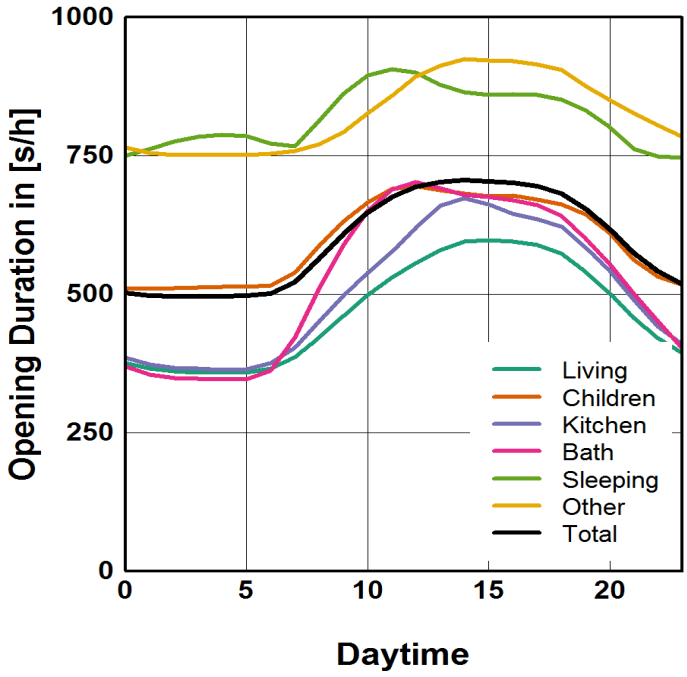

Figure 4.11 Day profiles of window opening for different room types.

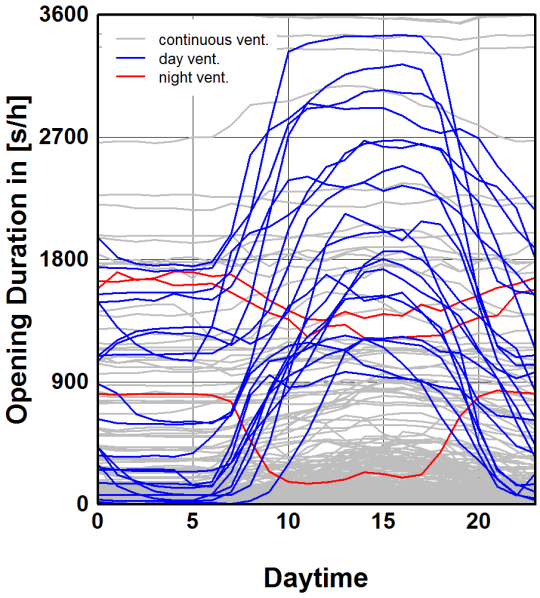

Figure 4.12 Window opening user profiles categorised in continuous, day and night ventilation for the living room.

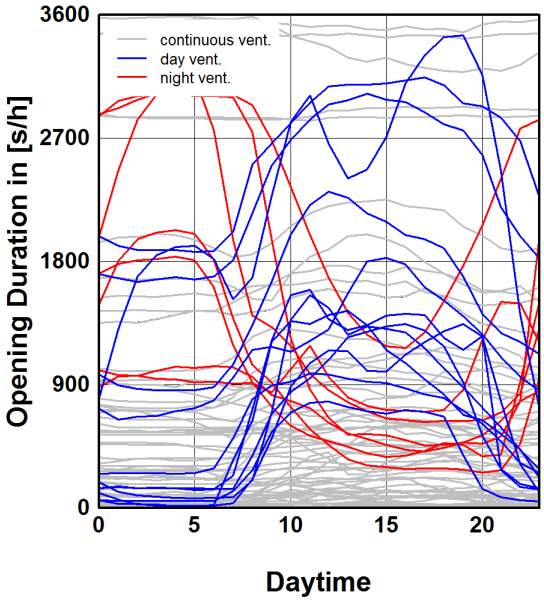

Figure 4.13 Window opening user profiles categorised in continuous, day and night ventilation for the sleeping room.

In Figure 4.12 and Figure 4.13 average day profiles for all houses are plotted for two different room types – living room and sleeping room. There are significant differences between user behaviour observed which again depend on the room type. In this case for example, the living room tends to be more ventilated during the day (blue), while the sleeping room also has a certain tendency for night ventilation (red). However, most of the user ventilate rather constant throughout the day (gray).

4.3.2.7 Other parameters

Other parameters which have not been investigated could influencing the opening behaviour could be external smell and noise disturbance as well as indoor air quality.

Another important aspect might be the window type (tilting possible?) and the orientation (south orientation receives more solar radiation), size and placement (close to the workplace) of the windows.

4.3.3 Modelling Approaches

Performing a correlation test for the status of the window opening (closed or open) displays a significant relation of the current state and its former states. The matrix in Figure 4.14 lists the auto-correlation for each time of the day. A correlation coefficient (according to Bravais Pearson) of 1 (dark filling) means a total correlation, where 0 (bright filling) indicates no correlation at all. The graphic draws the conclusion that the closer the last states of the window are, the greater its correlation to the current state. There is a higher correlation during night times which is not surprising as it is less likely that the window is opened or closed (=changing the current state) during night.

	1	2	3	4	5	6	7	8	9	0	11	12	13	14	15	16	17	18	19	20	21	22	23	24
1	1.00	0.93	0.89	0.87	0.86	0.84	0.81	0.74	0.66	0.60	0.55	0.51	0.49	0.47	0.47	0.45	0.44	0.45	0.45	0.46	0.48	0.51	0.55	0.59
2	0.93	1.00	0.97	0.95	0.93	0.92	0.88	0.80	0.69	0.61	0.55	0.51	0.49	0.46	0.46	0.44	0.44	0.44	0.44	0.45	0.46	0.49	0.53	0.58
3	0.89	0.97	1.00	0.99	0.97	0.96	0.91	0.83	0.71	0.61	0.55	0.50	0.48	0.45	0.45	0.43	0.42	0.43	0.43	0.43	0.45	0.48	0.51	0.56
4	0.87	0.95	0.99	1.00	0.99	0.97	0.93	0.85	0.72	0.62	0.55	0.50	0.47	0.45	0.45	0.43	0.42	0.42	0.42	0.43	0.44	0.47	0.50	0.56
5	0.86	0.93	0.97	0.99	1.00	0.99	0.94	0.86	0.73	0.62	0.55	0.51	0.47	0.45	0.45	0.43	0.42	0.42	0.42	0.43	0.44	0.47	0.50	0.55
6	0.84	0.92	0.96	0.97	0.99	1.00	0.96	0.88	0.74	0.63	0.56	0.51	0.47	0.45	0.45	0.43	0.42	0.42	0.42	0.42	0.44	0.47	0.50	0.55
7	0.81	0.88	0.91	0.93	0.94	0.96	1.00	0.91	0.76	0.65	0.57	0.52	0.48	0.45	0.45	0.43	0.42	0.43	0.43	0.44	0.45	0.48	0.51	0.56
8	0.74	0.80	0.83	0.85	0.86	0.88	0.91	1.00	0.86	0.71	0.63	0.56	0.52	0.49	0.49	0.48	0.46	0.47	0.47	0.47	0.48	0.50	0.52	0.56
9	0.66	0.69	0.71	0.72	0.73	0.74	0.76	0.86	1.00	0.85	0.72	0.64	0.59	0.56	0.56	0.54	0.53	0.53	0.52	0.52	0.53	0.54	0.54	0.56
10	0.60	0.61	0.61	0.62	0.62	0.63	0.65	0.71	0.85	1.00	0.85	0.73	0.67	0.63	0.63	0.60	0.58	0.57	0.57	0.56	0.56	0.56	0.56	0.57
11	0.55	0.55	0.55	0.55	0.55	0.56	0.57	0.63	0.72	0.85	1.00	0.87	0.76	0.70	0.70	0.65	0.62	0.61	0.60	0.59	0.59	0.58	0.57	0.56
12	0.51	0.51	0.50	0.50	0.51	0.51	0.52	0.56	0.64	0.73	0.87	1.00	0.87	0.77	0.77	0.71	0.67	0.65	0.64	0.62	0.61	0.60	0.57	0.55
13	0.49	0.49	0.48	0.47	0.47	0.47	0.48	0.52	0.59	0.67	0.76	0.87	1.00	0.88	0.88	0.78	0.73	0.69	0.67	0.65	0.62	0.60	0.57	0.54
14	0.47	0.46	0.45	0.45	0.45	0.45	0.45	0.49	0.56	0.63	0.70	0.77	0.88	1.00	1.00	0.88	0.79	0.73	0.71	0.67	0.64	0.61	0.57	0.54
15	0.47	0.46	0.45	0.45	0.45	0.45	0.45	0.49	0.56	0.63	0.70	0.77	0.88	1.00	1.00	0.88	0.79	0.73	0.71	0.67	0.64	0.61	0.57	0.54
16	0.45	0.44	0.43	0.43	0.43	0.43	0.43	0.48	0.54	0.60	0.65	0.71	0.78	0.88	0.88	1.00	0.89	0.80	0.75	0.70	0.67	0.63	0.58	0.54
17	0.44	0.44	0.42	0.42	0.42	0.42	0.42	0.46	0.53	0.58	0.62	0.67	0.73	0.79	0.79	0.89	1.00	0.89	0.81	0.74	0.69	0.65	0.59	0.55
18	0.45	0.44	0.43	0.42	0.42	0.42	0.43	0.47	0.53	0.57	0.61	0.65	0.69	0.73	0.73	0.80	0.89	1.00	0.90	0.80	0.73	0.67	0.61	0.57
19	0.45	0.44	0.43	0.42	0.42	0.42	0.43	0.47	0.52	0.57	0.60	0.64	0.67	0.71	0.71	0.75	0.81	0.90	1.00	0.89	0.79	0.71	0.64	0.58
20	0.46	0.45	0.43	0.43	0.43	0.42	0.44	0.47	0.52	0.56	0.59	0.62	0.65	0.67	0.67	0.70	0.74	0.80	0.89	1.00	0.88	0.76	0.67	0.60
21	0.48	0.46	0.45	0.44	0.44	0.44	0.45	0.48	0.53	0.56	0.59	0.61	0.62	0.64	0.64	0.67	0.69	0.73	0.79	0.88	1.00	0.87	0.75	0.65
22	0.51	0.49	0.48	0.47	0.47	0.47	0.48	0.50	0.54	0.56	0.58	0.60	0.60	0.61	0.61	0.63	0.65	0.67	0.71	0.76	0.87	1.00	0.87	0.73
23	0.55	0.53	0.51	0.50	0.50	0.50	0.51	0.52	0.54	0.56	0.57	0.57	0.57	0.57	0.57	0.58	0.59	0.61	0.64	0.67	0.75	0.87	1.00	0.87
24	0.59	0.58	0.56	0.56	0.55	0.55	0.56	0.56	0.56	0.57	0.56	0.55	0.54	0.54	0.54	0.54	0.55	0.57	0.58	0.60	0.65	0.73	0.87	1.00

Figure 4.14 Window opening correlation matrix for each time of the day.

4.3.3.1 Markov Chains / Survival / Failure Time Analysis

Markov Chains are used to simulate transition probabilities. They estimate for each point in time the probability that the window state closed-open is changing or not. Inhomogeneous Markov Chains are time dependent but do not take other parameters into account. Therefore, this approach is only partly suitable for estimating window opening. Another method would be Survival / Failure Time Analysis of which only the previous state is relevant and not the former progression.

4.3.3.2 Generalised Linear Models (GLM) / Logistic Regression

The standard linear models are based on the assumption, that there is a (monotonous) linear correlation between the input variables and the output (window opening). GLM enhance the standard model by specifying the model by the distribution of the data and the expected value. This is done using a linking function which can be constructed in many different ways. Binomial- or Bernoulli distributions are used for independent outcome between 0 and 1 and Poisson distribution is used for discrete outcome which can be counted.

The modelling via logistic regression can be done using a dummy coding (0 = closed, 1 = open). Thereby, the window states are considered to be independent which objects the conclusion found in the correlation matrix. Like Markov chains, such models cannot describe the time dependency of the window states and would result in misleading p-values.

4.3.3.3 GEE - generalized estimating equations

GEE is a further development based on the GLM. The distribution of GEE can be binomial, poisson or gamma. The main advantage of this approach is that it takes the dependencies of the former states into account. Furthermore, it can be used for continuous outcome values, hence, the opening duration can also be estimated. To predict the opening probabilities the binominal distribution is used, whereas the gamma distribution for the opening duration is applied.

4.3.4 GEE Window Opening Model

The window opening model has been created using the GEE approach to take the auto correlation of the measured data into account. The dataset has been randomly divided into two parts; one is used for building the model and one for its validation.

To determine the most important input parameters for the model, a step-by-step approach has been used. The procedure starts with the parameter with the smallest p-value of the significance test followed by the parameter with the second smallest p-value and so on. At each step the model has to be checked if all including factors together are still considered to be significant.

This approach estimates the following parameter as significant for the opening probability:

- Outdoor temperature
- Outdoor relative humidity
- Indoor temperature (of the hour before)
- Time of the day
- Room type

Those are the co-variables used in the GEE model.

The final model for the opening probability μ is specified as follows:

$$\mu = \frac{e^{(1.76 + 0.10\mathrm{Te} + 0.007\mathrm{RHe} - 0.074\mathrm{Ti} + 0.011\mathrm{TD} + 0.387\mathrm{LR} + 0.517\mathrm{BR} + 0{,}46\mathrm{SR})}}{1+e^{(1.76 + 0.10\mathrm{Te} + 0.007\mathrm{RHe} - 0.074\mathrm{Ti} + 0.011\mathrm{TD} + 0.387\mathrm{LR} + 0.517\mathrm{BR} + 0{,}46\mathrm{SR})}} \quad (4.16)$$

where

Te = external temperature
RHe = external relative humidity
Ti = indoor temperature
TD = time of the day
LR = living room, BR = bathroom, SR = sleeping room
If for example the opening probability for a bathroom should be predicted, BR is set to 1, whereas LR and SR are set to 0.

The validation of the model shows a good accordance of the predicted values and the validation dataset. Figure 4.15 displays the predicted values (green) over the measured values (purple). The values have been clustered into 50 equal classes sorted by their mean values.

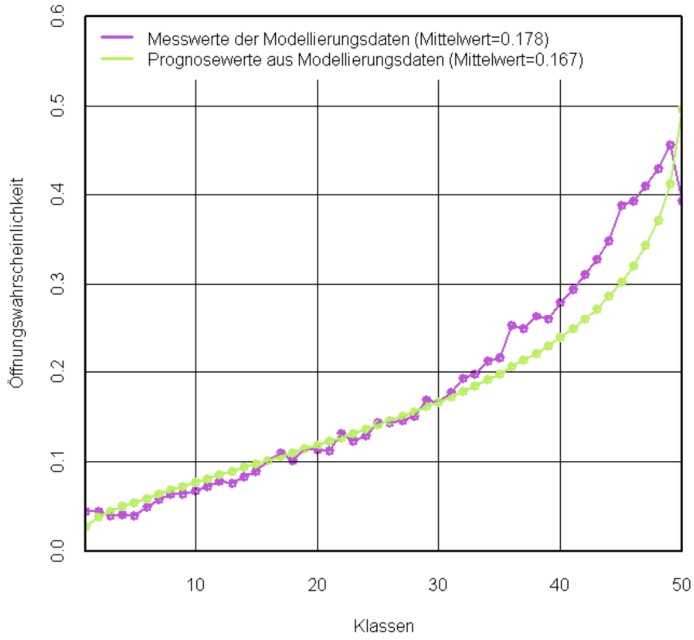

Figure 4.15 GEE model validation for window opening probability.

The same procedure for the opening duration estimates the following co-variables as significant:

- Outdoor temperature
- Outdoor relative humidity
- Indoor temperature (of the hour before)
- Wind speed
- Room type

Resulting in the following model:

$$\mu = e^{(6.1 + 0.10\mathrm{Te} - 0.27\mathrm{Ti} + 0.007\mathrm{RHe} - 0.02\mathrm{WS} + 0.19\mathrm{LR} - 0.28\mathrm{BR} + 0.58\mathrm{SR})} \quad (4.17)$$

where

Te = external temperature
RHe = external relative humidity
Ti = indoor temperature
WS = wind speed
LR = living room, BR = bathroom, SR = sleeping room

The lift plot indicates a good correspondence for durations up to 20min/hr (Figure 4.16).

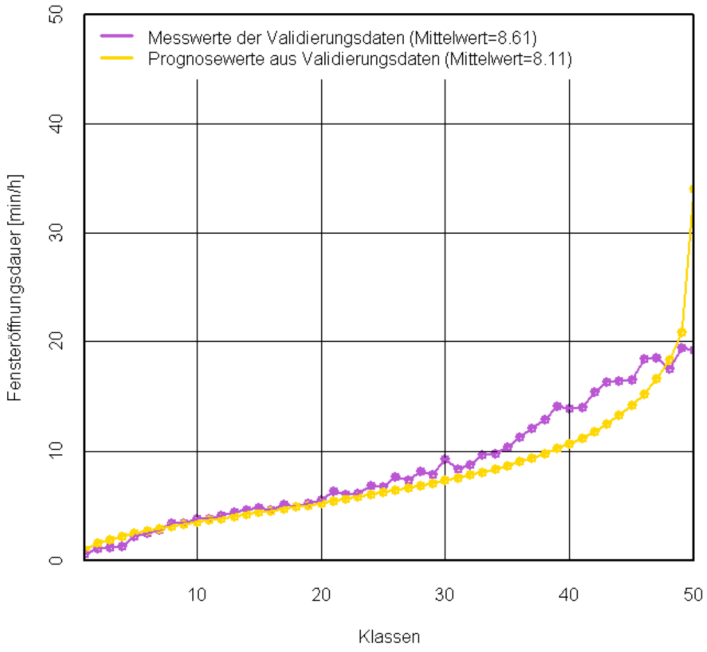

Figure 4.16 GEE model validation for window opening duration.

4.4 The Netherlands [TUE] - Statistical modelling of the UHI of Rotterdam

A neural network was trained in order to derive a data-driven model of the UHI intensity in Rotterdam. This model included the same weather parameters as described by [39] to determine the UHI intensity, meaning that wind speed, temperature, relative humidity, global horizontal irradiance and cloud cover were taken into account. In addition to these parameters the hour of the day, wind direction and solar elevation were added. The hour of the day was added based on its usage in existing time-based models [34] [87].

The hour of the day was also used as a UHI predictor in a neural network as reported by [35]. The hour of the day might be used by the network for accounting for the changing anthropogenic heat production over a day. The solar elevation was added to account for the effect of seasonal variation, which can potentially be learned by the trend in variation of the solar elevation over a year. Note that [35] used the date to account for the seasonal variation. Network A in Figure 4.17 shows the mean squared error (MSE) of the neural network that was trained with five weather parameters to determine the UHI intensity.

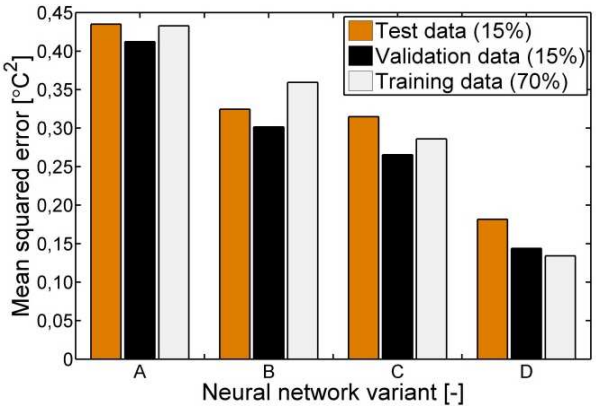

Figure 4.17 Mean squared error on test data, validation data and training data of four different neural networks.

Network A is trained with five UHI determining weather parameters, 17 neurons in the hidden layer, the training function was scaled conjugate gradient back propagation. Network B is trained with eight parameters, 17 neurons in the hidden layer and scaled conjugate gradient back propagation as training function. Network C is trained with eight parameters, 20 neurons in the hidden layer and Levenberg-Marquardt back propagation. Network D is trained with eight parameters for the hour in question as well as the preceding three hours, 20 neurons in the hidden layer and Levenberg-Marquardt back propagation as training function.

The improvement of the network performance by adding the parameters as described above is visible by comparing network A with network B. The addition of the parameters resulted in a change in the MSE on the validation data and test data of -26 % and -25 % respectively. A re-analysis of eight different training functions as well as nine different network architectures

resulted in a network with a lower MSE (network C in Figure 4.17). This network consisted of 20 neurons in the hidden layer with Levenberg-Marquardt back propagation as training function. The MSE with network C changed with -36 % and -28 % for the validation data and test data respectively when compared to network A. [52] used the maximum UHI intensity of the previous day as one of the predictors in a data driven models based on a multiple linear regression analysis. In this study the eight weather parameters of the preceding three hours are used in an addition to the weather parameters as described above, which to the best of our knowledge has not been done before to predict the UHI intensity. For the network training a reanalysis of the network architecture and training function was performed, the network with the lowest MSE on the validation data is shown a variant D in Figure 4.17. This network consisted of 20 neurons in the hidden layer with Levenberg-Marquardt back-propagation as training function. The MSE with network D changed with -65 % and -58 % for the validation data and test data respectively when compared to network A. The addition of the UHI intensity predictors of the previous hours therefore improved the neural network performance. A comparison was made between the measured temperature in the urban area and the urban modelled temperature as well as the measured rural temperature. Based on this comparison the advantage of using a model of the UHI can be shown. Figure 4.18(a) shows the rural, urban and urban modelled temperature of five continues days with a typical UHI are shown. The results show that the model reproduces the trend and intensity of the UHI in an accurate manner. Figure 4.18(b) shows the predicted UHI intensity for five days, in which there was a non-typical diurnal variation of the UHI. The results indicate that the neural network is accurate for this period as well.

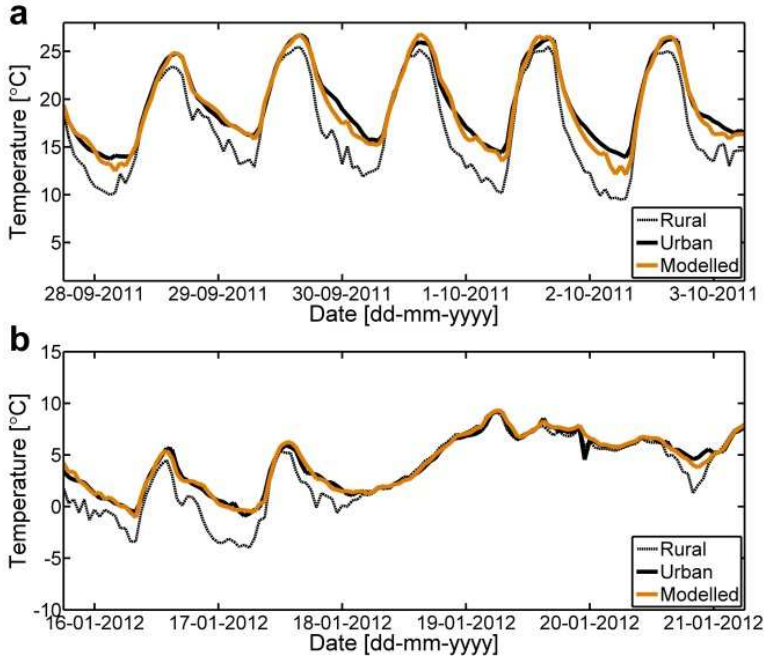

Figure 4.18 Measured en modelled urban temperature. (a) Shows the perdiction of the UHI for five days with a typical diurnal variation. (b) Shows the predicton during a period with a minimal UHI intensity.

In order to indicate the model accuracy over the whole period the regression coefficient was determined for both the case in which the modelled urban temperature and the rural temperature are used to represent the urban temperature, note that the latter is the commonly used method in building energy simulations. The adjusted coefficient of determination (R^2) for the neural network and the rural data are 0.996 and 0.980 respectively, therefore a stronger relation was found for the modelled urban temperature. The regression line on the data of the neural network is shifted 0.04 °C from the exact solution, and therefore shows a close fit to the measured data. Figure 4.19 shows the regression analysis. It can be seen that that there is a close agreement between the estimated urban temperature and the measured urban temperature.

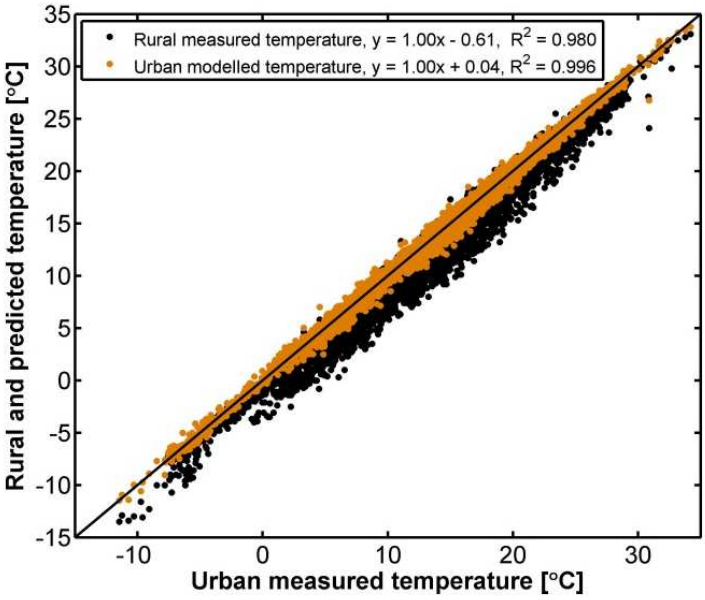

Figure 4.19 Comparison between the rural temperature, urban temperature and the modelled urban temperature.

The preceding section provided a systematic analysis on how to convert rural temperatures to urban temperatures by the use of a neural network. While the study has provided several new insights, it is also important to mention the limitations of this study:

- The applicability of the developed neural network is limited to prediction the UHI of Rotterdam;
- The study is based on the average UHI of Rotterdam, which was based on the measurements at five locations.

In spite of these shortcomings, the present study has provided new and valuable insights. It has been shown that the artificial neural network approach as first described by [50] and later by [51] [52] [39] and [35] does provide reliable results for the prediction of the UHI intensity of Rotterdam as well. Moreover, it has been shown that the addition of UHI determining parameters of the hours before the hour in question significantly improved the neural network performance (decrease in mean squared error of 65 % on validation data). This also indicates that the UHI intensity at a certain time is a result of the weather determining parameters at that time, as well as the previous hours.

5 ENERGY USE DATA FOR VALIDATION

5.1 Introduction

The fifth chapter addresses energy consumption data, presenting examples that can be used for validation of stochastic methodologies, applying the input data presented in section 3.

The consumption on electricity, gas, water and heating in buildings with different construction solutions were recorded as well as correlation between air change rates, living area dimensions and energy consumption were analyzed.

5.2 Estonia [TTU] – Energy use in Estonian Buildings

5.2.1 Electricity

The average annual use of electricity (lighting, household electricity and space heating in same cases) in brick apartment buildings was 35 kWh/(m²·a) (22–49 kWh/(m²·a)). In wooden apartment buildings the use of electricity was larger, 58 kWh/(m²·a) (26–103 kWh/(m²·a)), due to use of electricity for heating of domestic hot water and partially for space heating. The percentage of electricity use in apartments (from the total use of electricity) was 80–98 % in brick apartment buildings and 93–99 % in wooden apartment buildings. The average annual and monthly use of electricity in brick and wooden apartments is presented in Figure 5. 1 and Figure 5.2 respectively.

The use of electricity changed +15–-28 % from annual average in brick apartment buildings and +27–-44 % in wooden apartment buildings, mainly due to lower use of lighting.

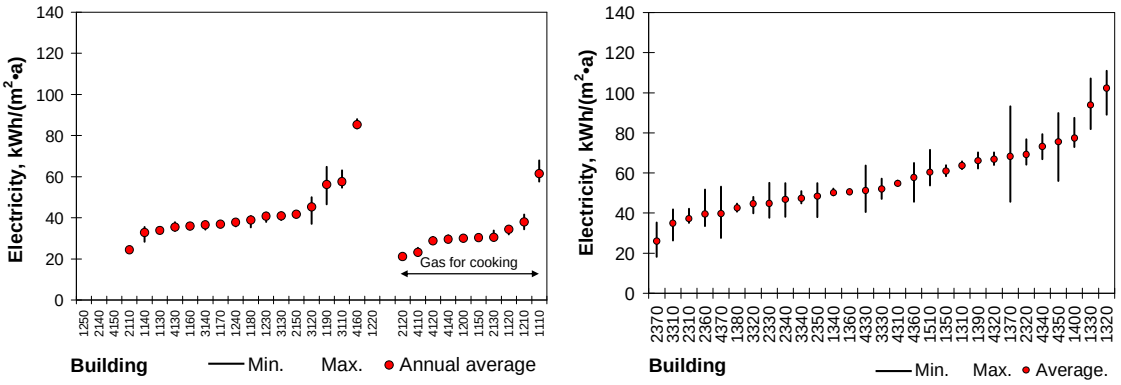

Figure 5. 1The average annual use of electricity in brick apartment buildings (left, district heating for space heating) and in wooden apartment buildings (right).

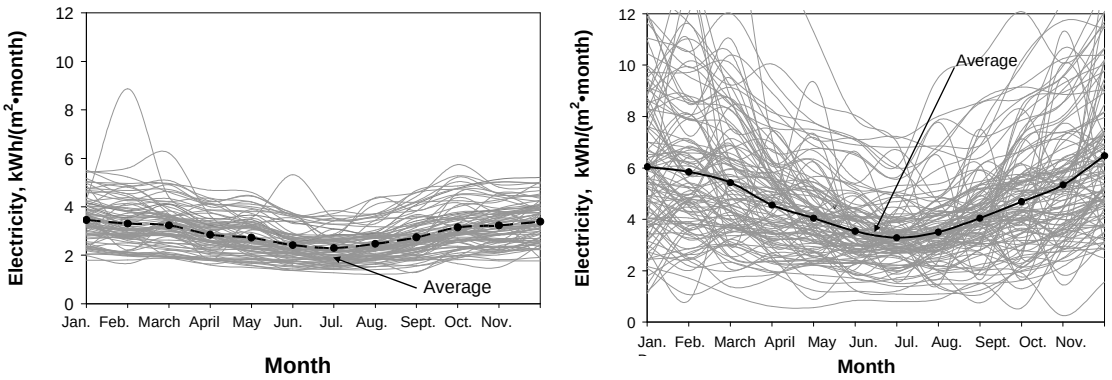

Figure 5.2 The monthly use of electricity in brick apartment buildings (left) and in wooden apartment buildings (right).

5.2.2 Gas

The annual average use of gas for cooking was 0.5 $m^3/(m^2 \cdot a)$ (st. dev. 0.34 $m^3/(m^2 \cdot a)$ and for cooking and heating of domestic hot water 3 $m^3/(m^2 \cdot a)$ (st. dev. 1.0 $m^3/(m^2 \cdot a)$) in brick apartment buildings, Figure 5.3. In buildings where gas was used for cooking, for heating of domestic hot water and for space heating (SH), the annual average use of gas was 26 $m^3/(m^2 \cdot a)$ in brick apartments buildings and 14.6 $m^3/(m^2 \cdot a)$ (st. dev. 9.7 $m^3/(m^2 \cdot a)$ in wooden apartment buildings.

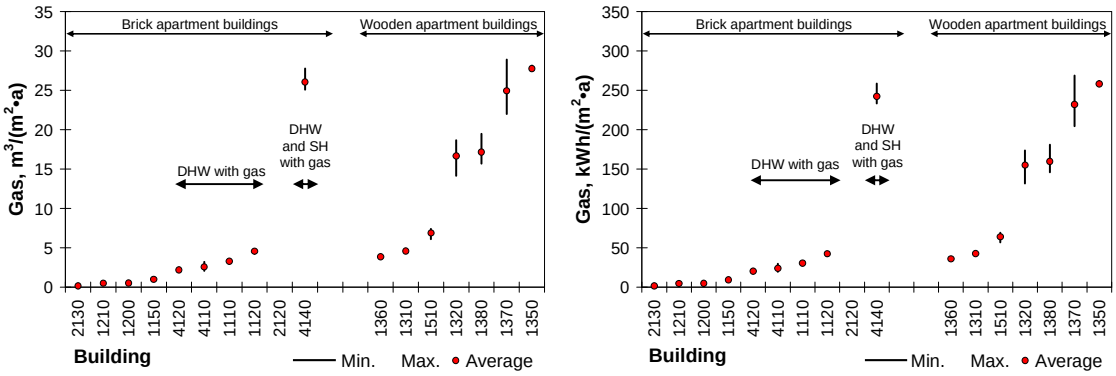

Figure 5.3 The average annual use of gas ($m^3/(m^2 \cdot a)$: left and $kWh/(m^2 \cdot a)$:right) in brick apartment buildings and in wooden apartment buildings.

5.2.3 Water

The annual average daily overall (hot and cold) water use was 3 $l/(m^2 \cdot d)$ (st. dev. 0.6 $l/(m^2 \cdot d)$) and 202 l/(apartm.·d) (st. dev. 64 l/(apartm.d)) in brick apartment buildings, and 2.8 $l/(m^2 \cdot d)$ (st. dev. 0.9 $l/(m^2 \cdot d)$) and 149 l/(apartm.·d) (st. dev. 109 l/(apartm.·d)) in wooden apartment buildings. The use of water was similar over the entire year; monthly average use of water was also similar. The percentage of domestic hot water from overall water use was 40 % on average. The average daily use of water in brick and wooden apartments is presented in Figure 5.4 andFigure 5.5 respectively.

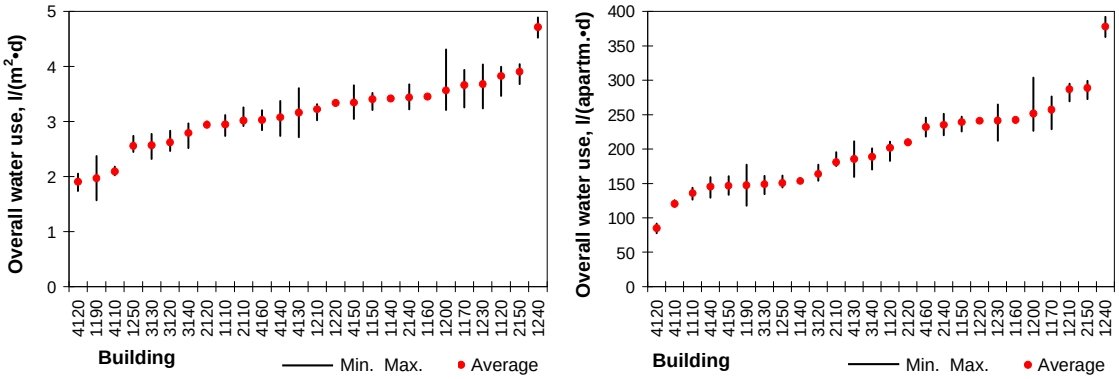

Figure 5.4 The daily average overall (hot and cold) water use in brick apartment buildings.

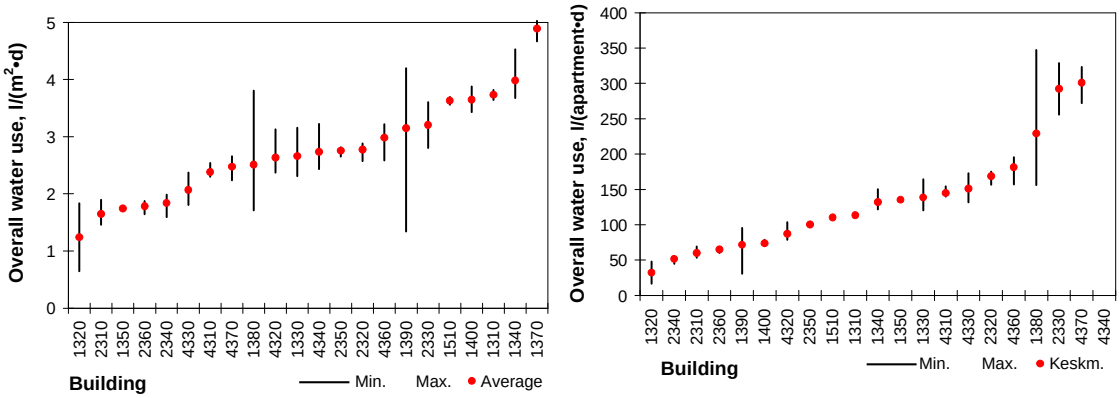

Figure 5.5 The daily average overall (hot and cold) water use in wooden apartment buildings.

The use of domestic hot water (DHW) was 35 l/(person·d) (st. dev. 10 l/(person·d)) in brick apartment buildings and 30 l/(person·d) (st. dev. 9 l/(in·d)), in wooden apartment buildings, see Figure 5.6.

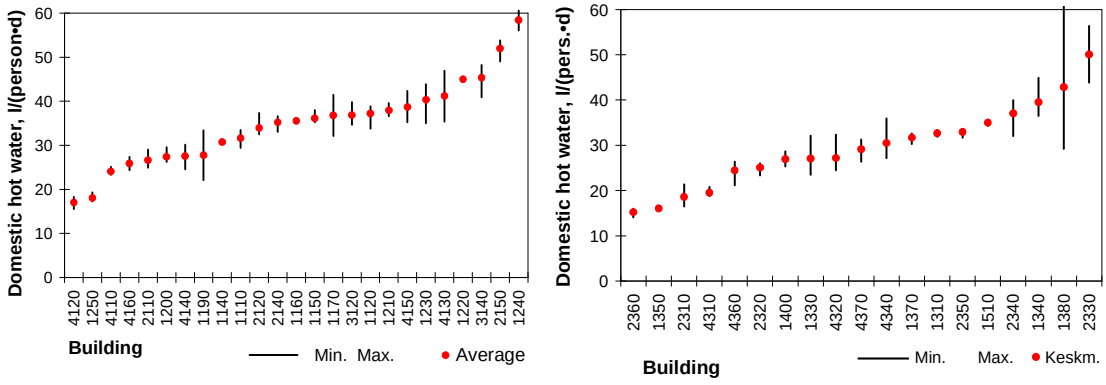

Figure 5.6 The daily average us of domestic hot water in brick apartment buildings (left) and wooden apartment buildings (right).

The use of DHW has decreased from 1990 almost twice, see Table 5.1 (mainly due to measurement of water use and higher energy prices).

Table 5.1 The personal use of domestic hot water in apartment buildings during 1999-2010.

	Kõiv & Toode 2005 (75 apartment buildings)						Brick apartment buildings	Wooden apartment buildings
	1999	2000	2001	2002	2003	2004	2009	2010
	Use of domestic hot water, l/(m²·d)							
Average	2.8	2.6	2.3	2.2	2.1	2.0	1.3	1.1
Range	1.6…3.6	2.1…3.3	1.8…3.1	1.7…2.8	1.6…2.6	1.7…2.7	0.7…1.8	0.5…2.0
	Use of domestic hot water, l/(person·d)							
Average	60	56	49	46	45	44	35	30
Range	34…77	44…71	38…66	37…59	35…56	36…58	17…58	15…50

5.2.4 Space heating

The energy used for space heating was analysed in brick apartment buildings with district heating. This energy should cover:

- heat losses through building envelope,
- heat loss through thermal bridges,
- heat loss due to infiltration,
- heat loss due to natural ventilation.

The measured energy from different locations and from different years was reduced based on heating degree days at a balanced temperature of +17 °C. The average energy use for space heating was 150 kWh/(m^2·a) (st. dev. 41 kWh/(m^2·a)). The heating energy use was larger in buildings with one pipe heat distribution system (complicated balance and temperature regulation) and in buildings with larger compactness (Figure 5.7).

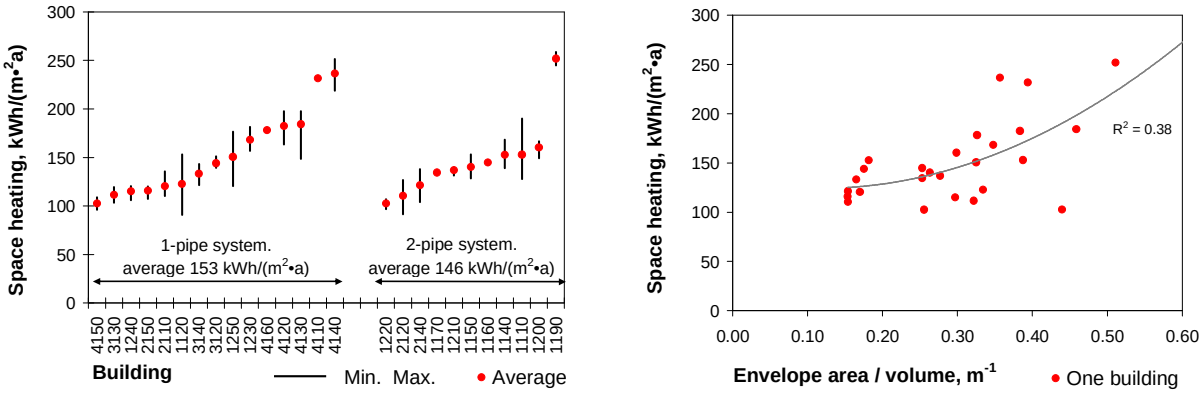

Figure 5.7 Energy use for space heating in brick apartment buildings depending on heat distribution system (left) and compactness of building (right).

5.2.5 Overall primary energy consumption

The overall primary energy consumption represents energy need in a building for space heating, ventilation, domestic hot water, lighting and appliances and is presented as the energy performance value (EPV). The EPV is calculated from delivered energy use with energy carrier factors:

- Wood, wood-based fuels, and other bio fuels: 0.75;
- District heating: 0.9;
- Fossil fuel (gas, coal etc.): 1.0;
- Electricity: 1.5 (changed to 2.0 in 2012).

The average energy performance value in brick apartment buildings was 238 kWh/(m^2·a) (st. dev. 48 kWh/(m^2·a)), see Figure 5.8.

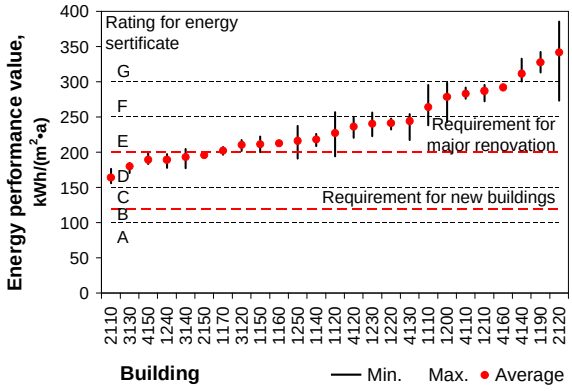

Figure 5.8 Energy performance value in brick apartment buildings.

In buildings without gas: 62 % was used for space heating, 13 %for domestic hot water and 25 % from electricity weighted delivered energy, Figure 5.9.

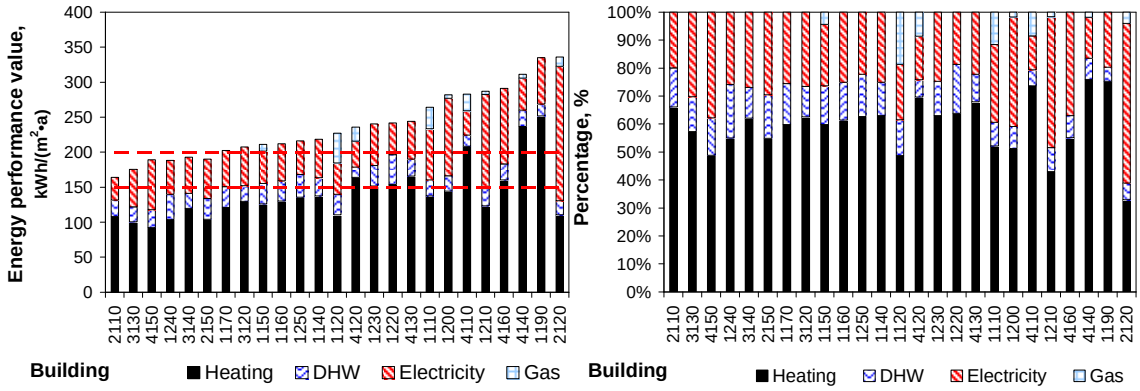

Figure 5.9 The structure (left) and percentage distribution (right) of energy performance value in brick apartment buildings.

5.3 Finland [TUT] – Energy use in Finnish buildings

5.3.1 Building air tightness

The results from building air tightness measurements and user questionnaires were further analysed. Figure 5.10 shows results of the total delivered energy consumption per ventilated floor area against the measured n_{50}-value.

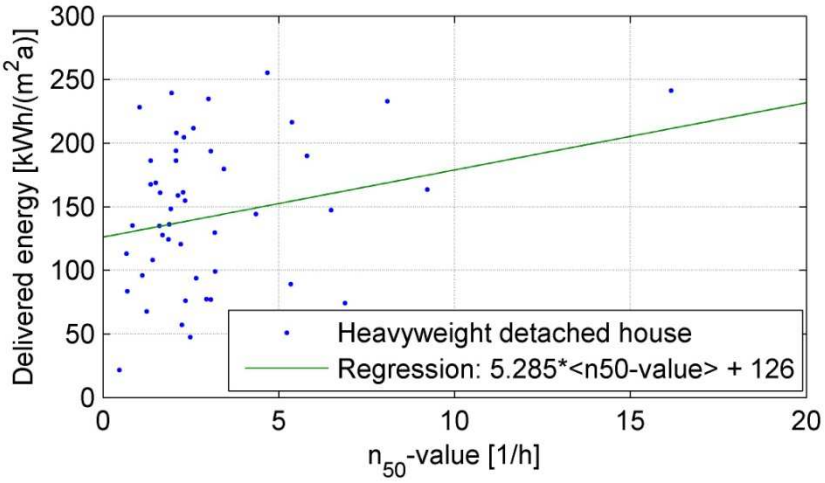

Figure 5.10 Heating degree day -normalized (to 4097 Kd) delivered energy consumption versus building n_{50}-value in Finnish heavyweight detached houses. Delivered energy consumption data from the years 2004-2005 was gathered with user questionnaires.

The values include sources for large variations e.g. different heat production systems and user behaviour. The corresponding polynomial coefficient in timber-framed detached houses was 4.202 kWh/(m^2a) / (1 h^{-1}).

The regression result is evaluated by comparing it to simple hand calculations: using a simple approximate method to calculate the space heating energy demand for air infiltration, we get $Q_{infiltration} = \rho_a c_{pa}(n_{50}/x)V_{ventilated}\Delta T\Delta t$ = 1.25 kg/m^3 · 1000 J/(kgK) · (1 h^{-1} / 25) · 2.5 m^3/m^2 · 16 K · 8760 hr = 4.867 kWh/(m^2a). The result is of the same order of magnitude than the result from the regression analysis. Simplifying even further and by assuming few more generic input values we get: 5 kWh/(m^2a) · 100 m^2 · 0.10 eur/kWh = 50 eur/a. Decreasing building air tightness value by 2 h^{-1}would roughly mean financial savings of 1000 euro in ten years through reduced heating costs.

Improved building air tightness has also other important benefits e.g. improved moisture-safety, reduced transport of microbes from outside, better heat recovery system efficiency (if installed) and reduced draft. Arranging proper ventilation is a prerequisite for good indoor air in all cases.

5.3.2 Size of the living area

Figure 5.11 shows a correlation between energy consumption and living area. The values include e.g. many different heat production systems and different user behaviour patterns.

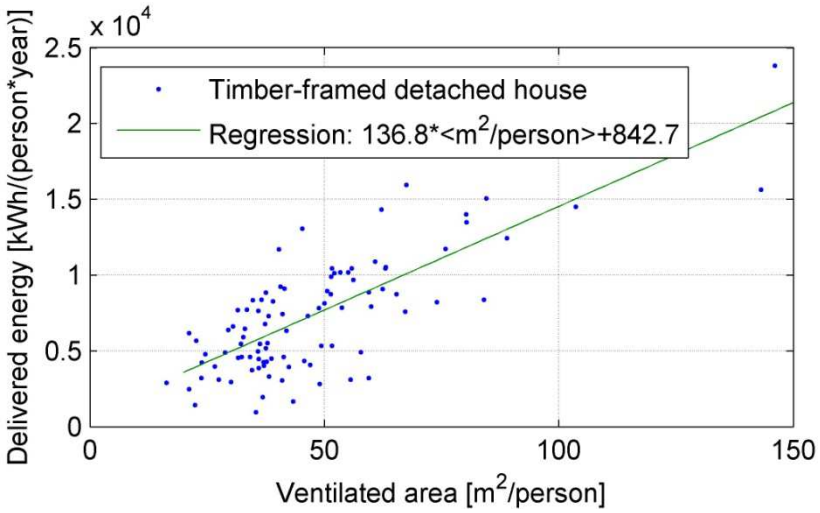

Figure 5.11 Smaller delivered energy consumption per person correlates with smaller living area per person. The median value for the number of residents is four.

The regression line for heavyweight detached houses was: 96.8*<m^2/(person*year)>+2458 (the result is in [kWh/(person*year]). The median value of for the number of residents is the same as for the timber-framed detached houses. The data could be further divided into subgroups to compare different design solutions.

If we assume an energy consumption reduction of 100 kWh/(m^2*year), a living space reduction of 10 m^2/person and an energy price of 0.10 eur/kWh, the annual savings in delivered energy would be 100 eur/(person*year). The size of the building and the room plan also depend on e.g. the current and future usage and aesthetic values.

5.3.3 Heat production method

The heating degree day –normalized delivered energy consumption was divided with the ventilated floor area and arranged into subgroups according to the heat production method. The results are presented in Table 5.2.

Table 5.2 The average, standard deviation and sample size of delivered energy per ventilated floor area in Finnish detached houses. The energy consumption values are from years 2002-2003 (timber-frame detached houses) and 2004-2005 (heavyweight detached houses). The delivered energy is normalized to heating degree days of 4097 Kd, with indoor temperature 17 °C.

	Heat production system	Average delivered energy [kWh/(m^2*year)]	Delivered energy standard deviation [kWh/(m^2*year)]	Sample size
Heavyweight detached houses	Ground source heat pump	102.8	50.6	15
	Electricity	171.3	52.9	24
	Oil	174.2	49.2	6
Timber-framed detached houses	Ground source heat pump	112.2	24.6	4
	Electricity	166.6	58.3	66
	Oil	147.8	61.0	14

The use of wood for space heating is included in the delivered energy, but is not analysed further. The standard deviation in delivered energy per ventilated floor area is close to 50 kWh/(m^2*year) in all the cases.

5.4 United Kingdom [UCL] – Energy use in the Warm Front study

5.4.1 Collected raw data

A total of 2901 sets of data (1255 pre-intervention, 1162 post-intervention and 242 both pre- and post-intervention) were collected from a subset of 2659 dwellings. However, as the post-processing of these data use the measured indoor and outdoor temperatures, data corresponding to the same sample of 1481 dwellings as presented on 3.4.8 will be shown here. Again, the data are cleaned of repeat measurements, and if both pre- and post-intervention measurements exist for the same dwelling, only the pre-intervention measurements are kept so that the data represents a single stock.

5.4.1.1 Total fuel consumption

The total fuel consumption for each house was recorded over the same 2–4 week period as the temperature and relative humidity monitoring presented on 3.4.8, by reading the gas and the electric meters each time the data loggers were placed and removed. For a further 100 dwellings that granted consent, utility billing data for the 1–2 year period was obtained.

5.4.1.2 Primary heating fuel and efficiency

These were recorded during the surveys of the dwellings.

5.4.2 Analysis

5.4.2.1 Post-processing of data

5.4.2.1.1 Normalized space heating fuel consumption (E-value)

Space heating fuel consumption was normalized to account for the variation in the difference between internal and external temperatures, and the ground floor area of the dwelling using the following relation:

$$\text{E-value} = {}^{1}\!/_{4\,\frac{Q}{DDA_f}} \tag{5.1}$$

where the E-value is the normalized space heating fuel consumption (W/K/m^2), Q is the space heating fuel consumption derived from the monitored total fuel consumption data, DD is the heating degree days calculated over the monitoring period, and A_f is the total ground floor area (m^2) of the dwelling.

The space heating fuel consumption was not directly monitored due to funding constraints and therefore instead estimated by subtracting the summer fuel load from the monitored total fuel data collected in winter. The summer fuel load was itself estimated using a regression model

derived to predict fuel consumption by non-heating appliances, based on the summer utility billing data and also surveyed data on appliance type, their frequency of use, and occupancy. More details can be found in [58].

The heating degree days, DD, were calculated for each dwelling by summing the temperature difference between the daily mean internal base temperature and the daily mean external temperature over the 2-4 week monitoring period. More details can be found in [58].

A total of 69 dwellings were excluded from further analysis, as a result of very low values for the E-value. In many cases, this was due to the primary heating fuel being solid fuel or paraffin, broken boilers, suspected vacated dwellings, or overestimation of either the non-heating fuel consumption or the heating degree days.

5.4.3 Stochastic data sets

Figure 5.12 shows the distribution of E-values, primary heating fuel type, and efficiency of primary heating fuel.

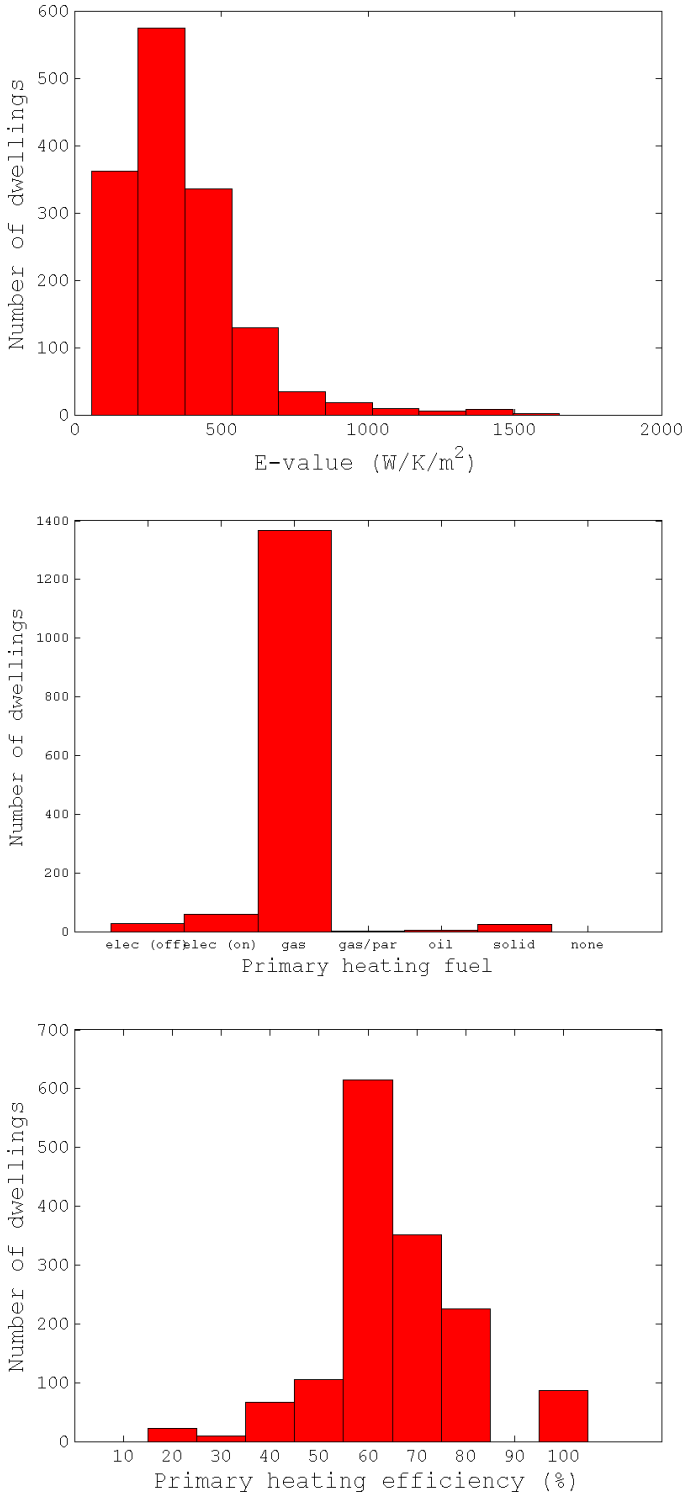

Figure 5.12 Distribution of E-values (top), primary heating fuel (middle), and primary heating efficiency (bottom).

6 CONCLUSIONS

6.1 Final Remarks

This report was built on data previously collected in different projects. A synthesis of the projects carried out by each institution was presented and details from the developed experimental campaigns, were described.

Input data was presented and divided into the following categories: stochastic material data, ventilation and airtightness, indoor loads and weather. Different codes may require different sets of stochastic data, which means that these cannot be considered ready to use stochastic sets but rather a base for each practitioner to build his required set of input data.

Each subchapter was arranged so that each set of collected raw data is introduced. The analysis to derive statistical distributions that was performed on the raw data was explained and the final stochastic data sets are presented. The focus was put on ensuring that the connection to measured data wouldn't be lost.

Synthetic data sets were included, demonstrating how additional sets of valuable information can be prepared with more advanced analysis. The examples included: extrapolation of material properties, determination of window opening behaviour and UHI intensity determination.

Energy consumption data, presenting examples that can be used for validation of stochastic methodologies, applying the input data presented in section 3, is also presented. The consumption on electricity, gas, water and heating in buildings with different construction solutions were recorded as well as correlation between air change rates, living area dimensions and energy consumption were analyzed.

The effort of the participating teams also allowed gathering extensive electronic raw data files that can be made available by the operating agent upon request. Those files include the following information:

- Belgium: [KUL] Airtightness data;
- Canada: [BCIT] Indoor Temperature and Humidity Summary Data;
- Estonia: [TUT] Indoor Temperature and Relative Humidity Data;
- Finland: [TTU] Finnish data on timber framed houses;
- Finland: [TTU] Finnish data on detached houses and apartments;
- Germany: [TUD] Material summary sheet template;
- The Netherlands: [TUE] Temperature and UHI data;
- Portugal: [UP] Airtightness data;
- Sweden: [SP] Airtightness data;
- Sweden: [LTH] Climate Sweden;
- United Kingdom: [UCL] Indoor climate and energy

7 REFERENCES

[1] EN ISO 13829 (2001). Thermal performance of buildings. Determination of air permeability of buildings. Fan pressurization method. CEN. Brussels

[2] Arumägi, E.; Kalamees, T. (2014). Analysis of energy economic renovation for historic wooden apartment buildings in cold climates. Applied Energy, 115, 540 - 548.

[3] Kuusk, K.; Kalamees, T.; Maivel, M. (2014). Cost effectiveness of energy performance improvements in Estonian brick apartment buildings. Energy and Buildings, 77, 313 - 322.

[4] Vinha, J., Korpi, M., Kalamees, T., Eskola, L., Palonen, J., Kurnitski, J., Valovirta, I., Mikkilä, A. & Jokisalo, J. (2005) Moisture and temperature conditions, ventilation and air tightness in timber framed one family houses. Research report 131. 102 p. + app. 10 p. Tampere University of Technology. Department of Civil Engineering. Structural Engineering Laboratory. Tampere. Finland. ISBN 978-952-15-2747-0. Publication in Finnish.

[5] Vinha, J., Korpi, M., Kalamees, T., Jokisalo, J., Eskola, L., Palonen, J., Kurnitski, J., Aho, H., Salminen, M., Salminen, K. & Keto, M. (2009) Air tightness, indoor climate and energy economy of detached houses and apartments.Research report 140. 148 p. + app. 19 p. Tampere University of Technology. Department of Civil Engineering. Structural Engineering Laboratory. Tampere. Finland. ISBN 978-952-15-2738-8. Publication in Finnish, English abstract included.

[6] ISO 11272:2001. Soil quality - Determination of dry bulk density

[7] ASTM C177 (2010). Standard Test Method for Steady-State Heat Flux Measurements and Thermal Transmission Properties by Means of the Guarded-Hot-Plate Apparatus.

[8] ASTM C518 (2010). Standard Test Method for Steady-State Thermal Transmission Properties by Means of the Heat Flow Meter Apparatus

[9] DIN EN 12664 (2001). Thermal performance of building materials and products - Determination of thermal resistance by means of guarded hot plate and heat flow meter methods - Dry and moist products with medium and low thermal resistance.

[10] ASTM E1269 (2011). Standard Test Method for Determining Specific Heat Capacity by Differential Scanning Calorimetry

[11] ASTM C1498 (2004). Standard Test Method for Hygroscopic Sorption Isotherms of Building Materials

[12] DIN EN ISO 12571 (2000). ISO 12571:2000 Hygrothermal performance of building materials and products. Determination of hygroscopic properties

[13] ASTM C1699 (2009). Standard Test Method for Moisture Retention Curves of Porous Building Materials Using Pressure Plates

[14] ASTM E96 /E96M (2010). Standard Test Methods for Water Vapor Transmission of Materials

[15] ISO 12572:2001 Hygrothermal performance of building materials and products. Determination of water vapour transmission properties.

[16] ISO 15148 (2003). Hygrothermal performance of building materials and products - Determination of water absorption coefficient by partial immersion (ISO 15148:2003)

[17] Plagge, R., Scheffler, G. and Nicolai, A. 2007. Experimental Methods to Derive Hygrothermal Material Functions for Numerical Simulation Tools, Buildings X Proceedings, Clearwater Beach, Florida.

[18] Zhao, J. 2012. Development of a Novel Statistical Method and Procedure for Material Characterization and a Probabilistic Approach to Assessing the Hygrothermal Performance of Building Enclosure Assemblies. Ph.D. Dissertation. Syracuse University, USA, pp.298

[19] Howard, L., 1833. Climate of London deduced from meteorological observations. 3rd ed. London: Harvey & Darton.

[20] Mills, G. 2003. Luke Howard and the Climate of London. Weather, Vol.63, no.6, pp.153–157.

[21] Oke, T. R. 1982. The energetic basis of the urban heat island. Quarterly Journal of the Royal Meteorological Society, Vol. 108, no. 455, pp.1–24.

[22] Oke T. R. 1987. Boundary layer climates. Methuen Co. NY, London, pp.1-435

[23] Taha, H. 1997. Urban climates and heat islands: albedo, evapotranspiration, and anthropogenic heat. Energy and Buildings, Vol. 25, No. 2, pp. 99–103.

[24] Santamouris M. 2001. Energy and climate in the urban built environment. London: James and James; 2001.

[25] Santamouris, M. 2007. Heat island research in Europe: The state of the art. Advances in building energy research, Vol. 1, pp. 123–150.

[26] Kolokotroni, M., Davies, M., Croxford, B., Bhuiyan, S., & Mavrogianni, A. 2010. A validated methodology for the prediction of heating and cooling energy demand for buildings within the Urban Heat Island: Case-study of London. Solar Energy, Vol. 84, No. 12, pp. 2246–2255.

[27] Stewart, I. D. 2011. A systematic review and scientific critique of methodology in modern urban heat island literature. International Journal of Climatology, Vol. 31, No. 2, pp. 200–217.

[28] Tomlinson, C. J., Chapman, L., Thornes, J. E., & Baker, C. J. 2011. Including the urban heat island in spatial heat health risk assessment strategies: a case study for Birmingham, UK. International journal of health geographics, Vol. 10, no. 1, pp. 42.

[29] Mavrogianni, A., Davies, M., Batty, M., Belcher, S., Bohnenstengel, S., Carruthers, D., Chalabi, Z., et al. (2011). The comfort, energy and health implications of London's urban heat island. Building Services Engineering Research and Technology, Vol. 32, No. 1, pp. 35–52.

[30] Gosling, S. N., Lowe, J. A., McGregor, G. R., Pelling, M., & Malamud, B. D. 2008. Associations between elevated atmospheric temperature and human mortality: a critical review of the literature. Climatic Change, Vol. 92, No. 3-4, pp. 299–341.

[31] Pirard, P., Van den torren, S., Pascal, M., Laaidi, K, Le Tertre, A., Cassadou, S., Ledrans, M., 2005, Summary of the mortality impact assessment of the 2003 heat wave in France, Euro Surveillance 2005, Vol 10, No. 7, pp. 153–6

[32] Brücker, G., 2005, Vulnerable populations: Lessons learnt from the summer 2003 heat waves in Europe. Eurosurveillance, Vol. 10, no. 7, pp. 147.

[33] Kosatsky, T., 2005, The 2003 European heatwave, Eurosurveillance, Vol. 10, no. 7, pp. 148-149

[34] Kershaw, T., Sanderson, M., Coley, D., & Eames, M., 2010. Estimation of the urban heat island for UK climate change projections. Building Services Engineering Research and Technology, Vol. 31, No. 3, pp. 251–263.

[35] Gobakis, K., Kolokotsa, D., Synnefa, a., Saliari, M., Giannopoulou, K., & Santamouris, M. 2011. Development of a model for urban heat islandprediction using neural network techniques. Sustainable Cities and Society, Vol. 1, No. 2, pp. 104–115.

[36] Assimakopoulos, M. N., Mihalakakou, G., & Flocas, H. a. 2007. Simulating the thermal Behaviour of a building during summer period in the urban environment. Renewable Energy, Vol. 32, No. 11, pp. 1805–1816.

[37] Hassid, S., & Santamouris, M. 2000. The effect of the Athens heat island on air conditioning load. Energy and Buildings, Vol, 32, pp. 131–141.

[38] Wilbanks, T.J., P. Romero Lankao, M. Bao, F. Berkhout, S. Cairncross, J.-P. Ceron, M. Kapshe, R. Muir-Wood and R. Zapata-Marti, 2007: Industry, settlement and society. Climate Change 2007: Impacts, Adaptation and Vulnerability. Contribution of Working Group II to the Fourth Assessment Report of the Intergovernmental Panel on Climate Change, M.L. Parry, O.F. Canziani, J.P. Palutikof, P.J. van der Linden and C.E. Hanson, Eds., Cambridge University Press, Cambridge, UK, 357-390.

[39] Kolokotroni, M., Zhang, Y., & Watkins, R., 2007.The London Heat Island and building cooling design. Solar Energy, Vol. 81, No. 1, pp. 102–110.

[40] Kolokotroni, M., Davies, M., Croxford, B., Bhuiyan, S., & Mavrogianni, A. 2010. A validated methodology for the prediction of heating and cooling energy demand for buildings within the Urban Heat Island: Case-study of London. Solar Energy, Vol. 84, No. 12, pp. 2246–2255.

[41] Taha, H. 1999. Modifying a mesoscale meteorological model to better incorpórate urban heat storage: A bulk-parameterization approach. Journal of Applied Meteorology, Vol 38, pp. 466–473.

[42] Bueno, B., Norford, L., Hidalgo, J., Pigeon, G., 2012. The urban weather generator, journal of Building Performance Simulation, DOI:10.1080/19401493.2012.718797

[43] Runnalls, K., Oke, T. 2000. Dynamics and controls of the near-surface heat island of Vancouver, British Columbia. Physical Geography. Vol. 21, pp. 283-304

[44] Erell, E., Williamson, T. 2006. Simulating air temperature in an urban street canyon in all weather conditions using measured data at a reference meteorological station. International Journal of Climatology, Vol. 26, No.12, pp.1671–1694

[45] Levermore, G., Cheung, H. 2012. A low-order canyon model to estimate the influence of canyon shape on the maximum urban heat island effect. Building Services Engineering Research and Technology, Vol. 33, No. 4, pp. 371–385.

[46] Bouyer, J., Inard, C., Musy, M. 2011. Microclimatic coupling as a solution to improve building energy simulation in an urban context. Energy and Buildings, Vol. 43, No. 7, pp. 1549–1559.

[47] Wilby, R. 2003. Past and projected trends in London's urban heat island. Weather, Vol. 58, pp. 251–260.

[48] Giridharan, R., Lau, S. S. Y., & Ganesan, S., 2005. Nocturnal heat island effect in urban residential developments of Hong Kong. Energy and Buildings, Vol. 37, No. 9, pp. 964–971.

[49] Morris, C., Simmonds, I., 2001. Quantification of the influences of wind and cloud on the nocturnal urban heat island of a large city. Journal of Applied Meteorology, Vol. 40, pp. 169–182.

[50] Santamouris, M. 2007. Heat island research in Europe: The state of the art. Advances in building energy research, Vol. 1, pp. 123–150.

[51] Mihalakakou, G., Flocas, H. A., Santamouris, M., Helmis, C. 2002. Application of neural networks to the simulation of the heat island over Athens, Greece, using synoptic types as a predictor. Journal of Applied meteorology, Vol. 41, pp. 519–527.

[52] Kim & Baik 2002 Kim, Y.H., Baik, J. 2002. Maximum urban heat island intensity in Seoul. Journal of Applied Meteorology, Vol. 41, pp. 651–659.

[53] Pallin, S. (2012). Probabilistic Risk Assessment of Energy Efficient Retrofitting Techniques - Focus on Multi-family Dwellings and the Effects of Changing Air Movements. Licentiate, Chalmers University, Gothenburg, Sweden.

[54] Stein J. (2010). Preliminary Results from Moisture Measurements in a Swedish Multi-family Dwelling Retrofitted with Interior Insulation. International Conference on Building Envelope Systems and Technologies (ICBEST), Volume 2, pp. 265-274, Vancouver, Canada.

[55] Levin, P., A. Jidinger, and A. Larsson, (2009). Preliminär objektrapport för Norrbacka-Sigtunahem: Etapp 1&2. Energimyndighetens beställargrupp för energieffektiva flerbostads-hus. Unpublished

[56] Oreszczyn, T., Hong, S., Ridley, I., & Wilkinson, P. (2006). Determinants of winter indoor temperatures in low income households in England. Energy & Buildings., 38(3), 245-52.

[57] Oreszczyn, T., Ridley, I., Hong, S. H., & Wilkinson, P. (2006). Mould and winter indoor relative humidity in low income households in England. Indoor built environment, 15(2), 125-35.

[58] Hong, S. H., Oreszczyn, T., & Ridley, I. (2006). The impact of energy efficient refurbishment on the space heating fuel consumption in English dwellings. Energy & Buildings, 38(10), 1171-1181.

[59] Hong, S. H., Gilbertson, J., Oreszczyn, T., Green, G., & Ridley, I. (2009). A field study of thermal comfort in low-income dwellings in England before and after energy efficient refurbishment. Building and Environment, 44(6), 1228-1236.

[60] Hamilton, I. G., Davies, M., Ridley, I., Oreszczyn, T., Barrett, M., Lowe, R., Hong, S., Wilkinson, P., and Chalabi, Z. (2011). The impact of houring energy efficiency improvements on reduced exposure to cold – the 'temperature take back factor'. Building Services Engineering Research and Technology, 32(1), 85-98.

[61] Grunewald, J., P. Häupl, and M. Bomberg. 2003. Towards an Engineering Model of Material Characteristics for Input to Ham Transport Simulations - Part 1: An Approach. Journal of Building Physics 26 (4):343-366.

[62] Zhao, J., Grunewald, J. and Plagge, R. 2013. Definition of generic materials by using a cluster analysis method. 2nd Central European Symposium on Building Physics, Vienna, Austria, Sept.9-11, pp 875-881.

[63] Everitt, B.S., Landau, S., Leese, M. and Stahl, D. 2011. Cluster analysis (5th edition). John Wiley & Sons. Chichester, West Sussex.

[64] ASHRAE. 2009. ASHRAE Handbook of Fundamentals. Atlanta, GA: American Society of Heating, Refrigerating and Air-Conditioning Engineers

[65] Kumaran, M.K. 1996. Final Report, IEA-Annex 24, Task 3: Material Properties, IRC/NRC, Canada.

[66] Kumaran, M.K., J.C. Lackey, N. Normandin, F.Tariku, and D. van Reenen. 2004. Heat, air and moisture transport properties of several North American bricks and mortar mixes. Journal of Testing and Evaluation,Vol 32, no 5, pp. 383–389

[67] Bekö G, Lund T, Nors F, Toftum J, Clausen G. Ventilation rates in the bedrooms of 500 Danish children. BuildEnviron 2010; 45(10):2289-95.

[68] Persily A. Evaluating building IAQ and ventilation with indoor carbon dioxide. ASHRAE Trans; 1997:193-204.

[69] ASTM .ASTM Standard D 6245-98 (2002), standard guide for using indoor carbon dioxide concentrations to evaluate indoor air quality and ventilation. American Society for Testing and Materials; 2002.

[70] Amstat.org [Internet]. Alexandria, VA: American Statistical Association; c2013 [cited 2013March11]. Available from: http://www.amstat.org/publications/jse/v13n1/olsson.html

[71] Appendix A Bekö et al. (2011) The APPENDIX is a (unpublished) conference paper written for the Indoor Air 2011 conference held in Austin, Texas

[72] EN 15251 (2007). Indoor environmental Input Parameters for Design and Assessment of Energy Performance of Buildings Addressing Indoor Air Quality, Thermal Environment, Lightning and Acoustics.

[73] ISO 9972 (1996). Thermal Insulation, Assessment of the airtightness of buildings, Fan Pressurization Method, ISO, Geneva.

[74] Hagentoft, Carl-Eric (2010). Probabilistic analysis of hygrothermal conditions and mould growth potential in cold attics. Impact of weather parameters, building systems and construction design characteristics. Annex 55 (RAP-RETRO) working paper to Copenhagen meeting. Chalmers University of Technology. Gothenburg. Sweden.

[75] EN ISO 13788 (2001). Hygrothermal performance of building components and building elements – Internal surface temperature to avoid critical surface humidity and interstitial condensation – Calculation methods. CEN. Brussels.

[76] Sanders, (1996) Internation Energy Agency Annex 24, Task 2 Environmental conditions

[77] Arfvidsson, J. (1998) Moisture transport in Porous Media. Modelling Based on Kirchhoff Potentials. PhD thesis. Lund University. Sweden.

[78] Boverket. (2009). Så mår våra hus - redovisning av regeringsuppdrag beträffandebyggnaders tekniska utformning m.m. ISBN-nummer: 978-91-86342-29-6, (in Swedish).

[79] Bagge H. (2011). Building Performance - Methods for Improved Prediction and Verification of Energy Use and Indoor Climate. Lund University, Building Physics, ISBN 978-91-88722-41-6, TVBH-1019.

[80] Allegrini, J., Dorer, V., & Carmeliet, J. 2012. Influence of the urban microclimate in street canyons on the energy demand for space cooling and heating of buildings. Energy and Buildings, Vol. 55, pp. 823–832.

[81] Cooley and Turkey 1965

[82] Carnahan, W., & Larson, R. 1990. An analysis of an urban heat sink. Remote Sensing of Environment, Vol. 33, pp. 65–71.

[83] Klysik, K., & Fortuniak, K. 1999. Temporal and spatial characteristics of the urban heat island of Lodz, Poland. Atmospheric Environment, Vol. 33, pp. 3885–3895.

[84] Runnalls, K., Oke, T. 2000. Dynamics and controls of the near-surface heat island of Vancouver, British Columbia. Physical Geography. Vol. 21, pp. 283-304

[85] Kalnay, E., Cai, M. 2003. Impact of urbanization and land-use change on climate. Nature, Vol. 423, pp. 528–532.

[86] Kim, Y., Baik, J. 2005. Spatial and temporal structure of the urban heat island in Seoul. Journal of Applied Meteorology, Vol. 44, pp. 591–605.

[87] Crawley, D. B. 2008. Estimating the impacts of climate change and urbanization on building performance. Journal of Building Performance Simulation, Vol. 1, No. 2, pp. 91–115.

[88] Rizwan, A. M., Dennis, L. Y. C., & Liu, C. 2008. A review on the generation, determination and mitigation of Urban Heat Island. Proceedings of BS2013: 13th Conference of International Building Performance Simulation Association, Chambéry, France, August 26-28 mitigation of Urban Heat Island. Journal of Environmental Sciences, Vol. 20, no. 1, pp. 120–128.

[89] Steeneveld, G. J., Koopmans, S., Heusinkveld, B. G., van Hove, L. W. a., & Holtslag, a. a. M. 2011. Quantifying urban heat island effects and human comfort for cities of variable size and urban morphology in the Netherlands. Journal of Geophysical Research, Vol. 116, No. D20, pp. 1–14.

[90] Tumanov, S., Stan-Sion, A., Lupu, A., Soci, C., & Oprea, C., 1999. Influences of the city of Bucharest on weather and climate parameters. Atmospheric Environment, Vol. 33, No. (24- 25), pp. 4173–4183.

[91] V. M. Nik, Climate Simulation of an Attic Using Future Weather Data Sets - Statistical Methods for Data Processing and Analysis . Sweden: Chalmers University of Technology, 2010. Available on http://publications.lib.chalmers.se/records/fulltext/114053/114053.pdf

[92] V. M. Nik, “Hygrothermal Simulations of Buildings Concerning Uncertainties of the Future Climate,” PhD, Chalmers University of Technology, Gothenburg, Sweden, 2012. Available on http://publications.lib.chalmers.se/records/fulltext/159222.pdf

[93] Wallenten, P. (2010), The treatment of long-wave radiation and precipitation in climate files for building physics simulations, Proceedings of the 11th International Conference on Thermal Performance of the Exterior Envelopes of Whole Buildings (Clearwater)